1983

Fatigue resistance of riveted steel truss bridge members and joints, PhD dissertation, September 1983.

Chun Kyung Seong

FATIGUE RESISTANCE OF RIVETED STEEL TRUSS BRIDGE MEMBERS AND JOINTS

by

Chun Kyung Seong

A Dissertation
Presented to the Graduate Committee
of Lehigh University
in Candidacy for the Degree of
Doctor of Philosophy
in
Civil Engineering

Lehigh University

September 1983

Certificate of Approval

Approved and recommended for acceptance as a dissertation in partial fulfillment of the requirements for the degree of Doctor of Philosophy.

August 25, 1983
(Date)

Professor Ben T. Yen
Professor in Charge

Accepted Sept. 23, 1983
(Date)

Special Committee directing
the Doctoral work of
Chun Kyung Seong

Professor Ti Huang
Committee Chairman

Professor John W. Fisher

Professor Allan W. Pense

Professor David A. VanHorn
(Ex Officio)

A C K N O W L E D G E M E N T S

This analytical study was performed at Fritz Engineering Laboratory, Lehigh University, Bethlehem, Pennsylvania. Dr. Lynn S. Beedle is Director of Fritz Engineering Laboratory and Dr. David A. VanHorn is Chairman of the Department of Civil Engineering.

The study was part of the "Fatigue Assessment of Sudan Railway Bridge" project sponsored by the World Bank.

The author is very gratefull for the continuing supervision, encouragement, many careful suggestion and critical review of this work by Dr. Ben T. Yen, Professor in charge of the dissertation.

The author also wishes to thank for the guidance of his doctoral committee consisting of Professors Ti Huang, John W. Fisher, Allan W. Pense and David A. VanHorn. Professor Allan W. Pense's teaching was not limited to academic knowledge but extended to Christianity.

Acknowledgements are also due to Mr. Hans Out who provided the fatigue crack growth test data on full size

riveted built-up floor beam of an old truss bridge (French Broad Ivy River Bridge) for the comparison of analytical work.

A special debt of gratitude is expressed to all the author's colleagues and Fritz Engineering Laboratory staff members. The help from Mrs. Dorothy Fielding in typing the special characters and Mr. WonKi Kim in preparing the drawings are gratefully acknowledged.

TABLE OF CONTENTS

A B S T R A C T	1
1. I N T R O D U C T I O N	3
1.1 General	3
1.2 Brief Summary of Previous Work	6
1.2.1 Load Distribution among Fasteners	7
1.2.2 Stress Distribution in Gusset Plate	8
1.2.3 Fatigue Tests on Riveted Joints	11
1.2.4 Fatigue Resistance Studies on Riveted Truss Bridges	15
1.3 Scope and Objectives of the Study	18
2. Analysis of Live Load Stresses in Truss Bridge Members	23
2.1 Introduction	23
2.2 Modelling of Truss Bridges	25
2.2.1 Two-Dimensional Models	26
2.2.2 Three-Dimensional Space Frame Models	28
2.2.3 Review of Results from Analytical Models	33
2.3 Stress Redistribution in Truss Bridges	37
2.3.1 Description of Truss Bridge and Modelling Details	39
2.3.2 Discussion of Stress Redistribution	41
3. Evaluation of Stress Intensity Factor by Singular Finite Element	45
3.1 Crack Tip Stress Field and $1/\sqrt{r}$ Singularity	46
3.2 $1/\sqrt{r}$ Singular Elements	49
3.2.1 General Information	49
3.2.2 Modification on Degenerated Triangular Element	53
3.2.3 Singularity in Degenerated Element	55
3.3 Calculation of Stress Intensity Factor	59
3.3.1 By Equality	60
3.3.2 By Virtual Crack Extension Method	61
3.3.3 Finite Element Computer Program QIFEVCEM	63
3.3.4 Comparison of Results	66
3.4 Estimation of Fatigue Life	67
4. Estimation of Stress Intensity Factor for Riveted Truss Members and Joints	71
4.1 General Assumptions	71
4.2 Riveted Built-up Truss Members--Detail 1	75
4.2.1 Geometry and Modelling	76
4.2.2 Results of Analysis	79
4.3 Riveted Truss Joints with Gusset Plates--Detail 2	83
4.3.1 Geometry and Modelling	85
4.3.2 Stress Distribution in Gusset Plates	88

4.3.3 Shear Force Distribution among the Rivets 89
4.3.4 Substructure Modeling 91
4.3.5 Results of Analysis 94
4.4 Riveted Connections with Splice Plates--Detail 3 99
4.5 Discussion 100
5. Fatigue Life of Riveted Truss Members and Joints 103
5.1 Fatigue Crack Growth Characteristics and Crack Sizes 104
5.2 Crack Growth Life Computations 108
5.2.1 Riveted Built-up Member -- Details without Bearing 111
5.2.2 Riveted Truss Joint -- Details with Bearing 112
5.2.3 Effects of Bending Moment 114
5.2.4 Comparison with AASHTO Fatigue Strength Provisions 116
5.2.5 Comparison with Fatigue Crack Growth Data of Riveted Beam Specimen 118
5.3 Comparison with Results from Previous Fatigue Tests 121
5.4 Crack Initiation Life and Fatigue Strength 124
5.5 Discussion 129
6. Summary and Conclusions 131
6.1 Main Findings and Conclusions 131
6.2 Suggestions

T A B L E S 139

F I G U R E S 168

R E F E R E N C E S 233

I. Isoparametric Finite Element Formulation 244
I.1 Isoparametric Finite Element [83] 244
I.2 Element Stiffness Matrix for the Isoparametric Element [40] 246
I.3 Consistent Nodal Forces and Pressure Loading Applied to Element Edges [40] 248

V I T A 255

LIST OF TABLES

Table 2-1:	Maximum Calculated Stresses in Various Truss Member	139
Table 2-2:	Cross-Section Properties of Kosti Bridge	140
Table 2-3:	Reduced Hanger Cross-Section Properties of Kosti Bridge	141
Table 2-4:	Maximum Calculated and Measured Stresses of Kosti Bridge Member	142
Table 2-5:	Change of Stresses in Truss Bridge Members due to 40 % Area Reduction in Hanger U_1L_1	143
Table 2-6:	Member forces and Stresses in Hanger for Various Reduction Steps	144
Table 3-1:	Stress-Intensity Factor for Center-Through Crack	145
Table 3-2:	Stress-Intensity Factor for Double-Edge Crack	146
Table 4-1:	Stress-Intensity Factor for Cracks in Built- up Truss Member under Tension of 68.95 MPa (10.0 ksi)	147
Table 4-2:	Stress-Intensity Factor for Cracks in Built-up Truss Member under Bending Moment Which Induces 68.95 MPa (10.0 ksi) at Extreme Fiber	148
Table 4-3:	Non-Dimensionalized Stress-Intensity Factor for Cracks in Riveted Built-up Truss Member	149
Table 4-4:	Coefficients of Functions F_t and F_b	150
Table 4-5:	Geometrical Variables of Riveted Truss Joint for Different Bearing Ratio	151
Table 4-6:	Stress-Intensity Factor for Cracks in Truss Joints under Tension of 68.95 MPa (10.0 ksi)	152
Table 4-7:	Stress-Intensity Factor for Cracks in Truss Joints under Bending Moment Which Induces 68.95 Mpa (10.0 ksi) at Extreme Fiber of Truss member	153
Table 4-8:	Non-Dimensionalized Stress-Intensity Factor for Cracks in Truss Joints	154
Table 4-9:	Coefficients of Functions G_t and G_b	155
Table 5-1:	S_R- N Provisions for Riveted Joints	156
Table 5-2:	Values of P and Q for Riveted Built-up Truss Members for m=3.0 and $C=3.829*10^{-12}$	157
Table 5-3:	Values of P and Q for Riveted Truss Joints for m=3.0 and $C=3.829*10^{-12}$	158

Table 5-4:	Measured and Estimated Fatigue Crack Length and Loading Cycles of Riveted Floor Beam	159
Table 5-5:	Result of Fatigue Tests on Double Lap Joints Bearing Ratio=2.74; from Reference [60]	160
Table 5-6:	Result of Fatigue Tests on Double Lap Joints Bearing Ratio=2.36; from Reference [60]	161
Table 5-7:	Result of Fatigue Tests on Double Lap Joints Bearing Ratio=1.83; from Reference [60]	162
Table 5-8:	Result of Fatigue Tests on Double Lap Joints Bearing Ratio=1.37; from Reference [60]	163
Table 5-9:	Result of Fatigue Test on Riveted and Bolted Joint, Bearing Ratio=0.89; from Reference [48]	164
Table 5-10:	Result of Fatigue Test on Riveted Joint ; from Reference [78]	165
Table 5-11:	Fatigue Crack Initiation, Propagation and Total Life of Riveted Details under Constant Stress Range (Tension only)	167

LIST OF FIGURES

Figure 2-1:	Typical Finite Element Mesh for Two-Dimensional Model	168
Figure 2-2:	Three-Dimensional Space Frame Model of Kohr Mog Bridge in sudan railway	169
Figure 2-3:	Three-Dimensional Space Frame Model of Kartoum Bridge in sudan railway	170
Figure 2-4:	Three-Dimensional Space Frame Model of Atbara Bridge in sudan railway	171
Figure 2-5:	Three-Dimensional Space Frame Model of Frankford Elevated Line Viaduct Trusses	172
Figure 2-6:	Three-Dimensional Space Frame Model of Fraser River Bridge in British Columbia, Canada	173
Figure 2-7:	Stress-Time Relationship of Hanger in Kosti Bridge	174
Figure 2-8:	Plan and Elevation of Kosti Bridge	175
Figure 2-9:	Three-Dimensional Space Frame Model of Kosti Bridge	176
Figure 2-10:	Stress-Time Relationship of Floor Beam in Kosti Bridge	177
Figure 2-11:	Stress-Time Relationship of Stringer in Kosti Bridge	178
Figure 2-12:	Stress Variation due to Damage in Member Cross-Section	179
Figure 3-1:	Coordinates, Displacement and Stress Field Ahead of a Crack Tip	180
Figure 3-2:	Singular Elements by Byskov, Tong and Pian, and Benzley	181
Figure 3-3:	Henshell and Barsoum's Quarter-point Isoparametric Elements. (a, b, c) Original singular Element, (d, e) Degenerated Singular Element	182
Figure 3-4:	Isoparametric Quadratic Two-Dimensional Elements	183
Figure 3-5:	Degeneration of Quadrilateral to Triangle	184
Figure 3-6:	Finite Element Mesh Along The Crack Line	185
Figure 3-7:	Change of Geometry due to Virtual Crack Extension δa	186
Figure 3-8:	Flow Diagram of Computer Program QIFEVCEM	187
Figure 3-9:	Modeling for Center-Through Crack	188
Figure 3-10:	Modeling for Double-Edge Crack	189
Figure 3-11:	Stress-Intensity Factor around the Crack Tip	190

Figure 4-1:	Locations of the Details of Study	191
Figure 4-2:	Detail of Riveted Built-up Truss Member Section--Detail 1	192
Figure 4-3:	Finite Element Model for Built-up Truss Member--Detail 1	193
Figure 4-4:	Non-Dimensionalized Stress Distribution across the Rivet Hole of Built-up Truss Member (15.24 cm for Gage and Pitch Distance)	194
Figure 4-5:	Effect of Pitch Distance on Function F_t of Detail 1	195
Figure 4-6:	Effect of Gage Distance on Function F_t of Detail 1	196
Figure 4-7:	Riveted Truss Joint Detail--Detail 2	197
Figure 4-8:	Simplified Riveted Truss Joint Model	198
Figure 4-9:	Finite Element Mesh for Global Analysis of Truss Joints--Detail 2	199
Figure 4-10:	Pratt Truss Joint Tested by Irvan [44]	200
Figure 4-11:	Contour Plot of Maximum Tensile Stress from Irvan's Test Results [44]	201
Figure 4-12:	Finite Element Mesh for Irvan's Test Detail	202
Figure 4-13:	Contour Plot of Maximum Tensile Stress from Finite Element Analysis	203
Figure 4-14:	Load Distribution among the Rivets	204
Figure 4-15:	Finite Element Mesh of Substructure Model for Detail 2	205
Figure 4-16:	Non-Dimensionalized Stress Distribution across the Rivet Hole of Truss Joint (Bearing Ratio = 1.66, Pitch = 81 mm)	206
Figure 4-17:	Effect of Bearing Ratio on Function G_t of Detail 2	207
Figure 4-18:	Detail of Riveted Member to Member Connection with Splice Plates--Detail 3	208
Figure 5-1:	Variation of P Due to Change of Initial Crack Size a_i for Riveted Built-up Truss Member	209
Figure 5-2:	Variation of P Due to Change of Initial Crack Size a_i for Riveted Truss Joint	210
Figure 5-3:	Effects of Initial Crack Size on Fatigue Life of Riveted Truss Members and Joints.	211
Figure 5-4:	Effects of Pitch Distances on	212

Fatigue Life of Riveted Built-up Truss Member(Gage Distance=15.24 cm)
Figure 5-5: Effects of Gage Distances on Fatigue Life of Riveted Built-up Truss Member(Pitch Distance=15.24 cm) 213
Figure 5-6: Effects of Bearing Ratio on Fatigue Life of Riveted Truss Joints 214
Figure 5-7: Effects of Pitch Distances on Fatigue Life of Riveted Truss Joints (Gage Distance=15.24 cm) 215
Figure 5-8: Effects of Bending Moments on Fatigue Life of Riveted Truss Joints 216
Figure 5-9: Details and Crack Locations of Riveted Floor Beam in Testing 217
Figure 5-10: Measured and Estimated Fatigue Crack Propagation in Riveted Floor Beam 218
Figure 5-11: Estimated Fatigue Strength and Test Result of Reference [60] for Bearing Ratio 2.74 and 2.36 ; R=0 219
Figure 5-12: Estimated Fatigue Strength and Test result of Reference [60] for Bearing Ratio 2.74 and 2.36 ; R=-1 220
Figure 5-13: Estimated Fatigue Strength and Test result of Reference [60] for Bearing Ratio 2.74 and 2.36 ; R=1/2 221
Figure 5-14: Estimated Fatigue Strength and Test result of Reference [60] for Bearing Ratio 2.36 and 1.83 ; R=0 222
Figure 5-15: Estimated Fatigue Strength and Test result of Reference [60] for Bearing Ratio 2.36 and 1.83 ; R=-1 223
Figure 5-16: Estimated Fatigue Strength and Test result of Reference [60] for Bearing Ratio 2.36 and 1.83 ; R=1/2 224
Figure 5-17: Estimated Fatigue Strength and Test result of Reference [60] for Bearing Ratio 1.83 and 1.37 ; R=0 225
Figure 5-18: Estimated Fatigue Strength and Test result of Reference [60] for Bearing Ratio 1.83 and 1.37 ; R=-1 226
Figure 5-19: Estimated Fatigue Strength and Test result of Reference [60] for Bearing Ratio 1.83 and 1.37 ; R=1/2 227
Figure 5-20: Estimated Fatigue Strength and Test result of Reference [48] for Riveted and Bolted Joints 228
Figure 5-21: Estimated Fatigue Strength and Test result of Reference [78] 229

Figure 5-22:	Fatigue Crack Initiation Behavior of A36 Steel [63]	230
Figure 5-23:	Cracks in Coped Section of Floor System	231
Figure 5-24:	$S_{r\,(net)}$-N_T Curves of Present Study and AASHTO Fatigue Category B, C and D	232
Figure I-1:	Consistent Nodal Force Vector For Uniformly Distributed Traction Force	249
Figure I-2:	Consistent Nodal Force Vector for Arbitrarily Distributed Traction Force	250
Figure I-3:	Consistent Nodal Force Vector for Traction force on Curved Edge	253

A B S T R A C T

The fatigue resistance of old riveted truss bridge members and joints was investigated in this dissertation. Clamping forces in rivets and friction between interfacing plates were considered not dependable and ignored. The components of riveted details were subsequently resolved into plane stress plates. Emphasis was placed on developing an analytical procedure for estimating fatigue crack propagation life of riveted truss details.

The analysis of member stresses was conducted by finite element modelling of a bridge span as a three dimensional space frame. Redistribution of stresses in truss bridge members when one developed a crack was examined by assuming the reduction of cross section occured throughout the member length. By using singular isoparametric plane stress elements, the fracture mechanics stress intensity factor for cracks emanating from rivet holes was evaluated through a virtual crack extension method.

Two types of details were studied : riveted built-up truss members with no transfer of load between component

plates and riveted truss joints where rivets transfer loads by bearing.

Results of analysis showed that pitch and gage distances of rivets affected stress concentration and stress intensity factor at rivet holes and consequently the fatigue crack propagation life of riveted built-up truss members. Bearing ratio was the controlling parameter for riveted truss joints. Higher bearing ratio resulted in shorter fatigue crack propagation life.

It was found that the fatigue crack growth life of riveted details could be conservatively represented by existing fatigue strength provisions for bridge design.

A more appropriate estimate of fatigue resistance was established through consideration of crack initiation and propagation. The estimate fatigue life of riveted details compared well with test results of previous studies.

Areas for further studies were pointed out.

CHAPTER 1

I N T R O D U C T I O N

1.1 General

With the introduction of wrought iron and steel into bridge construction practice, rivets were the standard fasteners for over 100 years. The development of the high strength structural bolts and the advanced techniques in welding around the 1950's significantly reduced the usage of riveted joints. At the present time, rivets are rarely used in new structural connections and most bridge members are connected by either high strength bolts or welding [26, 35, 44].

Even though the riveted joints are no longer used for bridge construction, a large number of riveted steel bridges are still continuing in service. Maintaining and upgrading of these structures are among many important tasks of modern bridge engineers.

In riveted or bolted joints, small micro-flaws are present at the edges of holes as a result of punching or drilling the fastener holes. It is well known that the stress concentration of a plate with a hole could be as

large as three times the nominal stress. These micro-flaws and stress concentrations play a significant role in fatigue crack propagation in riveted and bolted joints. As early as 1938, it was noticed that riveted joints provided less favorable fatigue strength than high strength bolted joints primarily due to the low clamping force of riveted joints [78]. Riveted and bolted joints could carry loads by bearing of the fasteners against the plates or by friction between the jointed plates, or by both actions.

When riveted or bolted joints carry loads by bearing, end fasteners undertake the highest proportion of the load resulting in high localized bearing stresses around the end fastener holes [60, 79].

For truss member connections, load transfer between a gusset plate and the built-up member causes non-uniform stress distribution known as shear lag [18, 54].

These conditions of high stress concentration, low clamping force, unequal load distribution among fasteners, localized bearing, and shear lag contribute to the fatigue strength of the riveted truss joints.

After experiencing considerable numbers of live load cycles, old riveted and bolted truss bridges have developed problems with fatigue cracking in the connection region of hangers, floor beams and stringers [3, 4, 24, 67, 79]. As a result, a great deal of research work have been undertaken on the fatigue resistance of riveted and bolted joints since 1930's, and specifications governing fatigue strength have been developed for the AMERICAN ASSOCIATION OF STATE HIGHWAY TRANSPORTATION OFFICIALS (AASHTO) and AMERICAN RAILWAY ENGINEERING ASSOCIATION (AREA) [1, 2].

The scarcity of fatigue failure of old riveted steel truss bridges could be regarded as the results of these specifications, as well as the relatively large safety margin inherent in early design practice, the clamping forces in rivets though unknown in magnitude, and the redundant nature of force transmittal in truss bridge structural systems.

Recent studies, based on statistical analysis of results from large number of test specimens and on results of analyses which utilize the concepts of linear elastic fracture mechanics, have led to a new set of

provisions for evaluation of the fatigue strength of welded structural joints [27].

The analytical assessment of fatigue strength of riveted members in old steel truss bridges is the primary emphasis of this dissertation.

1.2 Brief Summary of Previous Work

The fatigue behavior and strength of riveted truss joints become complicated because of uncertain clamping forces after long periods of use, unequal load distribution among the fasteners, shear lag effects in truss joints and the great variety of geometrical dimensions and component arrangements. Although there have been numerous studies from 1838 to the present on these individual factors of riveted connections, their fatigue strength has not yet been defined satisfactorily.

Some of the studies are mentioned very briefly below to point out the large number of influencing factors and the current state of knowledge.

1.2.1 Load Distribution among Fasteners

The first extensive static tests of riveted joints were reported in 1838 by William Fairburn [22]. Most of the early theoretical studies on riveted and bolted joints reviewed by De Jonge [45] and Hrennikoff [42] considered the load distribution among fasteners in the elastic range of behavior of the joints [10, 13, 28, 42]. The first extension of these studies into the inelastic range was made by Vogt [73], followed by Francis [29] and Rumpf [64]. These studies showed that the load distribution among fasteners of splice joints was unequal in both the elastic and inelastic load ranges of the joints and that the end fasteners carried the largest proportion of the load.

Tate and Rosenfeld [69] included a friction term in the load equation for bolts in joints in 1946 and Lobbet and Robb [49] obtained the effects of friction on the load distribution among fasteners in 1962.

Later, mathematical models were developed by Fisher [23] who established the load deformation relationship throughout the complete load range of the components in bolted joints and developed an iterative

type of computer program based on this model. These enabled with relative ease studies on the effects of various parameters, such as joint length, pitch, fastener diameter and shear ratio of the joints. Fisher and Rumpf's study [25] based on these theoretical developments was confirmed by tests, and excellent agreement between analysis and tests was observed.

Yen and Smillie presented in 1973 an analytical method to investigate the fastener load distribution in a multi-row joint and facilitated the study on the effects of number of fasteners in a row and the friction at the interfaces of the connected materials [81].

1.2.2 Stress Distribution in Gusset Plate

One of the important components in a riveted or bolted joint is the gusset plate which is needed to transfer the load from one member to another. The stress distribution pattern within a gusset plate is complicated and highly indeterminate. The stress distribution pattern must be in accordance with the load transfer between components and affects the fatigue strength of the truss joint.

Only a relatively few attempts have been made to

determine experimentally and analytically the stress distribution in gusset plates.

In 1952, Whitmore conducted an experimental investigation of stress distribution in gusset plates by using an aluminium gusset plate model simulating a lower chord joint of a Warren truss with a continous chord [75]. From the results, he proposed an effective width solution which assumed the maximum normal stress at the end of a member was distributed uniformly over an effective cross section of the gusset plate. The effective width of the section was obtained by constructing 30 degree lines from the outer rivets of the first row to intersect a line perpendicular to the member and passing through the last row of rivets. The line segment intercepted was then used as the effective width of a section to calculate the uniform stress caused by a force in the member.

Irvan [44] and Hardin [34] made an investigation of the primary stress in a double plane gusset plate of a pratt truss with or without chord splice. Their investigation was different from that of Whitmore on the assumption of effective width. The effective width by

Irvan and Hardin was also obtained by drawing lines at 30 degrees with respect to the member direction, but from an origin at the center of gravity of the rivet group, to intersect a line passing through the bottom row of fasteners.

Davis attempted an analytical study in 1967 in duplicating Whitmore's test by finite element analysis and confirmed his conclusions [20].

Vasarhelyi conducted an experimental and analytical study on a Warren truss joint model to improve the empirical basis of the stress analysis of gusset plates [72]. He concluded that the magnitudes of maximum stresses found in a gusset by various simplified methods were only slightly different; the major deviations were in the location of those maximum values.

In 1972, Struik presented an analysis of inelastic behavior to determine the ultimate strength of gusset plates for the first time [66]. He developed a finite element computer program capable of elastic and elastic-plastic analysis. The presence of fastener holes were accounted for by special elements with a hole. But no attempt was made to include the variation in load

partition among the fasteners as a result of deformations caused by the load and the load transfer between the gusset plate and the joinning members.

1.2.3 Fatigue Tests on Riveted Joints

The first important series of fatigue tests related to riveted joints was reported in 1921 and 1923 by Moore and Kommers [47, 52]. Their papers dealt with the fatigue of metals. In 1922, Wilson and Haigh conducted fatigue tests on plates with open holes [77].

To determine the material requirements and to formulate design specifications for riveted joints, many tests were carried out around 1930 in Germany for the Deutsche Stahlbau-Verbund and the Deutsche Reichsbahn-Gesellshaft. The test series of Graf [32] and Klöppel [46] were to investigate the effects of mill scale, holes and grooves, painting in double lap riveted joints, and placing rivets in open holes, the effect of small fluctuations of load on a bar with high initial stress, the effects of clamping force and of the tension-shear-bearing ratio (T : S : B) on the fatigue strengh of riveted joints.

In 1938, Wilson and Thomas conducted an extensive

program of fatigue tests on riveted joints in connection with the construction of the San Francisco-Oakland Bay Bridge, California [78]. They studied the effects of stress ratio, method of forming holes, T : S : B ratio and grip length in combination with carbon steel and manganese steel rivets and bolts with carbon, silicon and nickel steel plates. Bolts driven to fit as well as under-sized bolts were investigated.

In 1947, the Association of American Railroads (AAR) began an investigation of the fatigue failures in floor beam hangers of railway bridges at the request of Committee 15 of the American Railway Engineering Association (AREA) [3]. In connection with this investigation to explain the cause and remedy of these fatigue failures, Wyly advanced the working hypothesis that the index to the fatigue strength of a structural member is given by the magnitude of the tensile stress concentrations and the total tensile strain concentrations which were induced by rivet bearing. This was determined by examining stress distribution around rivet holes through strain measurement and photoelastic testing [3, 79]. He also proposed the replacing of rivets by non-bearing, high strength, high-clamping force

bolts as a remedy to minimize the effect of rivet bearing. This explanation was subsequently verified by the study of Carter, Lenzen and Wyly on the fatigue in riveted and bolted single lap joints [16].

Lenzen studied the relative fatigue strength of structural joints in 1949 [48]. He compared joints fabricated with hot and cold-driven carbon steel rivets and carbon steel bolts. He also performed tests to evaluate the initial tension in hot and cold-driven rivets and the clamping force of the bolts.

Baron and Larsen studied the effects of grip length of riveted and bolted joints and T : S : B ratio with A141 and A195 rivets using both punched and drilled holes [5].

Baron, Larson and Kenworthy extensively studied the effects of pitch, gage and edge distance on a variety of rivet patterns [6].

The effect of bolt tension on the fatigue strength of joints fastened by A325 bolts was studied by Munse, Wright and Newmark [55]. The tests indicated that the high strength bolted joints were generally superior to

similar riveted joints, whether subjected to static loads or fatigue type loads. Munse also tested bolted joints in which the bolts were torqued beyond the elastic limit [53].

Hansen [33] discussed tests on mild steel and high strength low-alloy steel fastened by A141 rivets and A325 bolts. His study showed that the clamping forces in rivets varied from 4.45 kN to 89.0 kN (1 to 20 kips) with 30 % less than 22.25 kN (5 kips) and 20 % greater than 48.95 kN (11 kips) in 19.1 mm (3/4 in.) diameter A141 rivets.

Reemsnyder presented an extensive literature survey and synthesized the numerous data of the previous work [61]. His investigation showed that the fatigue strength of riveted and high strength bolted joints is comparable to that of perforated and plain plates respectively for mild steel.

1.2.4 Fatigue Resistance Studies on Riveted Truss Bridges

Most of the above studies dealt with behavior of riveted or bolted joints idealy controlled in the laboratory environments. The study on the overall behavior and fatigue resistance of riveted truss bridges was not started until the late 1970's.

In 1976, Fisher and Daniels estimated the fatigue life of the 380 ft main span in the Fraser River Bridge at New Westminister, British Columbia, Canada [24]. They modeled the actual truss bridge as a three-dimensional space frame assuming continuity condition for gusseted joints and compared the live load stress spectrum defined by actual field measurement with the predicted spectrum by analytical models. It was concluded that, in order to assess accurately the significance of the applied loads, a space frame analysis would normally be required for all such structures.

Yen, Seong and Daniels studied the fatigue resistance of the Frankford Elevated Line Viaduct truss spans in 1980 [80]. They also used a three-dimensional space frame, with the concrete deck attached at bottom chords.

Between 1976 to 1981, Sweeney and Elkholy conducted a series of studies for the estimation of fatigue damage in truss bridges of Canadian National Railways [67]. These studies included field inspections, field measurements of stresses in truss details, comparison with results of bridge analysis, study of traffic volume trends, fatigue damage estimation, etc, in order to estimate the cumulative fatigue damage, and to predict the remaining fatigue life and necessary strengthening of the bridges to the same level of strength as other bridges of the Railways. The important general conclusions were that the fatigue strength category D of AASHTO specifications [1] is too conservative to be applied indiscriminantly to members of riveted truss bridges and that the replacement of the critical rivets in the floor beam to hanger connection by properly torqued high strength bolts will extended the fatigue life remarkably.

In connection with a general study on the Sudan Railroad system in order to assess the condition of the bridges and to evaluate any fatigue damages, a series of field tests as well as analytical studies were under taken by Lehigh University. De Luca developed several

analytical bridge models to simulate the behavior of a bridge structure in order to determine the applicable model by comparing analytical results with the field measurements [21]. He concluded that the three-dimensional model which assumed the stringers as simple beams between floor beams provided the best agreement between the results of field test and the analytical model. Marcotte studied the effect of loading type on the fatigue behavior of riveted connections in addition to estimating fatigue damage in the Blue Nile Bridge in Khartoum, Sudan [51]. On the other hand, Ward examined the redundancy of the force flow in truss bridges using three-dimensional truss models [74]. He also concluded that the three-dimensional space frame model provided the best approximation. The stress redistribution due to redundant force flow in a truss bridge was a localized characteristic and the presence of a fatigue damaged member did not ensure an increase in stress in the adjacent members. As far as a damaged member remains functional, the increase in stresses in adjacent members only occurs when reduction in cross sectional area of the damaged member is fairly extensive. This confirmed a conclusion of Yen, Seong and Daniels [80].

1.3 Scope and Objectives of the Study

From the brief review above, it can be concluded that, although there has been a substantial amount of work on the fatigue strength of riveted connections, most of the studies were based on tests of single or double lap joint specimens ideally controlled in laboratories. There is only very limited correlation between these laboratory test data and actual behavior of riveted truss bridge members under live load conditions.

The difficulties in determining the stress distribution in the component plates of a riveted joint and the great variety of geometric configurations of gusseted connections and truss joints inhibited the development of a simple and reliable analytical method to estimate the fatigue strength of these joints. The lack of an analytical method for evaluating the fatigue strength of riveted truss members and joints prevents bridge engineers from estimating quantitatively the expected fatigue life of a riveted truss bridge and from developing the necessary and effective retrofit procedure for fatigue damage of the bridge components.

From reviewing the results of the three dimensional

space frame analyses of truss bridges, it is clear that the applied live loads usually induce bending moments in addition to axial forces in the truss members but the twisting moments are usually negligible. Since all the forces and bending moments in truss members can be adequately resolved into in-plane stresses, the stress state of the individual component plates in built-up members, gusset plates of truss joints, and splice plates of members can all be treated as two-dimensional, plane stress elements if the clamping forces in rivets are negligible or not considered.

However, clamping forces do exist and studies and retrofitting of bridges showed that the variation in clamping force is possibly a major factor contributing to the scatter of experimental fatigue data of riveted joints [16, 26, 33, 61].

Consequently, the development of an analytical procedure for evaluation of fatigue strength of riveted truss members and joints could be approached in two ways. First, neglect the clamping forces in riveted members and joints, formulate an analytical procedure for plane stress component plates, correlate with experimental

results and field measurement results, and then try to correct for the effects of clamping forces. Second, try to develop analytical three dimensional models of riveted members and then correlate with test data and field study results. The first approach can readily be made, with the resulting fatigue strength of riveted members and joints being a lower bound (conservative). The second approach may eventually provide a more accurate estimate of fatigue strength, but a quick and rational analytical procedure of three dimensional members can not be developed instantly. In the light of the increasing reports of fatigue cracks in riveted truss bridges [3, 4, 24, 67, 80], the first approach is preferrable.

Therefore, the objectives of this study are to develop an analytical method for estimating the fatigue strength of riveted truss members and joints by investigating two-dimensional plates with holes where bearing pressure is applied by rivet without clamping force, to examine the various truss bridge models proposed by many studies for establishing a rational modelling technique which can provide information on stress distribution, and to correlate the analytical results with experimental and field data for evaluating

fatigue strength of riveted members and joints in truss bridges.

The study presented here consists of four phases, each in a separate chapter. The four phases are;

1. The comparative study of modelling technique and redundant behavior of truss bridges,
2. The selection of a finite element procedure for application to linear elastic fracture mechanics analysis of component plates,
3. The analytical estimation of stress intensity factor correction functions for the cracks at rivet holes of riveted truss members and joints, and
4. The estimation of fatigue life of riveted truss members and joints and the comparision of analytical results to previous experimental results.

In Chaper 2, several modelling techniques for truss bridges are compared. The main purpose of the comparision is to obtain a more rational stress distribution at the "fatigue critical" details of the truss bridges. The basic models to be compared are the two-dimensional plane frame model and three-dimensional

space frame models established by several studies. The behavior of redundant force flow in truss bridges is to be examined with respect to the reduction in the cross sectional area of the fatigue damaged member. Chapter 3 describes an effective way of calculating the fracture mechanics stress intensity factor by using appropriate singular finite elements. A brief historical review on the application of finite element method to fracture mechanics is also given. The accuracy of the selected singular element is checked against the results originated from different studies. The parametric studies on the stress intensity factors of the cracks in riveted built-up truss members and truss joints by using the singular finite element developed in Chapter 3 are described in Chapter 4. The purpose of these studies is to examine the effects of bearing ratio, pitch and gage distance as governing parameters of the fatigue strength of riveted truss joint and built-up truss members. In Chapter 5, the stress intensity factors as a function of crack length are correlated to fatigue life of truss members and joints by using a linear elastic fracture mechanics approach. The analytical results are compared to previous experimental results of several studies on riveted joints.

CHAPTER 2

ANALYSIS OF LIVE LOAD STRESSES IN TRUSS BRIDGE MEMBERS

2.1 Introduction

Whereas the maximum tensile stress in a railroad or highway bridge member is one of the primary factors which influence its resistance to yielding and fracture, the live load stresses are responsible for the initiation and growth of fatigue cracks. Therefore, in order to assess the fatigue strength of the truss bridge members and the safety of a truss bridge, accurate evaluation of the live load stresses in its members is essential.

In truss bridges, the main trusses support the deck system which includes floor beams, longitudinal stringers and the deck. Lateral bracing at the top chord and bottom chord level and the sway frames at panel points are added to resist wind loading and to improve the stability of the structure.

Usually, most of the riveted truss members except eyebars are rigidly connected at their junction to neighboring members. Therefore, live loads on the deck system induce axial force and bending moments in the

truss members. However, the magnitudes of member stresses due to bending moments, being controlled by the truss geometry and joint details, are usually small in comparison to those due to axial forces and have been considered to be secondary in nature.

As a result, the analysis and design of trusses have been based on the traditional assumption that all members are pin-connected, developing only axial member forces, and each truss behaves as a two-dimensional plane structure. The floor beams, stringers and bracings have been designed as simply supported beams. This approach is intended to give an upper bound solution to the member forces [19, 67, 74].

These assumptions are satisfactory for overall member size proportioning under static loading condition. In considering the fatigue strength under live loads and the potential of fracture of bridge members, the actual stress at a structural detail must be evaluated, not the upper bound average stress. The relatively small magnitudes of secondary bending stresses due to the actual condition of member connections may contribute to fatigue crack growth by being additive to the primary

direct stresses.

Fortunately, because of the highly redundant nature of riveted truss bridge structures, complete failure of a truss bridge very seldom took place.

In this chapter, various analytical modelling techniques, which can provide reasonable evaluation of stresses for fatigue life estimation, are discussed. The influence of fatigue damaged components and members is examined by assuming that the reduction of cross sectional area and moment of inertia due to fatigue damage occurs throughout the length of the member in order to get the maximum effect on the stress redistribution among the truss members.

2.2 Modelling of Truss Bridges

The basic analytical models used for truss bridges reviewed are the finite element models of two-dimensional plane truss and rigid frame model and the three-dimensional space frame model established by several previous studies [21, 51, 74, 80].

The two-dimensional finite element models are essentially the same in general consideration of loads

but slightly different in modelling of joint details.

The differences in three-dimensional models developed by various studies arise from the conditions of structural details characteristic to individual truss bridges. These include conditions of floor system restraints, such as stringer to floor beam connections or floor beam to truss connections, and the degree of participation of the ties and rails in resisting the bending of stringers and floor beams.

2.2.1 Two-Dimensional Models

Most of the two-dimensional finite element models can be distinguished into two groups, the plane truss models and the plane frame models.

A plane truss model is the most common model used for the analysis and design of truss bridge spans. Truss components are not considered to undertake bending and all truss joints are assumed pin connected. As a result, only axial forces are calculated in the plane truss models. Loads can be applied only at the truss joints as single concentrated loads.

In a plane frame model most of the members are

assumed capable of resisting bending and most of the joints are assumed rigidly connected. Bending moment in the plane of the frame can be developed in the component members. As a result each truss of a bridge is modelled as a two dimensional rigid frame. The loads to the trusses, however, remain the same as used in the plane truss models, that is, loads on each truss are introduced at panel points as concentrated loads.

Figure 2-1(a) shows the typical finite element mesh of two-dimensional plane truss or plane frame model. A plane truss model or a plane frame model does not take into consideration the floor system. A separate analysis was required to provide the stress conditions in the floor beams and stringers as well as the load magnitudes at the panel points of the two-dimensional truss or frame models [24].

For the two-dimensional models reviewed, a computer program was used to develop influence values of stresses due to axial forces and bending moments in members. This was done through loading the floor system at successive locations and applying the resulting panel point concentrated loads to the two-dimensional trusses.

The influence values for member stresses by axial forces or bending moments were used as input to a computer program which evaluated the stress-time relationship for the point of interest on the truss bridge for a given loading condition of vehicular wheel spacing and load magnitude. No dynamic effect was considered in the computation.

The computed stress-time relations were compared with field measured stress variations under live load to correlate the stresses of the analytical models and the real structure. Some of the comparisons are presented later with those from the three-dimensional models.

2.2.2 Three-Dimensional Space Frame Models

The three-dimensional finite element space frame models were developed to simulate the continuity conditions of all the structural joints in actual bridge spans, including the floor systems. Because results of analyses showed that twisting moments are negligible, beam elements were usually used for all members except for the lateral bracing members which had relatively low bending rigidity compared to the other members and the stringers and floor beams. Truss elements were adopted for these bracing members. In most cases, all six

degrees of freedom were allowed at all the finite element nodes which were not physically supported at the bridge.

Since prismatic bridge members were used in the models, judgement was needed to established the locations of the element connections between the hangers, floor beams and bottom chord members because the centers of gravity of the connecting members usually do not coincide. A common assumption is that all members are connected at the center of gravity of the bottom chord.

The three-dimensional models require large computational capacity of the computers but enable more realistic modelling of the truss spans. For the examination of fatigue cracks in actual bridges, for example, elaborate consideration of connection details can be made by careful discretization of the component parts. For general evaluation of member forces and bending moments, beam and truss elements are usually sufficient in modelling the bridge spans.

Some examples of three-dimensional space frame models are the following.

1. Kohr Mog Bridge in Sudan is a single track,

half-through pony truss span [21].

It has triangular buttress plates between the built-up hanger and the floor beam. These plates were taken into account in the three-dimensional model shown in Fig. 2-2 by adding triangular plate elements.

Also, the composite action of rails with stringers was considered as a variation of the three-dimensional model.

Four slightly different models in the assumption of floor beam to hanger connection and stringer to floor beam connection were analyzed to bound the actual behavior of truss bridge.

2. Blue Nile Bridge in Khartoum, Sudan is a Petit truss type through span bridge [51].

   A single railway track is carried by two lines of longitudinal stringers and the roadway is supported on a longitudinal trough. The stringers are connected to the transverse floor beams and troughs are also supported by the floor beams.

   Since the floor beams are non-prismatic members, an average depth was used to estimate the corresponding geometrical properties in the three-dimensional model shown in Fig.2-3. Floor beam connections

were assumed to be rigid.

3. Atbara Bridge in Sudan is a single track, Pratt through truss bridge, with pedestrian and automobile roadways supported from the outside of each truss [74].

   Several variations of the three-dimensional space frame model were developed by modifying the support conditions of the structure and the restraint conditions of floor beam to stringer connection. Figure 2-4 shows the typical space frame model used in this study.

4. The viaduct span of the Frankford Elevated Line in Philadelphia consists of three parallel trusses with the inbound and outbound tracks separated by the center (inner) truss. The railroad tracks are supported on concrete decks which are at about mid-depth of the trusses and encase the transverse floor beams and all web members of the center truss [80].

   The finite element three-dimensional space frame model of three-parallel trusses with a concrete slab is shown in Fig. 2-5. In this model, the floor beams and the concrete deck were assumed at the level of the truss lower chord. The concrete

encased floor beams and two rails between trusses were modelled as continuous beams at the level of the deck.

5. Fraser River Bridge in British Columbia is a single track, 115.8 m (380 feet) main span, through truss bridge and carries most of Canadian National Railways traffic to Vancouver [24].

   A three-dimensional finite element model was developed by taking advantage of symmetry as shown in Fig. 2-6. Because the study was concerned with stress resultants in the first hanger M_1L_1, only major load-carrying members were retained in the vicinity of the hanger M_1L_1. Nodes midway between the truss were constrained to displace only vertically and horizontally because of symmetry.

All these railroad bridge trusses are loaded by train wheels on the rails. In finite element analytical models, loads were applied at the nodes which connected the beam elements representing stringers and floor beams. Each loading case consisted of two unit vertical loads applied at corresponding nodes. By applying the loads at successive nodes, influence values for stresses in members can be obtained from the computer program.

Stress-time relationships for specific points of a member can then be computed, as it was described for two-dimensional models.

2.2.3 Review of Results from Analytical Models

The results of the example modelling are summarized in Table 2-1. These are total stresses (axial plus bending) from static analyses without considering the effects of impact. No transverse loading due to wind or train motion was considered in the analyses.

Also listed are the maximum measured stresses in the corresponding truss members. No significant changes in measured stresses of the truss components were observed between speeds of 15 km/h and 45 km/h for test train runs [21]. This condition enabled direct comparison between computed and measured stresses.

By examining the magnitudes of stresses in Table 2-1, a number of conclusions may be drawn.

(1) The two-dimensional plane truss models generally produced the highest stresses in all members except for the first and last hangers. Thus this model provided an upper bound value for axial stresses of main truss

members.

(2) The stresses computed for main truss members by plane truss and plane frame models were not significantly different. This indicates that the stresses induced by the in-plane bending moments were small.

(3) The calculated stresses, including those from the three-dimensional space frame models, were generally in good agreement with the measured values.

(4) For the three-dimensional space frame models, the truss support conditions only affected the bottom chord stresses. When pin and roller support conditions were used the bottom chord stresses were overestimated. When both ends were restrained against longitudinal displacement (pin / pin), the bottom chord stresses were underestimated.

(5) The assumed conditions of the connections between stringers and floor beams and floor beams and hangers did not significantly affect the nominal stresses in the main members of the trusses. Only the stresses in the floor system and at the floor beam to hanger connections were being influenced.

(6) The largest discrepancy among the stresses computed from different analytical models and obtained by measurements occurred in the areas of the connections between the floor beams and the hangers of the main trusses. The two-dimensional models assumed point loading from the floor system to the hangers at panel point thus ignored the influence of bending of the floor beams. The three-dimensional space frame models permitted close approximation of the continuity condition therefore should provide better correlation between computed and measured stresses.

To examine the computed stresses from the three-dimensional space frame model further, the measured strains and the estimated stress-time relations of a hanger are compared. Figure 2-7 shows the measured strain and the estimated stress-time relations of hanger U_1L_1 or U_6L_6 of Fig. 2-8. The traditional influence line from the plane truss analysis implies that the first and last hangers are not subjected to any stress until the loads are applied to the two neighboring panels. The influence lines from the two-dimensional plane frame and the three-dimensional space frame both indicate that these hangers are stressed by loads applied anywhere on

the structure. Consequently, all wheels of a train cause stresses in the hangers as the train pass through the bridge and the stress in the hanger predicted by the plane truss model would be lower than those from the frame models. This is evident from comparing the stress-time relations from computed and actually measured results, Fig. 2-7.

The stresses developed in the hanger by the space frame model are significantly higher than those developed by either of the two-dimensional models. This is due to the "rigid" connection of the floor beam to the hanger, resulting in bending of the hanger. Typically, bridge trusses have been designed using plane truss models. Hence, the stresses experienced by the hangers would be higher than predicted. Fatigue damage could therefore occur if the live load magnitudes are high and the loads are frequent. Fatigue cracks in hanger have been observed [26, 67].

Similar conditions exist for the ends of floor beams near the hangers. Traditional plane truss analysis ignores the bending restraint from the hanger to the floor beam, assuming that only shear is transmitted

between the floor beam and the lower chord-hanger panel point. The space frame models show that the floor beam stresses could be large. This explains, in a broad sense, why fatigue cracking of floor beams has been the most common problem reported in the literature [26, 67].

For the study of this dissertation, the emphasis is on riveted truss members. The most important and relevant result from the previous studies is that appropriate three-dimensional model of a truss bridge provides good approximations to member forces and stresses and closely simulates the actual behavior of the truss bridge.

Three-dimensional models are used in this study for examination of force and stress redistribution in truss bridges with cracked truss members.

2.3 Stress Redistribution in Truss Bridges

A truss bridge with rigid connections between component members is in essence a rigid frame structure with high degree of redundancy. Structures with redundancy do not collapse suddenly or undergo catastrophic failure if one member of the structure is

damaged slightly or even totally. The force or part of the force which is sustained by the member before damage can be redistributed to the neighboring members.

Damages of a truss member may be caused by over-stressing, fatigue crack growth, corrosion, or other events such as accidental impact. These local damages change the cross sectional properties of the member through reduction of area or stiffness. In order to get the maximum effect of these damages on force redistribution in truss bridge members, a reduction in the cross sectional area and stiffness of the entire member can be assumed. Thus, it is simple in principle that the effects of a damaged member on the behavior of a truss bridge can be studied by changing the cross sectional area and stiffness of the member and analyzing the bridge.

The three-dimensional space frame finite element model of a truss bridge provides a convenient and adequate tool for such analysis. By employing this procedure the force redistribution and resulting stresses in members of a viaduct truss span was examined [80]. Ward studied the change of member stresses and the

overall truss bridge behavior when half of the cross section of a hanger or a lower chord member was not effective, and when each of these member was completely incapable of resisting load [74].

In this section, it is examined how the stress in the cracked member of a truss bridge varies as force redistribution takes place when the crack becomes larger.

2.3.1 Description of Truss Bridge and Modelling Details

The Kosti Bridge of Sudan railway system is used in this part of study to see how the stress in the cracked member varies when the crack grows into different lengths successively. The bridge is a single track, through-Pratt truss bridge with pedestrian roadways located outside of the trusses. Member dimensions are tabulated in Table 2-2, and the bridge plan and elevation are shown in Fig. 2-8. The main truss and floor systems are composed of riveted built-up members of steel plates and angles.

The bridge was modelled as a three-dimensional space frame with rigid joints. Three-dimensional beam elements from SAP IV finite element library [9] were used for all members except the wind bracings which had small cross

sections compared to the other members. Truss elements were used for these bracing members. Hinge and roller support conditions were assumed at the two ends of the trusses.

Fig. 2-9 shows the three-dimensional space frame model. For ease in identifying the members, the west truss is identified as truss A and the east truss as truss B. The nodal number of the panel points increase numerically from north to south, that is left to right in Fig. 2-9. Each stringer between floor beams has two nodes at the third points.

In this model, two unit vertical loads were applied at the nodes which connect the stringers and floor beams or at the nodes on one-third point of stringers. This constitutes one load case. To calculate the influence values of the member forces, 12 load cases were considered on the south half of the span, taking advantage of symmetry of the truss span. Also, one set of two 445 kN (100 kips) vertical loads were applied at the first panel stringer to floor beam connections. Therefore, a total of thirteen load cases of applied forces were considered.

Because, as mentioned before, the stresses in the first hangers were usually underestimated, and a significant number of fatigue related problems in hangers have been reported in literature, the first hanger of truss A (U_1L_1A) was assumed in the model to have been damaged by a fatigue crack and reduction of the cross sectional area and moment of inertia was assumed to occur throughout the member length.

The hanger U_1L_1A is an I-shaped built-up member consists of four flange angles of unequal leg $4L_S$-127x89x11.1 mm (5x3-1/2x7/16 in.) connected by lacing in the web (see Table 2-3). The damaged condition of the hanger was simulated by successively reducing the original gross cross sectional area of the hanger by 5, 10, 20, and 40 per cent. The cross sectional properties for different steps of area reduction are shown in Table 2-3.

2.3.2 Discussion of Stress Redistribution

First of all, that the three-dimensional space frame model represented the actual conditions of the truss bridge is to be confirmed. The computed stress-time relations of hanger, floor beam and stringer shown in Figs. 2-7, 2-10 and 2-11, have similar shapes of the

corresponding measured curves. The computed and measured maximum stresses of some truss bridge members are tabulated in Table 2-4. The stresses in most of the members compare fairly well.

As a more and more reduction in cross sectional area was introduced in hanger U_1L_1A in the finite element model, only the members adjacent to the damaged hanger incurred significant increase in computed member stresses. These adjacent members undertook more bending moment as the reduction of area in the hanger got larger. Table 2-5 summarizes stresses in some of the members when the area of U_1L_1A was reduced by 40 per cent and the moment of inertia reduced accordingly. By comparing the stresses in the members when the hanger was intact, it can be stated that the influence of a damaged member was very minor beyond one or two panels from the member. The stress changes in the opposite truss, the floor system and the top bracing members were minimal.

To examine the changes of stress in the hanger itself as the cross sectional area was gradually reduced, calculated member forces and stresses of hanger U_1L_1A were summarized and are listed in Table 2-6. With more

reduction of area, all member forces decreased. The axial force and the bending moment in the plane of the truss (about weak axis of member) reduced slightly. The out-of-plane bending moment perpendicular to the truss changed significantly from 37.09 kN-m (328.2 k-in) to 18.43 kN-m (163.1 k-in), a 50 % reduction when the area was reduced 40 %. The combined effect of decreases in area and member forces was an increase in the maximum stress in the hanger. As shown in Table 2-6, the maximum stress in the hanger increased from 72.40 MPa (10.50 ksi) to 96.94 MPa (14.06 ksi).

The gradual increase of maximum stress in hanger is compared to the decrease in cross sectional area in Fig. 2-12. In this figure, the ratio of max. stress in damaged condition to the max. stress in undamaged (intact) condition for the lower end of the hanger is plotted against the percentage reduction in area. The change of stresses with respect to change of damaged cross section was small for small sizes of the crack. The rate of change increased gradually when the crack became larger. At 40 % reduction of area, the stress ratio was 1.34. At 50 % reduction of area, the ratio was 1.49 by Ward [74].

Based on the results of this and earlier studies [74, 80], it can be expected that as long as the damages in one or two truss members of a truss bridge are small, the structure would not undergo a change in its overall response to loads. The changes would be primarily increase of stresses in members adjacent to the damaged member. Even for the damaged member, the increase of maximum live load stress would be modest if the damaged area is less than twenty five to thirty per cent of the original area.

This phenomenon of only modest change in stress in a cracked truss member enables the adoption of the linear elastic fracture mechanics concept of fatigue crack growth to the evaluation of cracks in bridge truss members.

CHAPTER 3

EVALUATION OF STRESS INTENSITY FACTOR BY SINGULAR FINITE ELEMENT

The study of fatigue crack growth or propagation is, in modern days, usually by the linear elastic fracture mechanics approach. This approach is based on an analytical procedure which relates the stress-field magnitude and distribution in the vicinity of a crack tip to the nominal stress applied to the structural member and the geometry of the crack or crack-like discontinuity, and to the material properties.

The procedure provides a criterion for crack propagation by balancing the released energy of the structural member and the increase of surface energy resulting from presence of the crack. The state of a crack is expressed by the stress intensity factor which incorporates the crack condition and stress magnitude of the structural member. This factor is then compared with the "material properties" of the structural member to assess the growth of the crack [63, 83].

It was observed that the magnitude of stress levels in the structural member controlled the rate of crack

propagation and the fatigue crack most often propagated with increasing rate as the crack length increased. Consequently, the fatigue crack propagation behavior of structural members was correlated to the range of stress intensity factor [1, 63].

Theoretical, closed-form solutions of stress intensity factor are available for many ideal crack geometries and stress conditions [68]. There are, however, still substantial difficulties in evaluating the stress intensity factor for cracks in structural members with complicated geometry and stress conditions. In such situations, numerical analysis technique such as a finite element method may be used as described in this chapter.

3.1 Crack Tip Stress Field and $1/\sqrt{r}$ Singularity

In the immediate vicinity of a crack tip in a two-dimensional body, the stress and displacement fields are of the following form [59],

$$\begin{Bmatrix} \sigma_x \\ \sigma_y \\ \tau_{xy} \end{Bmatrix} = \frac{1}{\sqrt{2\pi r}} \begin{bmatrix} \cos\frac{\theta}{2}(1 - \sin\frac{\theta}{2}\sin\frac{3\theta}{2}) & -\sin\frac{\theta}{2}(2+\cos\frac{\theta}{2}\cos\frac{3\theta}{2}) \\ \cos\frac{\theta}{2}(1 + \sin\frac{\theta}{2}\sin\frac{3\theta}{2}) & \sin\frac{\theta}{2}\cos\frac{\theta}{2}\cos\frac{3\theta}{2} \\ \sin\frac{\theta}{2}\cos\frac{\theta}{2}\cos\frac{3\theta}{2} & \cos\frac{\theta}{2}(1-\sin\frac{\theta}{2}\sin\frac{3\theta}{2}) \end{bmatrix} \begin{Bmatrix} K_I \\ K_{II} \end{Bmatrix} + 0_{(r)}$$

(3.1)

$$\begin{Bmatrix} u \\ v \end{Bmatrix} = \frac{1+\nu}{4E}\sqrt{\frac{2r}{\pi}} \begin{bmatrix} (2k - 1)\cos\frac{\theta}{2} - \cos\frac{3\theta}{2}, & (2k + 3)\sin\frac{\theta}{2} + \sin\frac{3\theta}{2} \\ (2k + 1)\sin\frac{\theta}{2} - \sin\frac{3\theta}{2}, & -(2k - 3)\cos\frac{\theta}{2} + \cos\frac{3\theta}{2} \end{bmatrix} \begin{Bmatrix} K_I \\ K_{II} \end{Bmatrix} + 0_{(r)}$$

(3.2)

where u, v are the displacement components in the x, y directions at a point with polar coordinates, r and θ in the x-y plane as shown in Fig. 3-1. In Eq. (3.2), E is Young's modulus, ν is Poisson's ratio, $\kappa=3-4\nu$ for plane strain, $\kappa=\frac{3-\nu}{1+\nu}$ for plane stress, and K_I and K_{II} are the stress intensity factors which are functions of the structural member's geometry, crack length and the applied stress.

Equations (3.1) and (3.2) show that the distributions of the elastic-stress field and the deformation field in the vicinity of crack tip are invariant. The magnitude of the elastic stress field can be described by

single-term parameters, K_I and K_{II}, which correspond to Modes I and II respectively [63]. Consequently, the applied stress, the crack shape and size, and the structural member configuration affect the value of the stress intensity factor but do not alter the stress-field distribution. In a sense, K serves as a scale factor to define the magnitude of the crack tip stress and displacement fields.

Equation (3.1), which neglects higher order terms in "r", shows that the local stresses could rise to extremely high levels when r approaches very small values in comparison to other x-y planar dimensions. This situation is limited by the onset of plastic deformation (yielding) at the crack tip. While in fracture problems this plastification effect is often considered in stress intensity factor calculations based on plastic zone size, it is usually disregarded in evaluation of fatigue crack growth in structural members because the small stress ranges usually encountered [82].

The stress field adjacent to the crack tip, as defined by Eq. (3.1), is dominated by a inverse square-root singularity in "r" ($1/\sqrt{r}$) at the crack tip.

The displacement field adjacent to crack tip by Eq. (3.2) also varies with square-root of "r" ($\sqrt{r}$).

3.2 $1/\sqrt{r}$ Singular Elements

3.2.1 General Information

The application of finite element methods to the fracture mechanics problem has been quite extensive.

Around 1970, researchers attempted to use conventional finite elements such as the constant-strain triangle elements to calculate the stress intensity factor for complicated crack configulation. These approaches usually encountered difficulties because the results converged very slowly for elements in which the $1/\sqrt{r}$ singularity was not included.

Consequently, extremely refined finite element meshes were required to obtain a reasonable evaluation of the stress intensity factors. Frank's study [30] on fillet-welded connections showed the extremely refined meshes required for this approach.

Byskov [15] developed an cracked-element embodying the singularity and combined it with a standard finite

element expansion in a triangle, and integrate over its domain as shown in Fig.3-2.

Tong and Pian [71] adopted the hybrid-element concept and the complex variable technique for constructing a special super-element to be used jointly with conventional finite elements (Fig.3-2). This super-element provided very accurate results with a quite coarse element mesh near crack tip.

Benzley [11] represented the effects of the singularity near crack tip by introducing an enriched-element assuming bilinear element displacement with terms that give the proper singularity at the crack tip node (refer to Fig. 3-2).

$$u_i=\alpha_{i1}+\alpha_{i2}a+\alpha_{i3}b+\alpha_{i4}ab+K_I Q_{1i}(\rho,\theta)+K_{II}Q_{2i}(\rho,\theta)$$

Where α_{ij}= unknown coefficients, (3.3)

Q_{1i}= specific singular assumption.

This type of element is used in the finite element computer program CHILES by Benzley and Beisinger [12]. The computer program APES developed at Lehigh University by Taylor [70] included both a hybrid super-element and an enriched-element with cubic displacement functions for

a quadrilateral, 12 node, two-dimensional element.

Another type of element which is simple to apply is the quarter-point quadratic isoparametric element introduced by Henshell and Shaw [37], and almost simultaneously by Barsoum [7]. Their idea was to make use of the existance of singularity in the properties of a coordinate mapping introduced in isoparametric elements. An 8-noded isoparametric quadrilateral element was used for plane-strain and plane-stress crack problems and a 20-noded isoparametric brick element for three-dimensional problems. The required $1/\sqrt{r}$ singularity for elastic analysis was achieved by placing the mid-side nodes 5 and 8 at the quarter-point of sides 1-4 and 1-2 and near the crack tip at 1, as shown in Fig.3-3 (a).

Later, Barsoum found that the same singularity exists in a six-noded triangular element, degenerated from collapsing one side of an 8-noded quadrilateral element, and in a three-dimensional prism element, degenerated from collapsing one face of the 20-noded brick element (Fig.3-3). The degenerated elements lead to better results than the quadrilateral 8-noded(2-D) and

20-noded brick(3-D) elements for elastic fracture problems. This was explained mathematically by Hibbitt [39], that strain energy of the original quarter-point quadrilateral elements is unbounded, whereas the degenerated quarter-point elements in triangular form offer bounded strain energy. In other words, rectangular elements have $1/\sqrt{r}$ singularity only on the boundary but the triangular elements have the same singularity in the interior of the element as well as on the boundary.

In 1977, Barsoum showed that the triangular elements could have either $1/\sqrt{r}$ singularity or $1/r$ singularity depending upon whether the nodes on the crack tip are constrained to have the same displacements or left free (sliding node) to displace independent of each other. This $1/r$ singularity was used to study the blunting effect of the crack tip for the case of perfect plasticity [8].

This approach by isoparametric finite elements gave fairly good results with relatively coarse finite element meshes [7, 37].

3.2.2 Modification on Degenerated Triangular Element

The formulation of the isoparametric finite element is well documented [40, 83]. Appendix I provides the necessary calculations.

Irons [43] and Newton [56] showed that some of the shape functions for a quadratic isoparametric element require modification when the element is degenerated by coalescing the nodes of one edge. In Fig.3-4, the coalescing of nodes 1, 4, and 8 is achieved by giving the nodes 4 and 8 the same x, y co-ordinates of node 1, resulting in the collapsing of edge 1-8-4. Without modification on shape functions, each function presents a linear variation along any line radiating from the coalesced corner. This gives infinite curvature at the corner. The correct response of quadratic isoparametric triangle involves shape functions in which this variation should be parabolic along the line radiating from that corner, as shown in Fig. 3-5.

To correct this effect, Newton [56] presented the following modifications to form the shape functions (N^*'s) for triangular shape element.

$$N_1^* = N_1 + N_4 + N_8, \quad N_5^* = N_5, \quad N_7^* = N_7$$

$$N_2^* = N_2 + \delta N, \quad N_3^* = N_3 + \delta N, \quad N_6^* = N_6 - 2\delta N$$
$$\text{and } \delta N = \frac{1}{8}(1-\xi^2)(1-\eta^2) \tag{3.4}$$

After substituting the shape functions, (the N's of Eq. (I.3) in Appendix), the shape functions for triangular shape degenerated element became,

$$\begin{aligned}
N_1^* &= \frac{1}{2}\,\xi(\xi-1) \\
N_2^* &= \frac{1}{8}\,(1+\xi)(1-\eta)(\xi-\eta-\xi\eta-1) \\
N_3^* &= \frac{1}{8}\,(1+\xi)(1+\eta)(\xi+\eta+\xi\eta-1) \\
N_5^* &= \frac{1}{2}\,(1-\xi^2)(1-\eta) \\
N_6^* &= \frac{1}{4}\,(1-\eta^2)(1+\xi)^2 \\
N_7^* &= \frac{1}{2}\,(1-\xi^2)(1+\eta)
\end{aligned} \tag{3.5}$$

These modified shape functions also satisfied the necessary condition,

$$\Sigma\, N_i^* = 1 \tag{3.6}$$

to guarantee constant strain and rigid body motion conditions for convergence [83].

This modification is implemented in a computer program, QIFEVCEM which is discussed in Subsection 3.3.3, for the degenerated singular element as well as for regular elements of triangular shape.

3.2.3 Singularity in Degenerated Element

The singularity in the two-dimensional quarter-point isoparametric quadrilateral element was proved by Barsoum [7].

Singularity along the boundary of a quarter-point isoparametric degenerated triangular element can be investigated as following. As shown in Fig.3-4, the triangular element is degenerated from collapsing the side 1-8-4 of the quadrilateral element. The singularity is achieved by placing the mid-side nodes 5 and 7 at the quarter-points of the sides and near the crack tip. Along the side 1-5-2, after substituting (η=-1), the shape functions of Eq. (3.5) become,

$$N_1^* = \frac{1}{2}\,\xi\,(\xi-1)$$
$$N_2^* = \frac{1}{2}\,(1+\xi)\,\xi$$
$$N_5^* = 1-\xi^2 \qquad (3.7)$$

and,

$$N_3^* = N_6^* = N_7^* = 0$$

Since $x=N_1^*x_1+N_2^*x_2+N_5^*x_5$, by substituting $x_1=0$, $x_2=L$ and $x_5=\frac{1}{4}L$, then,

$$x = \frac{1}{2}\,(1+\xi)\,\xi\,L + \frac{1}{4}\,(1-\xi^2)\,L \qquad (3.8)$$
$$= \frac{1}{4}\,(1+\xi)^2\,L$$

Therefore,

$$\xi = [-1 + 2\sqrt{\frac{x}{L}}] \tag{3.9}$$

For the calculation of the Jacobian, the derivative of x with respect to ξ is,

$$\frac{\partial x}{\partial \xi} = \frac{1}{2}(1+\xi)\, L \tag{3.10}$$

By substituting Eq. (3.9) into Eq. (3.10), it is obtained:

$$\frac{\partial x}{\partial \xi} = \sqrt{L\, x} \tag{3.11}$$

Eq. (3.11) makes the inverse of the Jacobian singular at the crack tip (x=0, ξ=-1).

The displacements u and v along the side 1-5-2 are,

$$u = \frac{1}{2}\xi(\xi-1)u_1 + \frac{1}{2}\xi(\xi+1)u_2 + (1-\xi^2)u_5 \tag{3.12}$$

$$v = \frac{1}{2}\xi(\xi-1)v_1 + \frac{1}{2}\xi(\xi+1)v_2 + (1-\xi^2)v_5 \tag{3.13}$$

Differentiating u with respect to ξ results in:

$$\frac{\partial u}{\partial \xi} = \frac{1}{2}(2\xi-1)u_1 + \frac{1}{2}(2\xi+1)u_2 - 2\xi u_5 \tag{3.14}$$

Then, the strain in x-direction in terms of x is,

$$\epsilon_x = \frac{\partial u}{\partial x} = [J]^{-1}\frac{\partial u}{\partial \xi} = \frac{\partial \xi}{\partial x}\frac{\partial u}{\partial \xi} \tag{3.15}$$
$$= -\frac{1}{2}[\frac{3}{\sqrt{Lx}} - \frac{4}{L}]u_1 - \frac{1}{2}[\frac{1}{\sqrt{Lx}} - \frac{4}{L}]u_2 + [\frac{2}{\sqrt{Lx}} - \frac{4}{L}]u_5$$

It is apparent from Eq. (3.15) that strain in the

vicinity of crack tip has $1/\sqrt{r}$ singularity along the crack boundary.

The vertical displacement component, Eq. (3.13), can be written as the following, after employing Eq. (3.9),

$$v=v_1+ (-3v_1+4v_5-v_2)\sqrt{\frac{x}{L}} + (2v_1+2v_2-4v_5) \frac{x}{L} \qquad (3.16)$$

This equation will be used later to explain one of the methods for stress intensity factor calculation.

Next, the singularity inside the degenerated triangular element is to be examined. For simplicity, the singularity along the x-axis ($y=\eta=0$) is investigated. The equation x along the x-axis in terms of nodal point coordinates is,

$$x = N_1^*x_1+ N_2^*x_2+ N_3^*x_3+ N_5^*x_5+ N_6^*x_6+ N_7^*x_7 \qquad (3.17)$$

Substituting into Eq. (3.17) $x_1=0$, $x_5=x_7=\frac{1}{4}L$, $x_2=x_3=x_6=L$ and the value of N^*'s from Eq. (3.5) with $\eta=0$ then, expression for x in terms of ξ is obtained.

$$\begin{aligned} x &= \frac{1}{8}(1+\xi)(\xi-1)L + \frac{1}{8}(1-\xi^2)L + \frac{1}{4}(1+\xi^2)L + \frac{1}{8}(1-\xi^2)L \\ &= \frac{1}{4}(1+\xi)^2 L \end{aligned} \qquad (3.18)$$

This equation is identical to Eq. (3.8) for singularity along the element boundary and also makes the inverse of

the Jacobian singular at crack tip ($x=0, \xi=-1$).

Likewise, the displacement u along the x-axis ($\eta=0$) is,

$$u = \frac{1}{2}\xi(\xi-1)u_1 + \frac{1}{8}(\xi^2-1)u_2 + \frac{1}{8}(\xi^2-1)u_3 + \frac{1}{2}(1-\xi^2)u_5 + \frac{1}{4}(1+\xi)^2u_6 + \frac{1}{2}(1-\xi^2)u_7 \quad (3.19)$$

Differentiating u with respect to ξ, then, gives

$$\frac{\partial u}{\partial \xi} = \xi(u_1+\frac{1}{4}u_2+\frac{1}{4}u_3-u_5+\frac{1}{2}u_6-u_7) - \frac{1}{2}(u_1-u_6) \quad (3.20)$$

Therefore, the strain in the x-direction in terms of x, corresponding to Eq. (3.15), is,

$$\epsilon_x = \frac{1}{\sqrt{Lx}}\left(-\frac{3}{2}u_1 - \frac{1}{4}u_2 - \frac{1}{4}u_3 + u_5 + u_7\right) + \frac{2}{L}\left(u_1 + \frac{1}{4}u_2 + \frac{1}{4}u_3 - u_5 + \frac{1}{2}u_6 - u_7\right) \quad (3.21)$$

Eq. (3.15) and Eq. (3.21) show that the strain inside the element as well as along the element boundary has $1/\sqrt{r}$ singularity. The nodal variables u_i are determined during the finite element analysis by minimization of total potential energy of the structural member.

The 20-noded three dimensional isoparametric prism element with the quarter-point nodes in Fig.3-3 has the same $1/\sqrt{r}$ singularity on the face 1234 and 5678 as in a two dimensional singular element.

3.3 Calculation of Stress Intensity Factor

There are several ways to calculate stress intensity factors from the finite element analysis results.

The most convenient way is by substituting the computed values of stress or displacement for the known local crack tip stress or displacement equations [7, 17, 65]. Another way is by using the strain energy concept [36]. The stress intensity factor is computed from the relationship between the crack tip energy release rate and stress intensity factor. All the quantities necessary for this calculation are already computed during the finite element analysis.

In the approach by Benzley [11], the stress intensity factors are calculated in the simultaneous equation solution process of finite element methods because the interpolation functions u_i also include the unknowns K_I and K_{II} as shown in Eq. (3.3). But, as in the case of quarter-point isoparametric element which uses the same interpolation function as that of ordinary elements, the stress intensity factors must be derived from element stresses, displacements, or energy consideration after completing the finite element

analysis.

Although the local crack tip stress or displacement equations (Eq. (3.1) or Eq. (3.2)) are readily applicable, because of the intrinsic errors contained in a given finite element mesh, the calculation of K values from the individual nodal stress or displacement values can present erroneous results, particularily from stresses where errors are accumulated.

In this section, two very efficient methods developed in connection with quarter-point isoparametric element will be explained briefly.

3.3.1 By Equality

When Mode II effects are neglected from Eq. (3.2), the displacement v along the crack line 1-5-2 of Fig.3-6 is,

$$v = \frac{1+\nu}{4E}\sqrt{\frac{2r}{\pi}}\{(2\kappa+1)\sin\frac{\theta}{2} - \sin\frac{3\theta}{2}\} K_I + O(r) \qquad (3.22)$$

For line 1-5-2, $\theta=\pi$, then Eq. (3.22) becomes,

$$v = \frac{1+\nu}{4E}\sqrt{\frac{2r}{\pi}}(2\kappa+2) K_I + O(r) \ . \qquad (3.23)$$

If Eq. (3.23) is equated to Eq. (3.16), then,

$$K_I = \frac{E\sqrt{2\pi}}{(1+\nu)(\kappa+1)} \quad \frac{(-3v_1 - v_2 + 4v_5)}{\sqrt{L}}$$

or

$$= \frac{2G\sqrt{2\pi}}{(\kappa+1)} \quad \frac{(-3v_1 - v_2 + 4v_5)}{\sqrt{L}} \qquad (3.24)$$

where G is the shear modulus, L is the crack tip element size, E and κ are defined before in section (3.1). This method was used in references [7, 65].

3.3.2 By Virtual Crack Extension Method

In the energy method reviewed by Gallagher [31] and Rice and Tracey [62], the strain energy release rate per unit thickness due to a crack under constant load condition is,

$$\Gamma = - \frac{d\Pi}{da} \qquad (3.25)$$

where Γ is the energy release rate per unit thickness, $d\Pi$ is the changes in total potential energy of a body with unit thickness and da is the change of crack length.

From Griffith theory, for plane-strain condition,

$$\Gamma = \frac{1-\nu^2}{E} [K_I^2 + K_{II}^2] + \frac{1+\nu}{E} K_{III}^2 \qquad (3.26)$$

and for plane stress condition,

$$\Gamma = \frac{1}{E} [K_I^2 + K_{II}^2 + K_{III}^2] \qquad (3.27)$$

Among the several techniques to determine Γ, Hellen [36] introduced a very practical method known as virtual crack extension method. In considering the crack extension under constant loading, there are differences in the stiffness values of the elements near crack tip due to the change of geometry as shown in Fig.3-7.

The total potential energy can be expressed as the strain energy minus the work done by the forces,

$$\Pi = \frac{1}{2} \{u\}^T [K] \{u\} - \{u\}^T \{q\} \tag{3.28}$$

Considering a small virtual increase δa in crack length with no change in external load including thermal effects, the variation of Π with respect to constant load is,

$$\delta\Pi = \frac{1}{2} \{u\}^T [\delta K] \{u\} + \{\delta u\}^T [K] \{u\} - \{\delta u\}^T \{q\} - \{u\}^T \{\delta q\} \tag{3.29}$$

Since $[K] \{u\} = \{q\}$, this can be reduced to,

$$\delta\Pi = \frac{1}{2} \{u\}^T [\delta K] \{u\} - \{u\}^T \{\delta q\} \tag{3.30}$$

where $\{u\}$ is the vector of nodal displacements,
$\{q\}$ is the vector of corresponding nodal forces, and
$[K]$ is the structural stiffness matrix of a body with unit thickness.

In the subsequent analysis, since the crack tip

forces and thermal effects will not be assumed, the vector $\{\delta q\}$ will be null and can be dropped. Then,

$$\delta\Pi = \frac{1}{2} \{u\}^T [\delta K] \{u\} \tag{3.31}$$

Therefore,

$$\Gamma = - \frac{d\Pi}{da} = - \frac{1}{2} \{u\}^T \left[\frac{dK}{da} \right] \{u\} \tag{3.32}$$

The stiffness variation matrix $[\delta K]$ is null for all elements not containing the crack tip, since the only changes in geometry is at the crack tip and the adjoining mid-side nodes of degenerated isoparametric elements.

Because this method considers the difference of stiffness of a small number of elements between slightly different finite element meshes around the crack tip, the inherent geometric mesh errors are largely cancelled and the numerical errors are less accumulative than by the methods which involve displacements and stresses.

3.3.3 Finite Element Computer Program QIFEVCEM

The quarter-point quadratic isoparametric triangular element for the solution of linear elastic fracture mechanics problems is simple to use because quadratic isoparametric elements exist in almost all general

purpose finite element method computer programs. And it has been proved that these elements satisfy inter-element continuity as well as the constant strain and rigid body motion conditions. Also, as mentioned previously, the procedure gives sufficient accuracy with relatively coarse mesh.

For these reasons, the quarter-point quadratic isoparametric 2-D elements are used in a computer program, QIFEVCEM, to calculate the stress intensity factor at the crack tip in riveted members and joints of truss bridges. The name QIFEVCEM is an acronym for Quarter-point Isoparametric Finite Element and Virtual Crack Extension Method.

As mentioned before, the strains and stresses in the degenerated elements with quarter point nodes are singular at the degenerated corner. In other words, the inverse of the Jacobian matrix [J] does not exist at that corner. By using numerical integration of Gaussian Quadrature, this problem can be avoided. A 9 point Gaussian quadrature integration rule (3*3) was used for the singular element and 4 point integration rule (2*2) for the regular element.

In the computer program QIFEVCEM, during the finite element analysis of initial crack position, element stiffness matrices are stored on tapes for later use. For the solution of large simultaneous equations, $[K]\{u\} = \{q\}$, a blocking technique [76] is used. After computing the nodal displacements, $\{u\}$, of the structural system, a slightly different mesh pattern for virtual crack tip positions are generated and then, only the stiffness matrices of the elements around the virtual crack tip positions are calculated for the estimation of the energy release rate, Γ, values.

Since the virtual crack extension method does not require solving another set of simultaneous equation, the change of the stiffness matrix from initial crack position can be calculated repeatedly for any number of different lengths and directions of virtual crack extension with only small increase of computer time. By changing the virtual crack direction at the crack tip, the maximum value of $\frac{d\Pi}{da}$ can be determined for a constant virtual crack length da. The direction of the virtual crack corresponding to the maximum Γ will be the direction of crack propagation according to the maximum energy release rate criterion.

A flow diagram of computer program QIFEVCEM is shown in Fig. 3-8.

3.3.4 Comparison of Results

For the comparison of results from the computer program of this study with results from previous research [7, 65, 70], several well-known crack configurations were analyzed by using the computer program QIFEVCEM. These configurations include plates with center-through cracks and plates with double-edge cracks. Different patterns of modelling the crack tip with singular elements are shown in Fig.3-9 and in Fig.3-10. These models have very coarse finite element meshes in order to show the degree of accuracy of computer program QIFEVCEM. Since the models have symmetric configurations, the resuting energy differences have to be doubled before calculating the stress intensity factor K.

The results of finite element analyses of these example models are summarized in Table 3-1 and Table 3-2. Also included are the theoretical values available in reference [68]. The virtual crack length used in this comparison were between 1/100 to 1/10000 of crack tip element size. Small virtual crack lengths gave increasingly more refined results. The recommended

virtual crack length is in the order of 1/100 to 1/5000 of crack tip element size [36]. The results compared very well.

The stress intensity factors for center-through cracks of Fig. 3-9 with different virtual crack directions are plotted in Fig. 3-11 against the angle θ. The curve shows a sinusoidal variation of stress intensity factor K around the crack tip. The highest value occurs at $\theta=0^{o}$, indicating the crack would propagate perpendicular to the applied stress.

Since, in computer program QIFEVCEM, the singular finite elements which represent the $1/\sqrt{r}$ singularity in the vicinity of crack tip were used, very reasonable values of stress and strains were obtained with relatively coarse meshes. Also the accuracy in calculating the stress intensity factors at the crack tip was enhanced by using virtual crack extension method. The deviation from the handbook solution for stress intensity factor of example models in Fig.3-9 and Fig.3-10 was considered less than 1.5 %.

3.4 Estimation of Fatigue Life

Since the fatigue crack growth process takes place at the crack tip, it is reasonable to assume that the process must be a function of the crack tip stress field and consequently of the stress intensity factor [57].

Around 1960, Paris proposed the following relationship between the stress intensity factor range (ΔK) and the crack growth rate ($\frac{da}{dN}$) based on empirical data [57],

$$\frac{da}{dN} = C\ \Delta K^m \tag{3.33}$$

where a is the crack length, N is the number of stress cycle, and C and m are constants for the material.

Numerous studies on fatigue crack growth of different materials and different structural details have shown that Eq. (3.33) provides a reasonable estimate of fatigue crack growth response in the practical range of engineering application [38, 58, 63].

The range of stress intensity factor ΔK can, in general, be expressed as,

$$\Delta K = f(a)\ S_r \sqrt{\pi\ a} \tag{3.34}$$

where, S_r is the nominal stress range in the structural member and f(a) is the correctional function against

member geometry, crack shape and stress gradient. The quantity $S_r\sqrt{\pi a}$ is used as a reference value for the range of stress intensity factor of crack length a.

When Eq. (3.33) is rearranged after substitution of ΔK by the expression of Eq. (3.34), and is integrated between the limits of the initial crack length a_i and the final crack length a_f , the fatigue life N_g of a component can be defined as,

$$N_g = \frac{1}{C\ S_r^{\ m}} \int_{a_i}^{a_f} (f(a)\ \sqrt{\pi\ a}\ )^{-m}\ da \qquad (3.35)$$

This equation provides a necessary means to estimate the life of fatigue crack propagation of a structural component provided the values of S_r, a_i, a_f, C, m and the function f(a) are known. The existance in Eq. (3.35) of S_r, the stress range, means that only live load stresses need to be taken into account for fatigue crack growth analysis.

If it is assumed that the fatigue behavior of a component is largely, if not totally, a function of crack growth, and P is defined by,

$$P = \int_{a_i}^{a_f} [f(a)\ \sqrt{\pi\ a}\ ]^{-m} da \qquad (3.36)$$

then, the fatigue life of a structural component is

$$N_g = \frac{P}{C\ S_r^{\,m}} \tag{3.37}$$

This equation can be expressed in the familiar form of the log-log relationship between S_r and N_g normally observed for most structural details.

$$\log N_g = \log \frac{P}{C} - m \log S_r \tag{3.38}$$

Direct correlation of S_r-N_g results from Eq. (3.38) and from laboratory tests has been well established for some welded structural details and components [1, 26, 30].

In this study, the fatigue life of riveted truss members and joints (assuming no clamping forces) is investigated analytically using singular finite elements and the virtual crack extension method of this chapter.

CHAPTER 4

ESTIMATION OF STRESS INTENSITY FACTOR FOR RIVETED TRUSS MEMBERS AND JOINTS

4.1 General Assumptions

Although the finite element technique has been applied extensively to fatigue and fracture problems of rolled and welded structural members, the analytical estimation of the fatigue strength of riveted truss members and joints by finite element and fracture mechanics techniques has not yet been reported before this study. This is possibly due to the difficulties in assessing the clamping and frictional forces, the complicated load transfer between riveted components and the effects of the infinite variations of joint geometry and details.

This study attempted to examine the fatigue strength of three details:

1. riveted built-up truss members,
2. riveted truss joints with gusset plates, and
3. riveted connections with splice plates.

The general locations of these details are shown in Fig.4-1.

To achieve a practical estimate of the stress intensity factor for a riveted member or joint, several important assumptions were made. The first and most crucial was that clamping forces in the rivets were not dependable. Consequently no friction between the interfaces of the component plates was considered. This assumption may not be adequate for riveted truss bridge members and joints with "reliable" clamping forces in rivets, but it simplified drastically the complexity of a three-dimensional problem into a two-dimensional plane-stress problem. Without clamping force and friction, the riveted joints were assumed to be in bearing condition. The resulting estimated fatigue strength could be low but it would be a lower bound strength of riveted members and joints.

Second, all the initial flaws and cracks were assumed as through the thickness of the component plates. In practical conditions, the initiation of cracks most likely would start from the re-entrant corner at the rivet hole and the plate surface where cold-work damage by punching or drilling would be most severe. The initial crack could be a circular or an elliptical corner crack. Therefore, this assumption would also lead to

conservative estimates while facilitating the two-dimensional plane stress analysis.

Third, the possible crack path was assumed to be known, being a straight line starting at the side of a rivet hole and extending to the outside edge of the plate following a shortest path. Previous studies [16, 61] had the following observations.

1. If a rivet was not in bearing but the clamping force of rivets was low, the fatigue crack started at the side of the hole on the gage line and propagated following the gage line across the net section.
2. When the fastener was in bearing, the fatigue crack started at the point of maximum stress, which is above the center of the hole a distance of about 1/6 of the hole diameter. The crack then curved downward normal to the stress trajectory.
3. If the clamping force was high, as in the case of high-strength bolts, the fatigue crack started at the edge of a ply in the gross section. The crack propagated across the gross section and usually missed the holes.
4. In truss joints similar to the Detail 2 of Fig.4-1,

the failure cracks usually began at the edge of the rivet hole nearest the toe of a hanger angle or channel. The cracks usually progressed toward the edge and subsequently extended to the back of the angle or channel.

These general observations from previous studies indicated that the crack path is dependent upon clamping forces and bearing. Because of the extreme difficulties in determining and modelling the exact path of the cracks in the details, it is assumed to follow a straight line along the transverse diameter of the rivet hole, as suggested by the analytical results in Section 3.4, earlier.

With these assumptions, the calculation of stress intensity factor is a two-dimensional problem with a known crack path and the computer program QIFEVCEM could be used. The quadratic isoparametric finite element was best suited in this case of circular rivet hole since it does not require a very fine finite element mesh to model the circular boundary with curve-sided elements and it has the ability to represent the $1/\sqrt{r}$ singularity with simple modification of this element.

The SAP IV [9] computer program was used for global analysis of the structure. This computer program was intended for the analysis of linear elastic systems. Hence, the linear elastic behavior of the structural members and joints was an implicit assumption. Young's modulus was taken as 206850 MPa (30000 ksi) and Poisson's ratio was set at 0.3.

4.2 Riveted Built-up Truss Members--Detail 1

For riveted truss bridge members, built-up sections with flat plates and rolled sections are most common. Figure 4-2 depicts this type of built-up truss member.

The members were assumed to have symmetric configuration about the cross-sectional axes. The double symmetry was assumed to remain even when a fatigue crack developed at a rivet hole. This assumption imposed a hypothetical geometric condition to the finite element investigation but did not seriously affect the results of ΔK at the rivet hole.

The important characteristic or assumption of this detail was that, away from the truss joints with gusset plates or away from spliced connection, there was no

force transmittal between the component plates of the built-up member. The rivets in this member did not produce significant bearing forces onto the rivet holes of the component plate. The role of the rivets in this member was to maintain the cross-sectional shape of the member.

Consequently, any component plate of a built-up member was regarded as equivalent to the fundamental two-dimensional plate with rivet holes commonly assumed in studying such members. With the ΔK values readily computed by the SAP IV and QIFEVCEM computer program, the effects of geometric variations such as pitch and gage distances of the rivets on the fatigue strength of this detail can be examined.

4.2.1 Geometry and Modelling

A cover plate with a simple rivet pattern as shown in Fig. 4-2 was chosen for this part of study. Plates with a staggered rivet pattern or a multi-line rivet pattern were not included in the study but the procedure of their analysis would be the same.

The finite element model for the portion of plate at a rivet hole is shown in Fig. 4-3. The rivet hole used

here has 23.8 mm (15/16 in.) diameter for a ◆=22.2 mm (◆=7/8 in.) rivet.

To reduce the bandwidth of the stiffness matrix for the analysis, nodal point numbering was started from the inside edge of the rivet hole, increased along the half circle and then continued on the next larger semi-circle.

To avoid repeated renumbering of nodal points of the models for different crack lengths, extra nodal points were provided near the crack line. For the different crack tip location of each model, the boundary conditions and coordinates of some of these extra nodal points were modified for input.

A total of 336 nodal points and 118 quadratic isoparametric elements were used for the model of Fig. 4-3. Four quarter-point isoparametric singular elements were used at the crack tip of each model with a different crack length. The size of singular elements at the crack tip was varied from 2.08 mm to 5.08 mm (0.08 in. to 0.20 in.) and the virtual crack extension length for stress intensity factor calculation was equal to 1/10000 of crack tip element size.

To examine the effects of pitch distance on the stress intensity factor at the crack tip, pitch distances were varied as 101.6 mm, 152.4 mm, 203.2 mm and 304.8 mm (4.0 in., 6.0 in., 8.0 in. and 12.0 in. respectively) while the gage distance was kept as 152.4 mm (6.0 in.). The effects of gage distance were examined for 101.6 mm, 127.0 mm, 152.4 mm and 203.2 mm (4.0 in., 5.0 in., 6.0 in. and 8.0 in.) for a fixed pitch distance of 152.4 mm (6.0 in.). The basic model had both pitch and gage distance at 152.4 mm (6.0 in.). The change of gage distance and pitch distance was facilitated by adding or deleting outside rows and columns of elements to the basic rivet hole model of Fig. 4-3.

In the models, displacements perpendicular to the planes of symmetry at the nodes on basic model boundary were prevented except at the rivet hole and the cracked area. The cross section A-B-C between two rivet rows would have uniform elongation when the member was under uniform tension and linearly varied elongation when under bending moment.

Therefore, the loading condition for this model was simulated by prescribed equivalent displacements along

the edge A-B of Fig. 4-3.

Stress intensity factors were calculated for 9 different crack lengths for two different loading conditions, under tension and under bending moment, separately.

4.2.2 Results of Analysis

To examine the stress distribution around the rivet hole, the basic model without any crack was first analyzed using program QIFEVCEM. The pitch and gage distances of this model were 152.4 mm (6.0 in.). Figure 4-4 is a plot of the distribution or stress-concentration factors of the longitudinal stresses on the line E-F across the rivet hole and perpendicular to the member axis.

Figure 4-4 showes that, for this model, the stress concentrations on the two sides of the rivet hole are about the same when the plate is under tension force. Away from the hole, at the edge of the plate, the stress concentration factor is less than one.

When bending of the plate took place, the tension portion of the plate was analyzed adding to the stresses

from tensile forces. The outside edge A-F was subjected to higher tensile stress and consequently the stress was higher at this side of the rivet hole (point G) than at the opposite edge.

The stress intensity factors for a crack at or near point G were computed. Table 4-1 summarizes the stress intensity factor for the basic model for nine different crack lengths under uniform tension of 68.95 MPa (10.0 ksi). The notation PnGm in this table represents a model with pitch distance and gage distances of n and m inches, respectively.. Table 4-2 lists the values under bending moment which induced 68.95 MPa (10.0 ksi) tensile stress at the extreme fiber of the plate at position A of Fig. 4-2. Table 4-3 shows the non-dimensionalized stress intensity factor f(a) of the same crack lengths.

$$f(a) = \frac{K}{\sigma_{net}\sqrt{\pi\, a}} \tag{4.1}$$

in which K is the computed stress intensity factor and σ_{net} is the applied nominal net section stress.

The numerical values of the non-dimensionalized stress intensity factors may be expressed in terms of the crack lengths, a. An analytical solution for a plate with

a hole similar to the basic model of this study suggested the following form of equation [68],

$$K = [(1-\lambda)F_t(\frac{a}{R+a}) + \lambda F_b(\frac{a}{R+a})]\ \sigma_{net}\sqrt{\pi a} \qquad (4.2)$$

$$\text{or}\quad f(a) = (1-\lambda)F_t(\frac{a}{R+a}) + \lambda F_b(\frac{a}{R+a})$$

where, a = crack length,
R = rivet hole radius,
F_t= correction function for uniform tension,
F_b= correction function for bending moment,
and, $\lambda = \frac{\text{extreme fiber tensile stress due to bending}}{\text{maximum extreme fiber tensile stress}}$

Equation (4.2) implies that the stress intensity factor for combined axial force and bending moment is by the method of superposition [14]. The correction functions F_t and F_b are based on net-section stress (σ_{net}) and have the form of polynomial of $\frac{a}{R+a}$.

$$F_t=a_0+a_1(\frac{a}{R+a})+a_2(\frac{a}{R+a})^2+a_3(\frac{a}{R+a})^3+a_4(\frac{a}{R+a})^4 \qquad (4.3)$$

$$F_b=b_0+b_1(\frac{a}{R+a})+b_2(\frac{a}{R+a})^2+b_3(\frac{a}{R+a})^3+b_4(\frac{a}{R+a})^4 \qquad (4.4)$$

Fourth order polynomials of Eqs. (4.3) and (4.4) were used to fit the values of non-dimensionalized stress intensity factors of Table 4-3. The fourth order polynomial was found to provide a standard error of estimate less than 0.004 for all cases of pitch and gage distances, corresponding to an error of less than 0.5 %. The range of $\frac{a}{R+a}$ values was varied from 0.149 to 0.677 corresponding to a crack length from 2.08 mm (0.082 in.)

to 24.04 mm (0.946 in.). Table 4-4 gives the values of the coefficients a_i and b_i of the polynomial functions F_t and F_b of each model geometry.

The values of a_0 and b_0 of Table 4-4 have a significant meaning. These values are the stress concentration factors at the rivet hole for each case of plate geometry with different pitch and gage distances.

With the functions F_t and F_b known, the stress intensity factor can be evaluated over a wide range of geometrical conditions and crack lengths. Figure 4-5 shows the effects of pitch distances on the correction function F_t when the gage distance is kept at a constant value of 152.4 mm (6.0 in.) in the model of Fig. 4-3. Figure 4-6 is a similar plot showing the effects of gage distances.

It is clear from examining Fig.4-5 and Fig.4-6 that the magnitude of the correction functions (thus stress intensity factor) increase with increasing pitch and gage distances. In other words closer rivet pitch and gage distances produce a less severe stress intensity near the crack at a rivet hole.

Also Figs. 4-5 and 4-6 show that the effects of the pitch distance on the stress intensity factor is more pronounced than those of the gage distance.

For a given condition of pitch and gage distances, the correction fuctions F_t and F_b decrease with increase in crack length. However, the stress intensity factor K, as expressed by Eq. (4.2) or Tables 4-1 and 4-2, increases with increasing crack lengths. Its result is an increase of crack growth rate under live load on the truss bridge. This will be examined later in Chapter 5.

4.3 Riveted Truss Joints with Gusset Plates--Detail 2

In a steel truss bridge, the joint or panel point details usually have complicated geometrical configurations because different members coming from various directions meet together. Gusset plates normally are used, onto which are connected the flanges of the truss members. In order to examining the transfer of forces or stresses between members and gusset plates so as to estimate the stress intensity factors at rivet holes, drastic simplifications were necessary in modelling the gusset-plated details. The simplifications should not alter the overall behavior of the structural joints and

should provide satisfactory estimate of stress distributions. In this section, the simplifications, modelling technique and the final results of analysis of gusset-plated details are discussed.

The basic assumptions for Detail 1 were also adopted here for truss joints. The truss joints considered were also assumed to have symmetric configuration about the member axes. The crack locations in the gusset-plated joints of Detail 2, however, did not need to be symmetric since substructuring technique was used for the calculation of stress intensity factors of different crack lengths.

Again, the clamping forces in rivets were assumed not reliable and were ignored. The important characteristics of this detail was that there was force transmittal between the truss members and gusset plates through the rivets. The force transmittal produced bearing on the rivet hole edges resulting in a high stress concentration at rivet holes. The stress concentration at the end or last row of rivet holes was further raised by the unequal load distribution among rows of rivets.

Therefore, for this detail, the bearing ratio of the net cross-sectional area of the joining member divided by the rivet bearing area played an important role in force partition among fasteners and stress distribution around the rivet holes. The stress intensity factors of riveted truss joints of different geometry were calculated considering the bearing ratio as a parameter. Since it was difficult to keep the shear ratio as a constant without changing the overall geometry of the joint, the shear ratio was also varied with bearing ratio.

4.3.1 Geometry and Modelling

Figure 4-7 shows an example of the actual configuration of riveted truss joint details. It represents the hanger to bottom chord joints where fatigue cracks at rivet holes have been found.

The drastically simplified joint for this study is shown in Fig. 4-8. The simplification was based on the examination of stress distribution in gusset plates to be presented in Subsection 4.3.2.

Table 4-5 lists the geometrical dimensions of joints varied to achieve different values of bearing ratio. The notation Bxyz in this table represents a model with

bearing ratio x.yz and the following a or b is for a model with 101.6 mm (4.0 in.) or 152.4 mm (6.0 in.) pitch distance, respectively. Four different values of bearing ratio, 1.66, 2.09, 2.79 and 2.85, were considered, covering the range of the practical values of truss joint bearing ratio. Also, in order to examine the effects of pitch distance on the stress intensity factor of riveted truss joint, 101.6 mm (4.0 in.) and 152.4 mm (6.0 in.) pitch distances were included for a bearing ratio 2.79. These bearing ratios are average values for all rivets in a truss joint model. The model B285 has considerably small shear ratio compared to other details.

As shown in Fig. 4-8, the rivet pattern in the model detail had two lines of rivets in equal pitch distance. It had 4 rows of rivets for lower bearing ratios and 3 rows of rivets for the higher bearing ratio. By taking into consideration symmetry, the model was assumed to compose of a flat plate ($W_g x L_g$ in dimension) to simulate the gusset plate and a single T-section to simulate the two flange angles of the hangers. The width of gusset plates (W_g) of each model was chosen to be wider than the effective width proposed by Whitmore [75]. The T-section was equivalent to two angles of 102 x 76 x 12.7 mm

(4x3x1/2 in.) for the 1.66 bearing ratio and two angles of 127 x 89 x 12.7 mm (5x3-1/2x1/2 in.) for the other bearing ratios. The rivet holes had 23.8 mm (15/16 in.) diameter for ϕ=22.2 mm (ϕ=7/8 in.) rivets.

For the analysis of the global joint models, the SAP IV finite element computer program [9] was used. Figure 4-9 shows the finite element mesh for a joint model. A total of 790 nodal points and 744 plane stress elements were used for the gusset plate and T-section, and 8 beam elements simulated the rivets in this model. The far end of the gusset plate was assumed "fixed" and the flange-to-web junction line of the tee was restrained from displacement in the direction of the web.

Uniform tension forces and pure bending moments were applied separately at the end of the member to induce 68.95 MPa (10.0 ksi) tensile stress at the flange tip on gross section. The distance from the gusset-plated joint to the point of force input was over three times the flange width and well beyond the limit of the stress singularity region.

The displacements and rivet shear forces from the global analysis were to be used as input for the models

of substructure representing the vicinity of the most severely stressed rivet hole area. Displacement input to the substructure model was taken directly or interpolated from the global analysis output.

4.3.2 Stress Distribution in Gusset Plates

To examine the adequacy of the model in Figs. 4-8 and 4-9, a gusset plate of Irvan's test [44] was analyzed in this study using the SAP IV computer program. The same modelling technique described earlier in the previous section was used.

Figure 4-10 shows the joint tested by Irvan in 1957. The "contour" plot of maximum tensile stress obtained from the test is shown on Fig. 4-11. These two figures are taken directly from reference [44].

The finite element mesh of the simplified model of Irvan's test joint is shown in Fig. 4-12. Plane stress elements were used for the gusset plate and the joining members. Two different levels of planes were connected by beam elements representing the rivets. A Total of 716 nodal points, 527 plane stress elements and 50 beam elements were used.

The maximum tensile stresses from the finite element analysis were used to construct equal stress "contour lines" which are plotted in Fig. 4-13 to compare with those of Fig. 4-11. The results were not exactly the same but a notable resemblance exists between the two contour patterns except for the location of the maximum stresses. The magnitude of the stresses were in the same order. A more thorough comparison was not made without more information on the test conditions. Overall, the comparison showed that the model of two plates connected by beam elements simulating rivets could be used to model the truss joint for global analysis. The simplified model of Figs. 4-8 and 4-9 thus was chosen to represent typical portion of riveted truss joints with gusset plates.

4.3.3 Shear Force Distribution among the Rivets

The finite element model of Fig. 4-9 provided the shear forces in the participating rivets. The beam elements used in this model to simulate rivets had a length equal to half of the total thickness of the two interfacing plates. The nodes connected by the beam elements were allowed to move in two perpendicular directions in the planes of the plates. All the other

degrees of freedom such as rotation about any axis and displacement perpendicular to the plates were restrained. Consequently, the result of analysis included the shear forces in the planes of the plates and bending moments of the rivets. The stiffness of the beam elements (rivets) had very little effect on shear force distribution among the rivets. This was examined by changing the stiffness of the beam element from the value of an actual size rivet to 10^5 times of this value.

The magnitudes of calculated shear forces in a line of rivets are shown in Fig. 4-14. The shear forces in the direction of the truss member are plotted as hollow bars. Also shown are shear forces in the perpendicular direction which were induced by the Poisson's effect.

The overall shape of shear force distribution pattern in Fig. 4-14 was similar to that of bearing joints after major slip [26]. The end rivets undertook greater loads than did the rivets near the midlengths of the joint. The bearing condition at the end rivets changed to the higher bearing ratio 2.31, 2.93, 3.32 and 3.43 from the average values of 1.66, 2.09, 2.79 and 2.85 respectively. Such agreement further confirmed the

adequacy of the simple model.

The computed shear forces in the two perpendicular directions were to be applied as bearing pressure at the rivet holes in the substructure model. The moments at the ends of the beam elements (rivets) were ignored so as to keep the substructure model a two-dimensional one.

4.3.4 Substructure Modelling

Close examination of the stress distribution in the component plates of the riveted joint showed that the vicinity of the first row of rivets was the most highly stressed region in the truss member. In the gusset plates, the highest stressed region was at the last row of rivets. This was in agreement with the shear force distribution among the rivets.

Therefore, these critical regions of joint component plates were selected for substructure modelling to study the stress intensity factor and crack propagation behavior. To reduce the amount of interpolation on the boundary condition, 16 elements (4x4) around a first row rivet in the flange of the truss member and a last row rivet of gusset plate were chosen for the substructure with rivet hole. These regions are shown in Fig. 4-9 as

a shaded area.

Figure 4-15 shows the finite element discretization of the substructure model to be analyzed by computer program QIFEVCEM. The crack at the rivet hole was modeled by two lines of nodal points immediately adjacent to each other but not connected. Sixteen elements with parabolically curved sides were used to model the circular edge of a rivet hole very accurately.

A total of 582 nodal points and 208 quadratic isoparametric elements were used in modelling the substructure. Eight quarter-point isoparametric singular elements were used at the crack tip of each model with a different crack length. The size of the singular elements and the virtual crack extension length for stress intensity factor calculations were about the same as used in the analysis of riveted built-up members (Detail 1).

To reduce the bandwidth, nodal point numbering was started from the node at the crack on the edge of the rivet hole and increased along the circle to the other side of the crack, then continued to the next larger circles. A numbering scheme similar to that of Detail 1

was adapted to avoid repeated renumbering of nodal points of the models for different crack length.

The boundary conditions of the substructure model were determined from the global analysis model. The displacements of the corresponding nodal points of the global analysis model and the substructure model were transfered directly as boundary conditions. For the substructure nodes in between the global model nodes, the displacements were interpolated. Since the length of an element along the boundary of the substructure model was equal to the length of the corresponding element in the global model, only the displacements of the mid-edge nodes of the isoparametric elements needed to be interpolated.

This condition of prescribed boundary displacements was the same for the substructure model of the truss member and that of the gusset plate. The only difference is that the truss member substructure model had three edges with prescribed boundary displacements and one free edge, whereas that of the gusset plate had four edges with prescribed boundary displacements.

The rivet shear forces from the global model

analysis were applied as bearing pressure on the edge of the rivet hole of the substructure model. The rivet shear forces in the directions along and perpendicular to the truss member were transformed respectively to sine fuction normal pressure distributed around 180 degrees of the rivet hole boundary as shown in Fig. 4-15.

By using the computer program QIFEVCEM, stress intensity factors were calculated for the member flange models and the gusset plate models for different crack lengths and bearing ratios under tension and under bending moment, separately. The results are presented in the next section.

4.3.5 Results of Analysis

Because of the assumption of bearing pressure at the rivet hole of joints with gusset plates, stress concentration higher than that in built-up members was expected. To examine this condition, a substructure model of a rivet hole without a crack was analyzed. The model was for a member at a joint with bearing ratio of 1.66 and a pitch distance of 81 mm (3.2 in.). Figure 4-16 is the plot of distribution of longitudinal stresses across the line through the rivet hole.

By comparing the values in Figs. 4-4 and 4-16, it is obvious the latter has much higher stress concentration at the rivet hole. This implies that fatigue cracking is more likely at truss joints than at truss members which do not have bearing pressure at rivet holes.

The values of stress intensity factors for different length of cracks in truss joints under uniform tension and bending moment are summarized in Table 4-6 and Table 4-7. The stress intensity factors are for joints with nine different crack lengths, with four different bearing ratios, and under a uniform tension of 68.95 MPa (10.0 ksi) or under a bending moment which induces 68.95 Mpa (10.0 ksi) tensile stress at the extreme fiber of joining member flanges. The corresponding non-dimensionalized stress intensity factors computed by using Eq. (4.1) are listed in Table 4-8.

To obtain the values in Table 4-8, the net-section stresses for a member at a joint were readily calculated. For gusset plates, the net section stresses could not be determined because of the uncertainty as to how much of the gusset plate cross-section contributed to the stress distribution. The infinite variation of gusset plate

shapes and the contribution of the other members at the joint do not allow accurate determination of the effective cross-section.

However, for most truss joints, the gusset plates are thicker and wider than the member flange plates, and the stresses are found (in section 4.3.4) to be higher in the flange plates. Consequently the cracks in gusset plates are less critical than the cracks in flange plates of members at the joint. Therefore, correlation of fatigue crack growth with stress intensity factor of the cracks was made only for the flange plates of the members at the truss joints, not for gusset plates.

For the correlation of the stress intensity factor with fatigue life of truss members at joints, an equation with the same form of Eq. (4.2) was used.

$$K = [(1-\lambda)G_t(\frac{a}{R+a}) + \lambda G_b(\frac{a}{R+a})]\ \sigma_{net}\sqrt{\pi\, a} \qquad (4.5)$$

where, G_t= correction function for uniform tension,
G_b= correction function for bending moment,
and, the other variables are the same as for Eq.(4.2).

The correction fuctions G_t and G_b include the effect of bearing pressure at rivet hole. As it is for F_t and F_b in Eqs. (4.3) and (4.4), G_t and G_b are functions of

crack length and rivet hole radius.

$$G_t = c_0 + c_1\left(\frac{a}{R+a}\right) + c_2\left(\frac{a}{R+a}\right)^2 + c_3\left(\frac{a}{R+a}\right)^3 + c_4\left(\frac{a}{R+a}\right)^4 \qquad (4.6)$$

$$G_b = d_0 + d_1\left(\frac{a}{R+a}\right) + d_2\left(\frac{a}{R+a}\right)^2 + d_3\left(\frac{a}{R+a}\right)^3 + d_4\left(\frac{a}{R+a}\right)^4 \qquad (4.7)$$

Again, a fourth order polynomial was found to fit adequately the non-dimensionalized stress intensity factor of Table 4-8 as a function of $\frac{a}{R+a}$. The coefficients for the two correction functions of joints with different bearing ratios are summarized in Table 4-9.

The coefficients c_0 in Table 4-9 increase with the increasing bearing ratio of the joint. The coefficients c_0 of Table 4-9 are much higher than the corresponding coefficients a_0 in Table 4-4 for built-up members. This indicates the effects of bearing pressure on stress concentration at the rivet hole. The stress concentration in this detail is almost doubled compared to that in built-up members which do not have bearing pressure at rivet hole. A factor of two was previously observed in the experimental studies on riveted connections by Carter, Lenzen and Wyly [16] as well as by Parola, Chesson and Munse [60]. This high stress concentration at the rivet holes of the joints was caused by the presence of rivet holes in the plate, bearing

forces around the rivet holes and high partition of load at the rivets of the end row. The small differences in results of Table 4-9 for wide variations in geometry and loading conditions of the joint show that the bearing ratio of the joint is the controlling parameter compared to the other parameters.

Figure 4-17 shows the variation of function G_t for four different bearing ratios. This figure indicates that joints with high bearing ratio are subjected to higher stress concentration at rivet holes and always have higher stress intensity factors than joints with lower bearing ratios for any crack length, no matter what shear ratio the joints have.

This observation is in good agreement with the experimental results which indicated that there was an increase in fatigue strength with a decrease in bearing ratio [60].

The results in Table 4-9 show that the correction function G_b for bending moment is not as strongly affected by bearing ratios as was G_t for tension. This is due to the fact that the variation of shear force partition among the rivtets when the joint is under

bending moment does not differ much for different bearing ratios as indicated in Fig. 4-14.

The effects of pitch distance on correction function G_t are also indicated in Fig. 4-17. For pitch distances of 101.6 mm (4.0 in.) and 152.4 mm (6.0 in.) with the same bearing ratio, 2.79, the joint with the longer pitch distance has slightly a lower correction function G_t. This trend appears to be opposite to that for riveted built-up members as shown in Fig. 4-5. The dominant factor, however, is the bearing ratio.

4.4 Riveted Connections with Splice Plates--Detail 3

Quite often truss members have splices between panel points. This type of joint is used to accomodate changes in cross sections and to facilitate fabrication and erection of the bridge. Figure 4-18 shows an example of this connection with splice plates.

In this detail, the width of the flange splice plates are usully the same or narrower than the width of the truss member flange while the gusset plates in truss joints are always wider. Also, in this detail, the web of the truss members are usually connected with splice

plates too. The differences in this detail from the gusset-plated joints result in lower bearing ratios for this detail than for the joint with gusset plates. Furthermore, when all components of a member are spliced, the effects of shear lag are less than for gusset plates. All these conditions reduce the magnitude of stress concentration at the rivet holes.

Therefore, the overall behavior of member connections with splice plates is more favorable than that of a truss joint with gusset plates. However, because forces are transmitted through the splice plate, the connection is not expected to have the same strength as riveted built-up members without splice plates.

The analytical procedure for a riveted truss joint with gusset plates can be applied directly to this detail without much modification. The differences in size between the gusset and splice plates would not significantly affect the results.

Consequently, appropriate results of stress intensity factor from Eq. (4.5) could be applied conservatively to spliced joints.

4.5 Discussion

In this chapter, the stress intensity factors of cracks at rivet holes were calculated for two different riveted truss details with relative ease by using quadratic isoparametric plane stress elements and the virtual crack extension method of computer program QIFEVCEM.

The effects of pitch and gage distances in riveted built-up member on the stress concentration at rivet holes with no crack, and on stress intensity factors of cracks at rivet holes, were explored by assuming no clamping forces in the rivets.

Examination of the results on the riveted built-up member showed that the larger the gage and pitch distances of rivet hole, the higher the stress concentration and stress intensity factors. The effects of pitch distance was more pronounced than those of gage distance.

The stress intensity factors or correction function, G_t, of the cracks in riveted truss joints were always higher than those (F_t) in riveted built-up truss members. The results of analysis showed that the stress

concentration at rivet holes is almost doubled in riveted joints than in riveted built up members because of bearing forces at rivet holes and unequal load distribution among rivets. This implies that rivet holes in the truss joint region are more susceptible to development and faster propagation of fatigue cracks than the rivet holes in a built-up member away from joints and connections.

When the portion of maximum tensile stress due to bending increases, that is, the ratio λ increases, the magnitude of stress intensity factor correction function f(a) of Eq. (3.34) actually decreases because the effects of correction fuctions F_t and G_t to f(a) are considerably larger than those of F_b and G_b as shown in Tables 4-4 and 4-9.

In next chapter, the result of stress intensity factor estimation will be utilized for evaluation of fatigue strength of riveted truss members and joints.

CHAPTER 5

FATIGUE LIFE OF RIVETED TRUSS MEMBERS AND JOINTS

The total fatigue life (N_T) of a structural detail is the sum of the number of cycles required for crack initiation (N_i) and the number of cycles required for crack propagation (N_g) to the final crack size at the failure of the structural component.

$$N_T = N_i + N_g \tag{5.1}$$

In riveted truss members and joints, the crack initiation stage would take much longer time than in the welded details as clamping forces exert out-of-plane compressive stresses around rivet holes and alter the condition of stress concentration. After initiation of fatigue cracks from the initial flaws, which could have resulted from punching or drilling of the rivet holes, the propagation stage would begin. The crack initiation life of riveted truss members and joints is crudely estimated in this chapter using empirical formulas for blunt-tipped flaws.

The fatigue crack propagation life of riveted truss details is estimated by using the linear elastic fracture mechanics approach and utilizing fatigue crack growth

test data from other studies. The effects of pitch and gage distances of riveted built-up truss members and the effects of bearing ratio of riveted truss joints on the fatigue crack propagation life are examined using the stress intensity factor functions evaluated in the previous chapter.

Finally, the results of analytical procedure are compared with some existing experimental data of various references to gain insight on the fatigue strength of riveted members and joints.

5.1 Fatigue Crack Growth Characteristics and Crack Sizes

To estimate the fatigue crack propagation life of a specific riveted truss detail, evaluation of Eq. (3.35) is required for that detail. The evaluation depends on having knowledge of the crack growth characteristics of the material and detail, an expression for ΔK, and information on initial and final crack sizes.

The crack growth characteristics of materials are usually determined empirically through testing of precracked "fracture mechanics" specimens for which an

analytical expression for the stress intensity factor (K) is known. From measurements of crack sizes, the increases in size corresponding to increments of loading cycles are related to the stress intensity factor range ΔK in the form of Eq. (3.33).

The crack propagation characteristics of structural details differ from those of plain materials in that geometrical conditions, welding effects, and other factors influence the crack growth behavior. Many investigators have reported results of fatigue crack growth characteristics for structural steels and details [27, 30, 41, 57, 63]. From the test results of plain welded details, Hirt and Fisher [41] found the exponent, m, of Eq. (3.33) to be about 3.0 and the mean value of the constant, C, to be 3.925×10^{-12} $m^{11/2}/MN^3$cycle (2.05×10^{-10} $in^{11/2}/kip^3$ cycle). For a conservative upper bound value of C for structural details made of ferrite-pearlite steel, 6.893×10^{-12} $m^{11/2}/MN^3$ cycle (3.60×10^{-10} $in^{11/2}/kip^3$ cycle) was proposed by Barsom [63]. By assuming that the crack growth stage of plain welded structural details and of riveted structural details are comparable, characteristic values of m = 3.0 and C = 3.829×10^{-12} $m^{11/2}/MN^3$ cycle

$C\left(m^{11/2}/MN^3 \text{ cycle}\right) = .0139\,14634\; C\left(in^{11/2}/Kip^3 \text{ cycle}\right)$

(2.0×10^{-10} $in^{11/2}/kip^3$ cycle) were chosen for this study. This assumption appeared rational since currently fatigue strength category C and D of welded structural details [1, 2] are being utilized for riveted structural members and joints. More important is the fact that the structural steels are not greatly different in fatigue crack growth characteristics. It was assumed that the characteristic values of m and C remained constants for all values of ΔK.

With the chosen values of m and C, Eq. (3.33) on crack growth rate became,

$$\frac{da}{dN} = 3.829 \times 10^{-12} \Delta K^3 \qquad (5.2)$$

where a = crack length (m),

$\frac{da}{dN}$ = crack growth rate (m/cycle)

and ΔK= stress intensity factor range ($MPa\sqrt{m}$).

Little information is available on the initial crack sizes at the edges of rivet holes in truss members and joints. Small initial cracks under rivet heads can not yet be detected without removing of the rivet. However, it is generally known that the initial flaw sizes at rivet holes are related to the methods of forming the rivet holes. Each of the methods produces different microscopic geometrical and metallurgical structural

conditions for the initiation of fatigue cracks and different initial crack sizes, a_i.

An inspection by Fisher on the truss members of the Assiniboine River Bridge, Nattress, Manitoba, Canada resulted in estimated depth and length of elliptical edge cracks at four rivet holes to be 0.254 to 0.508 mm (0.01 to 0.02 in.) and 3.18 to 6.35 mm (1/8 to 1/4 in.), respectively [67]. The bridge was constructed in 1906 and in service for nearly 70 years.

For this study, an initial through-thickness crack of 0.0254 to 0.508 mm (0.001 to 0.02 in.) were assumed.

The final crack size was assumed as the length when the crack reached the outside edge of the component plate, point F of Figs. 4-3 and 4-15. This final crack length is approximately equivalent to a thirty eight percent reduction of the cross-sectional area of the structural details under consideration. Experimental observations of beams have demonstrated that crack instability is not likely in the multi-component member. Examination on the effects of reduction of cross-sectional area on the stress redistribution of a truss member was discussed in Chapter 2. It was shown in Fig.

2-12 that an area reduction of 30% or 35% and corresponding reduction of moment of inertia of an entire truss member would not increase significantly the stress in the member. This condition permitted the calculation of fatigue crack growth life using a constant magnitude of stress range, S_r in Eq. (3.38).

5.2 Crack Growth Life Computations

To evaluate the fatigue crack propagation life for the details in this study, the value of P as defined in Eq. (3.36) must be calculated. For m = 3.0,

$$P = \int_{a_i}^{a_f} [\, f(a) \sqrt{\pi a} \,]^{-3} \, da \qquad (5.3)$$

where $f(a)=(1-\lambda)F_t(\frac{a}{R+a}) + \lambda F_b(\frac{a}{R+a})$
for riveted built-up members

or $f(a)=(1-\lambda)G_t(\frac{a}{R+a}) + \lambda G_b(\frac{a}{R+a})$
for riveted truss joints.

The magnitudes of P were numerically estimated for different values of initial crack size a_i varing from 0.0254 mm (0.001 in.) to 0.762 mm (0.03 in.). Integration of Eq. (5.3) was performed by a computer program which could handle from three to a maximum of sixteen integration point Gaussian Quadrature for each

division. The number of divisions depended on the required accuracy. A maximum of twelve divisions dividing the crack length between a_i and a_f was used according to the assumed initial crack size.

The required accuracy was arbitrarily set by,

$$\frac{P_i - P_{i-1}}{P_{i-1}} \leq 10^{-5} \tag{5.4}$$

where P_i is the P value calculated by i integration point Gaussian Quadrature. The singularity in the integrand when a_i approaches zero is accounted for by dividing the crack length between a_i and a_f with increments $2a_i$, $8a_i$,---,$2N^2a_i$ (N=1,2,---,12) sequentially for each division length.

For most of the cases, seven integration point Gaussian Quadrature was accurate enough to satisfy the accuracy requirement for small initial crack size. The larger the assumed a_i, the smaller mumber of integration point in Gaussian Quadrature was required. Figures 5-1 and 5-2 show the variation of P with a_i for different rivet hole arrangement of each riveted structural detail. The final crack size, a_f, had a fixed value of 38.9 mm (1.53 in.) for all details except for the truss joint

B166. For detail B166, the final crack size was 28.7 mm (1.13 in.).

From Figs. 5-1 and 5-2 it can be stated that for initial crack size larger than 0.0508 mm (0.002 in.), the changes of P were minimal. This condition implied that the first term of Eq. (3.38) is a constant, and log N_g is linearly proportional to log S_r. In other words, fatigue crack propagation life is governed by the applied stress range alone, a phenomenon well observed for welded structural details. For very small initial crack sizes, the values of P were found to be higher, resulting in higher values of N_g in Eq. (3.38) and longer fatigue life. The initiation of cracks will be discussed later.

The logarithmic forms of S_r-N curve of Eq.(3.38) used for riveted joints in the specifications of several countries are shown in Table 5-1 [50]. In Table 5-1, the values of Q, where Q = log (P/C) of Eq. (3.38), varies from 11.40 to 12.74 for m = 3 and for fatigue life less than 2.5×10^6 cycles. From these values the magnitudes of P can be calculated if C is known. If $C=3.829 \times 10^{-12}$ (2.0×10^{-10}), then the magnitudes of P are between 0.957 $m^{-1/2}$ and 21.0 $m^{-1/2}$. These magnitudes

cover the values calculated for different rivet hole arrangement of each riveted structural detail in Figs. 5-1 and 5-2.

5.2.1 Riveted Built-up Member -- Details without Bearing

The integration of Eq. (5.3) for P was performed for seven different geometrical conditions of riveted built-up truss members. From the values of P, the logarithmic relationship of Eq.(3.38) can be estimated. When Q = log (P/C) and m = 3 in Eq.(3.38), it becomes,

$$\log N_g = Q - 3 \log S_{r\ (net)} \tag{5.5}$$

The stress range $S_{r\ (net)}$ is based on net-section stresses of built-up member. Table 5-2 summarizes the calculated values of P and Q of Eqs.(5.3) and (5.5) for three values of initial crack sizes and for three cases of bending moment plus tension. The effect of bending moments were calculated for a_i=0.508 mm (0.02 in.) only.

From the value in Table 5-2, $S_{r\ (net)}$- N_g relations for crack propagation life can be constructed. Figure 5-3 shows three lines of Eq.(5.5) for built-up member of 152.4 mm (6.0 in.) pitch and gage distance with different initial crack sizes. It confirms that for any applied stress range, smaller initial crack size requires more

stress cycles to fail a riveted truss member.

To examine the effects of pitch and gage distances on fatigue crack growth life of built-up members, stress-life relationship for members with different pitch distances and the same gage distance of 125.4 mm (6.0 in.) are plotted in Fig. 5-4. Figure 5-5 is for members with different gage distances but the same pitch distance. It is interesting to conclude from Figs. 5-4 and 5-5 that built-up members with smaller pitch and gage distance have longer cycle life than those with rivet holes placed further apart. Also the effects of pitch distance on fatigue crack growth life is more pronounced than the effects of gage distance.

5.2.2 Riveted Truss Joint -- Details with Bearing

Table 5-3 lists the calculated values of P of Eq. (5.3) and Q of Eq. (5.5) for five truss joints with different bearing ratio. For each bearing ratio, calculation was made for three different initial crack sizes. Also the values for three cases with bending moment plus tension were calculated for a_i=0.508 mm (0.02 in.).

The P values in Table 5-3 are generally much smaller

than those in Table 5-2. This signifies the severity of stress concentration in bearing joints in comparison to built-up members without bearing. The bearing forces at rivet holes elevate stress concentration around rivet holes (see Subsection 4.3.5) and subsequently reduce the magnitude of P.

The effects of initial crack size on bearing joints can be detected from Fig. 5-3. The stress range S_r is again based on net section stresses. For riveted joint with the same bearing ratio and pitch distance, small initial crack size can sustain longer crack growth life, as it can for built-up truss members. The lower fatigue life of bearing joints is evident.

Figure 5-6 shows the effects of bearing ratio on the fatigue crack propagation life of truss joints. Four values of bearing ratio are compared, 1.66, 2.09, 2.79 and 2.85. The smaller the bearing ratio, the longer is the fatigue crack propagation life when the joints are under the same stress range. Among the four cases, the joint with the 2.85 bearing ratio (B285) has a cosiderably lower shear ratio but the trend of longer fatigue crack propagation life for lower bearing ratio is

not affected by this condition. Therefore, it can be concluded that the fatigue life of a riveted joint is a function of the bearing ratio when the clamping forces of the rivets and the friction between component plates are negligible. This analytical result is in good agreement with the experimental results of earlier studies [16, 60].

To examine the effects of pitch distance of riveted truss joints, Eq.(5.5) was plotted in Fig. 5-7 for two different pitch distances, 101.6 mm and 152.4 mm (4.0 in. and 6.0 in.) with the same bearing ratio of 2.79 (B279a and B279b). It is noted that the joint with longer pitch distance has longer fatigue life. This result for bearing joints is opposite to that for built-up members without bearing which is depicted in Fig. 5-4.

5.2.3 Effects of Bending Moment

Riveted members and joints in truss bridges are subjected to bending moments as well as to axial forces as indicated in Chapter 2. The effects of bending moment on stress intensity factor at crack tip of truss members and joints were expressed in Eqs.(4.2) and (4.5) as the parameter λ which is the ratio of extreme fiber tensile stress due to bending alone to the maximum extreme fiber

tensile stress.

To examine the effects of bending on fatigue life of riveted built-up truss members and joints, Eq.(5.5) was plotted in Fig. 5-8 for four values of λ for some selected geometrical conditions of each detail. The built-up member has a 152.4 mm (6.0 in.) pitch and gage distance (P6G6); the truss joint has a 2.79 bearing ratio and a 101.6 mm (4.0 in.) pitch distance (B279a).

Figure 5-8 shows that under the same maximum extreme fiber tensile stress, members and joints subjected to higher bending moment (higher λ) tend to have longer fatigue crack propagation life than those with lower or no moment. This is rational since the magnitude of stress at rivet holes, where fatigue cracks usually grow, is lower than at the extreme fiber when stresses are introduced by both bending moment and axial force. The higher the bending moment, the lower the stress at the rivet hole compared to the extreme fiber.

This tendency of longer life for higher bending moment resulted for both details, built-up members without bearing and truss joints with bearing. The important fact is that the analysis is based on the same

maximum tensile stress at the extreme fiber. In most cases of truss bridge analysis, the bending moments in members and joints are ignored. Thus, the extreme fiber tensile stress is often underestimated, resulting in overestimation of fatigue crack growth life. More attention and more study should be directed to the effects of bending moments.

5.2.4 Comparison with AASHTO Fatigue Strength Provisions

So far, in this chapter, the fatigue crack growth life of riveted members and joints was estimated using fatigue crack growth characteristics of welded structural details. The S_r- N_g relationship of some welded details have been adopted as fatigue strength provisions for designing bridges [1, 2, 27]. It is therefore of interest to compare the results of this study with the design provisions.

The strength curves for AASHTO and AREA fatigue strength categories B, C and D are plotted in Fig. 5-8 with the computed fatigue crack growth life of riveted built-up members and joints from this study. Category B is for plain welded members, C for welded stiffeners and short attachments, and D for intermediate length attachments. AASHTO and AREA use category D as a

lower bound for fatigue strength of riveted joint with lower clamping force and bearing ratios of about 1.5. Hence, the estimates from analytical procedure should not differ much. The geometrical conditions of the riveted members and joints for this comparison were arbitrarily chosen to be of shorter life among the geometrical conditions.

It is seen from Fig. 5-8 that riveted members without bearing have crack propagation life comparable to that of Category C. Riveted truss joints can be considered to be represented by Category D. This agrees very well with the current practice of assuming Category C and D for riveted members and joints.

To rephrase the results of the above comparison, it can be stated that, if clamping forces of rivets and frictional forces between component plates of riveted members and joints are ignored, the AASHTO and AREA fatigue strength provisions for welded structural details could be used for fatigue crack growth life of these members and joints. Category C strength would be for built-up members, and Category D for riveted truss joints. This usage would be conservative because the

beneficial effects of clamping forces, as well as the initiation stage of fatigue phenomenon, were ignored.

5.2.5 Comparison with Fatigue Crack Growth Data of Riveted Beam Specimen

To examine the accuracy of the analytical procedure for riveted members and joints, comparison of analytical and experimental results must be made. There are in existance at the time of this study very little fatigue crack growth data on riveted members and joints. Some full size riveted built-up floor beams of an old truss bridge are being tested in Fritz Engineering Laboratory, Lehigh University. One of these test beams developed a few fatigue cracks of which the increases of length were recorded. A comparison of the measured and computed crack growth life is presented below.

The full size built-up floor beam was taken from a truss bridge designed and constructed around 1903, in service for nearly 80 years as a railway bridge. The test beam had a 5.94 m (19.5 ft.) long I-shaped steel built-up section composed of a 975 x 12.7 mm ($38\frac{3}{8}$x$\frac{1}{2}$ in.) web plate and four 125 x 125 x 12.7 mm (6x6x$\frac{1}{2}$ in.) equal legged flange angles jointed with 22.2 mm (7/8 in.) diameter rivets in a staggered pattern. The pitch

distance of the staggered rivet is 152.4 mm (6.0 in.). This test beam was subjected to repeated loads at approximately the third points with the middle part of the test beam under uniform bending moment. Cracks propagated in this middle portion.

The component plates of the test beam in this region of uniform bending moment did not transfer load among themselves. Therefore, the portion of the member where the cracks occured represented a typical Detail 1 condition: a riveted built-up member without bearing.

After 18.3 million test load cycles, several cracks were found at the rivet holes of a bottom flange angle as shown in Fig. 5-9. The applied net-section stress range at the elevation of the rivet holes was estimated to be about 64.1 MPa (9.3 ksi). Stress estimation was based on measured strains at the extreme fiber. The stress ratio, (R), that is, the ratio of minimum to maximum stress, was about 0.1.

The crack growth was measured for several increments of load cycles until the cracks reached the outside edge of the flange angle. The measured crack length and the number of load cycles are summarized in Table 5-4. The

cracks when first detected were out from under the respective rivet head and were already fairly long cracks but were still very difficult to be detected.

Three cracks, 4ST, 8NT and 12ST were chosen for the comparison of analytical estimation and test results of fatigue crack propagation life. The rivet pitch distance of the floor beam was 152.4 mm (6.0 in.) so the specimen was comparable to built-up member detail P6G4. Figure 5-10 shows the test results and the analytical estimation of the crack propagation life in the form of cycle versus crack length lines. The estimated loading cycles for each increment of crack length are also summarized in Table 5-4.

Table 5-4 and Fig. 5-10 show that the measured crack growth was much slower than the computed value. During testing, it required 11.2 million load cycles for an increase of 52.1 mm (2.05 in.) in length for crack 4ST, and 8.4 million and 5.4 million cycles respectively for a 31.7 mm (1.25 in.) increase of cracks 8NT and 12ST. On the other hand, the analytical procedure predicts only 2.61 million loading cycles for the same crack length increase for the crack 4ST and 1.16 million cycles for

the cracks 8NT and 12ST.

The differences in this comparison were expected, although not as great as observed. The computed life was based on the condition of no clamping force and friction and the adoption of crack growth characteristics of welded details. A major effect appears to be the bond between component plates of floor beam from paint and corrosion products. This prevents crack opening. The rivets in the test beam were tight and produced clamping forces, although unknown in magnitude. Furthermore, the built-up component plates were in bonding condition due to long years of weathering, developing high frictional resistance at the interfaces of the component plates. These clamping forces in rivets and friction between interfacing plates possibly affected the crack growth very strongly.

5.3 Comparison with Results from Previous Fatigue Tests

A fairly large number of experimental studies on fatigue of riveted joints have been conducted. One series was done by Parola, Chesson and Munse [60] in 1965. They examined the effects of bearing pressure on fatigue strength of riveted joints through testing of 120

specimens of double lap joints having four 22.2 mm (7/8 in.) diameter rivets arranged in a square pattern. The values of bearing ratio varied from 1.37, 1.83, 2.36 to 2.74 which are comparable to those of the present study. The specimens were subjected to repeated loading of complete reversal, zero to tension, or half tension to maximum tension. The stress magnitude of their tests were converted into stress ranges and the test data were plotted as $S_{r\ (net)}$- N diagrams. Regression lines corresponding to Eq. (5.5) were established through least square fit. The slope, m, and the intercept, Q, of each regression line were calculated and are summarized in Tables 5-5, 5-6, 5-7 and 5-8.

For the purpose of comparison later, the test data and regression lines of Tables 5-5 to 5-8 are presented in groups. In Figs. 5-11, 5-12 and 5-13, the test data points of bearing ratios 2.74 and 2.36 of reference [60] and the corresponding least square fit lines are plotted on log-log scale for repeated loading of zero to tension, complete reversal and half tension to maximum tension, respectively. Figures 5-14, 5-15 and 5-16 are for the test data points of double lap joints with bearing ratios 2.36 and 1.83, and Figs. 5-17, 5-18 and 5-19 for joints

with bearing ratio 1.83 and 1.37.

The least square fit regression lines of the experimental results show that the values of the slope, m of Eq. (5.5), are different from 3.0, the value assumed earlier from welded structural members and AASHTO design provisions. Also, the corresponding values of Q for Eq. (5.5) differ appreciably from approximately 12.0 listed in Table 5-3. Without a comprehensive evaluation of the test variables and failure conditions, a significant set of values for m and Q can not be established.

Another set of fatigue tests on riveted double lap joint was conducted by Lenzen [48]. The joints had nine rivets arranged in a square pattern with a bearing ratio of 0.89. The results are summarized in Table 5-9 and plotted in Fig. 5-20. The slope m and intercept Q determined by least square fit are 5.45 and 18.69, respectively. Earlier fatigue test data of riveted double lap joint by Wilson and Thomas [78] are summarized in Table 5-10 and plotted in Fig. 5-21. Bearing ratio was between 0.84 to 1.50. The regression line slope is m=3.65 and the intercept Q=14.26.

Because the test data from earlier studies included

the effects of crack initiation as well as those of crack propagation but the analytical estimates are based on crack propagation alone, modification of estimates must be made.

5.4 Crack Initiation Life and Fatigue Strength

As it has been pointed out at the beginning of this chapter, the fatigue strength of riveted built-up members and joints most likely includes a crack initiation stage as well as a crack growth stage. With m=3.0 and C=3.829×10^{-12} (*) (2.0×10^{-10}) (**) values of Eq. (3.33), the crack growth life can be estimated by following the procedure of Section 5.2. The crack initiation life needs to be examined.

Although, a method is not available at the present for direct evaluation of fatigue crack initiation life of riveted members and joints, an indirect way of estimation can be made through application of mechanics.

The fatigue crack initiation data of A36 steels are shown in Fig. 5-22 [63], a log-log scale plot in terms of the number of cycles for fatigue crack initiation (N_i) and the ratio of range of stress intensity factor to the

* $m^{11/2}/MN^3 cycle$

** $in^{11/2}/Kip^3 cycle$

square root of blunt notch-tip radius $\frac{\Delta K_I}{\sqrt{\rho}}$. The least square fit of these data provides an equation,

$$N_i = 5.37 \times 10^{22} \left(\frac{\Delta K_I}{\sqrt{\rho}}\right)^{-6.27} \qquad (5.6)$$

for $\frac{\Delta K_I}{\sqrt{\rho}} > 448$ MPa (65 ksi).

The elastic stress σ_{yy} in the vicinity of narrow elliptical notches in a structural component under tensile stress is represented by the following equation:

$$\sigma_{yy} = \frac{K_I}{\sqrt{2\pi r}} \cos\frac{\theta}{2}\left(1+\sin\frac{\theta}{2}\sin\frac{3\theta}{2}\right) + \frac{K_I}{\sqrt{2\pi r}}\frac{\rho}{2r}\cos\frac{3\theta}{2} \qquad (5.7)$$

where the coordinates r and θ are the same as defined in Fig. 3-1. The center of the narrow elliptical notch is located at $\rho/2$ behind the crack front [63]. The material element at the notch tip ($r=\rho/2$, $\theta=0$) is subjected to the highest stress or the largest stress fluctuation and, in general, is the origin of fatigue crack initiation. The maximum stress on this element is obtained by substituting the notch tip coordinates into Eq. (5.7).

$$\text{max. } \sigma_{yy} = \frac{2}{\sqrt{\pi}} \frac{K_I}{\sqrt{\rho}} \qquad (5.8)$$

Likewise, for the same element of a structural component under cyclic loading, the maximum stress range is,

$$\text{max. } \Delta\sigma_{yy} = \frac{2}{\sqrt{\pi}} \frac{\Delta K_I}{\sqrt{\rho}} \tag{5.9}$$

A rivet hole in a riveted structural detail is a geometrical discontinuity which intensify the nominal net section stress in the vicinity of the rivet hole. Because the edges of rivet holes are where initial flaws or notches most likely to occur, the maximum stresses at notch tips at rivet holes are very high. Fatigue cracks usually initiate at these notches.

The local maximum stress range at the tip of a notch at the rivet hole is assumed to relate to the nominal net section stress range of the structural component by Eq. (5.10).

$$\text{max. } \Delta\sigma_{yy} = K_t \, S_{r\,(net)} \tag{5.10}$$

where K_t is the stress concentration factor for the edge of the rivet hole and $S_{r\,(net)}$ is the nominal stress range based on net section area. The notch tip radius is generally not known and is difficult to obtain. For an upper bound estimate of crack initiation life, the rivet hole itself is considered as a blunt notch with a tip radius ρ=R. Equations (5.9) and (5.10) then combine with ρ = R into

$$K_t \, S_{r\,(net)} = \frac{2}{\sqrt{\pi}} \frac{\Delta K_I}{\sqrt{R}} \tag{5.11}$$

By substituting ΔK_I from Eq. (5.11) and $\rho = R$ into Eq. (5.6), the fatigue crack initiation life of riveted detail is then approximated by

$$N_i = 5.37 \times 10^{22} \left\{ \frac{\sqrt{\pi}}{2} K_t \, S_{r\,(net)} \right\}^{-6.27} \qquad (5.12)$$

The stress concentration factor, K_t, is readily available from Eqs. (4.2) and (4.5) by equating crack length, a, to zero. The resulting values are listed in the second column of Tables 4-9 and 4-4.

Equation (5.12) is fairly simple. It contains the stress concentration factor to account for the effects of geometry, and the nominal net section stress range. Since the same stress range is the variable in Eq. (3.37) for fatigue crack growth life, N_g, Eqs. (3.37) and (5.12) can be summed directly as indicated by Eq. (5.1) to provide estimates of total fatigue life of riveted built-up members and joints.

When values of m=3.0 and $C=3.829 \times 10^{-12}$ $m^{11/2}/MN^3$ cycle (2.0×10^{-10} $in^{11/2}/kip^3$ cycle) are used in Eq. (3.37), which in turn is substituted with Eq. (5.12) into Eq. (5.1), then the expression for fatigue life of riveted built-up members and riveted truss joints becomes:

$$N_T = 1.147 \times 10^{23} \{K_t S_{r\,(net)}\}^{-6.27} + \frac{P}{3.829 \times 10^{-12}} \{S_{r\,(net)}\}^{-3.0} \quad (5.13)$$

The fatigue crack initiation life (N_i), fatigue crack growth life (N_g) and the total fatigue life (N_T) of each detail of this study are summarized in Table 5-11 for two constant stress ranges of 137.9 MPa (20 ksi) and 275.8 MPa (40 ksi) of tension loading only.

From Eq. (5.13), the $S_{r\,(net)}$ versus N_T relations for riveted truss joints with bearing ratio of 1.66, 2.09, 2.79 and 2.85 are computed and are plotted in Figs. 5-11 to 5-21 to compare with results of testing. The lines of the estimated total fatigue life are not straight lines but the curvature is small.

In Figs. 5-11 to 5-19, the bearing ratios of the analysis do not coincide with those of the test specimens, but are bounded by the bearing ratios of the tests. For all cases in these figures, the analytical S_r (net)- N_T lines are almost parallel to the regression lines and are located close to those lines. The closeness of the analytical and regression lines is encouraging, indicating the feasibility of using the analytical procedure for fatigue life estimation.

5.5 Discussion

Although the analytical approach of this study can provide reasonable estimates of fatigue life for riveted built-up members and joints, there are numerous assumptions to be examined and many questions to be answered. The first and foremost is the ignorance of clamping and frictional forces between the component plates. These forces strongly affect the state of stress at the rivet holes and the transmission of forces between plates. Disregarding these forces reduced the stress analysis from three dimensional to two dimensional; it also rendered the results of analysis a lower bound solution.

The linear elastic fracture mechanics approach to crack growth analysis as taken in this study relies heavily on experimental results. The crack growth characteristics must be determined by tests. Unfortunately, there has been very little information of crack growth tests on riveted members and joints. One of the reasons that there is lack of such data is that the study of crack growth is a relatively new development. More influencial is probably the condition that there are so many variables for riveted members and joints. A

systematic experimental evaluation of the effects of the significant variables on the crack growth behavior is essential.

The incorporation of the fatigue crack initiation phase into the fatigue life estimate of riveted members and joints appears to be appropriate and necessary. Careful correlation between physical and geometrical conditions of rivet holes and crack development needs to be undertaken. The influence of notch tip radius, the effects of maximum stress and stress range, the possible level of crack initiation threshold, etc, all require careful study.

When most of these questions are answered, then the accuracy of the current approach can be improved and the analytical procedure can be applied to other riveted joints. (The riveted joint of Fig. 5-23 is an example.)

At the present, it can be stated that the procedure of this study is acceptable. In fact, since the analytical results compared very well with the results of available tests, it becomes certain that the S-N relations for riveted built-up members and joints will not be too far from those lines superimposed on the current AASHTO and AREA Provisions shown in Fig. 5-24.

CHAPTER 6

SUMMARY AND CONCLUSIONS

This dissertation presents an analytical approach to estimate the fatigue life of riveted built-up truss members and joints under cyclic tension and bending moments. Some important findings, conclusions, and suggestions for evaluation of fatigue resistance of truss bridges are summarized here. Areas for further studies are pointed out.

6.1 Main Findings and Conclusions

1. Truss members and joints are subjected to bending as well as axial forces due to the rigidity of joint connections. A three dimensional model of truss bridge spans, including the bridge deck system, generally provides better estimates of truss member forces and better simulation of actual behavior of the spans than do two dimensional plane truss or plane frame models. Since the fatigue strength of members and joints is controlled by local stresses, only an appropriate three-dimensional rigid frame model of a truss span including the deck system can be used to evaluate the live load stresses in the members and joints of

truss bridges.

2. The analysis of Kosti Bridge in Sudan Railroad showed that the effects of a damaged member are localized; only the members adjacent to the damaged member are subjected to slightly high stresses. For the damaged member, the stresses based on net remaining cross section do not increase much if the damaged area is less than 30 % of the original effective area because of force redistribution among the adjacent members. If the stress magnitudes are referenced to the undamaged net-sectional area, the numerical values are lower as the crack grows. This condition justifies the use of nominal stress range based on undamaged net section for evaluation of fatigue strength.

3. In this study, structural details in riveted truss bridges were classified into two types. One is riveted built-up truss members which do not transmit significant forces between the component plates. The other is riveted truss joints in which force transmittal occurs between member flanges and gusset plates by rivet bearing. The riveted

built-up member differs from riveted truss joint on the basis that the former is not in bearing condition but the latter is in high bearing condition at rivet holes. No clamping or frictional force at the interface of the components were considered. Stress distribution in the component plates and particularly at rivet holes were evaluated by using quarter-point quadratic isoparametric finite elements, and stress intensity factors at crack tips were calculated by using a virtual crack extension method. The stress concentration in riveted built-up truss members was found to be as high as 2.60 at the rivet holes. The stress concentration at rivet holes in truss joints with bearing was higher. The higher the bearing ratio, the higher the stress concentration.

4. Correction functions for stress intensity factors were formulated for the riveted details with cracks. When the crack length was zero, the functions give the magnitudes of stress concentration at the rivet hole.

5. The effects of pitch and gage distance on fatigue

life were derived from analysis. Riveted built-up members with smaller pitch and gage distances and no bearing have longer fatigue life. The effects of pitch distance are more pronounced than the effects of gage distance.

6. Riveted truss joints with higher bearing ratios were found to have a higher stress concentration at rivet holes than joints with smaller bearing ratios. Subsequently, riveted joints with higher bearing ratios have shorter fatigue life. This finding substantiates the test results from earlier studies by others.

7. Riveted bearing joints with longer pitch distances were found to have longer fatigue life compared to those with shorter pitch distance. This finding is in contrast to that for riveted built-up truss member without bearing. Confirmation by testing is necessary.

8. If maximum extreme fiber tensile stresses were the same, higher bending stresses caused lower stress concentrations at rivet holes and slower fatigue

crack propagation. If the average net section tensile stresses in riveted members were the same, higher bending moment would cause faster crack propagation at rivet holes.

9. By assuming that crack growth characteristics of riveted built-up members and joints were the same as those of welded members and joints, this study showed that the existing AASHTO fatigue strength provisions could be used conservatively for fatigue crack growth life estimation of riveted members and joints.

10. Comparison between results of this analysis and of fatigue tests indicated that fatigue crack growth characteristics should be utilized for evaluation of fatigue life of fatigue strength of such members and joints. The crack growth in riveted members and joints are slower than that in welded members and details.

11. Inclusion of the crack initiation phase was found necessary in estimating fatigue life of riveted members and joints. Upper bound estimates were

made assuming the initial flaw to be the rivet hole. Results of analysis agreed fairly well with test data from others.

12. Modelling of a crack with quarter-point quadratic isoparametric finite elements around the crack tip which provided an accurate approximation of $1/\sqrt{r}$ singular stress distribution and the virtual crack extension method enhanced the accuracy in calculating stress intensity factor at the crack tip. With these analytical tools, it was possible to model accurately cracks emerging from rivet holes with moderately fine meshes of the finite element model.

6.2 Suggestions

1. Riveted truss bridges should be analyzed as three dimensional frame structures including the floor systems. Stresses due to bending moment should be considered.

2. The provisions of specifications on the fatigue strength of riveted members and connections can be separated into two groups: the riveted built-up

members and the riveted joints with bearing.

3. Current fatigue strength provisions of AASHTO and AREA can be used conservatively for evaluation of fatigue crack growth in riveted members and joints. Category D may be used for riveted bearing joints, and Category C for built-up truss members. Stresses are to be based on net cross sections.

4. Experimental studies on fatigue crack initiation and propagation are necessary and must be conducted systematically with proper consideration of clamping force, bearing ratio, and geometrical parameters.

5. An analytical procedure needs to be developed for evaluation of force and stress distributions in joints with clamping forces. The magnitudes of clamping forces and the frictional forces between component plates, or some quantities representing them, should be the primary factors of investigation.

6. The quarter-point isoparametric finite element and

virtual crack extension method can be expanded into three dimensional isoparametric elements without difficulty. The utilization of such three dimensional elements for solving stress distribution and fatigue crack growth in complicated structural members and joints are suggested.

7. The analytical procedure of this study is applicable to the study of fatigue crack growth in plane stress welded structural details. Analysis of some welded details should be conducted to confirm results, as well as to obtain new results.

Table 2-1: Maximum Calculated Stresses in Various Truss Member

Member	2-d Model		3-D Model		Measured Stress (MPa)	Remark
	Truss (MPa)	Frame (MPa)	Pin\Pin (MPa)	Pin\ Roller		
Bottom Chord (L_4L_5)	10.14	9.52	N.A.	N.A.	6.20	Ref. [74] Atbara
Hanger (U_6L_6)	22.06	24.62	29.17	31.58	51.71	
Floor Beam	N.A.	N.A.	24.55	38.96	35.10	
Stringer	N.A.	N.A.	41.99	43.99	44.33	
Top Chord (U_4M_4)	-37.44	-36.82	-35.92	-36.61	-36.41	
Bottom Chord (L_3L_4)	39.37	39.03	14.14	37.65	27.03	Ref.
Bottom Chord (L_2L_3)	41.03	41.58	16.41	40.13	26.34	[21] Kohr-Mog
Diagonal (U_1L_2)*	47.71	45.99	40.89	42.96	42.34	
Hanger (U_2L_2)	-23.72	-23.58	-20.82	-27.00	-14.14	
Floor Beam (center)	N.A.	N.A.	29.44	50.82	49.37	
Stringer (center)	N.A.	N.A.	27.44	36.19	39.99	
Top Chord ($U_{15}U_{17}$)	-20.81	-21.65	N.A.	-19.04	-16.47	
Bottom Chord ($L_{12}L_{13}$)	19.84	22.94	N.A.	22.09	23.79	Ref.
Bottom Chord ($L_{11}L_{12}$)	19.84	21.12	N.A.	20.53	21.99	[51] Blue Nile
Diagonal ($U_{14}L_{15}$)	30.56	16.51	N.A.	14.86	12.82	
Hanger ($U_{13}L_{13}$)	28.35	19.52	N.A.	24.14	25.63	
Floor Beam (center)	N.A.	N.A.	N.A.	20.48	20.14	
Stringer (center)	N.A.	N.A.	N.A.	30.90	78.71	

* : Stress were measured and compared on the side of the member on which bending moment caused compressive stress.

Table 2-2: Cross-Section Properties of Kosti Bridge

Member	Composition	Area cm^2	I_x cm^4	I_y cm^4	K_t cm^4
L_0U_1 L_7U_6	-610x11.1 mm 2 -381x102mmx42# 2FL-102x12.7 mm	252.3	65294.	117637.	161.
U_1U_2, U_2U_3 U_3U_4, U_4U_5 U_5U_6	-610x12.7 mm 2 -381x102mmx45# 2FL-102x15.9 mm	281.3	71309.	137906.	188.
L_0L_1, L_1L_2 L_5L_6, L_6L_7	2 -381x11.1 mm 2 -102x102x11.1mm -635x9.5 mm	187.9	26251.	83910.	72.
L_2L_3 L_3L_4 L_4L_5	2 -381x11.1 mm 2 -267x11.1 mm 2 -102x102x11.1mm 1 -635x12.7 mm	267.2	44409.	119744.	121.
U_1L_1, U_6L_6	4 -127x89x11.1mm	91.1	22600.	3559.	39.
U_2L_2, U_3L_3 U_4L_4, U_5L_5	4 Bulb angles 4B -152x89mmx14.2#	107.9	27670.	7139.	34.
M_1L_1, L_6M_6	4 -127x89x9.5 mm	78.7	19677.	3051.	25.
U_1L_2, U_6L_5	4B -178x89mmx21.6#	163.9	42589.	9279.	53.
U_2L_3, U_5L_4	4B -178x89mmx16.8#	127.5	31608.	6840.	93.
U_3L_4, U_4L_3	4 -89x89x11.1mm	74.1	17517.	1338.	33.
Floor Beam	4 -152x152x14.3mm -914x11.1 mm	267.6	358611.	5600.	160.
Stringer	4 -127x89x11.1mm -787x9.5 mm	166.1	164944.	2682.	62.

Table 2-3: Reduced Hanger Cross-Section Properties of Kosti Bridge

Reduction Steps in Hanger $4L_s$-127*89*11.1mm	Area cm^2	I_x cm^4	I_y cm^4	K_t cm^4
Original Section 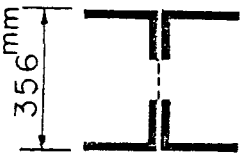	91.10	22600.0	3559.2	39.5
5 % Reduction 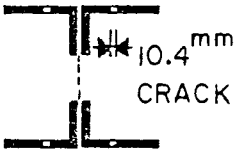	86.52	21226.3	3293.2	37.6
10 % Reduction 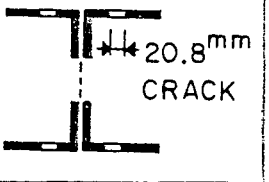	82.00	19902.5	3031.0	35.8
20 % Reduction 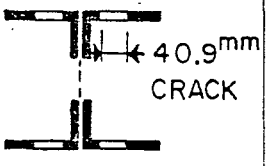	72.91	17203.7	2502.7	32.0
40 % Reduction 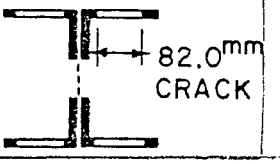	54.65	11788.3	1442.4	24.5

Table 2-4: Maximum Calculated and Measured Stresses of Kosti Bridge Member

Member		3-D Model Computed Stress (MPa)	Field Measured Stress (MPa)	Remark
Top Chord	(U_3U_4)	-37.78	-39.51	
Bottom "	(L_3L_4)	15.44	28.20	
Bottom "	(L_4L_5)	9.93	22.62	*Sidewalk
Diagonal	(L_4U_5)	24.34	22.62	
Hanger	(U_4L_4)	4.90	No Reading	
Hanger	(U_5L_5)	9.65	5.65	
Floor Beam	(L_3AL_3B)	46.27	50.82	
Stringer	(L_3L_4A)	37.92	47.02	
Stringer	(L_3L_4B)	37.92	45.16	

Table 2-5: Change of Stresses in Truss Bridge Members due to 40 % Area Reduction in Hanger U_1L_1

Member	Without Area Reduction in Hanger (MPa)	With 40 % Area Reduction in Hanger (MPa)	Per Cent Change (%)
Hanger (U_1L_1A)	72.40	96.96	33.9
Diagonal (M_1L_1A)	31.25	35.59	13.9
Diagonal (U_1L_2A)	-8.72	-10.78	23.6
Diagonal (U_2L_3A)	-8.79	-8.47	-3.6
Bottom Chord (L_0L_1A)	25.37	29.86	17.7
Bottom Chord (L_1L_2A)	14.86	17.46	17.5
Bottom Chord (L_2L_3A)	9.72	10.27	5.7
Hanger (U_1L_1B)	72.28	74.62	3.2
Floor Beam (L_1AL_1B)	17.95	18.18	1.3
Top Chord (U_1U_2A)	-12.51	-13.45	7.5

Table 2-6: Member forces and Stresses in Hanger for Various Reduction Steps

(Under one set of 445 kN (100 kips) axle loading between truss joint L_1A and L_1B)

	Force	Intact	5 % Reduc.	10 % Reduc.	20 % Reduc.	40 % Reduc.
Forces at Lower Joint of Hanger	Axial Force (kN)	382.53	381.02	379.37	375.63	365.63
	Moment in plane of truss (kN-m)	0.326	0.322	0.317	0.302	0.242
	Moment perpendicular to plane of truss(kN-m)	37.09	34.79	32.56	27.92	18.43
Stresses Based on Reduced Area	Maximum at Lower Joint of Hanger (MPa)	72.40	74.47	76.74	81.98	96.94
	Maximum at Upper Joint of Hanger (MPa)	58.47	60.74	63.23	69.02	85.50

Table 3-1: Stress-Intensity Factor for Center-Through Crack

(1)By Virtual Crack Extension Method

Virtual Crack Length δ	Energy Release Rate G	Stress Intensity Factor K
1/10 of l	9.4546 kN/m	44.228 MPa$\sqrt{m}$
1/100 of l	10.3285 "	46.227 "
1/500 of l	10.4073 "	46.403 "
1/1000 of l	10.4160 "	46.425 "
1/5000 of l	10.4248 "	46.443 "
1/10000 of l	10.4248 "	46.445 "
1/50000 of l	10.4265 "	46.447 "
1/100000 of l	10.4265 "	46.447 "

(2)By Equality 49.642 MPa$\sqrt{m}$

(3)By Handbook f_a=1.186 46.188 MPa$\sqrt{m}$

Reference Value : $\sigma\sqrt{\pi a}$ = 38.944 MPa$\sqrt{m}$

Where l = 0.0508 m (2.0 in.)

a = 0.1016 m (4.0 in.)

σ = 68.95 MPa (10.0 ksi)

Table 3-2: Stress-Intensity Factor for Double-Edge Crack

Stress Intensity Factor K for Fig. 3-10 (a)

	4-Element	6-Element	12-Element	Reference* Value
APES prog.	1.92	2.01	2.05	a/w = 0.4
QIFEVCEM		1.967	2.001	K = 2.006

*Tada's modification of Irwin's interpolation formula [68]

Non-Dimensional Value ($F=\frac{K}{\sigma\sqrt{\pi a}}$) for Fig. 3-10 (b)

	a/w = 0.25	a/w = 0.50	a/w = 0.75
Handbook Value	1.126	1.184	1.449
J-Integral	1.109 (1.5 %)	1.162 (1.9 %)	1.437 (0.8 %)
Equality	1.108 (1.6 %)	1.164 (1.7 %)	1.439 (0.7 %)
QIFEVCEM	1.110 (1.4 %)	1.169 (1.1 %)	1.442 (0.5 %)

Deviation < 1.5 % from the Handbook Value [68]

Table 4-1: Stress-Intensity Factor for Cracks in Built-up Truss Member under Tension of 68.95 MPa (10.0 ksi)

Crack Length cm	Stress-Intensity Factor (MPa$\sqrt{m}$)							
	P4G6	P6G6	P8G6	P12G6	P6G4	P6G5	P6G6	P6G8
0.208	12.41	12.69	12.83	13.75	13.14	12.68	12.69	12.70
0.417	14.03	14.41	14.61	15.69	14.91	14.34	14.41	14.43
0.625	14.45	14.95	15.22	16.37	15.41	14.92	14.95	14.96
0.833	14.63	15.26	15.60	16.78	15.76	15.26	15.26	15.27
1.091	14.71	15.46	15.86	17.22	15.99	15.46	15.46	15.48
1.349	14.83	15.73	16.29	17.71	16.24	15.70	15.73	15.75
1.667	14.91	15.96	16.74	18.29	16.49	15.98	15.96	16.03
1.984	14.93	16.26	17.18	18.87	16.73	16.23	16.26	16.28
2.492	15.29	17.14	18.46	20.52	17.57	17.09	17.14	17.15

Unit : MPa $\sqrt{m}$

1.0 ksi $\sqrt{in}$ = 1.1 MPa $\sqrt{m}$

Table 4-2: Stress-Intensity Factor for Cracks in Built-up Truss Member under Bending Moment Which Induces 68.95 MPa (10.0 ksi) at Extreme Fiber

Crack Length cm	Stress-Intensity Factor (MPa$\sqrt{m}$)							
	P4G6	P6G6	P8G6	P12G6	P6G4	P6G5	P6G6	P6G8
0.208	8.319	8.202	7.990	8.105	7.316	7.622	8.202	9.047
0.417	9.525	9.448	9.262	9.352	8.475	8.772	9.448	10.38
0.625	9.966	9.969	9.795	9.881	8.968	9.325	9.969	10.90
0.833	10.27	10.37	10.23	10.26	9.423	9.744	10.37	11.29
1.091	10.56	10.77	10.65	10.70	9.872	10.17	10.77	11.65
1.349	10.90	11.22	11.21	11.17	10.37	10.63	11.22	12.07
1.667	11.29	11.73	11.85	11.74	10.96	11.21	11.73	12.58
1.984	11.64	12.31	12.50	12.32	11.54	11.78	12.31	13.07
2.492	12.51	13.61	14.02	13.74	12.89	13.10	13.61	14.29

Unit : MPa $\sqrt{m}$

1.0 ksi $\sqrt{in}$ = 1.1 MPa $\sqrt{m}$

Table 4-3: Non-Dimensionalized Stress-Intensity Factor for Cracks in Riveted Built-up Truss Member

Under Tension

a/(R+a)	P4G6	P6G6	P8G6	P12G6	P6G4	P6G5	P6G6	P6G8
0.149	1.808	1.849	1.869	2.003	1.804	1.799	1.849	1.922
0.259	1.446	1.485	1.505	1.616	1.447	1.440	1.485	1.543
0.344	1.215	1.257	1.280	1.377	1.221	1.223	1.257	1.307
0.412	1.066	1.111	1.136	1.222	1.082	1.083	1.111	1.155
0.478	0.936	0.984	1.009	1.096	0.959	0.958	0.984	1.023
0.531	0.849	0.900	0.932	1.014	0.876	0.876	0.900	0.936
0.583	0.768	0.822	0.862	0.942	0.800	0.802	0.822	0.857
0.625	0.705	0.767	0.811	0.890	0.744	0.746	0.767	0.798
0.677	0.644	0.722	0.778	0.864	0.697	0.701	0.722	0.750

Under Bending Moment

a/(R+a)	P4G6	P6G6	P8G6	P12G6	P6G4	P6G5	P6G6	P6G8
0.149	1.190	1.173	1.142	1.159	1.081	1.103	1.173	1.284
0.259	0.963	0.955	0.936	0.946	0.886	0.898	0.955	1.042
0.344	0.823	0.823	0.809	0.816	0.765	0.779	0.823	0.893
0.412	0.734	0.741	0.732	0.733	0.696	0.705	0.741	0.801
0.478	0.660	0.673	0.665	0.668	0.637	0.643	0.673	0.723
0.531	0.612	0.631	0.630	0.627	0.602	0.604	0.631	0.673
0.583	0.571	0.593	0.599	0.594	0.572	0.573	0.593	0.631
0.625	0.539	0.570	0.579	0.571	0.553	0.552	0.570	0.601
0.677	0.517	0.562	0.580	0.568	0.551	0.548	0.562	0.587

Non-dimensional Value : $K_i / \sigma_{net}\sqrt{\pi a}$

Table 4-4: Coefficients of Functions F_t and F_b

Function F_t

Detail Type	a_0	a_1	a_2	a_3	a_4	Std. Error of Estimate
P4G6	2.4639	-5.1370	5.4044	-3.1883	0.8035	0.00197
P6G6	2.5644	-5.9269	8.8671	-9.3971	4.8572	0.00224
P8G6	2.5821	-5.9083	8.8461	-9.4954	5.1705	0.00258
P12G6	2.7735	-6.4306	9.9822	-11.038	6.1468	0.00319
P6G4	2.5084	-5.8174	8.5150	-8.4982	4.0910	0.00278
P6G5	2.5393	-6.3186	10.792	-12.506	6.5347	0.00191
P6G6	2.5644	-5.9269	8.8671	-9.3971	4.8572	0.00224
P6G8	2.6592	-6.0669	8.7465	-8.8202	4.4017	0.00218

Function F_b

Detail Type	b_0	b_1	b_2	b_3	b_4	Std. Error of Estimate
P4G6	1.6253	-3.5324	4.6744	-4.0700	1.9161	0.00146
P6G6	1.6339	-3.9713	7.0707	-8.5388	4.8752	0.00178
P8G6	1.5582	-3.5015	5.6557	-6.5741	3.9916	0.00225
P12G6	1.5906	-3.6343	5.8835	-6.7531	3.9755	0.00194
P6G4	1.4915	-3.5012	5.9588	-6.8156	3.8651	0.00227
P6G5	1.5618	-4.0783	8.1427	-10.465	6.0044	0.00135
P6G6	1.6339	-3.9713	7.0707	-8.5388	4.8752	0.00178
P6G8	1.7791	-4.1863	6.8814	-7.8248	4.3542	0.00190

Table 4-5: Geometrical Variables of Riveted Truss Joint for Different Bearing Ratio

Detail Type	No.of Rivet Row	Bearing Ratio (B)	Shear Ratio (S)	Rivet Diameter (D) mm	Gage Distance (g) mm	Pitch Distance (p) mm
B166	4	1.66	1.21	22.2	121.9	81.3
B209	4	2.09	1.52	Ditto	152.4	101.6
B279a	3	2.79	2.028	Ditto	Ditto	Ditto
B279b	3	2.79	2.028	Ditto	Ditto	152.4
B285	3	2.85	0.76	Ditto	Ditto	101.6

Detail Type	Member Width (w_m)mm	Member Thknss (t_m)mm	Member NetArea $A_{net}mm^2$	Gusset Width (w_g)mm	Gusset Thknss (t_g)mm
B166	2032	12.7	3750	528	15.9
B209	2540	Ditto	4718	660	Ditto
B279a	Ditto	Ditto	Ditto	609	Ditto
B279b	Ditto	Ditto	Ditto	660	Ditto
B285	Ditto	4.8	1807	660	6.4

Table 4-6: Stress-Intensity Factor for Cracks in Truss Joints under Tension of 68.95 MPa (10.0 ksi)

Crack Length cm	Member Flange (MPa$\sqrt{m}$)					Gusset Plate	
	B166	B209	B279a	B279b	B285	B166	B209
0.208	16.55	19.39	20.56	20.00	19.00	10.26	11.87
0.417	17.91	20.98	22.17	21.49	20.47	10.94	12.71
0.625	17.73	20.77	21.87	21.14	20.18	10.69	12.49
0.833	17.34	20.29	21.30	20.53	19.64	10.33	12.13
1.091	16.72	19.50	20.41	19.60	18.80	9.79	11.58
1.349	16.30	18.84	19.67	18.82	18.10	9.34	11.10
1.667	15.87	18.16	18.90	18.02	17.38	8.74	10.56
1.984		17.69	18.37	17.45	16.88		10.09
2.403		17.27	17.89	16.94	16.43		9.45

Unit : MPa $\sqrt{m}$

1.0 ksi $\sqrt{in}$ = 1.1 MPa $\sqrt{m}$

Table 4-7: Stress-Intensity Factor for Cracks in Truss Joints under Bending Moment Which Induces 68.95 Mpa (10.0 ksi) at Extreme Fiber of Truss member

Crack Length cm	Member Flange (MPa$\sqrt{m}$)				
	B166	B209	B279a	B279b	B285
0.208	8.517	9.629	9.679	9.695	8.827
0.417	9.483	10.675	10.728	10.719	9.776
0.625	9.665	10.827	10.879	10.848	9.906
0.833	9.734	10.841	10.887	10.841	9.908
1.091	9.746	10.752	10.791	10.728	9.813
1.349	9.859	10.709	10.741	10.667	9.762
1.667	10.043	10.733	10.756	10.670	9.770
1.984		10.839	10.855	10.759	9.855
2.403		11.113	11.123	11.013	10.092

Unit : MPa $\sqrt{m}$

1.0 ksi $\sqrt{in}$ = 1.1 MPa $\sqrt{m}$

Table 4-8: Non-Dimensionalized Stress-Intensity Factor for Cracks in Truss Joints

Under Tension

a/(R+a)	B166	B209	B279a	B279b	B285
0.149	2.556	3.082	3.268	3.179	3.327
0.259	1.956	2.358	2.491	2.415	2.534
0.344	1.581	1.906	2.007	1.939	2.039
0.412	1.339	1.612	1.693	1.631	1.719
0.478	1.128	1.354	1.417	1.361	1.438
0.531	0.989	1.176	1.228	1.175	1.245
0.583	0.866	1.020	1.062	1.012	1.076
0.625		0.911	0.946	0.899	0.957
0.669		0.808	0.837	0.792	0.847

Under Bending Moment

a/(R+a)	B166	b209	B279a	B279b	B285
0.149	1.141	1.377	1.384	1.386	1.387
0.259	0.899	1.079	1.085	1.084	1.086
0.344	0.748	0.894	0.898	0.895	0.899
0.412	0.652	0.775	0.778	0.775	0.778
0.478	0.571	0.672	0.674	0.670	0.674
0.531	0.519	0.602	0.603	0.599	0.603
0.583	0.476	0.543	0.544	0.539	0.543
0.625		0.502	0.503	0.498	0.502
0.669		0.468	0.468	0.464	0.467

Table 4-9: Coefficients of Functions G_t and G_b

Function G_t

Detail Type	c_0	c_1	c_2	c_3	c_4	Std. Error of Estimate
B166	3.6385	-8.4688	8.7834	-4.8840	1.2739	0.00196
B209	4.4386	-10.928	13.926	-12.090	5.3298	0.00194
B279a	4.7272	-11.765	15.066	-13.073	5.7515	0.00214
B279b	4.6169	-11.605	14.937	-12.996	5.7155	0.00217
B285	4.8171	-12.013	15.369	-13.299	5.8402	0.00227

Function G_b

Detail Type	d_0	d_1	d_2	d_3	d_4	Std. Error of Estimate
B166	1.5708	-3.3168	3.0747	-1.1710	0.2239	0.00070
B209	1.9446	-4.6175	6.2412	-5.8846	2.9000	0.00083
B279a	1.9439	-4.5045	5.7136	-5.0160	2.4074	0.00090
B279b	1.9602	-4.6630	6.2518	-5.8813	2.9253	0.00111
B285	1.9564	-4.6130	6.0948	-5.6141	2.7446	0.00072

Table 5-1: S_R- N Provisions for Riveted Joints

Basic Equation : Log N = Q - m Log S_R

Country	Intercept Q	Slope m	Limit	Remark
	12.182	3.0	$N<10^7$	Riveted Joint
England	15.637	5.0	$N>10^7$	with Clamping
(1977)	11.398	3.0	$N<10^7$	Riveted Joint
	14.330	5.0	$N>10^7$	Without Clamping
United States AASHTO 1977	11.820	3.0	$N<5.9*10^6$	S_r=48 Mpa for $N>5.9*10^6$
Switzerland SIA 1979	12.739	3.0	$N<2.5*10^6$	S_r=130 MPa for $N>2.5*10^6$
Netherland	14.120	4.0	$N<2.0*10^6$	
	20.000	7.0	$N>2.0*10^6$	

Table 5-2: Values of P and Q for Riveted Built-up Truss Members for m=3.0 and $C=3.829*10^{-12}$

P for Eq.(5.3)

λ		0.0		0.1	0.2	0.3
a_i cm	0.00254	0.00508	0.0508	0.0508	0.0508	0.0508
P4G6	11.483	10.061	7.555	8.150	8.816	9.565
P6G6	9.435	8.171	5.929	6.469	7.081	7.779
P8G6	8.637	7.400	5.205	5.741	6.356	7.067
P12G6	6.792	5.793	4.020	4.519	5.105	5.798
P6G4	10.265	8.914	6.517	7.128	7.826	8.630
P6G5	10.048	8.744	6.418	7.021	7.708	8.496
P6G6	9.435	8.171	5.929	6.469	7.081	7.779
P6G8	8.433	7.300	5.291	5.742	6.247	6.818

Q for Eq.(5.5)

P4G6	12.477	12.420	12.295	12.328	12.362	12.398
P6G6	12.392	12.329	12.190	12.228	12.267	12.308
P8G6	12.353	12.286	12.133	12.176	12.220	12.266
P12G6	12.249	12.180	12.021	12.072	12.125	12.180
P6G4	12.428	12.367	12.231	12.270	12.310	12.353
P6G5	12.419	12.359	12.224	12.263	12.304	12.346
P6G6	12.392	12.329	12.190	12.228	12.267	12.308
P6G8	12.343	12.280	12.140	12.176	12.213	12.251

Table 5-3: Values of P and Q for Riveted Truss Joints for m=3.0 and $C=3.829*10^{-12}$

P for Eq.(5.3)

λ		0.0		0.1	0.2	0.3
a_i cm	0.00254	0.00508	0.0508	0.0508	0.0508	0.0508
B166	4.753	4.311	3.524	4.059	4.711	5.515
B209	3.754	3.510	3.075	3.520	4.059	4.716
B279a	3.296	3.094	2.733	3.148	3.654	4.278
B279b	3.790	3.573	3.186	3.637	4.182	4.846
B285a	3.164	2.973	2.632	3.038	3.534	4.188

Q for Eq.(5.5)

λ		0.0		0.1	0.2	0.3
a_i cm	0.00254	0.00508	0.0508	0.0508	0.0508	0.0508
B166	12.094	12.051	11.964	12.025	12.090	12.158
B209	11.991	11.962	11.905	11.963	12.025	12.091
B279a	11.935	11.907	11.854	11.915	11.980	12.048
B279b	11.996	11.970	11.920	11.978	12.038	12.102
B285a	11.917	11.890	11.837	11.899	11.965	12.035

Table 5-4: Measured and Estimated Fatigue Crack Length and Loading Cycles of Riveted Floor Beam

Crack 4ST

Crack Length, a cm (in.)	N (tested) cycle	ΔN (tested) cycle	ΔN (estimated) cycle
3.68 (1.45)	18 259 000	0	0
4.83 (1.90)	21 000 000	2 741 000	922 000
6.10 (2.40)	23 672 000	5 413 000	1 644 000
7.24 (2.85)	25 944 000	7 685 000	2 115 000
7.37 (2.90)	26 683 000	8 424 000	2 160 000
8.89 (3.50)	29 507 000	11 248 000	2 608 000

Crack 8NT

Crack Length, a cm (in.)	N (tested) cycle	ΔN (tested) cycle	ΔN (estimated) cycle
5.72 (2.25)	18 259 000	0	0
6.60 (2.60)	21 000 000	2 741 000	417 000
7.37 (2.90)	23 672 000	5 413 000	707 000
8.51 (3.35)	25 944 000	7 685 000	1 056 000
8.89 (3.50)	26 683 600	8 424 000	1 155 000

Crack 12ST

Crack Length, a cm (in.)	N (tested) cycle	ΔN (tested) cycle	ΔN (estimated) cycle
5.72 (2.25)	18 259 000	0	0
7.87 (3.10)	21 000 000	2 741 000	872 000
8.89 (3.50)	23 672 000	5 413 000	1 154 000

Table 5-5: Result of Fatigue Tests on Double Lap Joints Bearing Ratio=2.74; from Reference [60]

Specimen Mark	Stress Ratio (R)	Stress Range (MPa)	Applied Cycles (Cycle)	Remark	S_r-N Curve Slope (m)	Intercept (Q)
1FR8	-1.0	220.6	66500	Nor.Cl.		
1FR9	"	165.5	390400	"		
1FR10	"	165.5	1907300	"		
1FR11	"	193.1	945200	"		
1FR16	"	282.7	221200	"	4.140	15.224
1FR17	"	193.1	929300	"		
1FR20	"	289.6	103800	"		
1FR21	"	165.1	1836400	"		
1FR12	"	165.5	138400	Red.Cl.		
1FR28	"	165.5	615500	"		
1FR29	"	275.8	36000	"	3.901	14.121
1FR31	"	275.8	44000	"		
1FR1	0.0	206.9	56900	Nor.Cl.		
1FR2	"	193.1	71400	"		
1FR3	"	193.1	80900	"		
1FR4	"	124.1	417200	"	4.368	14.866
1FR5	"	137.9	315700	"		
1FR6	"	124.1	685600	"		
1FR13	"	96.5	542800	Red.Cl.		
1FR14	"	96.5	1358700	"		
1FR19	"	206.9	35300	"		
1FR23	"	206.9	48800	"	3.991	13.907
1FR27	"	137.9	305700	"		
1FR30	"	137.9	278200	"		
1FR15	0.5	103.4	951400	Nor.Cl.		
1FR18	"	131.0	232000	"	6.353	18.776
1FR22	"	131.0	193100	"		
1FR24	"	131.0	84100	Red.Cl.		
1FR25	"	131.0	83100	"	3.244	11.790
1FR26	"	103.4	180100	"		

**Nor.Cl.---Normal Clamping in Rivets
Red.Cl.---Reduced Clamping in Rivets

Table 5-6: Result of Fatigue Tests on Double Lap Joints Bearing Ratio=2.36; from Reference [60]

Specimen Mark	Stress Ratio (R)	Stress Range (MPa)	Applied Cycles (Cycle)	Remark	S_r-N Curve Slope (m)	Intercept (Q)
2FR3	-1.0	220.6	1104900	Nor.Cl.		
2FR5	"	220.6	1354400	"		
2FR12	"	220.6	914700	"		
2FR14	"	179.3	2686200	"	6.600	21.463
2FR29	"	358.5	42500	"		
2FR30	"	365.4	26600	"		
2FR31	"	258.6	441000	"		
2FR1	0.0	151.7	1470500	Nor.Cl.		
2FR2	"	206.9	878100	"		
2FR6	"	206.9	1526900	"		
2FR7	"	206.9	82700	"		
2FR8	"	151.7	3979200	"		
2FR9	"	131.0	5035600	"	4.266	15.460
2FR10	"	144.8	989300	"		
2FR11	"	206.9	92000	"		
2FR15	"	206.9	1045600	"		
2FR16	"	151.7	331000	"		
2FR17	"	117.2	4663600	"		
2FR18	"	124.1	2014300	Red.Cl.		
2FR19	"	124.1	1314700	"		
2FR21	"	193.1	127000	"	5.472	17.630
2FR27	"	124.1	1239800	"		
2FR28	"	193.1	137700	"		
2FR13	0.5	120.7	2505000	Nor.Cl.		
2FR20	"	124.1	3386600	"		
2FR22	"	127.6	227400	"		
2FR23	"	103.4	3045200	"	9.485	25.751
2FR24	"	120.7	604900	"		
2FR25	"	127.6	271700	"		
2FR26	"	120.7	1320100	"		

**Nor.Cl.---Normal Clamping in Rivets
Red.Cl.---Reduced Clamping in Rivets

Table 5-7: Result of Fatigue Tests on Double Lap Joints Bearing Ratio=1.83; from Reference [60]

Specimen Mark	Stress Ratio (R)	Stress Range (MPa)	Applied Cycles (Cycle)	Remark	S_r-N Curve Slope (m)	Intercept (Q)
3FR8	-1.0	220.6	1632600	Nor.Cl.		
3FR9	"	220.6	954700	"		
3FR10	"	220.6	695900	"		
3FR13	"	220.6	2535200	"		
3FR25	"	331.0	330600	"	3.896	15.205
3FR27	"	220.6	778800	"		
3FR29	"	331.0	159200	"		
3FR30	"	275.8	461800	"		
3FR31	"	275.8	681200	"		
3FR14	"	331.0	83000	Red.Cl.		
3FR22	"	331.0	123200	"	1.459	8.682
3FR28	"	220.6	182800	"		
3FR1	0.0	206.9	153900	Nor.Cl.		
3FR2	"	206.9	243700	"		
3FR3	"	206.9	114700	"		
3FR4	"	165.5	668300	"	9.597	27.405
3FR5	"	165.5	1317000	"		
3FR6	"	165.5	1160900	"		
3FR11	"	151.7	5104000	"		
3FR16	"	165.5	203500	Red.Cl.		
3FR19	"	206.9	71800	"	5.545	17.664
3FR20	"	117.2	1634500	"		
3FR12	0.5	134.5	4877500	Nor.Cl.		
3FR15	"	141.3	792700	"		
3FR17	"	131.0	1340400	"	10.70	29.063
3FR18	"	127.6	3581400	"		
3FR21	"	155.1	431000	"		
3FR23	"	155.1	66200	Red.Cl.		
3FR24	"	155.1	75800	"	6.743	19.621
3FR26	"	131.0	221200	"		

**Nor.Cl.---Normal Clamping in Rivets
Red.Cl.---Reduced Clamping in Rivets

Table 5-8: Result of Fatigue Tests on Double Lap Joints Bearing Ratio=1.37; from Reference [60]

Specimen Mark	Stress Ratio (R)	Stress Range (MPa)	Applied Cycles (Cycle)	Remark	S_r-N Curve Slope (m)	Intercept (Q)
4FR5	-1.0	275.8	168500	Nor.Cl.		
4FR9	"	220.6	391500	"		
4FR10	"	220.6	1142800	"		
4FR11	"	220.6	1012400	"	5.321	18.334
4FR16	"	358.5	52200	"		
4FR19	"	358.5	66200	"		
4FR15	"	193.1	1716200	Red.Cl.		
4FR24	"	331.0	52900	"		
4FR28	"	193.1	456400	"	5.074	17.546
4FR30	"	331.0	62400	"		
4FR1	0.0	206.9	563700	Nor.Cl.		
4FR2	"	206.9	266400	"		
4FR3	"	206.9	1758600	"		
4FR4	"	165.5	3730600	"	4.822	16.972
4FR6	"	165.5	1005200	"		
4FR8	"	172.4	1419400	"		
4FR13	"	124.1	943500	Red.Cl.		
4FR17	"	206.9	106200	"		
4FR20	"	206.9	185400	"	3.901	14.199
4FR25	"	151.7	609000	"		
4FR12	0.5	141.3	842300	Nor.Cl.		
4FR14	"	141.3	845700	"		
4FR21	"	134.5	1351800	"		
4FR26	"	158.6	256700	"	7.592	22.258
4FR27	"	137.9	979700	"		
4FR31	"	158.6	510900	"		
4FR18	"	158.6	98700	Red.Cl.		
4FR22	"	137.9	198400	"		
4FR23	"	124.1	419300	"	5.077	16.220
4FR29	"	158.6	134000	"		

**Nor.Cl.---Normal Clamping in Rivets
Red.Cl.---Reduced Clamping in Rivets

Table 5-9: Result of Fatigue Test on Riveted and Bolted Joint, Bearing Ratio=0.89; from Reference [48]

Specimen Mark	Stress Ratio (R)	Stress Range (MPa)	Applied Cycles (Cycle)	Remark	S_r-N Curve Slope (m)	Intercept (Q)
C-4	-1.0	275.8	183200	C.D.R.		
C-5	"	311.7	40200	"		
C-6	"	280.6	163400	"		
C-7	"	248.2	342900	"		
C-8	"	248.2	198900	"	5.424	18.363
C-9	"	248.2	317900	"		
C-10	"	216.5	443000	"		
C-11	"	213.7	1257300	"		
C-12	"	213.7	1441100	"		
A-7	"	275.8	228300	H.D.R		
A-8	"	283.4	200900	"		
A-9	"	280.6	197700	"		
A-10	"	250.3	236200	"	5.788	19.478
A-11	"	248.2	490000	"		
A-12	"	248.2	562900	"		
D-7	"	275.8	338900	Bolt.J.		
D-8	"	275.8	574600	"		
D-9	"	280.0	360700	"		
D-10	"	257.9	1181300	"		
D-11	"	248.2	1061100	"	5.123	18.229
D-12	"	248.2	1400600	"		
D-13	"	281.3	326400	"		
D-14	"	277.9	810500	"		
D-15	"	206.9	1640900	"		

**C.D.R. --- Cold Driven Rivets
H.D.R. --- Hot Driven Rivets
Bolt.J.--- Bolted Joint

Table 5-10: Result of Fatigue Test on Riveted Joint ; from Reference [78]

Specimen Mark	Stress Ratio (R)	Stress Range (MPa)	Applied Cycles (Cycle)	Remark	S_r-N Curve Slope (m)	Intercept (Q)
Riveted Joints with 0.84-1.50 Bearing Ratio						
B12-6	0.0	275.8	165000			
B12-2	"	241.3	424000	"		
B12-4	"	206.9	1028000	"		
B12-1	"	241.3	284000	"		
B12-10	"	193.1	594000	"		
B13-1	"	241.3	339000	"		
B13-2	"	227.5	361000	"		
B13-3	"	206.9	812000	"		
B14-1	"	241.3	482000	"		
B14-2	"	227.5	632000	"		
B14-3	"	206.9	1874000	"		
B34-1	"	206.9	530000	"		
B34-2	"	179.3	1814000	"		
B34-3	"	186.2	1257000	"		
B16-1	"	193.1	414000	"		
B16-2	"	172.4	1395000	"	3.647	14.256
B16-3	"	165.5	1345000	"		
B17-1	"	206.9	520000	"		
B17-2	"	193.1	760000	"		
B17-3	"	172.4	715000	"		
B18-1	"	227.5	315000	"		
B18-2	"	206.9	1089000	"		
B18-3	"	193.1	448000	"		
B19-1	"	206.9	1221000	"		
B19-2	"	220.6	647000	"		
B19-3	"	200.0	961000	"		
B20-1	"	206.9	2311000	"		
B20-2	"	227.5	527000	"		
B20-3	"	217.2	904000	"		
B7-1	"	206.9	302000	"		
B7-2	"	193.1	407000	"		
B7-3	"	172.4	865000	"		
B27-1	"	227.5	125000	"		
B27-2	"	206.9	510000	"		
B27-3	"	186.2	1520000	"		

(Table 5-10 is Continued)

Specimen Mark	Stress Ratio (R)	Stress Range (MPa)	Applied Cycles (Cycle)	Remark	S_r-N Curve Slope (m)	Intercept (Q)
Riveted Joints with 0.84-1.26 Bearing Ratio						
B12-3	-1.0	413.7	66000	Nor.Cl.		
B12-5	"	386.1	75000	"	5.325	18.717
B12-11	"	344.8	171000	"		
B12-12	"	275.8	521000	"		
B12-7	0.5	137.9	1244000	Nor.Cl		
B12-8	"	155.1	889000	"	5.046	16.967
B12-9	"	124.1	2765000	"		
Riveted Joints with Very High Bearing Ratio (B=4.90)						
B1-1	0.0	117.2	46000	"		
B1-2	"	102.7	1217000	"		
B1-3	"	88.9	2276000	"		
B31-1	"	102.7	679000	"		
B31-2	"	117.2	517000	"		
B31-3	"	87.6	1714000	"	9.391	24.801
B32-1	"	117.2	225000	"		
B32-2	"	102.7	2087000	"		
B32-3	"	111.7	1389000	"		
B33-1	"	117.2	109000	"		
B33-2	"	102.7	2089000	"		
B33-3	"	111.7	186000	"		
Plates with Mill Scale with neither Hole nor Joints						
B37-1	0.0	206.9	3036000	Carbon		
B37-2	"	234.4	725000	"	11.59	33.217
B37-3	"	220.6	655000	"		
Plates with Mill Scale with Drilled Hole But no Joints						
B38-1	0.0	158.6	703000	Carbon		
B38-2	"	227.5	62000	"	6.247	19.533
B38-3	"	137.9	1332000	"		

Table 5-11: Fatigue Crack Initiation, Propagation and Total Life of Riveted Details under Constant Stress Range (Tension only)

Riveted Built-up Member (Detail 1) ($Nx10^3$)

Details	S_r=137.9 MPa (20 ksi)			S_r=275.8 MPa (40 ksi)		
	N_i	N_g	N_T	N_i	N_g	N_T
P4G6	15500	752	16200	200	94.1	294.1
P6G6	12000	590	12600	156	73.8	229.8
P8G6	11500	518	12000	149	64.8	213.8
P12G6	7360	400	77600	95.3	50.0	145.3
P6G4	13800	649	14500	179	81.1	260.1
P6G5	12800	639	13400	166	79.7	245.9
P6G6	12000	590	12600	156	73.8	229.8
P6G8	9580	527	10100	124	65.9	189.8

Riveted Truss Joint (Detail 2) ($Nx10^3$)

Details	S_r=137.9 MPa (20 ksi)			S_r=275.8 MPa (40 ksi)		
	N_i	N_g	N_T	N_i	N_g	N_T
B166	1340	351	1690	17.4	43.9	61.3
B209	386	306	692	5.0	38.3	43.3
B279a	260	272	532	3.4	34.0	37.4
B279b	301	317	619	3.9	39.7	43.6
B285	231	262	493	3.0	32.8	35.8

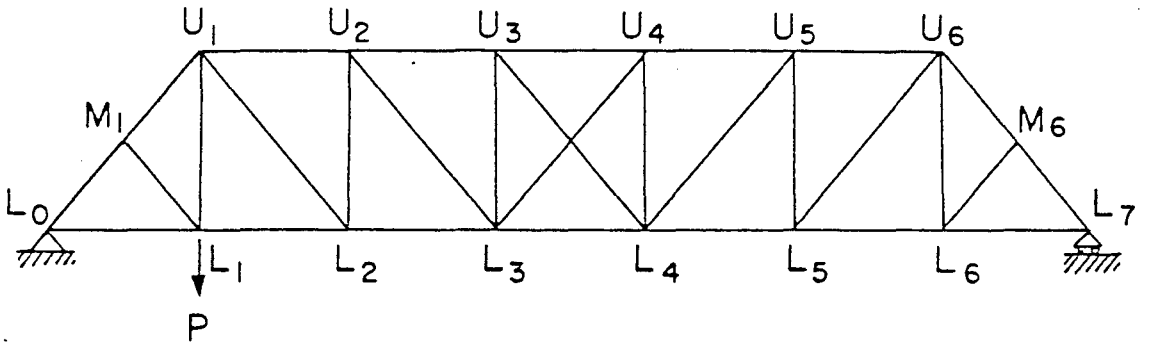

(a) Two-Dimensional Model

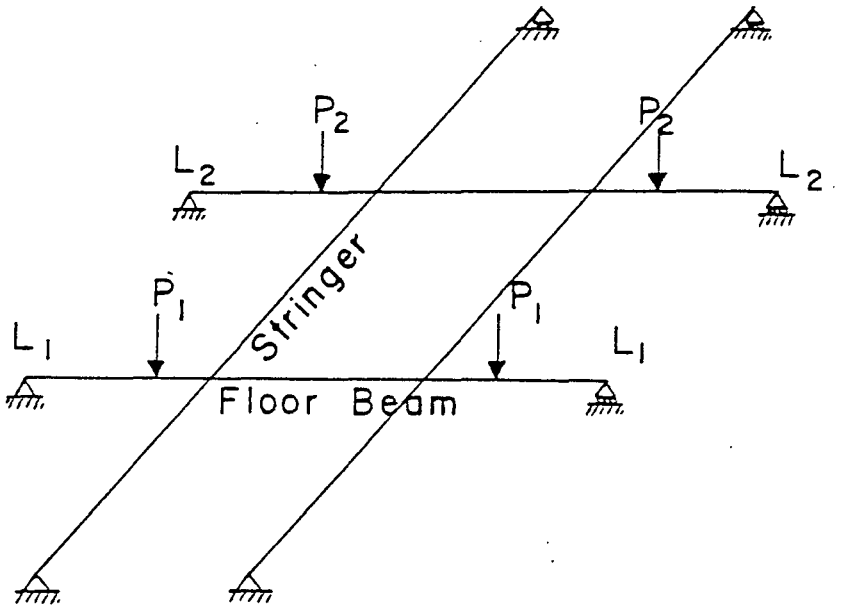

(b) Floor System Model

Fig. 2.1 Typical Finite Element Mesh for Two-Dimensional Model

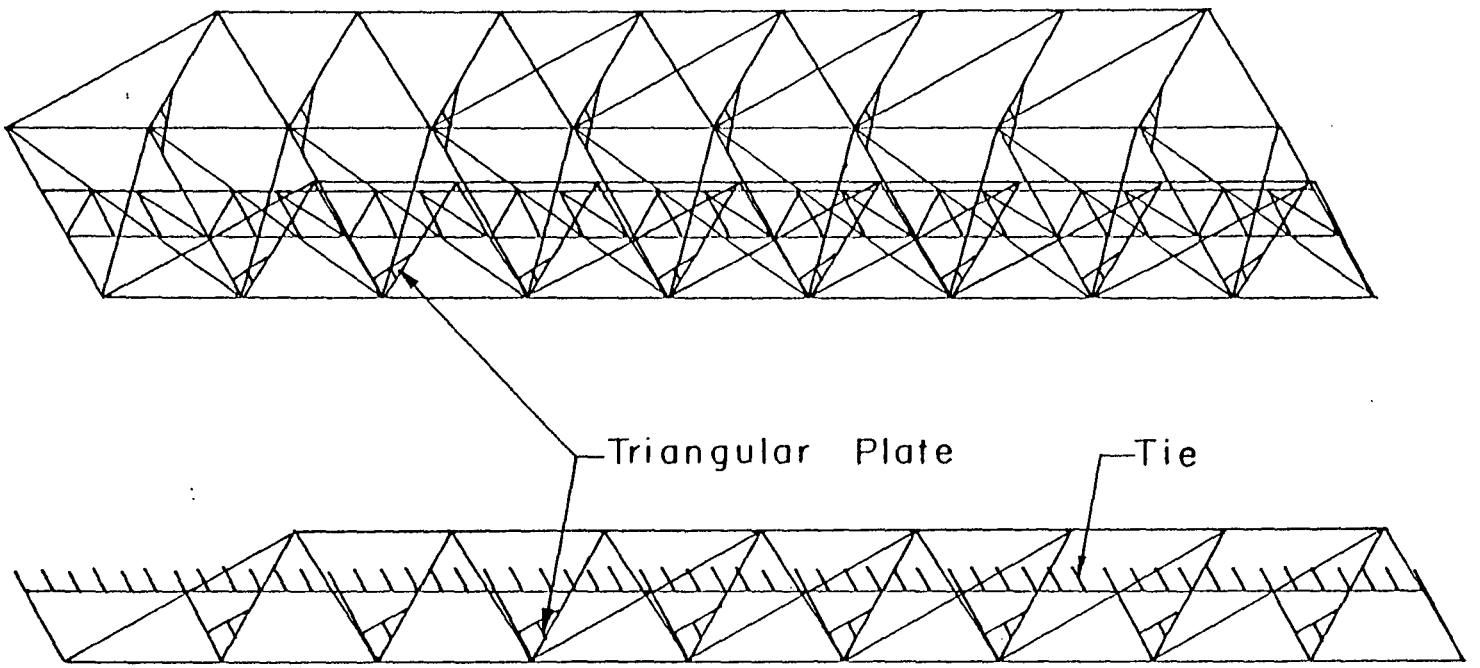

Fig. 2.2 Three-Dimensional Space Frame Model of Kohr Mog Bridge in Sudan Railway

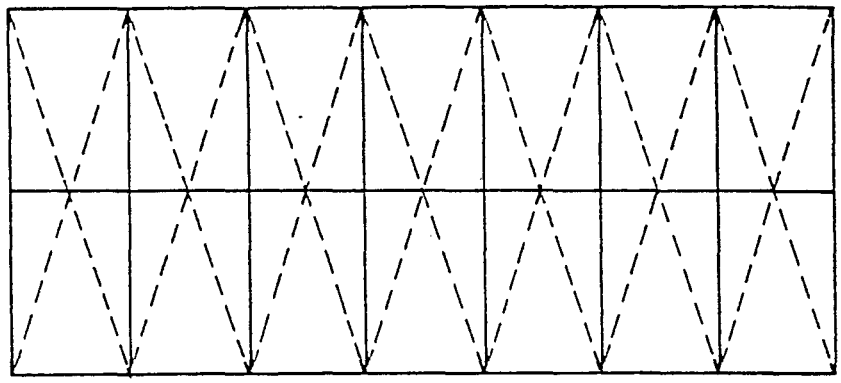

Top Bracing System

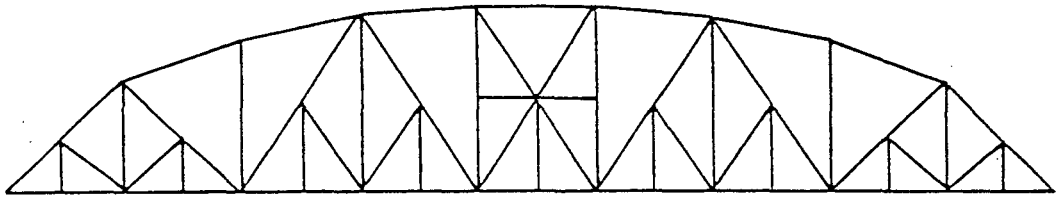

East and West Trusses

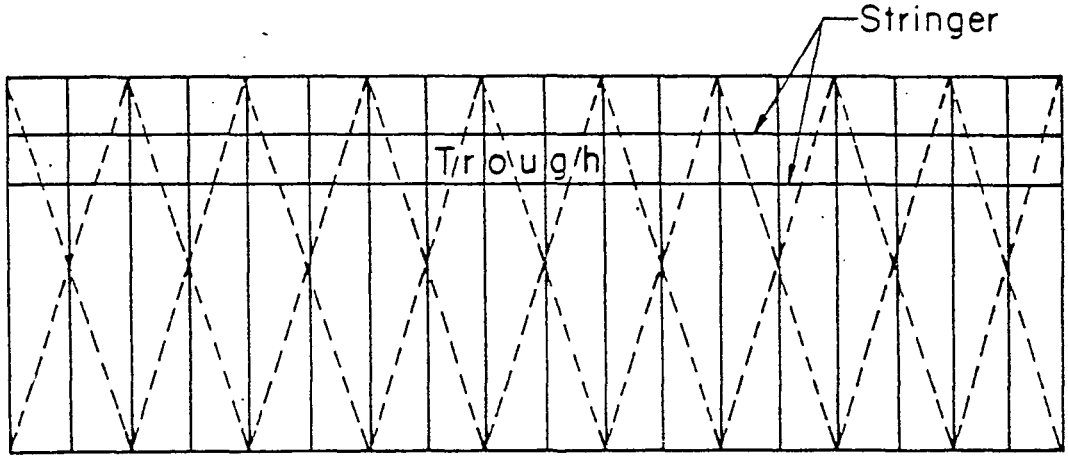

Floor System

Fig. 2.3 Three-Dimensional Space Frame Model of Kartoum Bridge in Sudan Railway

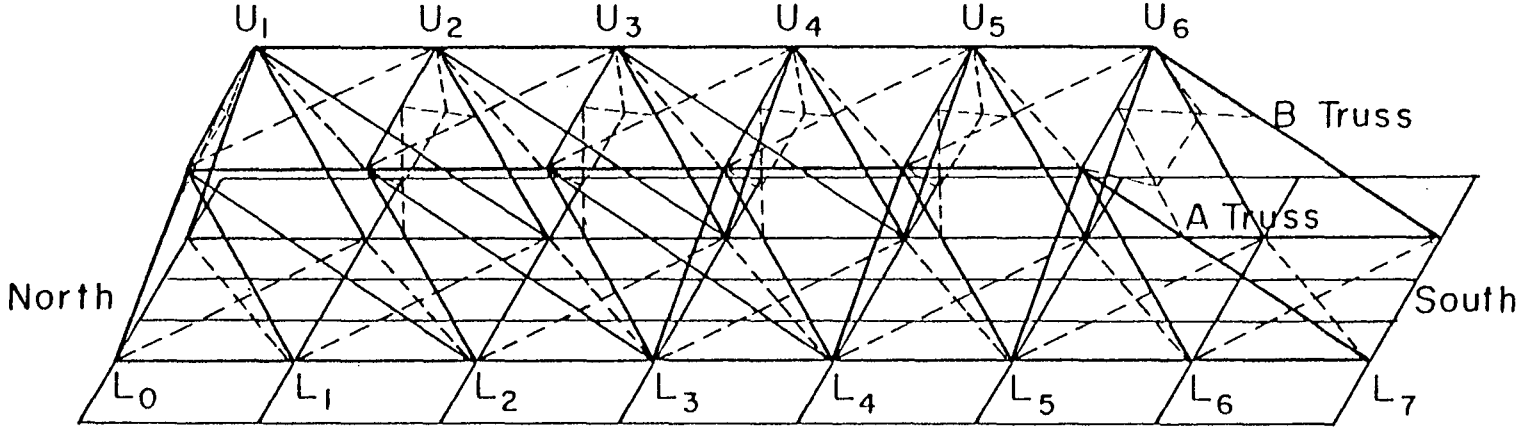

Fig. 2.4 Three-Dimensional Space Frame Model of Atbara Bridge in Sudan Railway

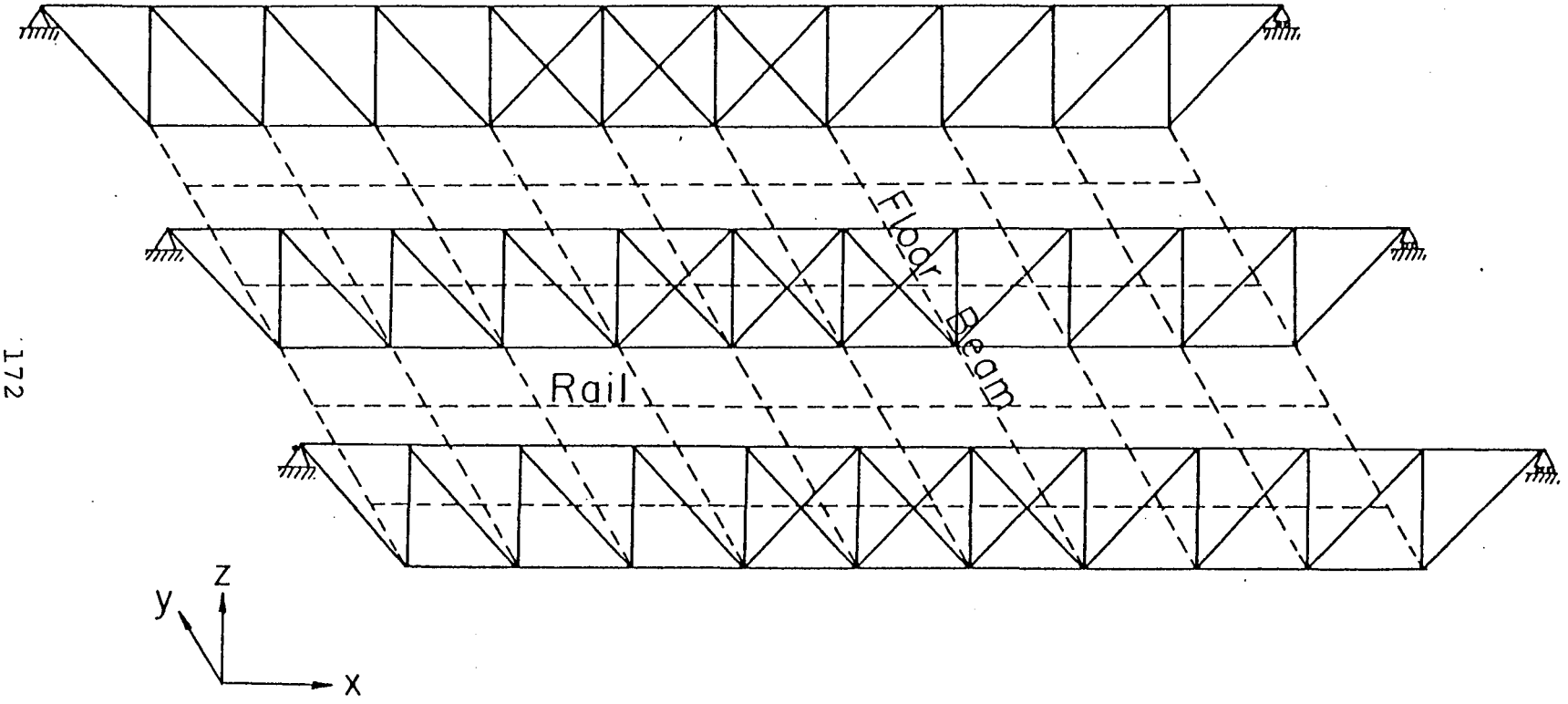

Fig. 2.5 Three-Dimensional Space Frame Model of Frankford Elevated Line Viaduct Trusses

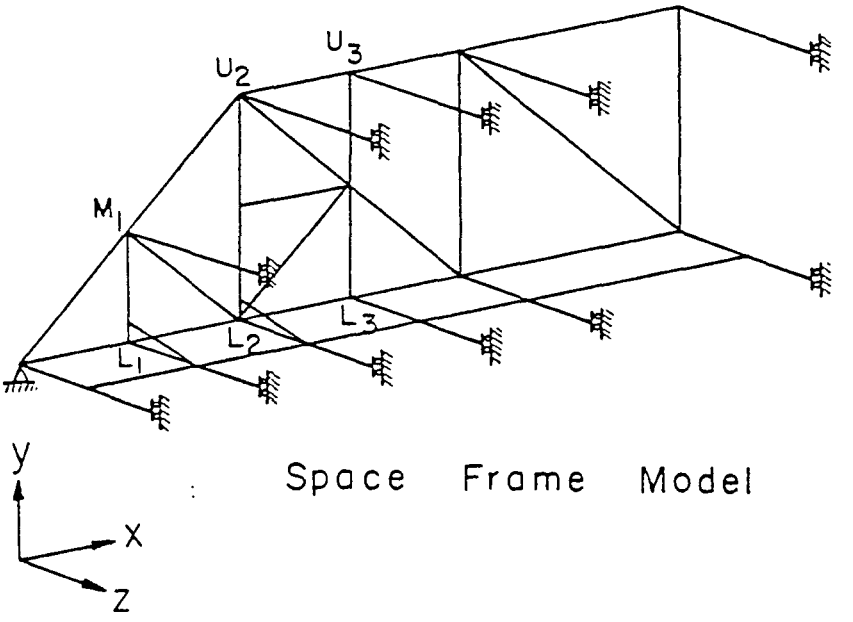

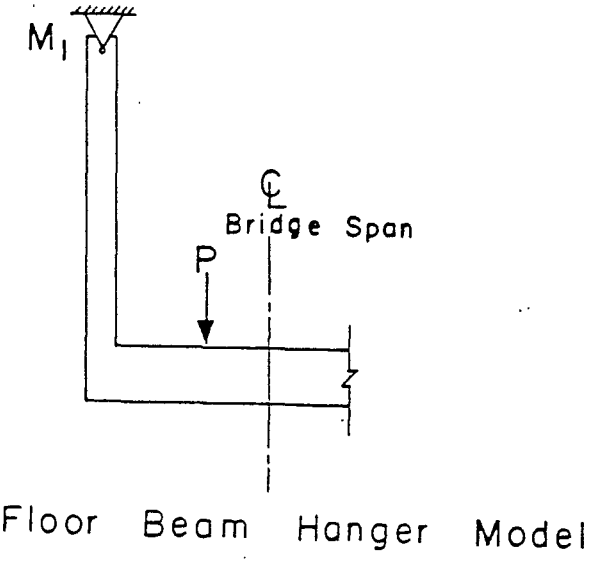

Fig. 2.6 Three-Dimensional Space Frame Model of Fraser River Bridge in British Columbia, Canada

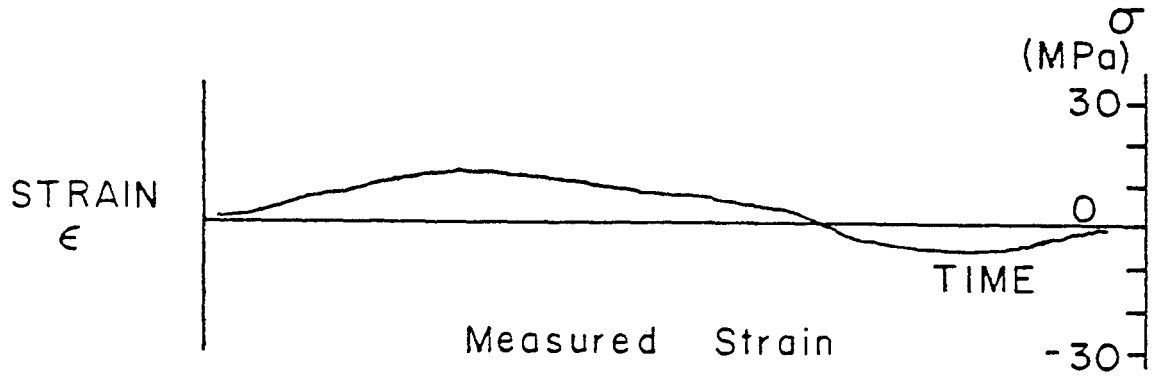

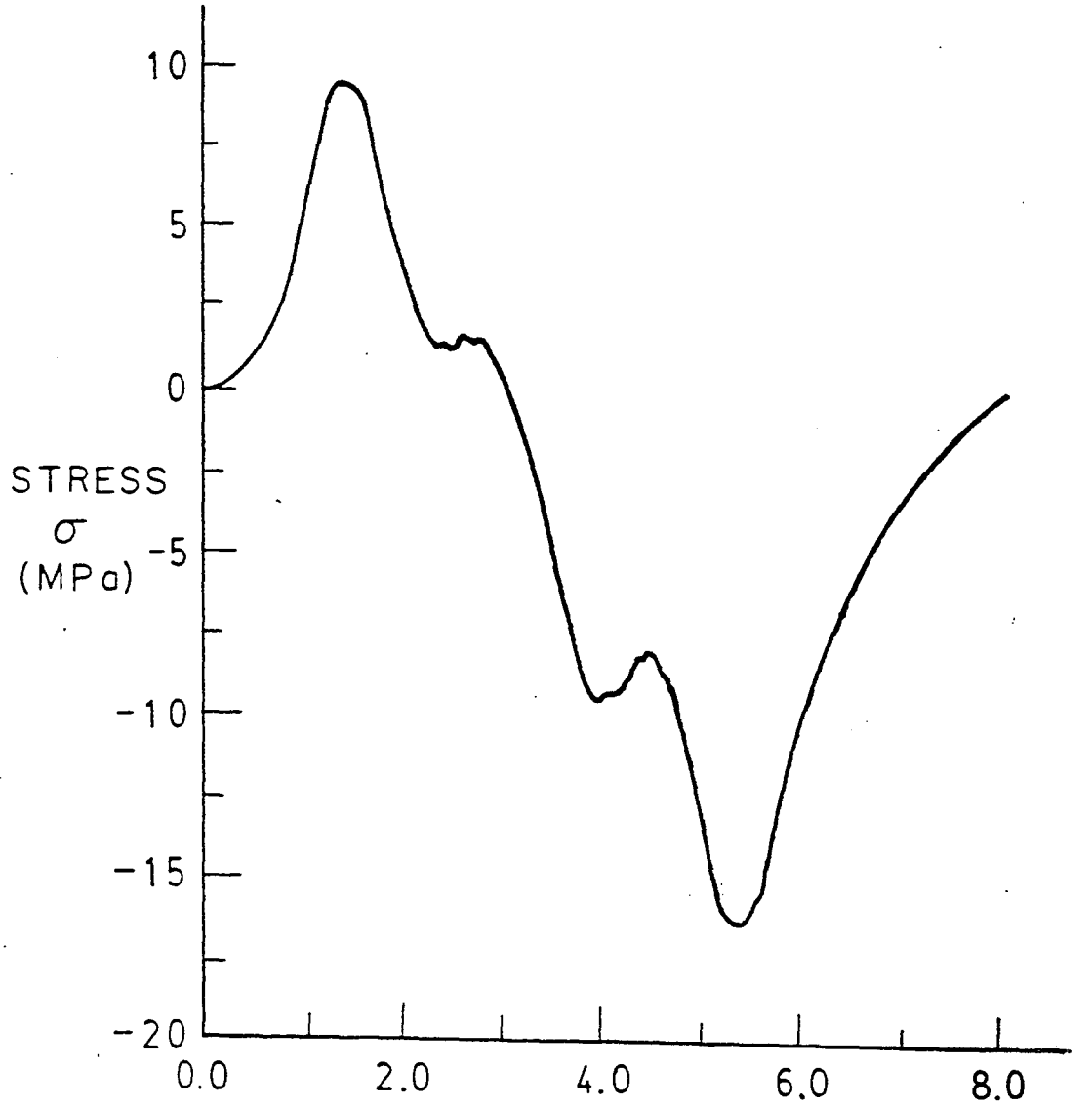

Figure 2-7: Stress-Time Relationship of Hanger in Kosti Bridge

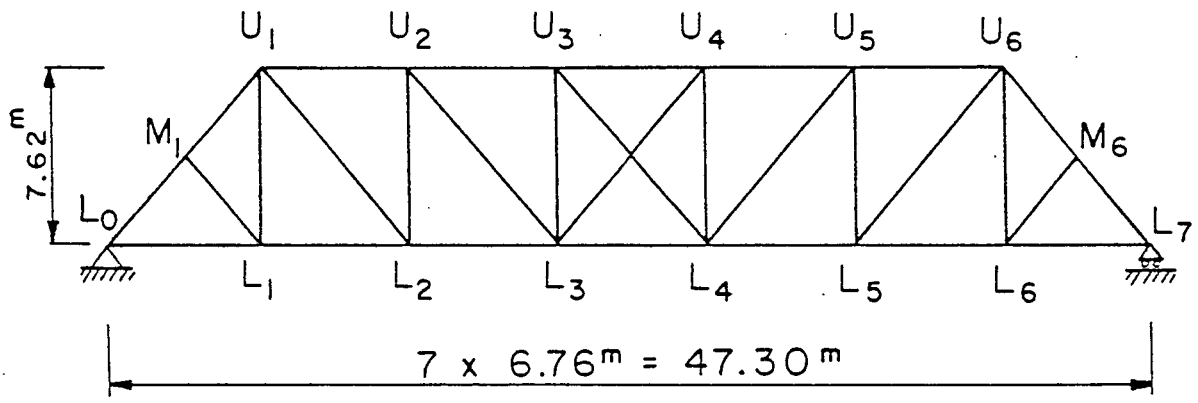

Typical Elevation

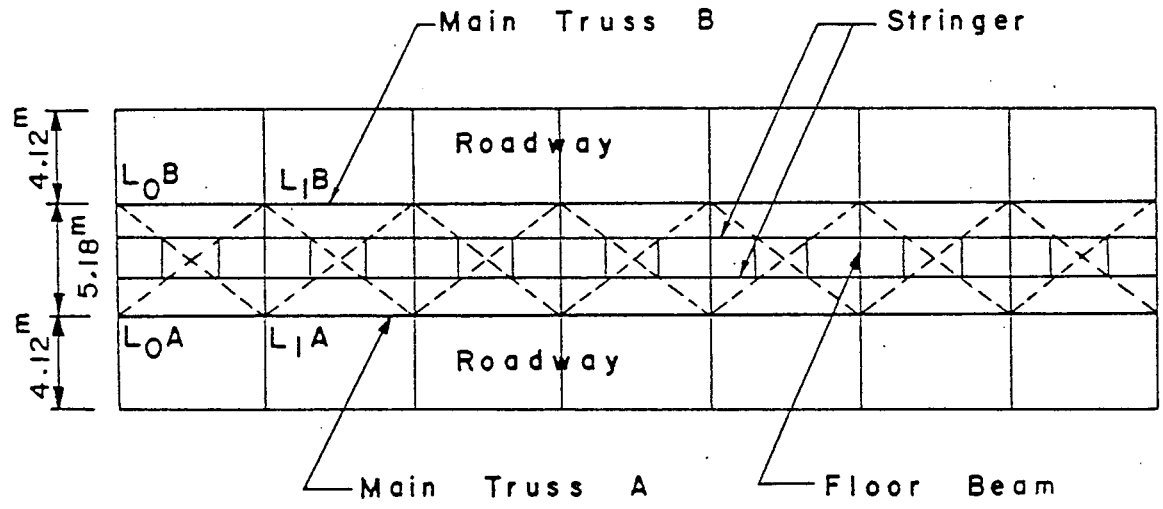

Typical Plan

Fig. 2.8 Plan and Elevation of Kosti Bridge in Sudan Railway

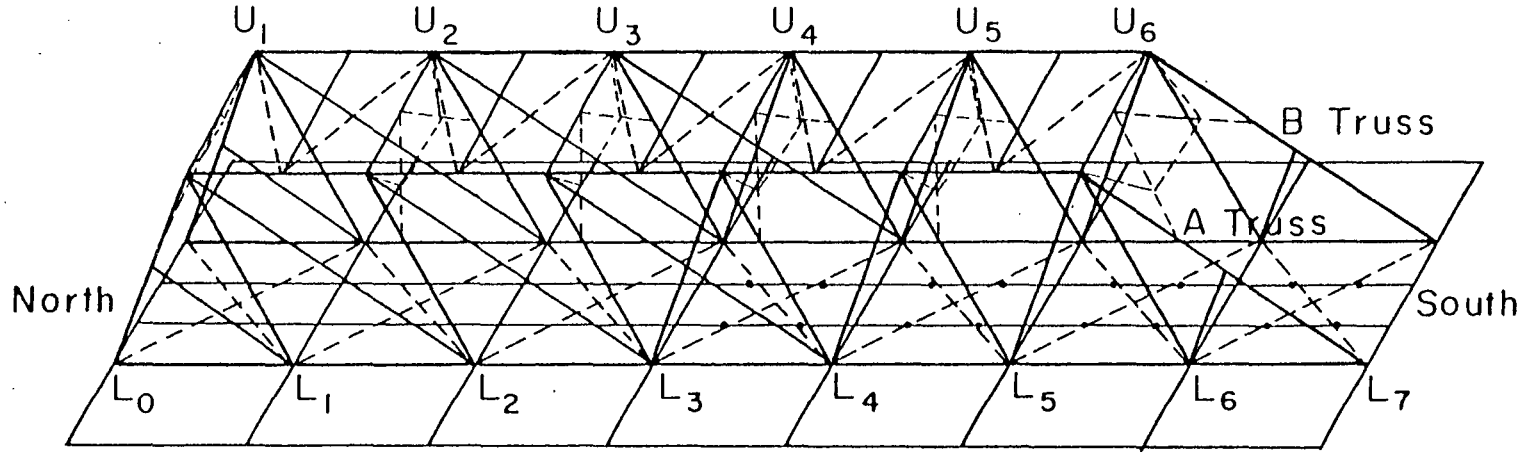

Fig. 2.9 Three-Dimensional Space Frame Model of Kosti Bridge in Sudan Railway

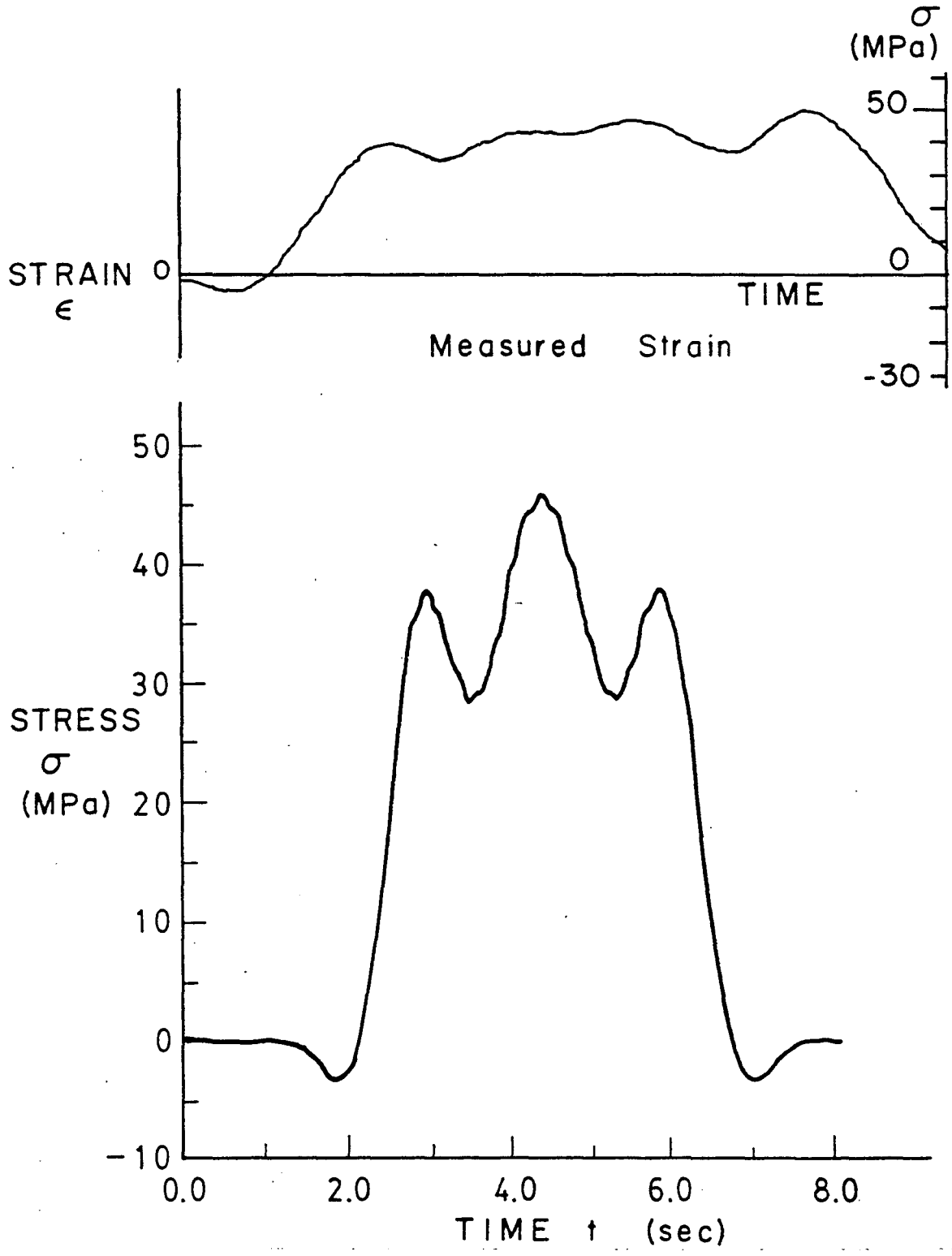

Fig. 2.10 Stress-Time Relationship of Floor Beam in Kosti Bridge

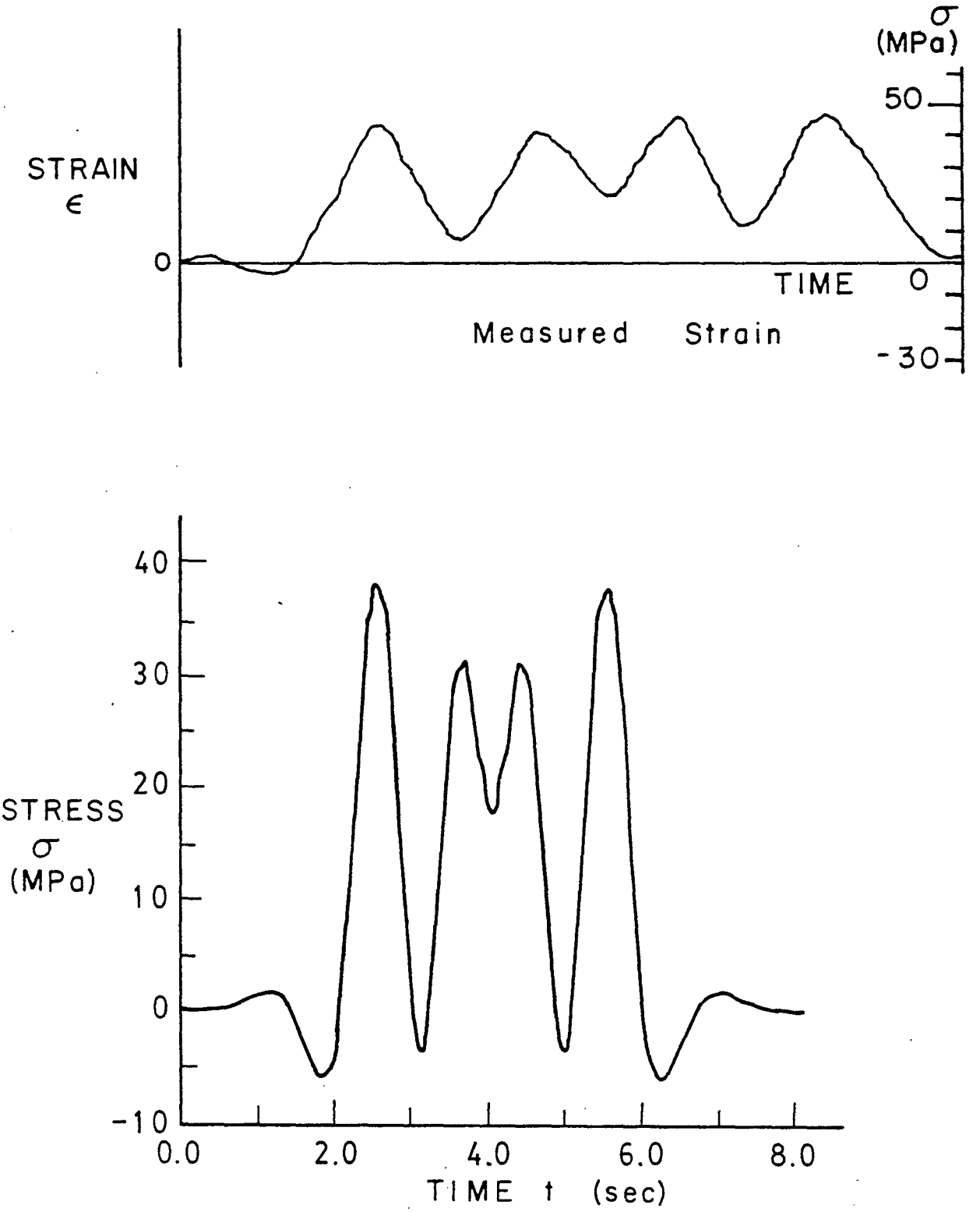

Fig. 2.11 Stress-Time Relationship of Stringer in Kosti Bridge

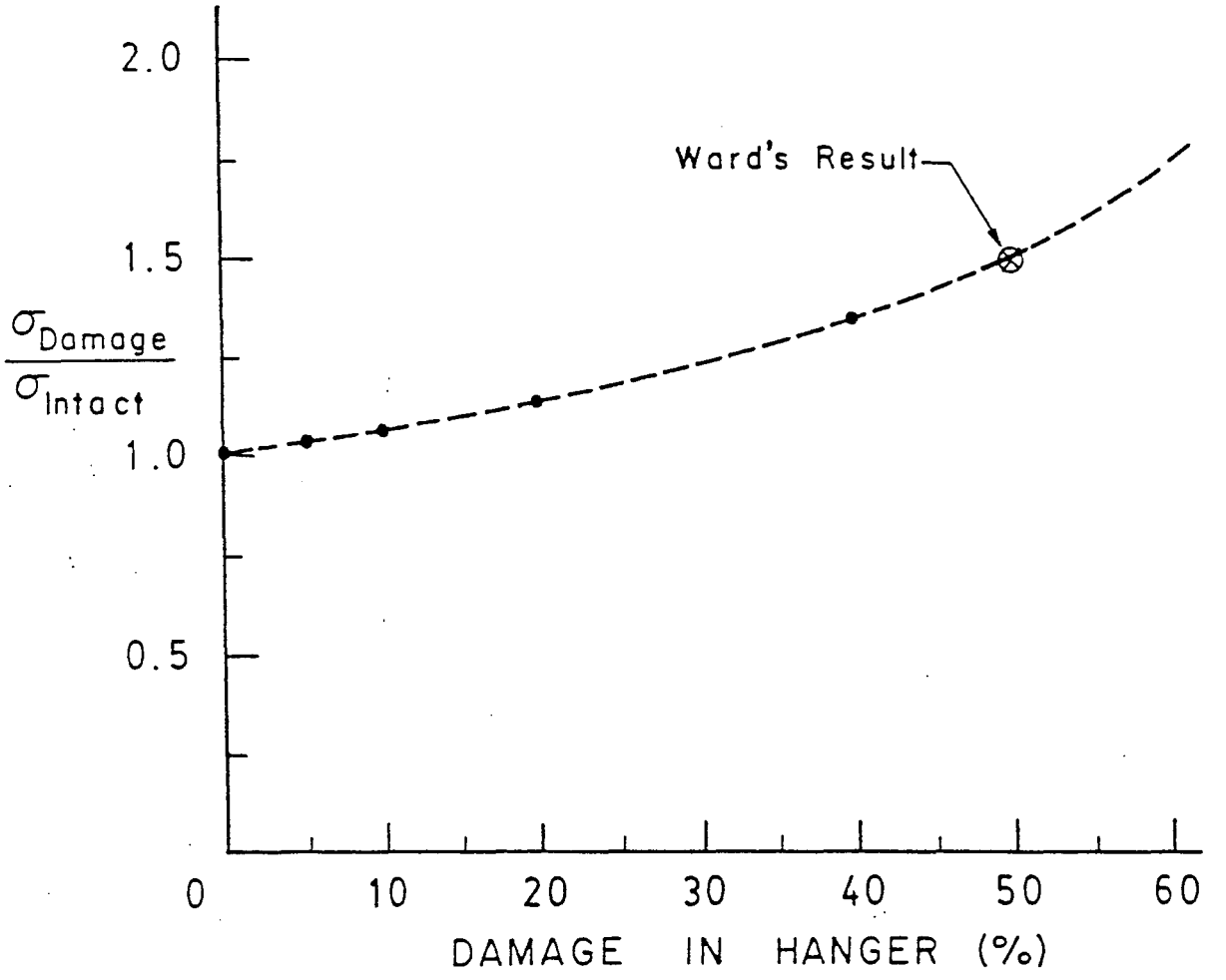

Fig. 2.12 Stress Variation due to Damage in Member Cross-Section

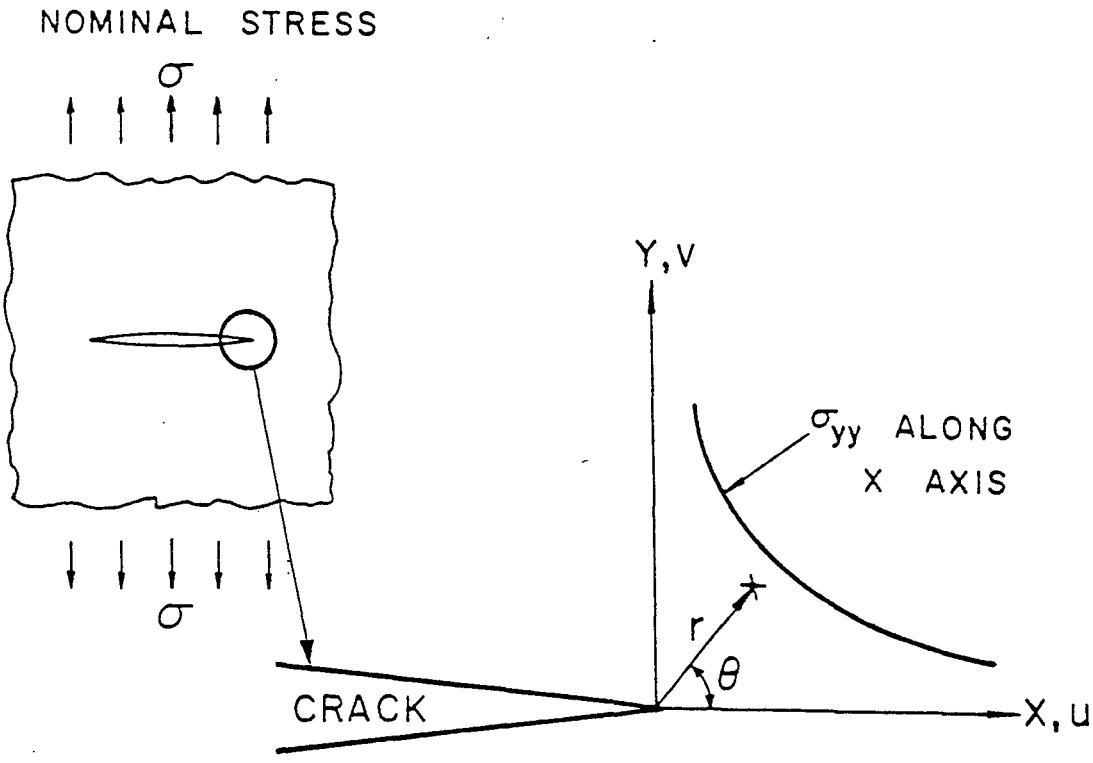

$$\sigma = \frac{K}{\sqrt{2\pi r}} f(\theta) \quad : \quad \frac{1}{\sqrt{r}} \text{ SINGULARITY}$$

$$u = \frac{K}{G}\sqrt{\frac{r}{2\pi}}\, g(\theta) \quad : \quad \sqrt{r} \text{ VARIATION}$$

Fig. 3.1 Coordinates, Displacement and Stress Field Ahead of a Crack Tip

BYSKOV (1970)	Cracked Triangle Displacement Formulation	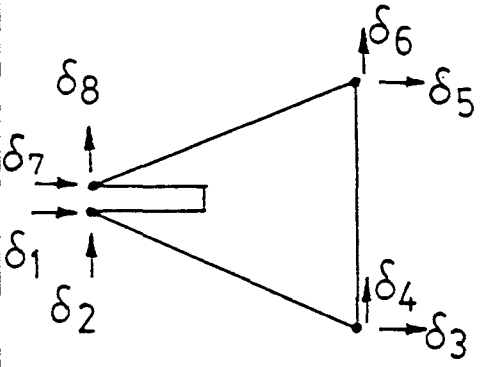
TONG and PIAN (1973)	Special Super Element Hibrid Formulation	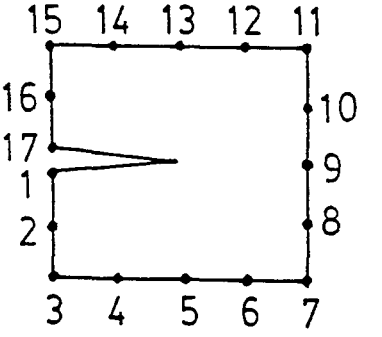
BENZLEY (1974)	Enriched Element Displacement Formulation	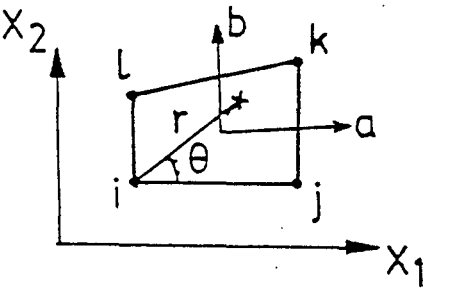 $U_i = \alpha i_1 + \alpha i_2 a + \alpha i_3 b + \alpha i_4 ab$ $+ K_I Q_{1i}(r,\theta) + K_{II} Q_{2i}(r,\theta)$

Fig. 3.2 Singular Elements by Byskov, Tong and Pian, and Benzley

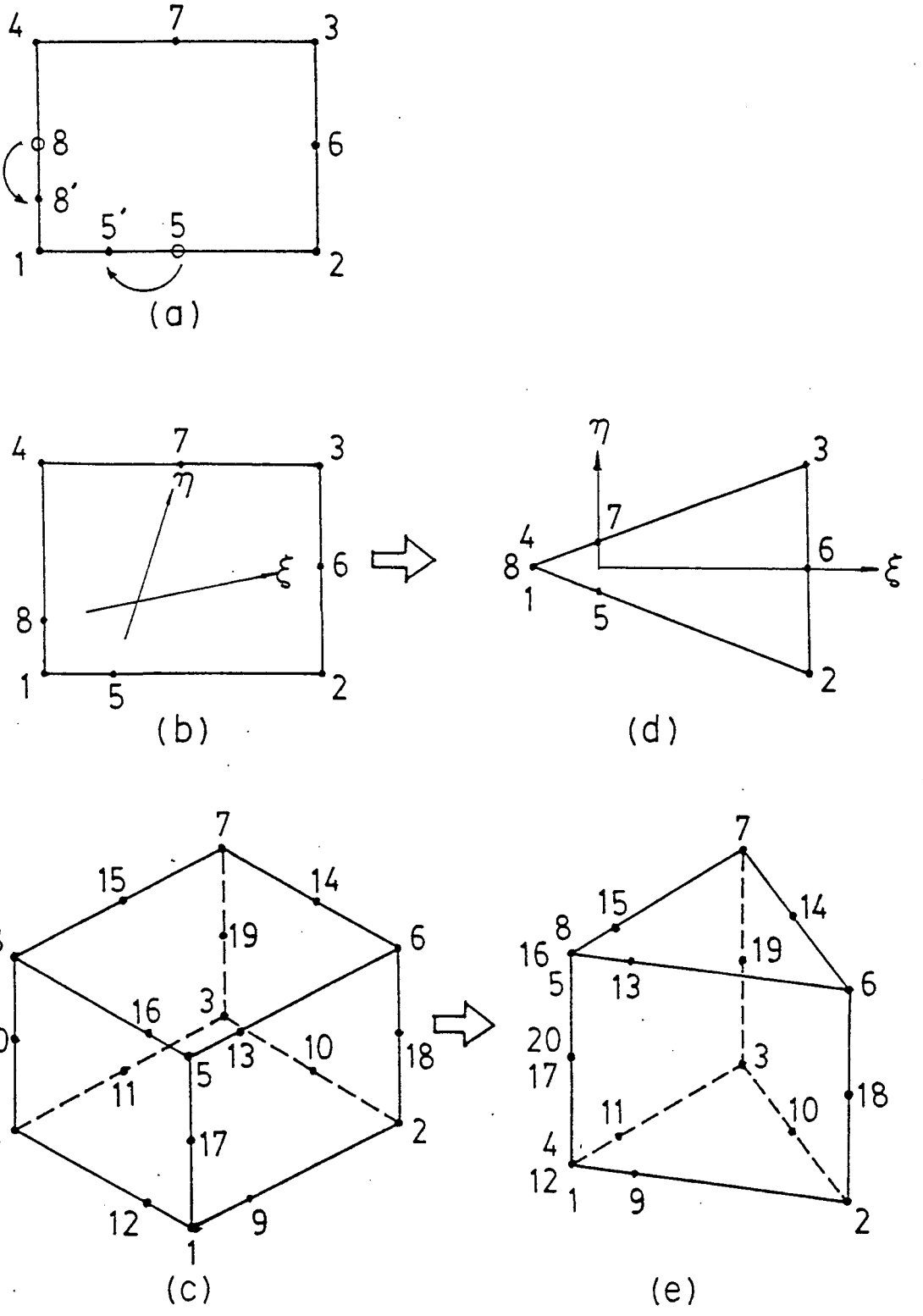

Fig. 3.3 Henshell and Barsoum's Quarter-point Isoparametric Elements
(a,b,c) Original Singular Element
(d,e) Degenerated Singular Element

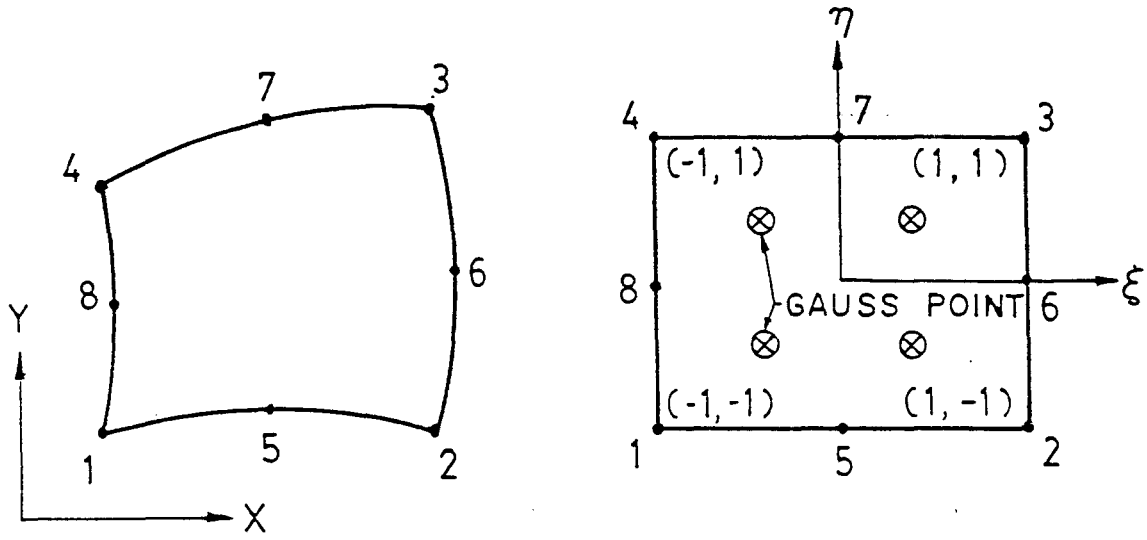

(a) REGULAR ELEMENT

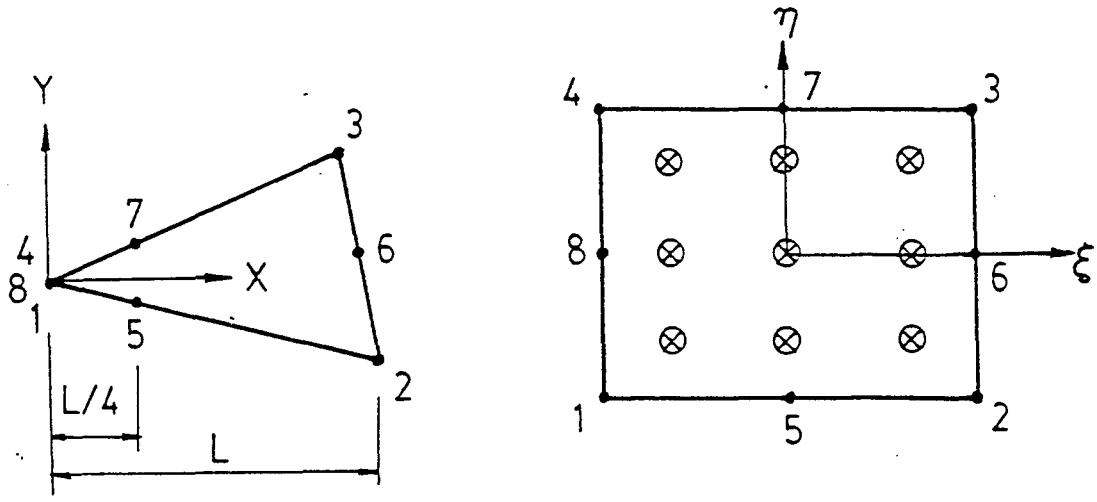

(b) DEGENERATED SINGULAR ELEMENT

Fig. 3.4 Isoparametric Quadratic Two-Dimensional Elements

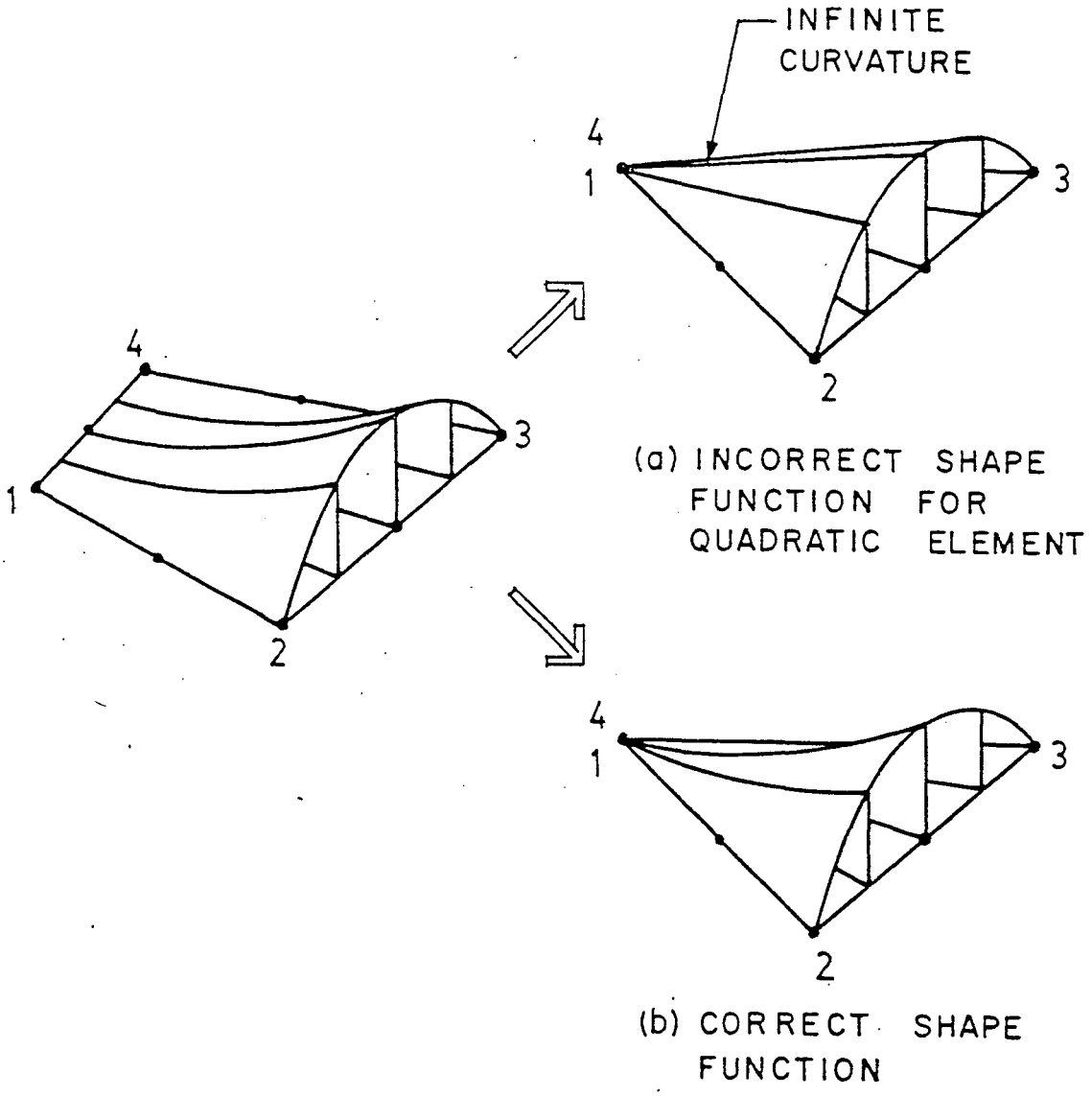

Fig. 3.5 Degeneration of Quadrilateral to Triangle

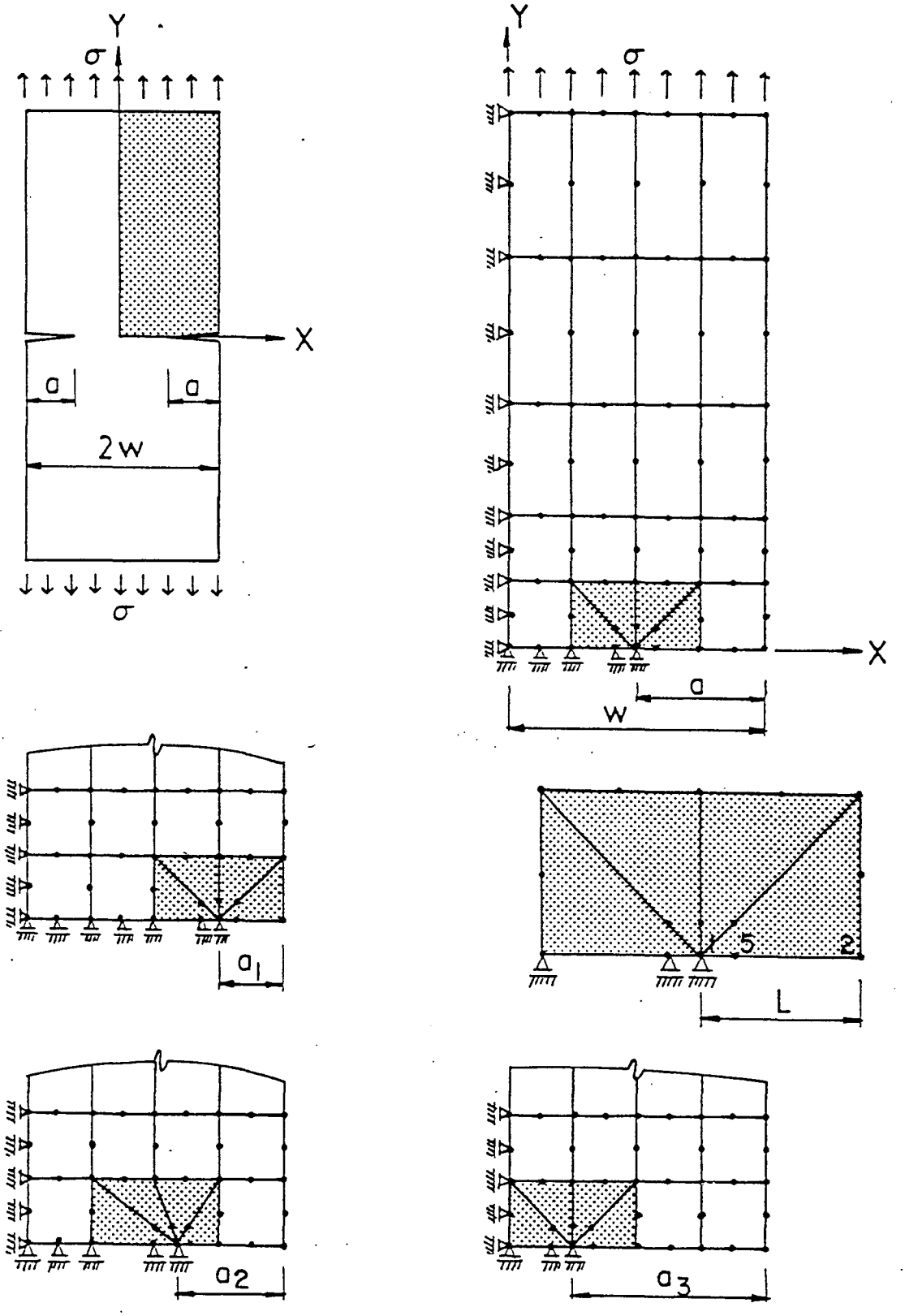

Fig. 3.6 Finite Element Mesh Along the Crack Line

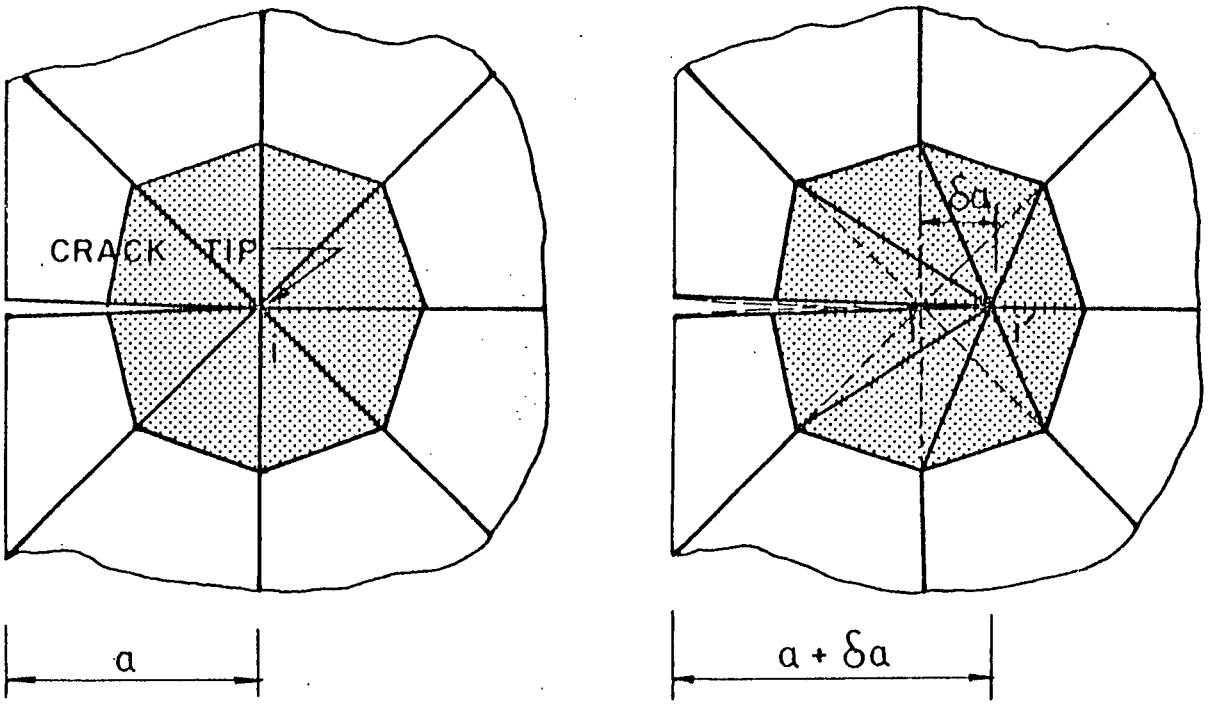

(a) ORIGINAL CRACK GEOMETRY

(b) CRACK GEOMETRY AFTER VIRTUAL CRACK EXTENTION

Fig. 3.7 Change of Geometry due to Virtual Crack Extension δa

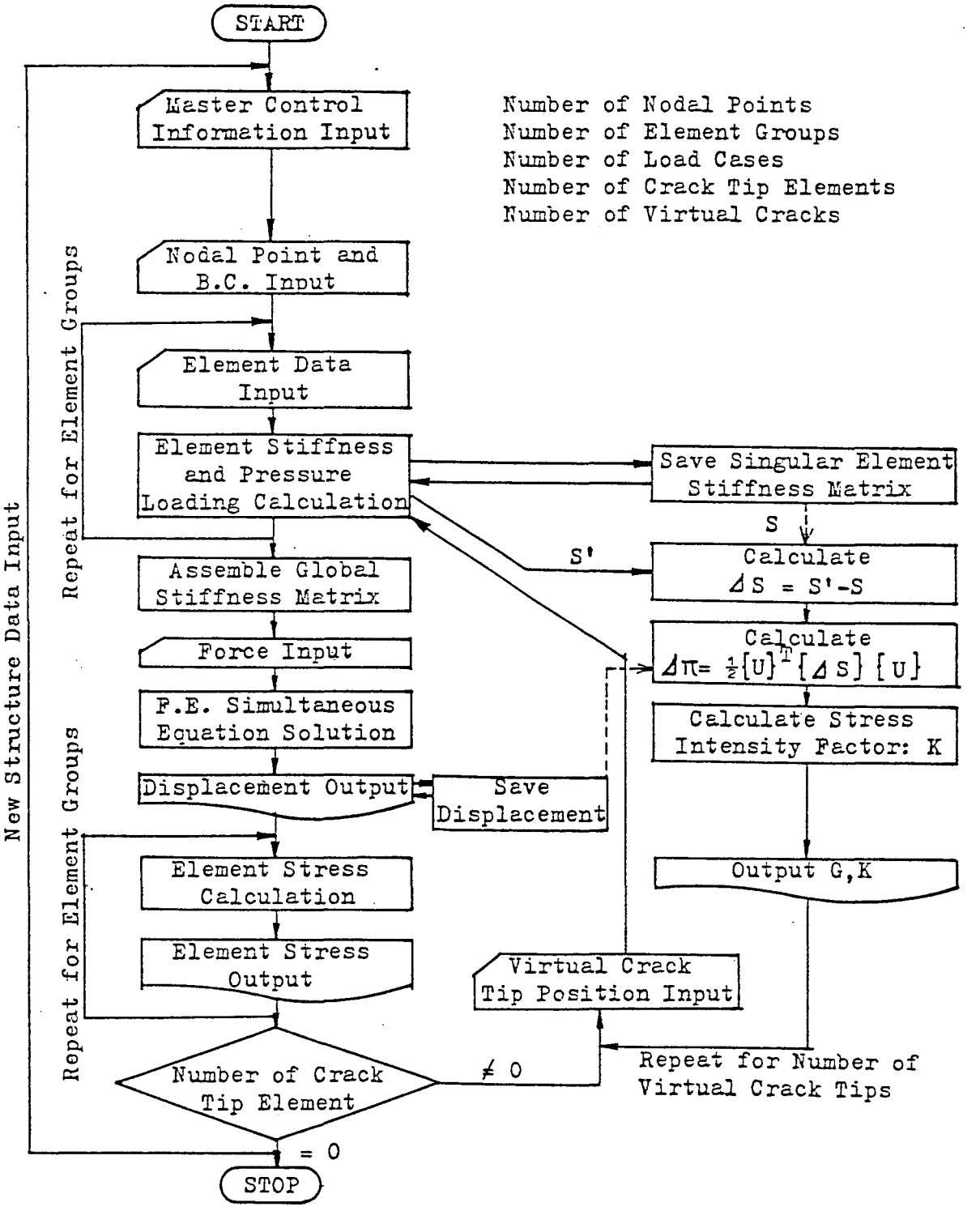

Fig. 3.8 Flow Diagram of Computer Program QIFEVCEM

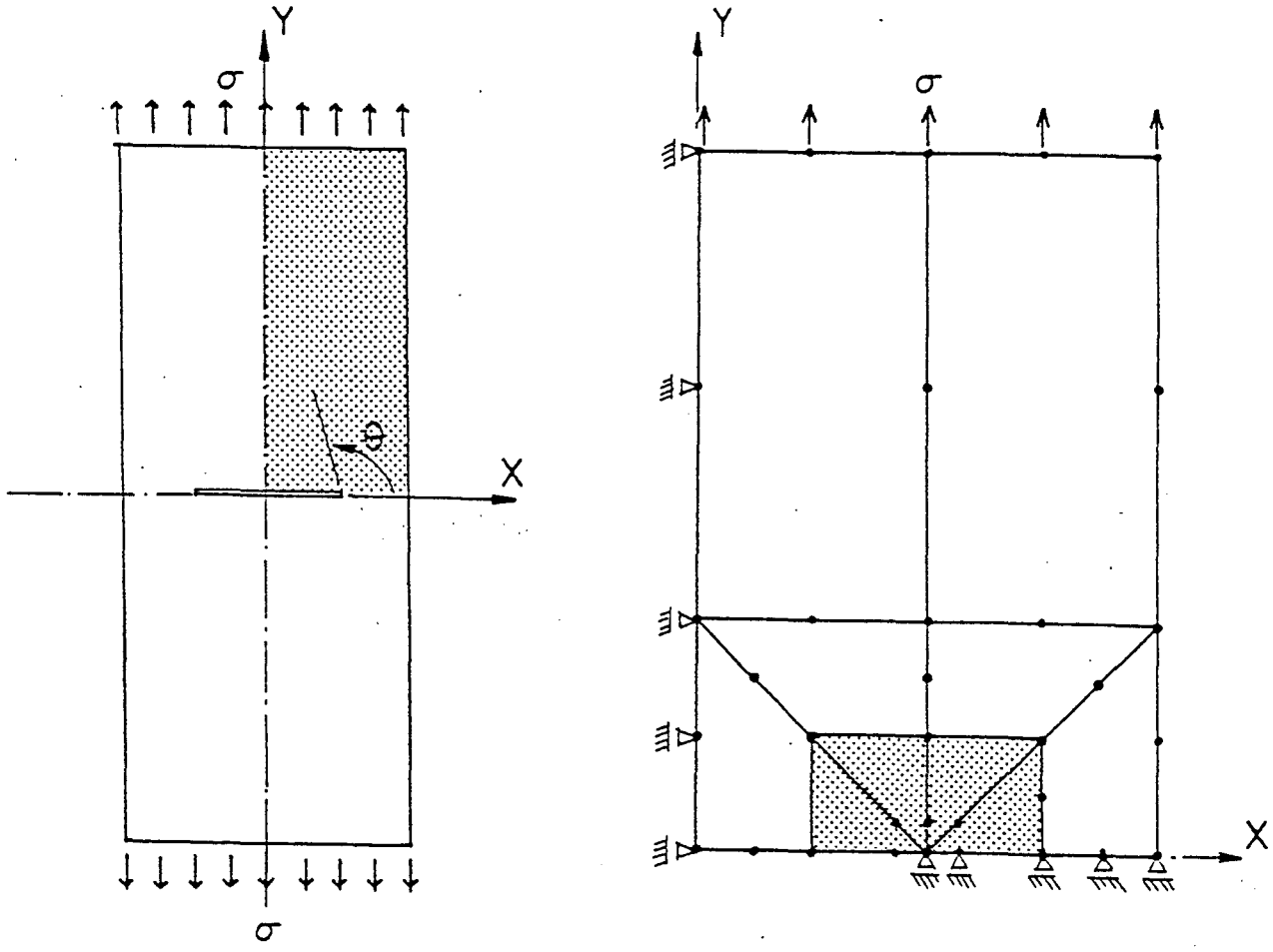

Fig. 3.9 Modeling fir Center-Through Crack

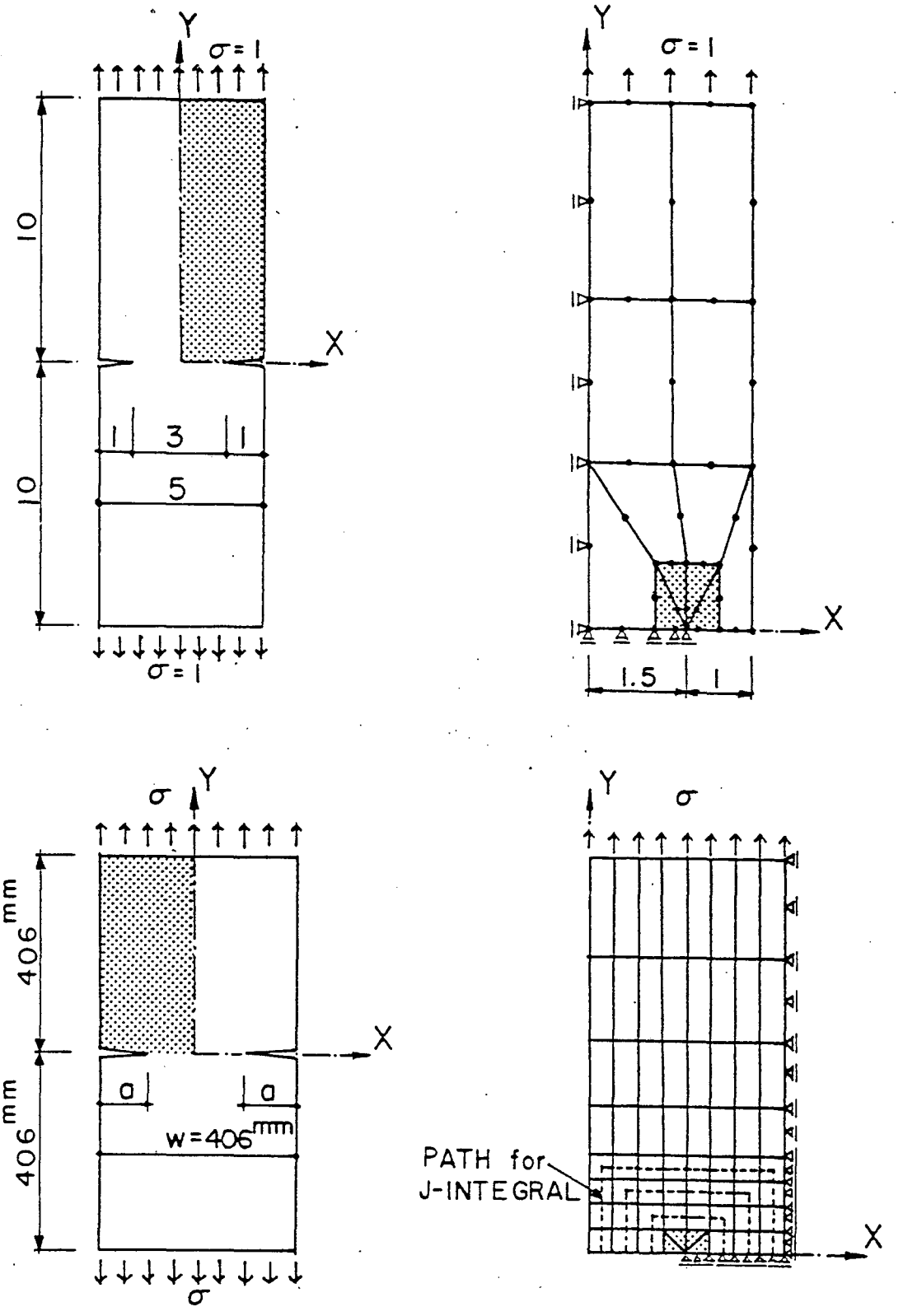

Fig. 3.10 Modeling for Double-Edge Crack

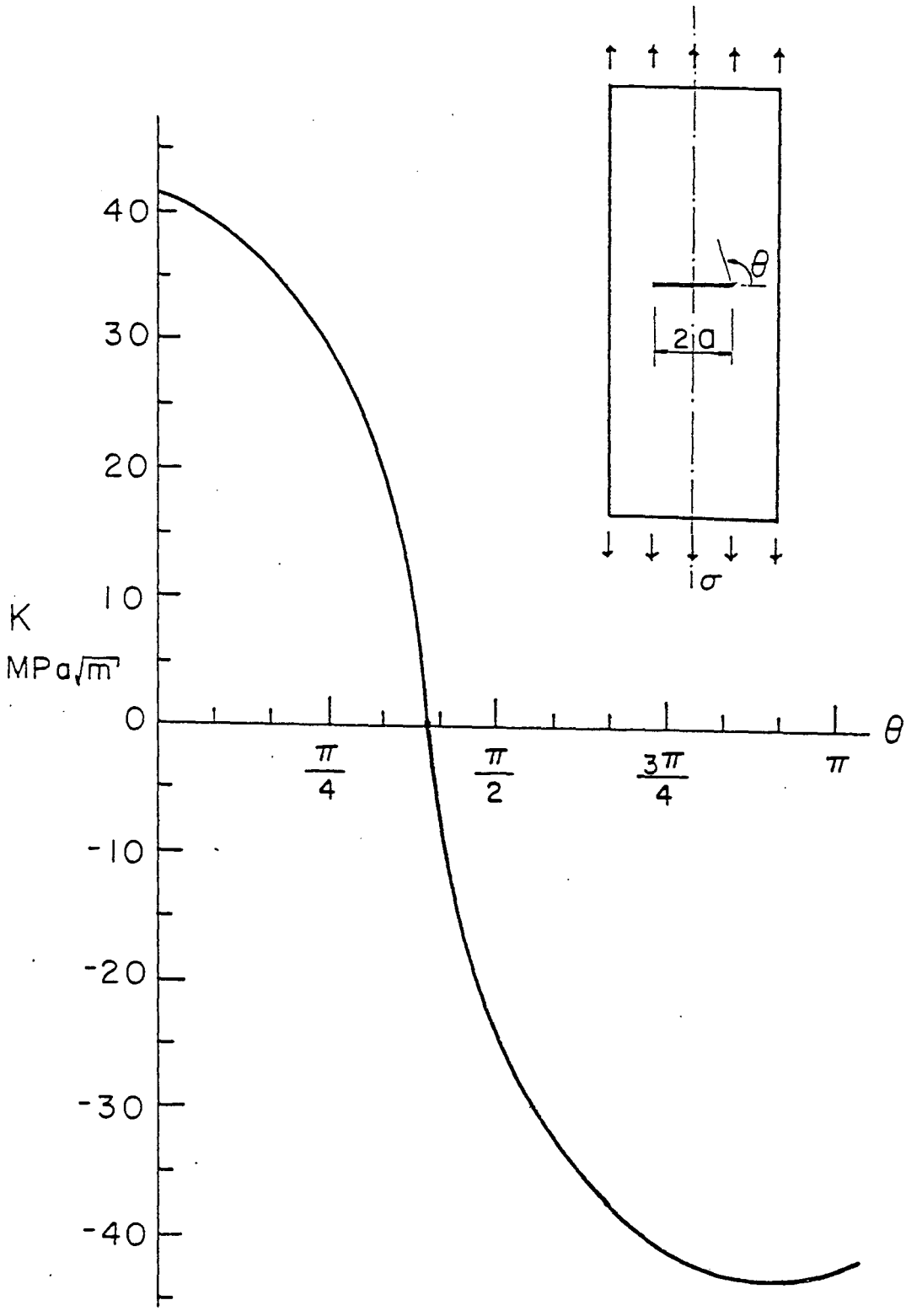

Fig. 3.11 Stress-Intensity Factor around the Crack Tip

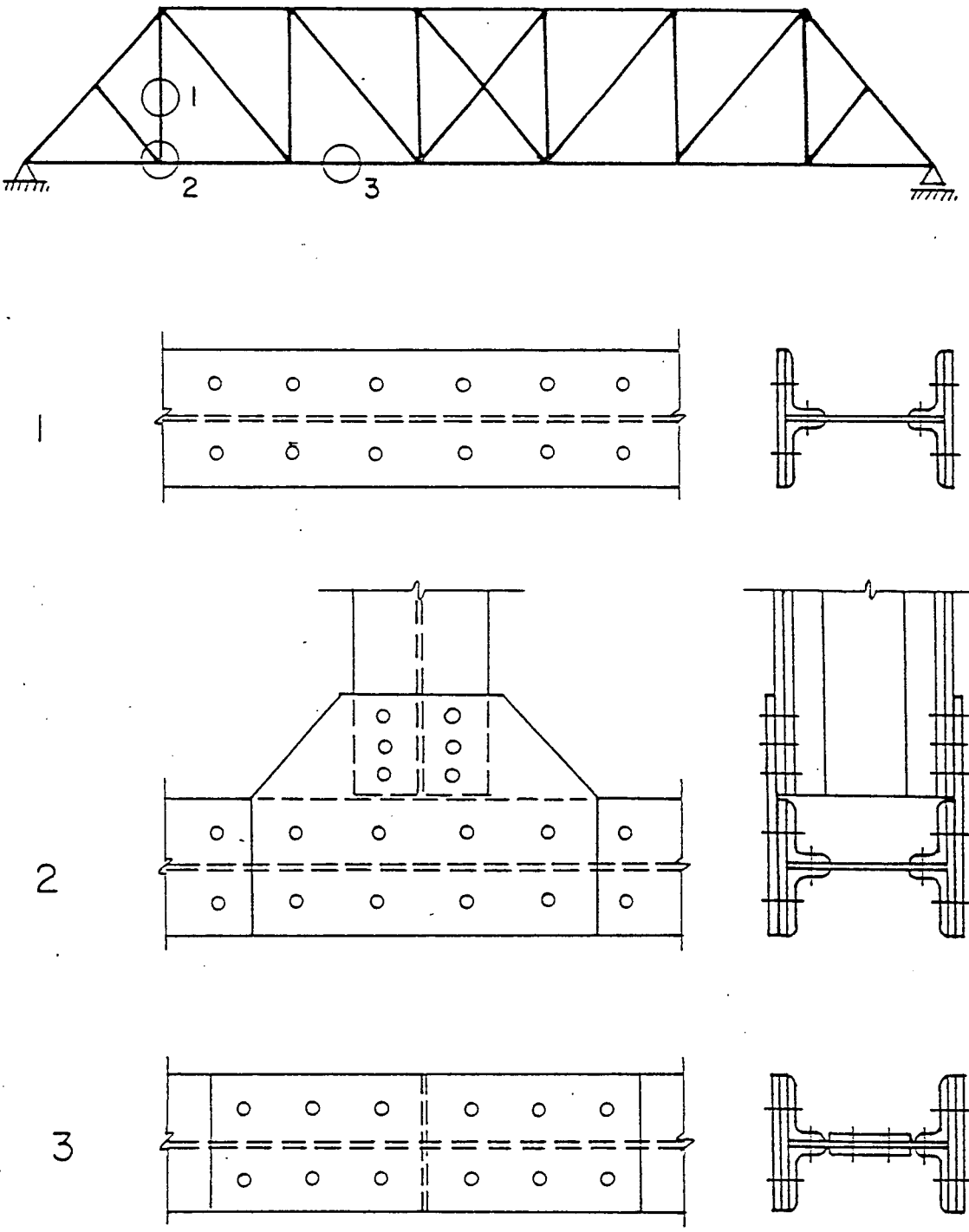

Fig. 4.1 Locations of the Details of Study

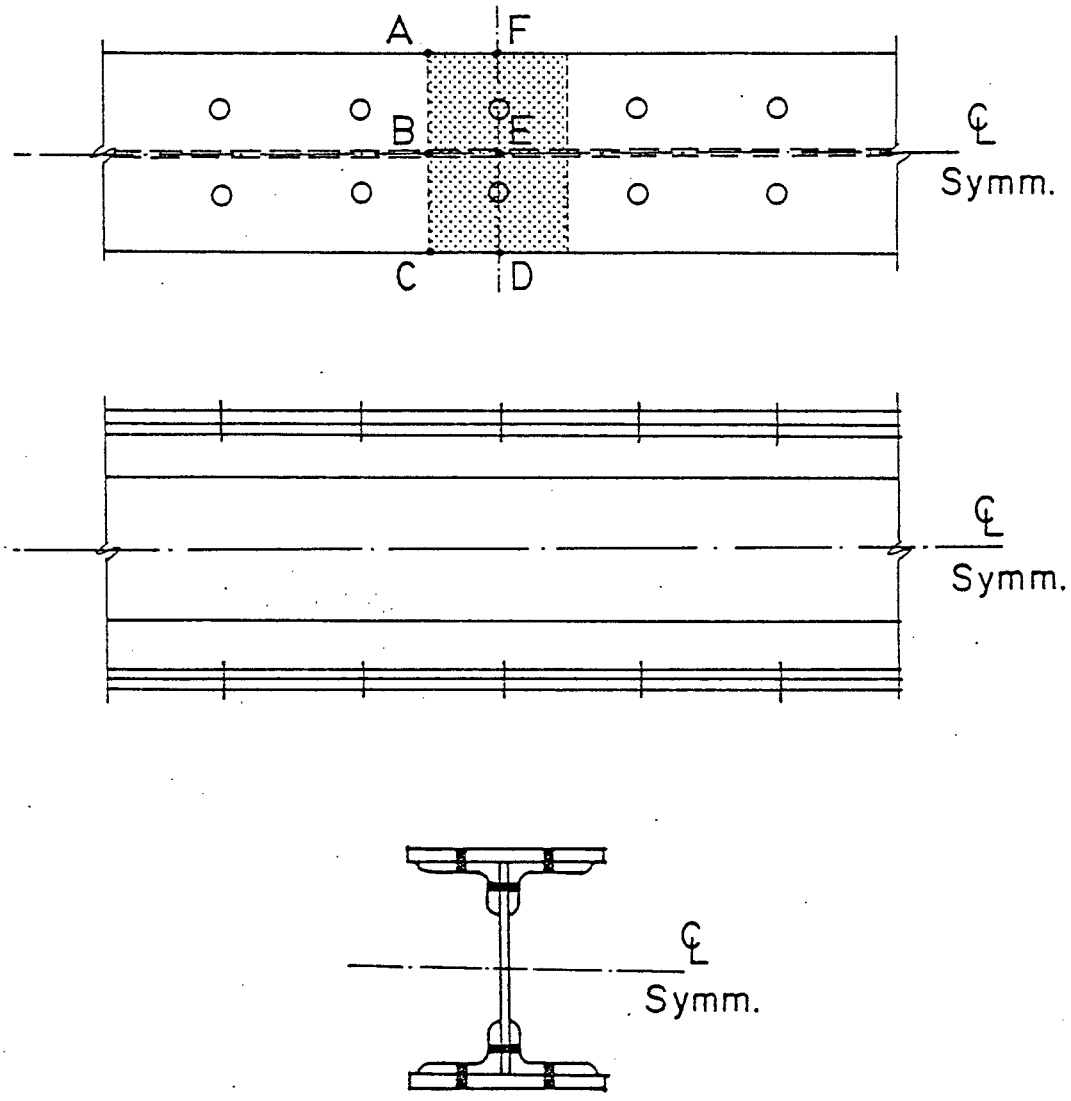

Fig. 4.2 Detail of Riveted Built-up Truss Member Section

Detail 1

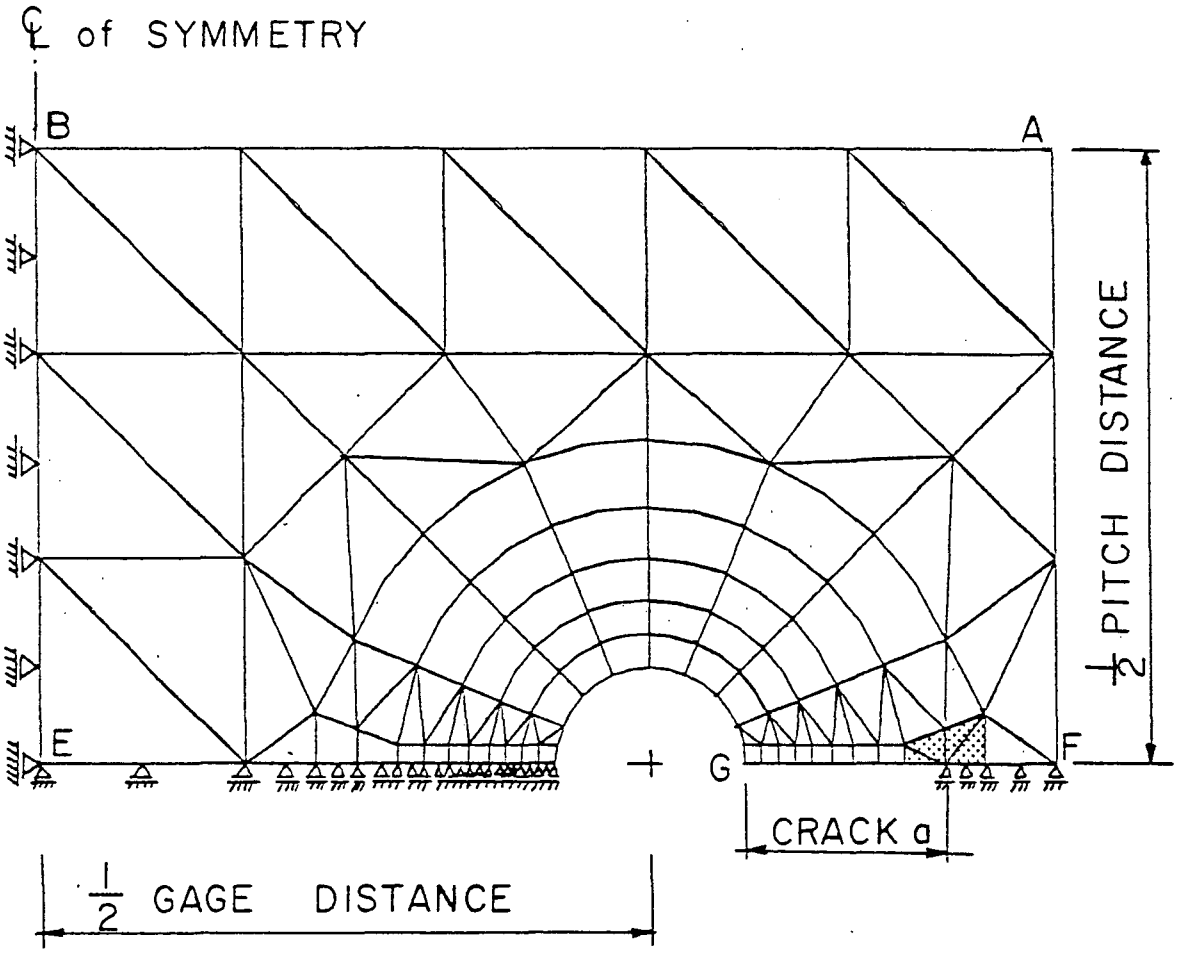

Fig. 4.3 Finite Element Model for Built-up Truss Member - Detail 1

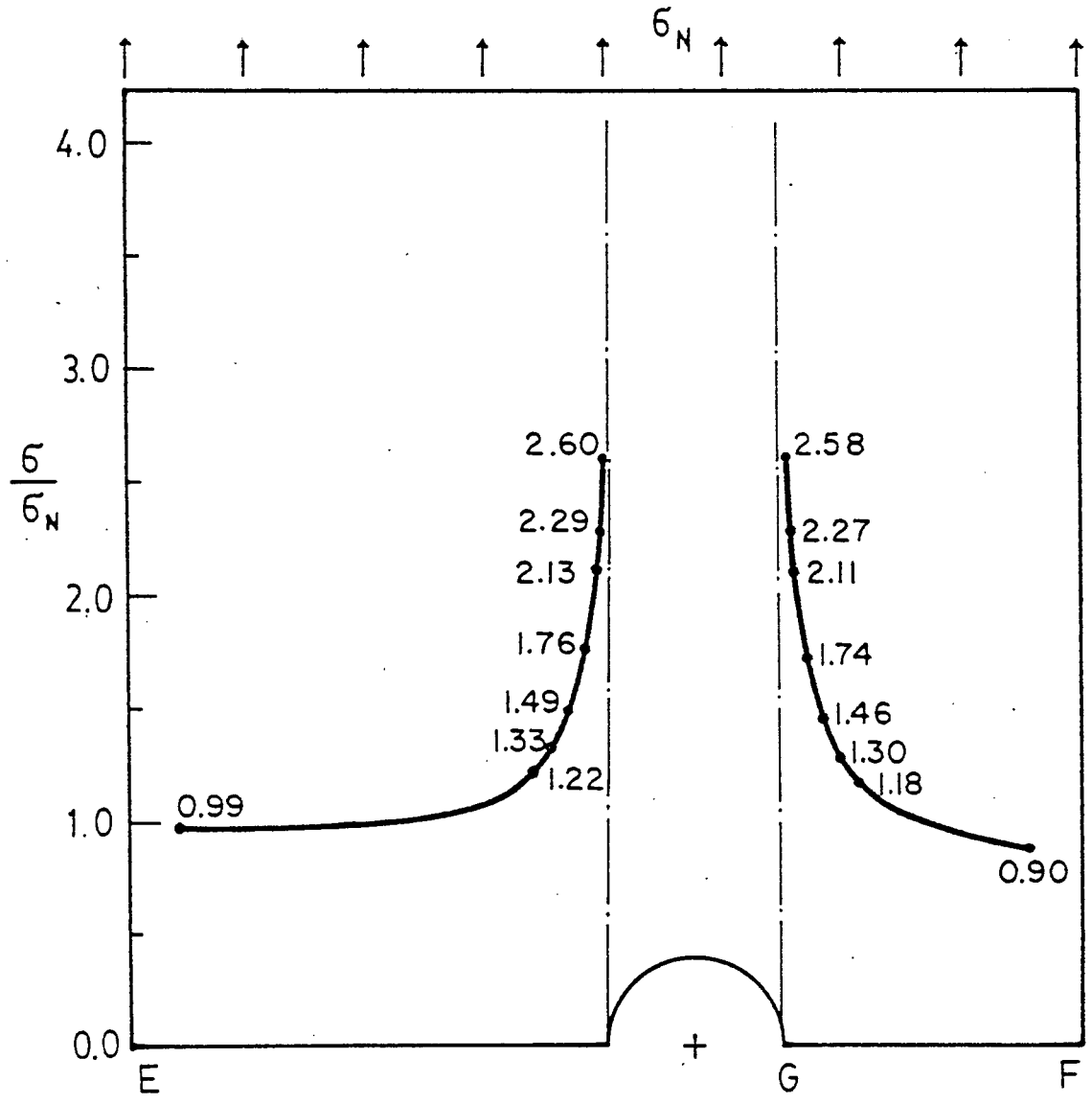

Fig. 4.4 Non-Dimensionalized Stress Distribution across the Rivet Hole of Built-up Truss Member

(15.24 cm for Gage and Pitch Distance)

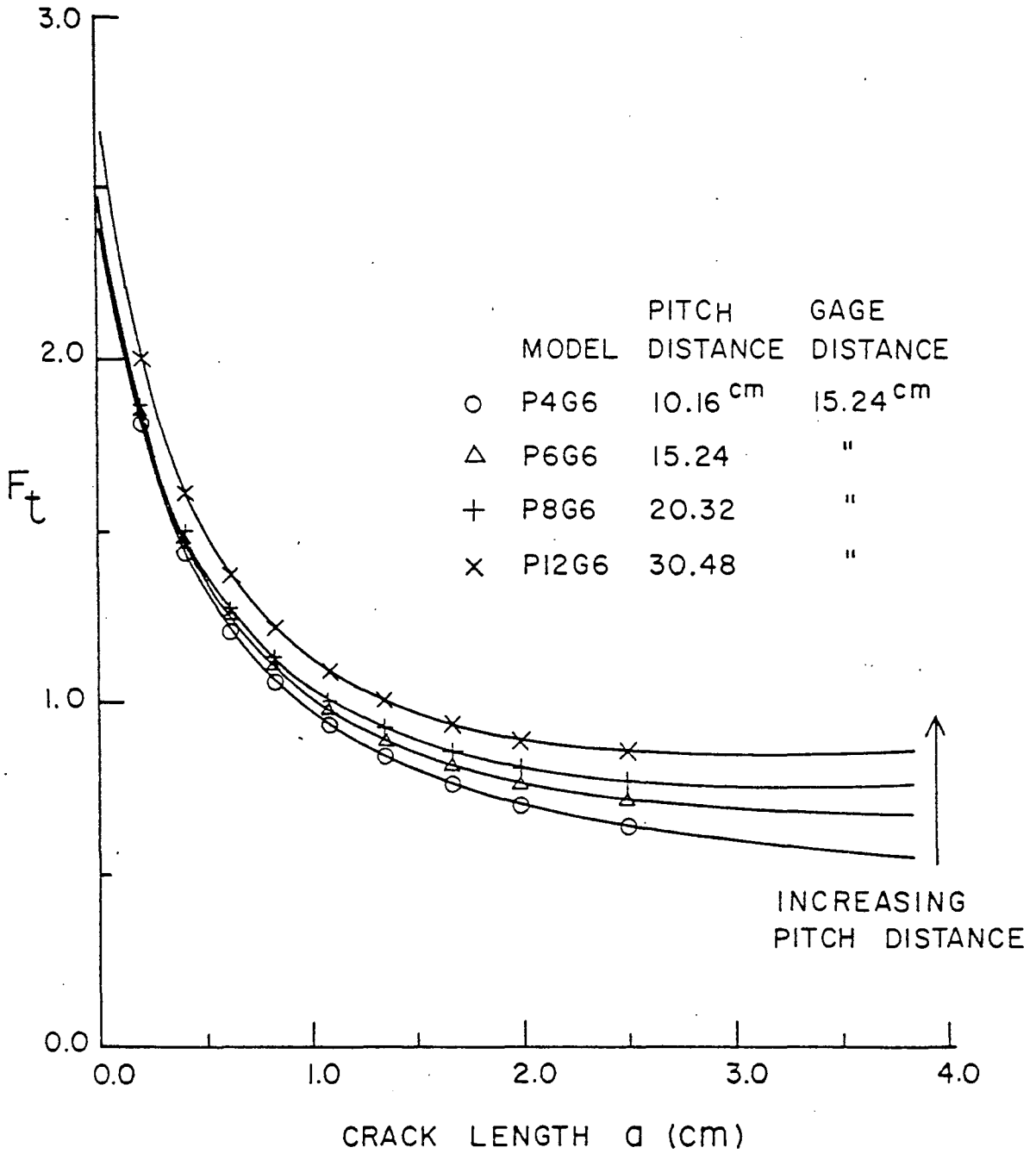

Fig. 4.5 Effect of Pitch Distance on Function F_t of Detail 1

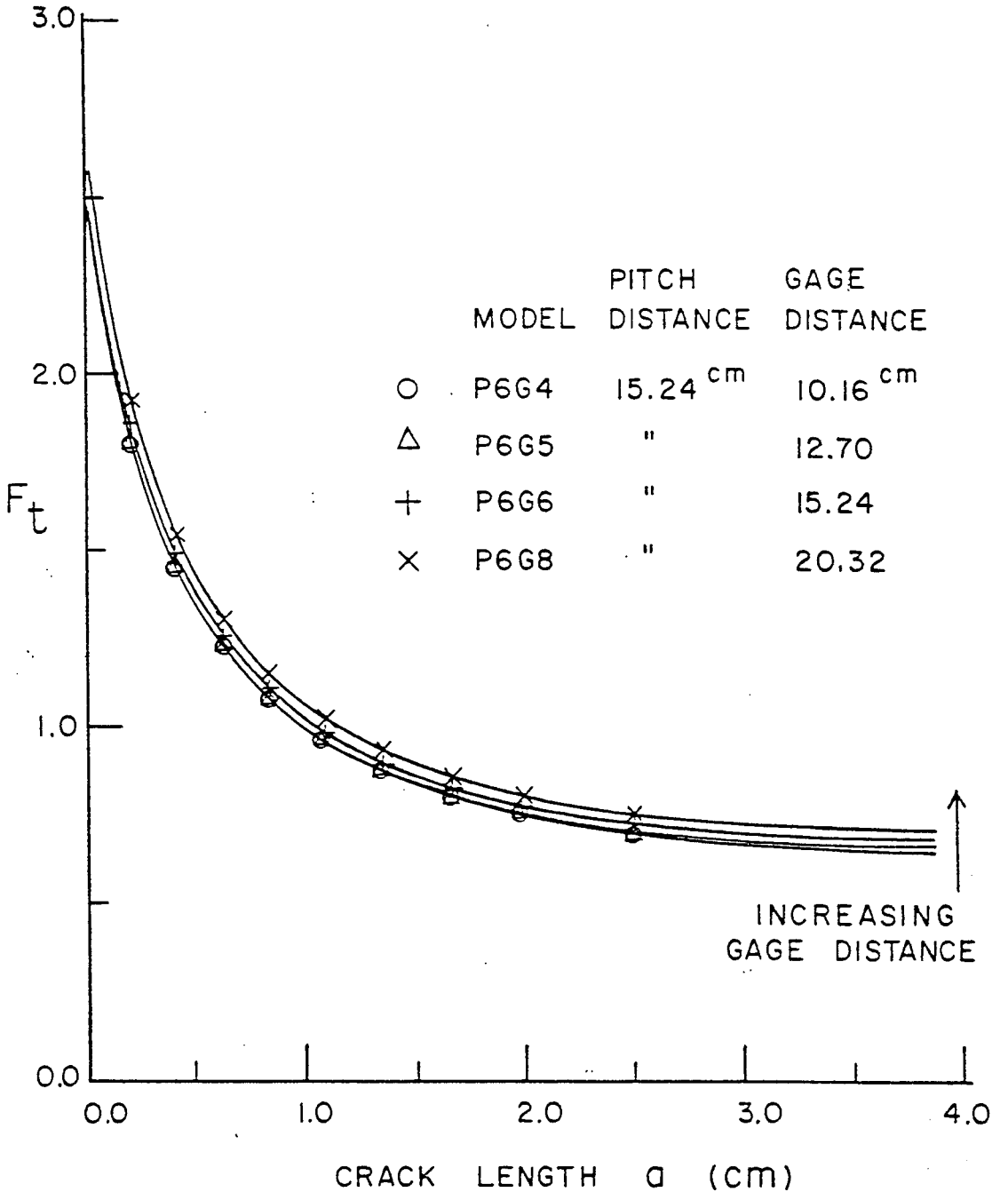

Fig. 4.6 Effect of Gage Distance on Function F_t of Detail 1

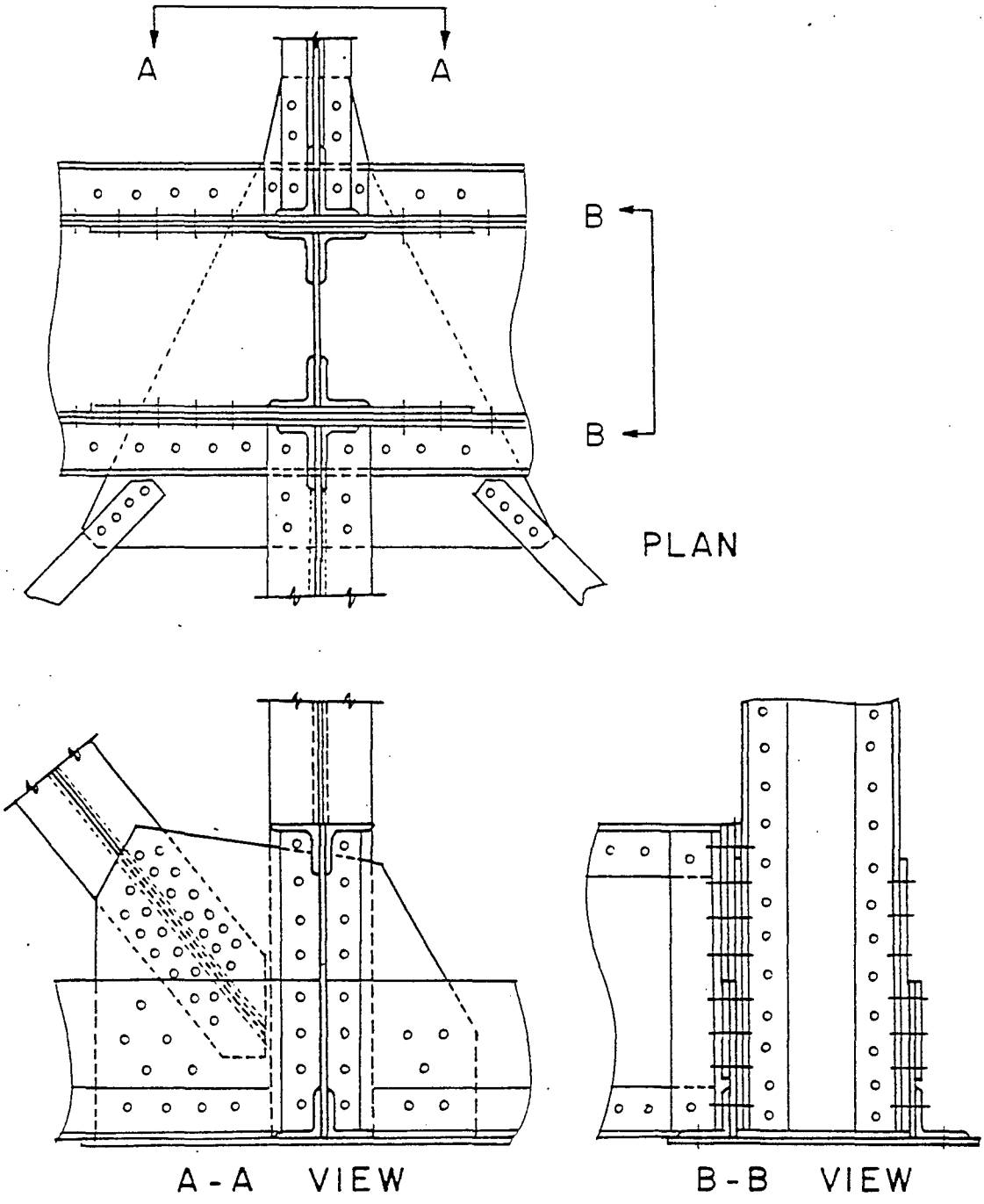

Fig. 4.7 Riveted Truss Joint Detail - Detail 2

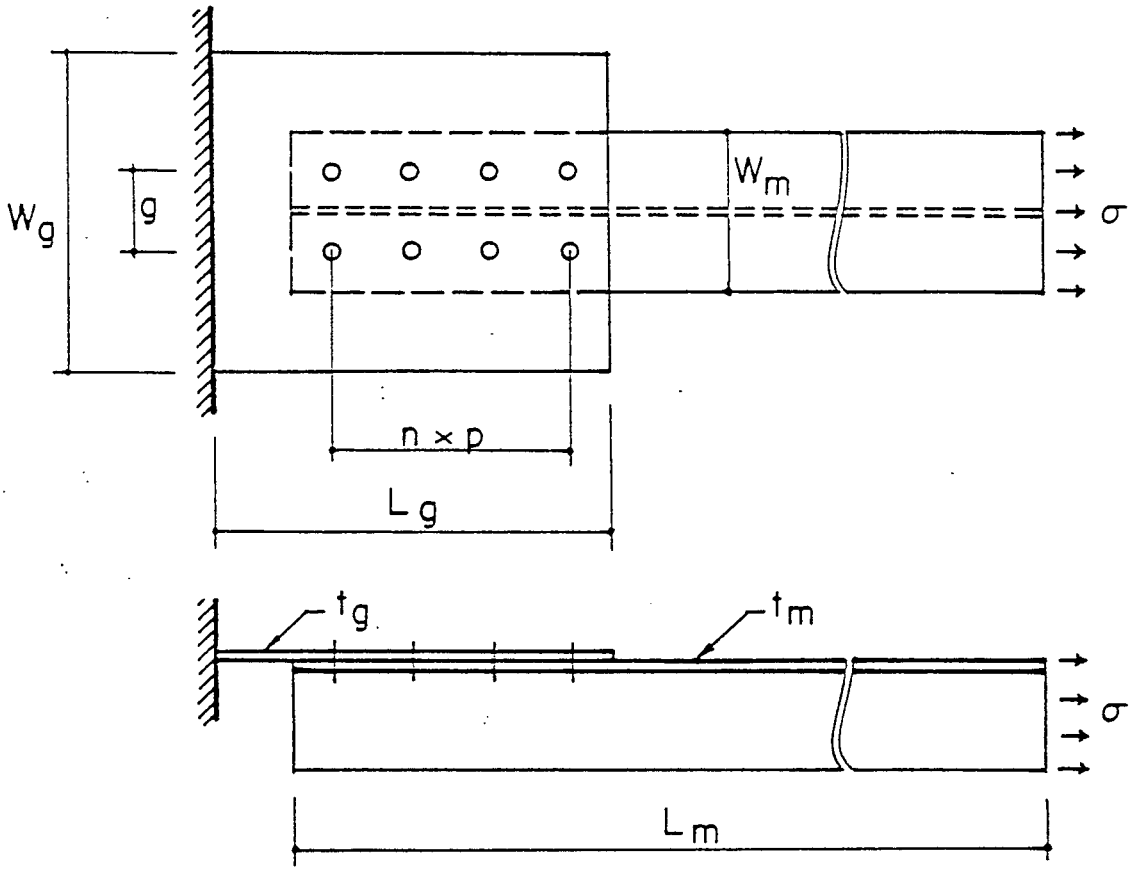

Fig. 4.8 Simplified Riveted Truss Joint Model

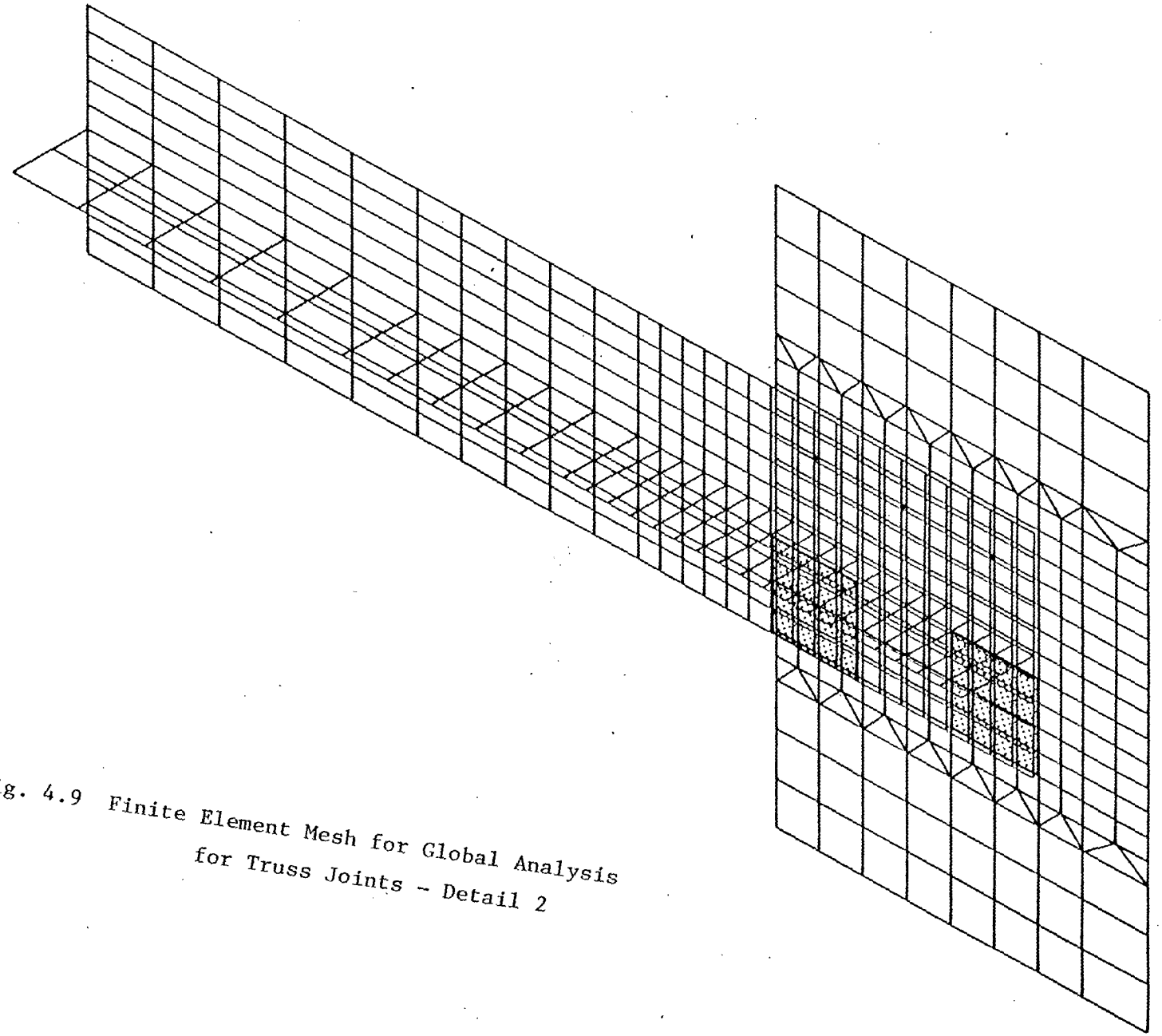

Fig. 4.9 Finite Element Mesh for Global Analysis for Truss Joints - Detail 2

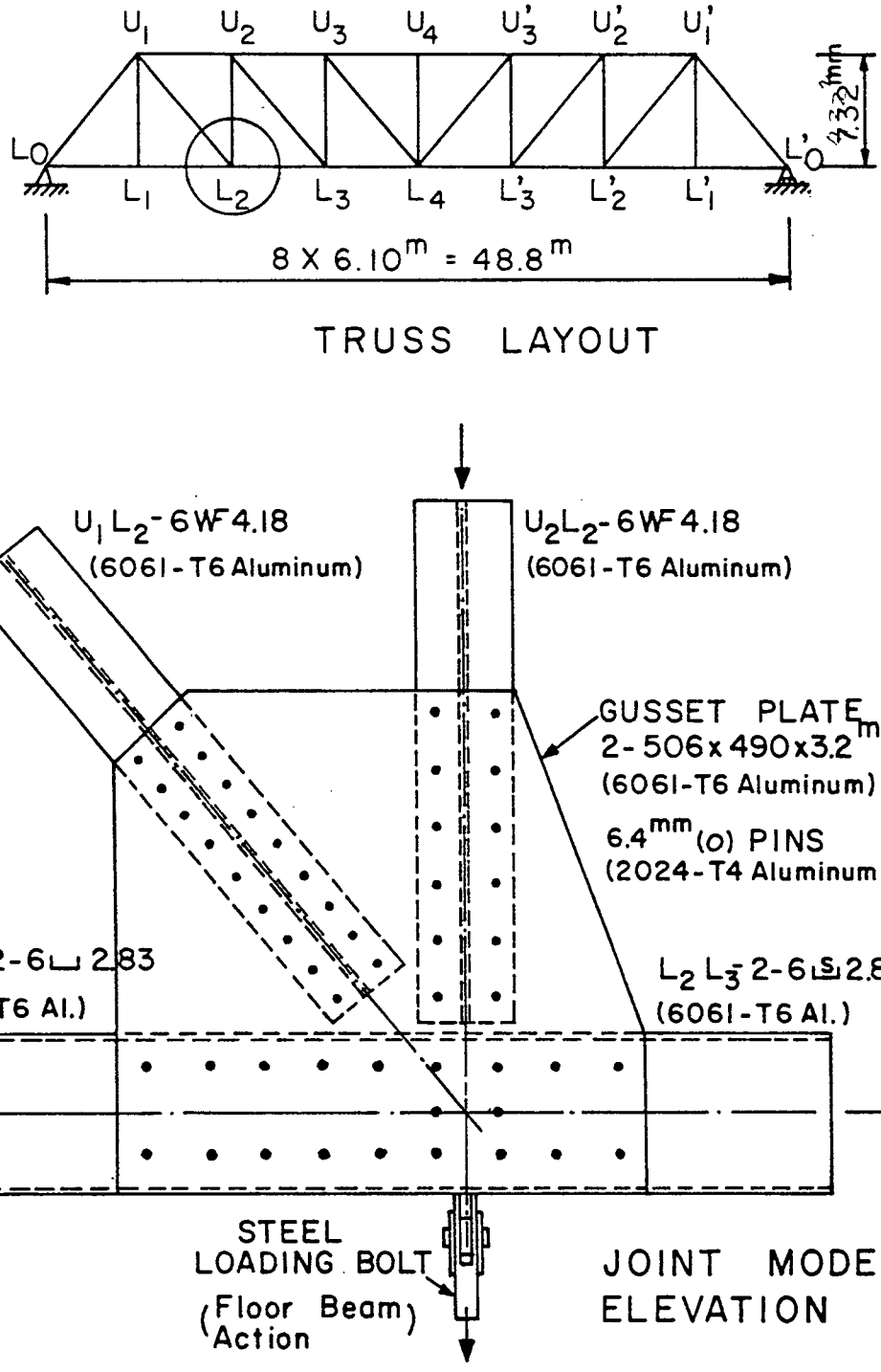

Fig. 4.10 Pratt Truss Joint Tested by Irvan [44]

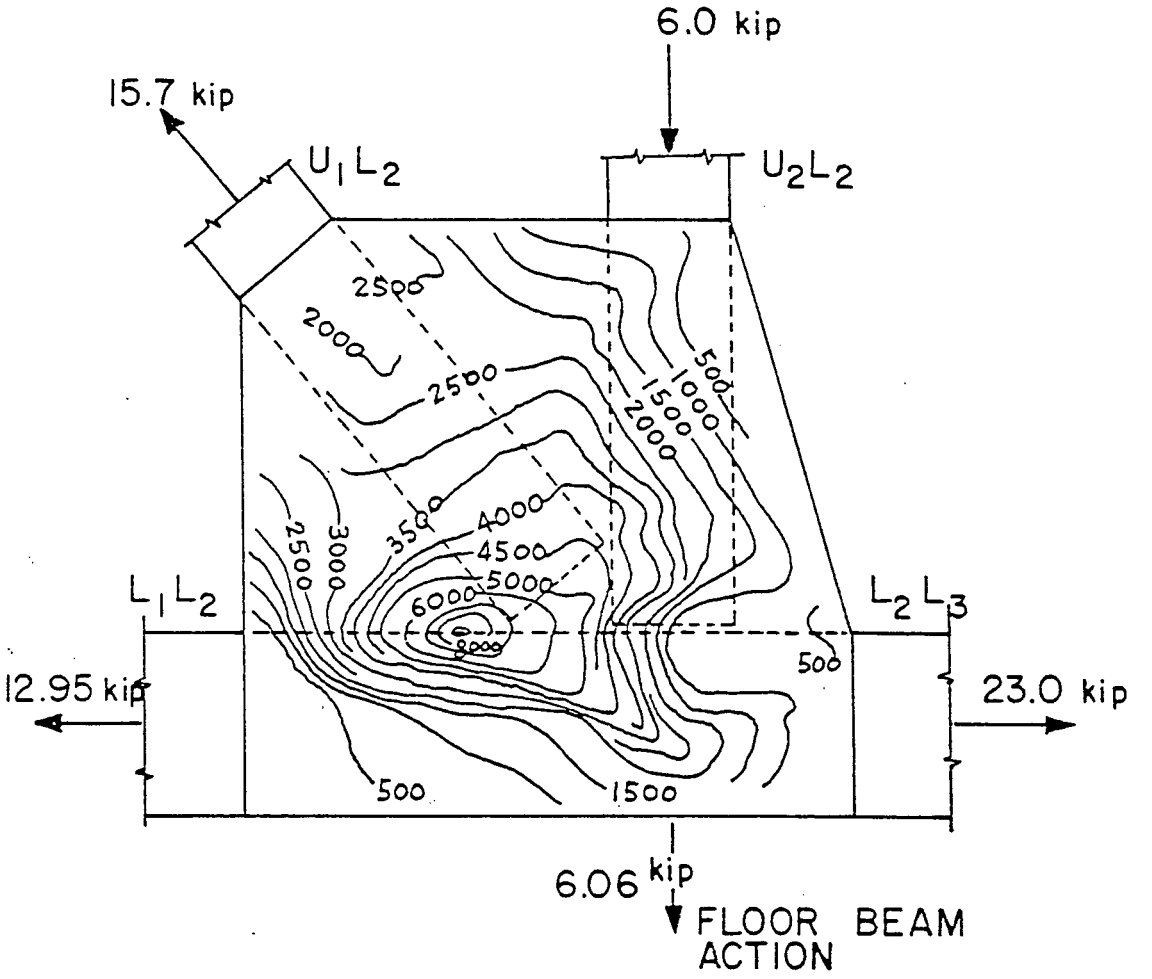

Fig. 4.11 Contour Plot of Maximum Tensile Stress from Irvan's Test Results [44]

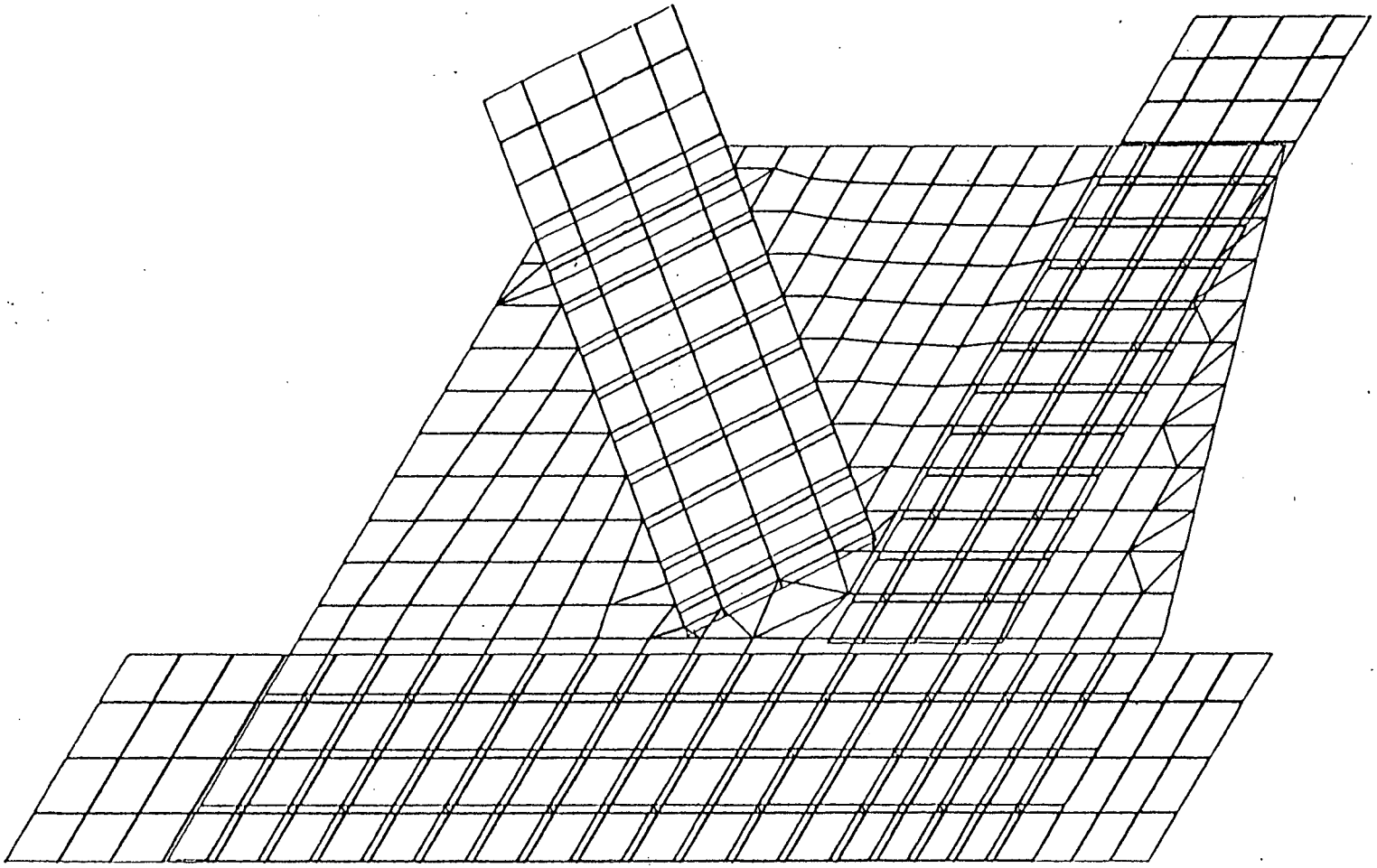

Fig. 4.12 Finite Element Mesh for Irvan's Test Detail

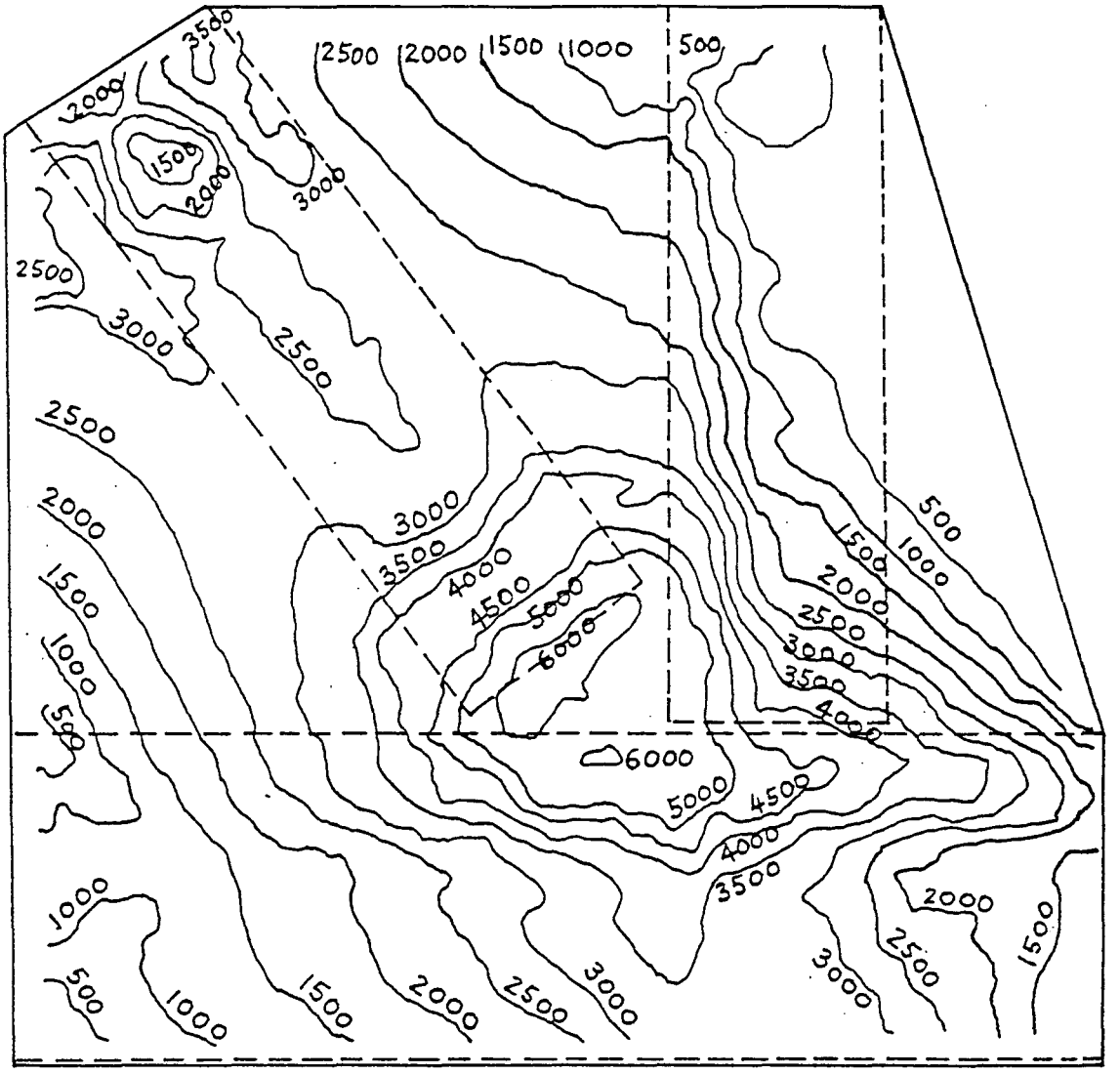

Fig. 4.13 Contour Plot of Maximum Tensile Stress from Finite Element Analysis

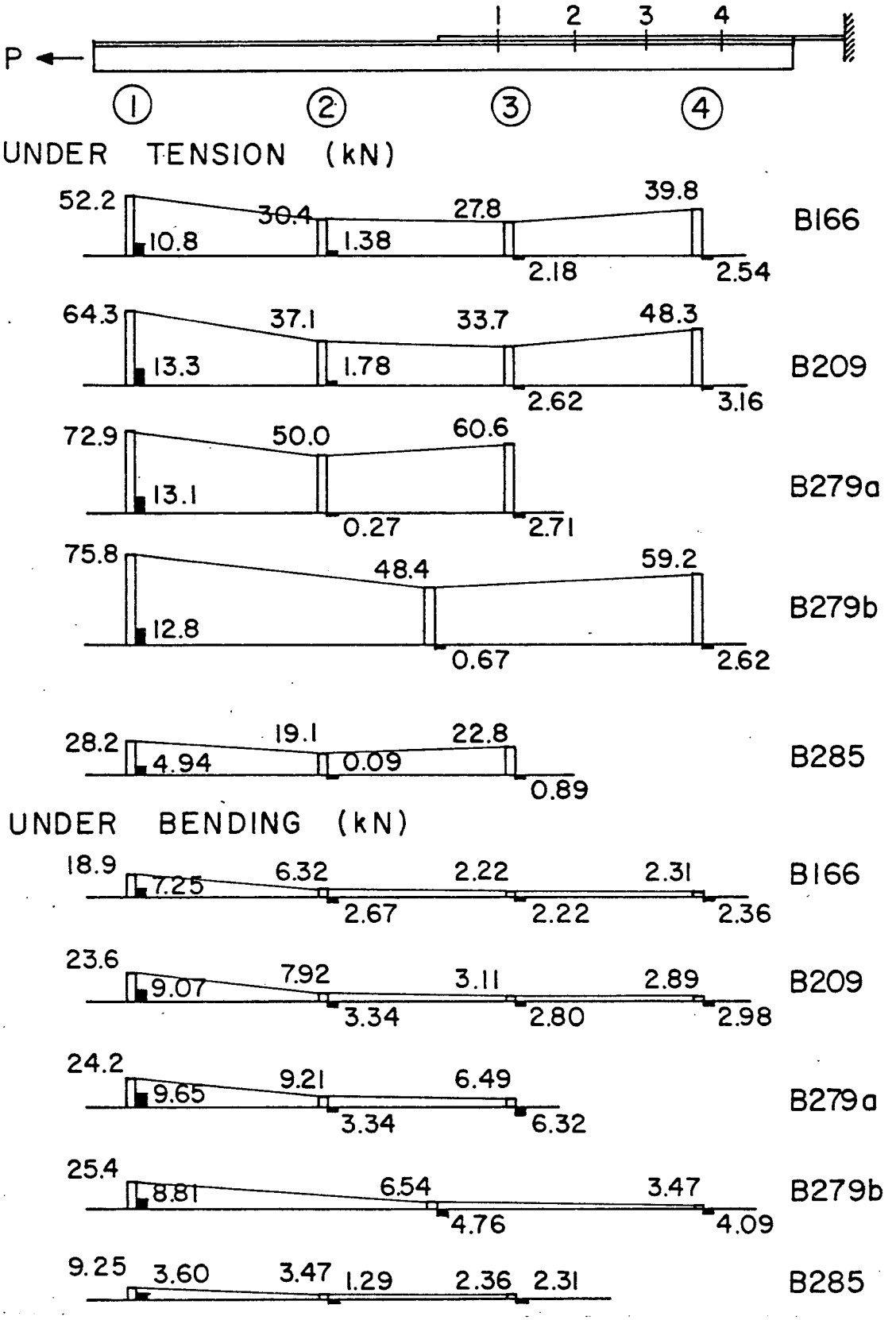

Fig. 4.14 Load Distribution Among the Rivets

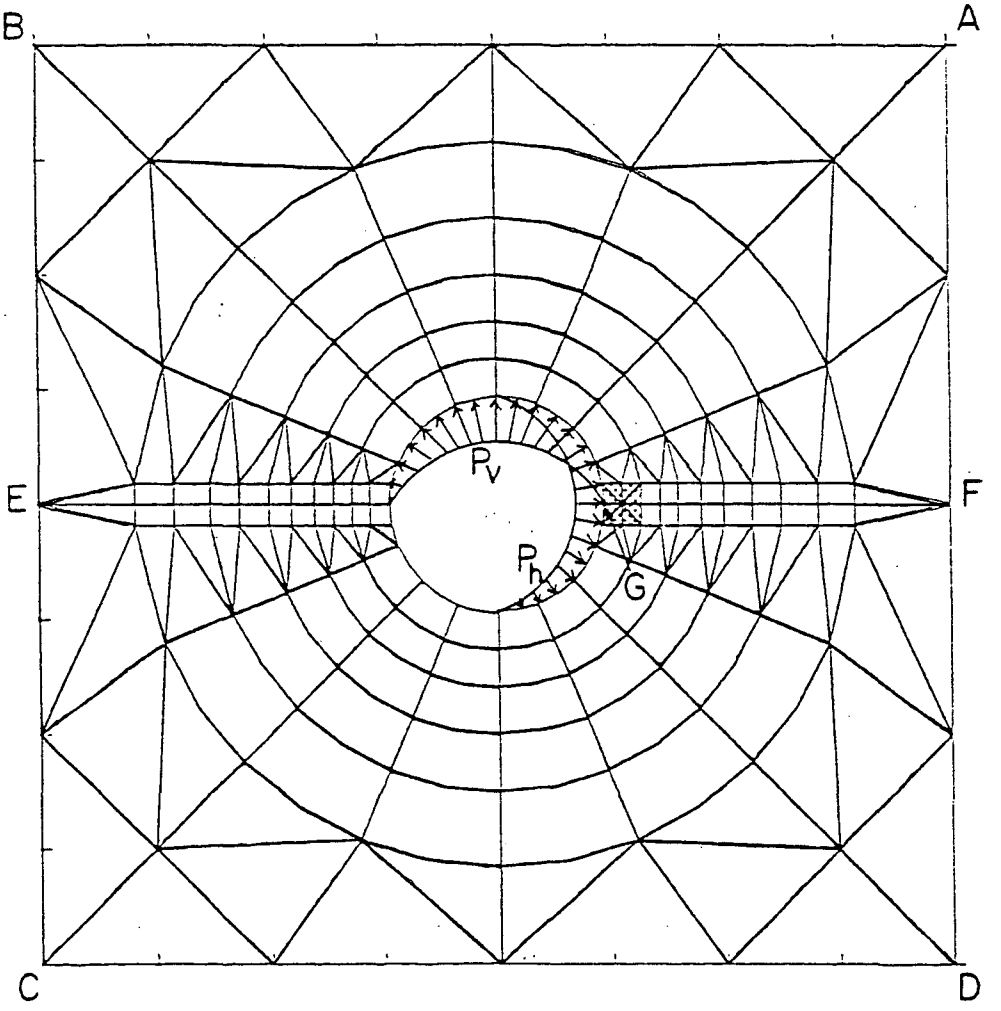

Fig. 4.15 Finite Element Mesh of Substructure Model for Detail 2

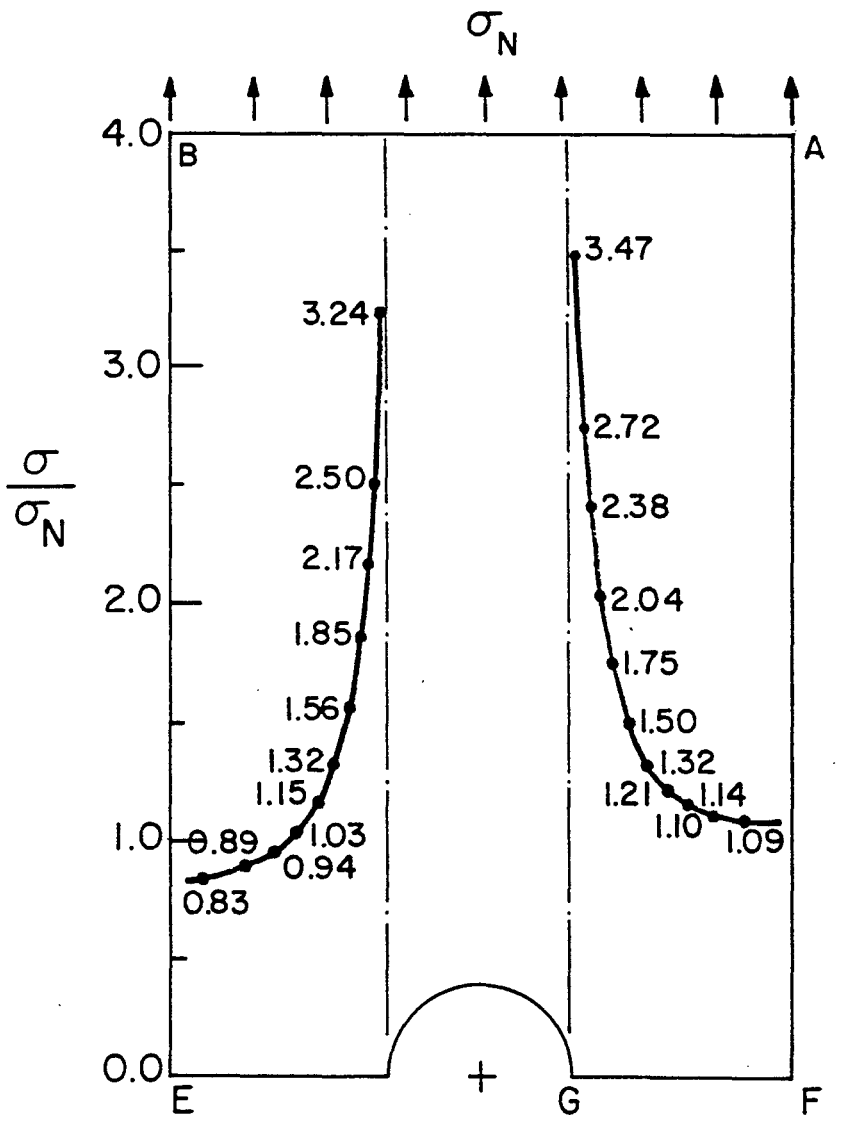

Fig. 4.16 Non-Dimensionalized Stress Distribution across the Rivet Hole of Truss Joint (Bearing Ratio = 1.66, Pitch = 81 mm)

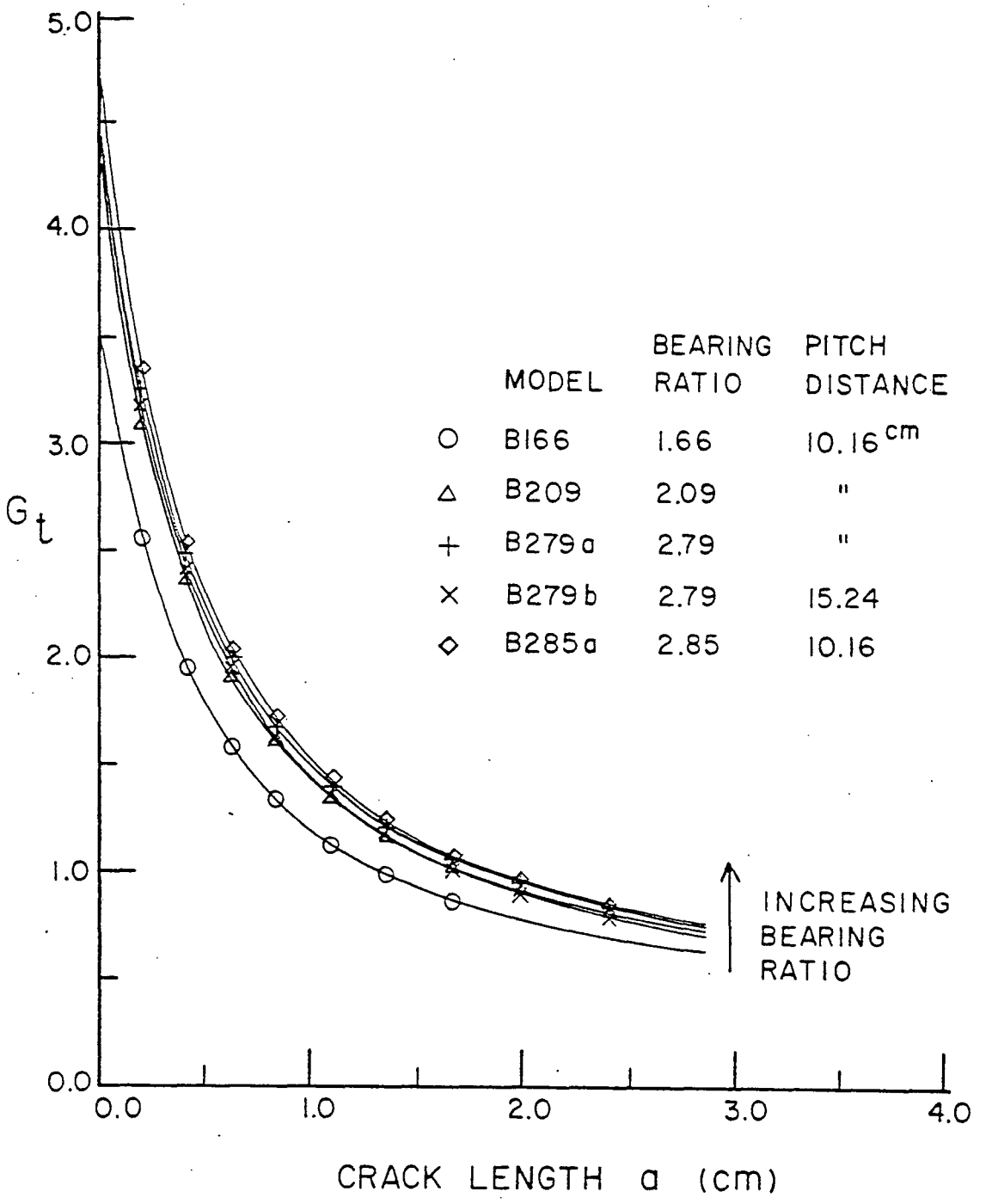

Fig. 4.17 Effect of Bearing Ratio on Function G_t of Detail 2

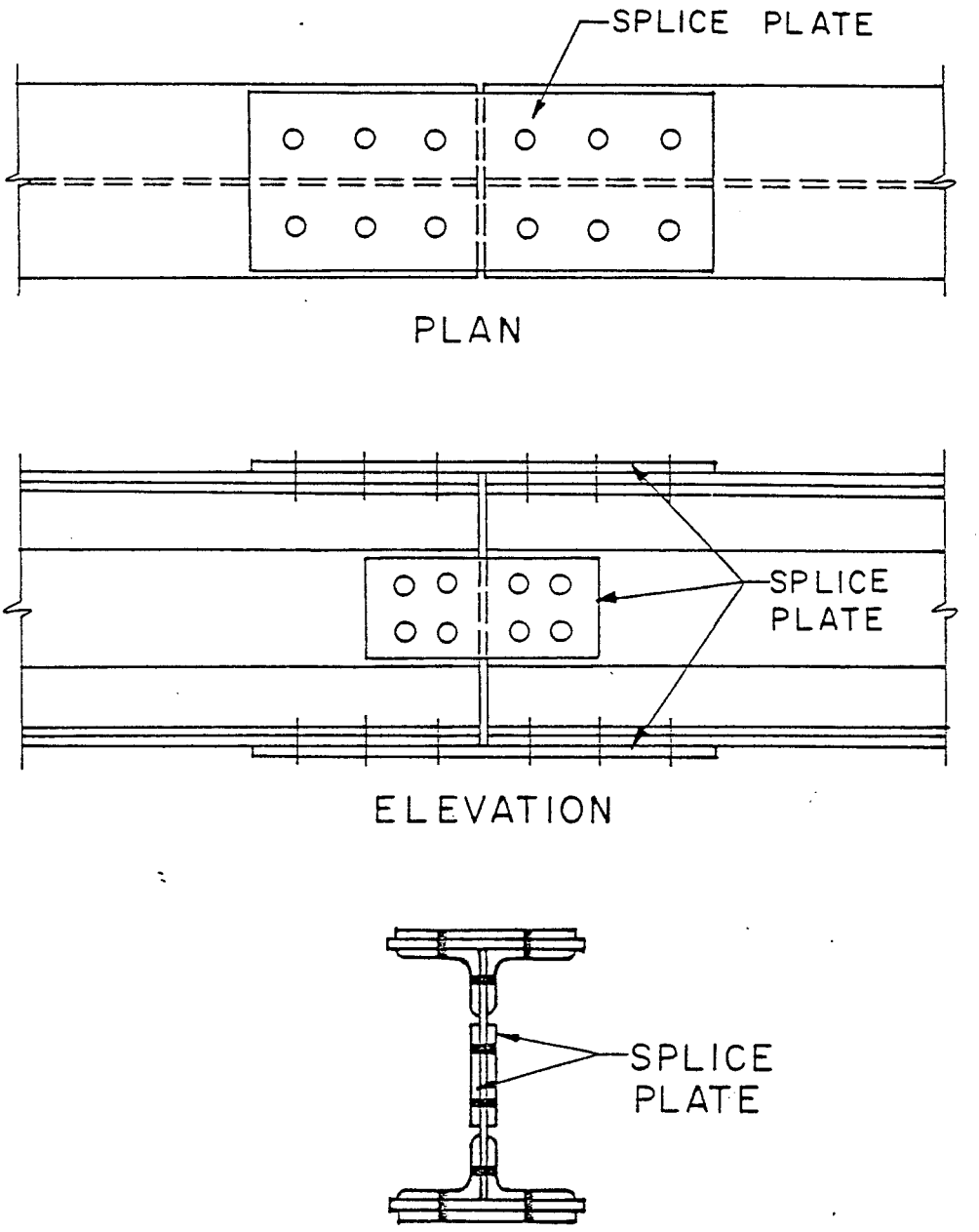

Fig. 4.18 Detail of Riveted Member to Member Connection with Splice Plates - Detail 3

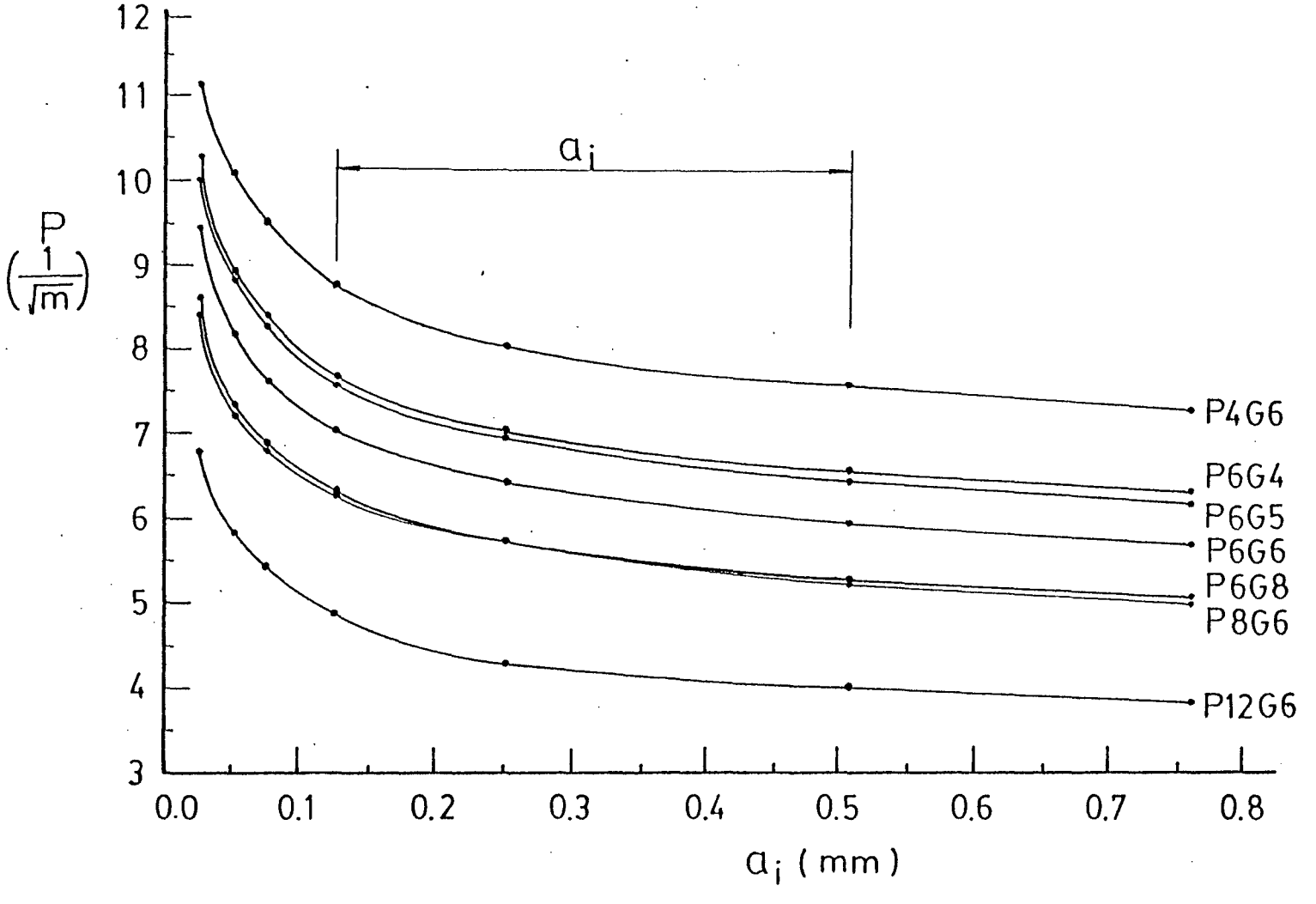

Fig. 5.1 Variation of P Due to Change of Initial Crack Size a_i for Riveted Built-up Truss Member

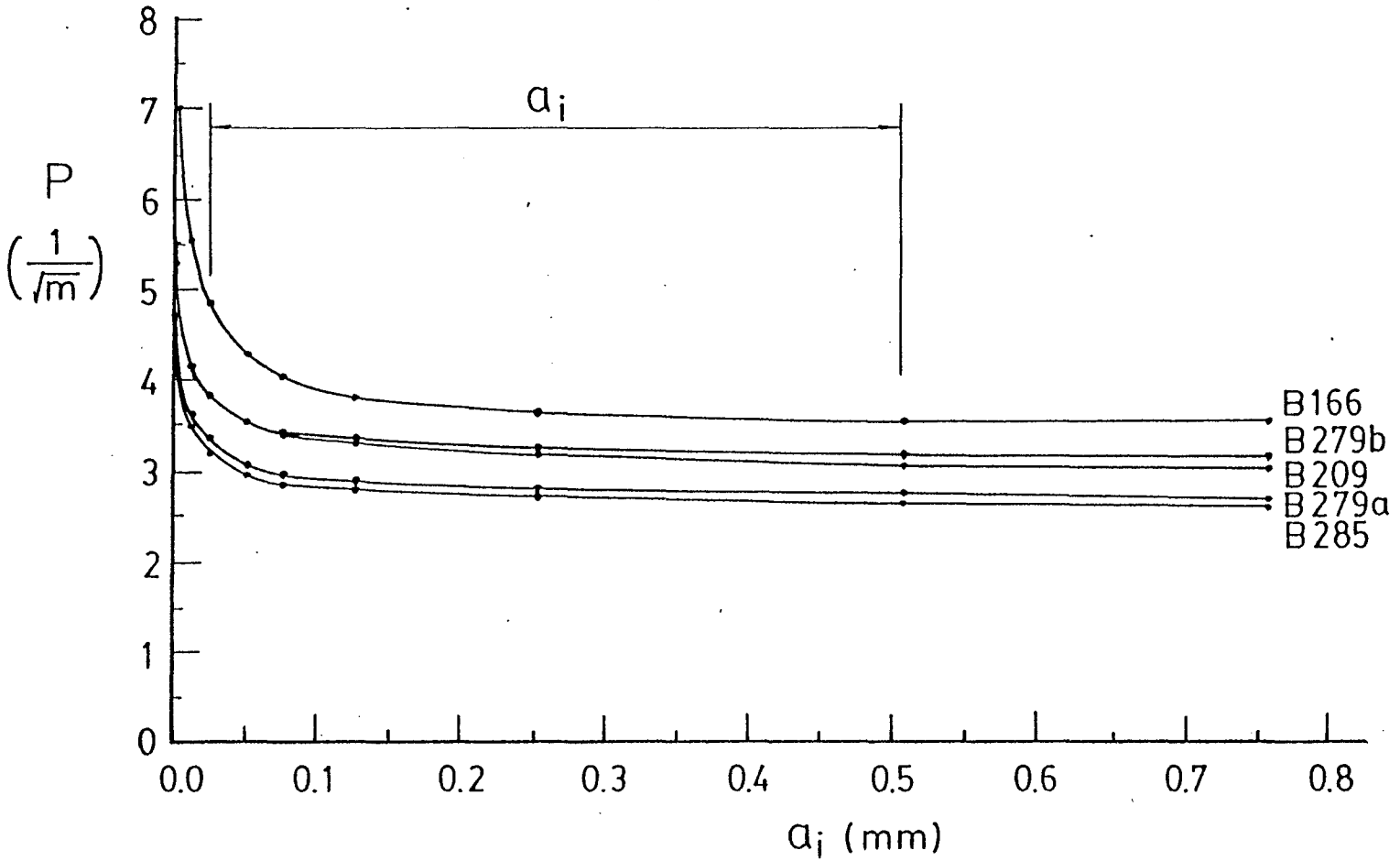

Fig. 5.2 Variation of P Due to Change of Initial Crack Size a_i for Riveted Truss Joint

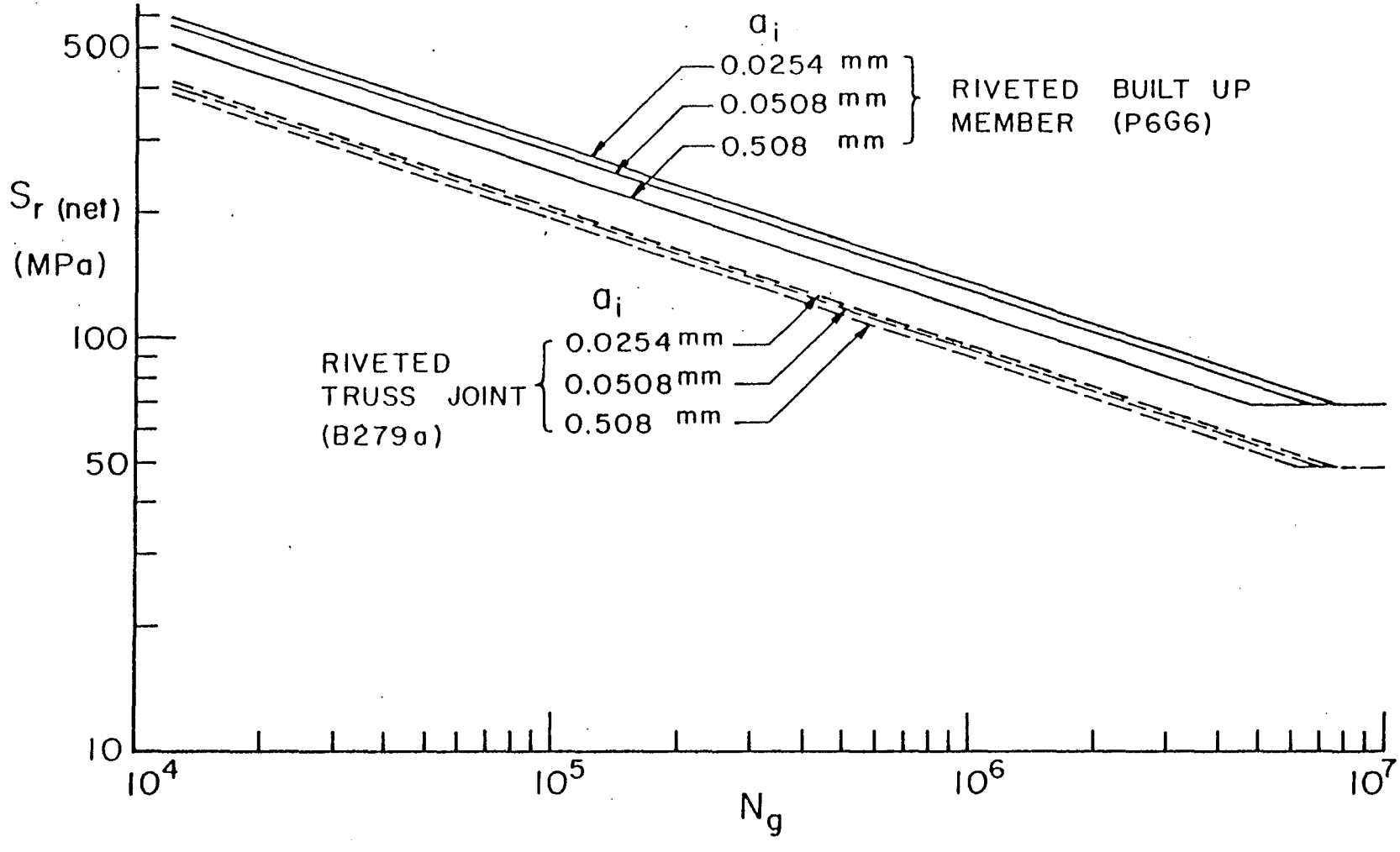

Fig. 5.3 Effects of Initial Crack Size on Fatigue Life of Riveted Truss Members and Joints

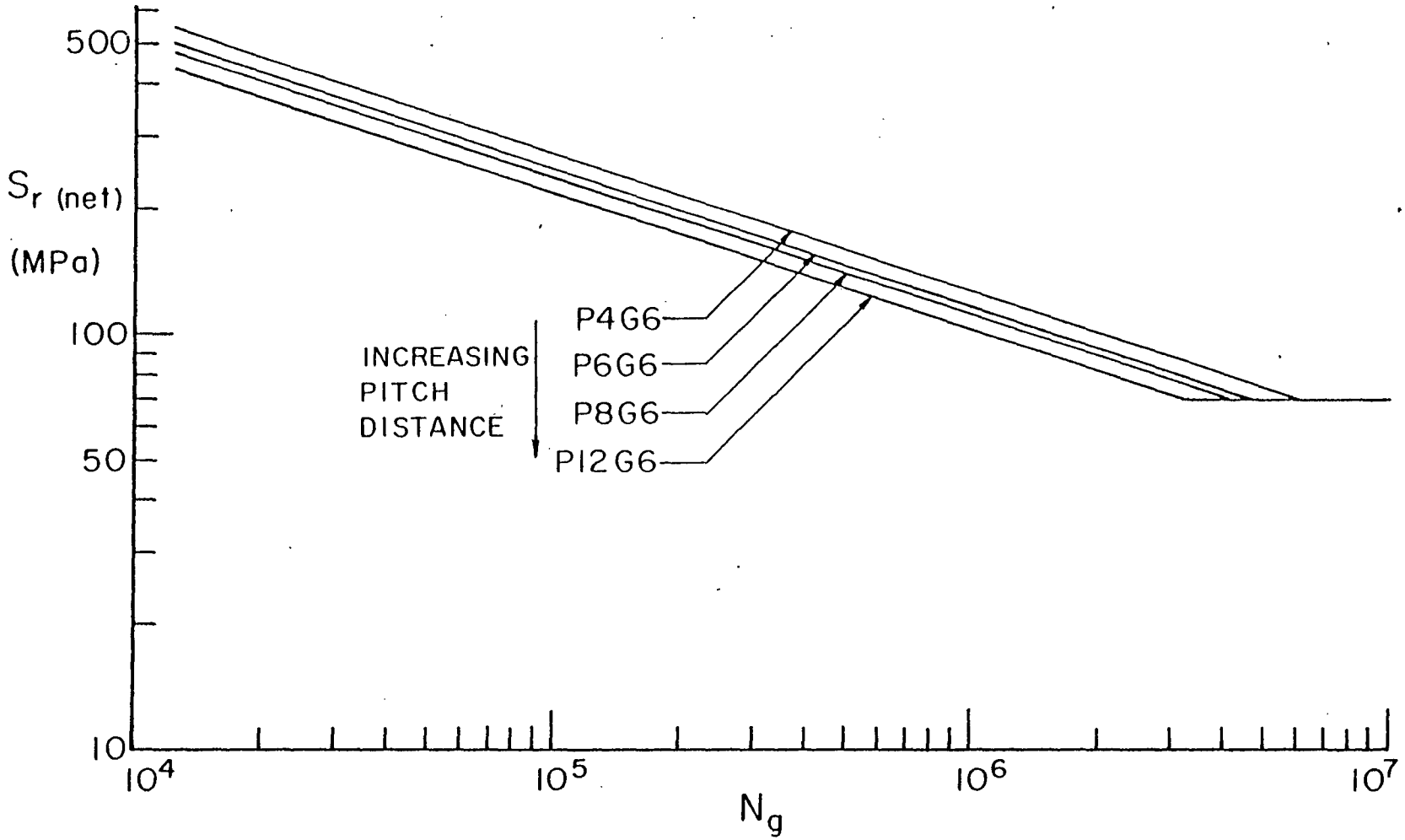

Fig. 5.4 Effects of Pitch Distances on Fatigue Life of Riveted Built-up Truss Member

(Gage Distance = 15.24 cm)

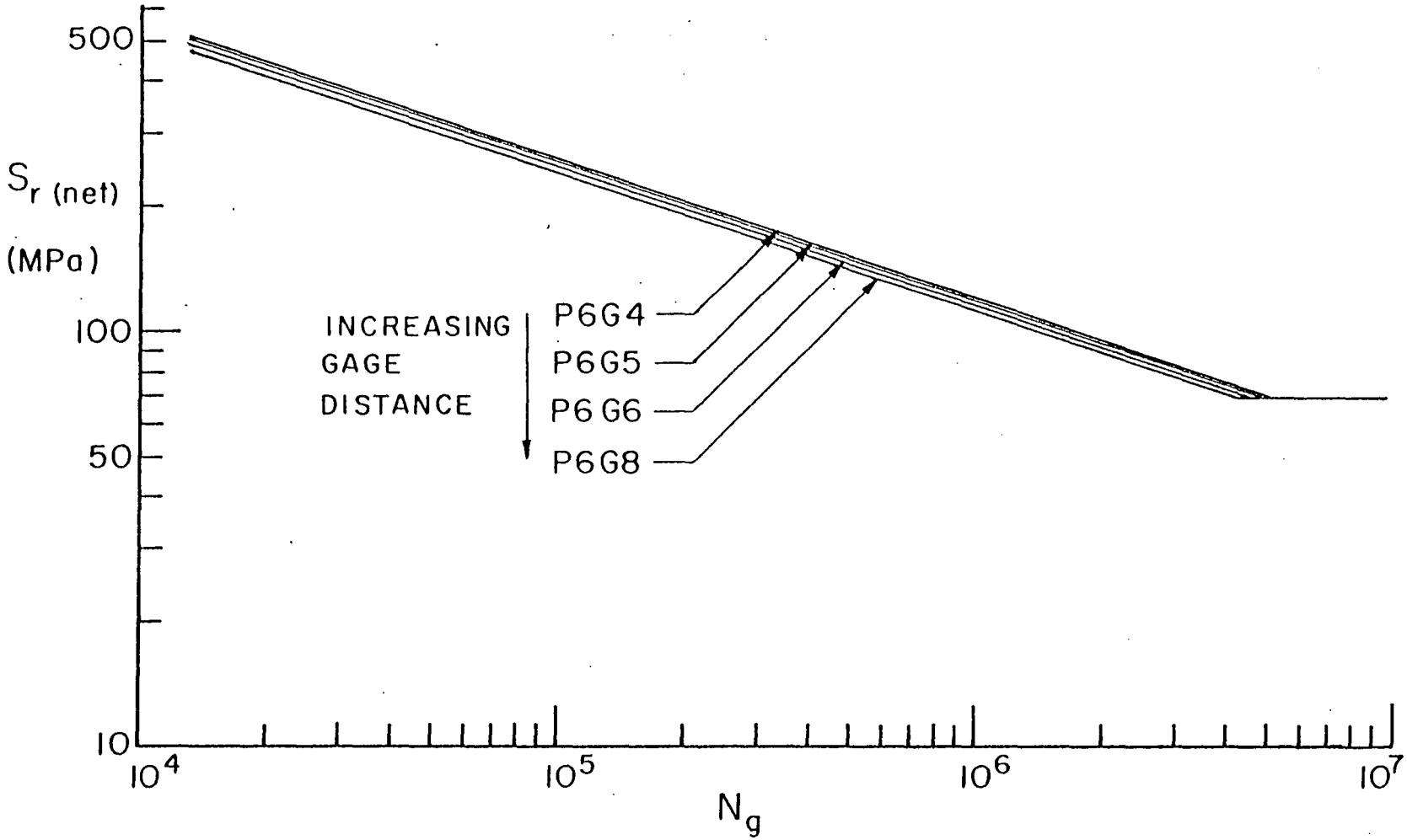

Fig. 5.5 Effects of Gage Distances on Fatigue Life of Riveted Built-up Truss Member

(Pitch Distance = 15.24 cm)

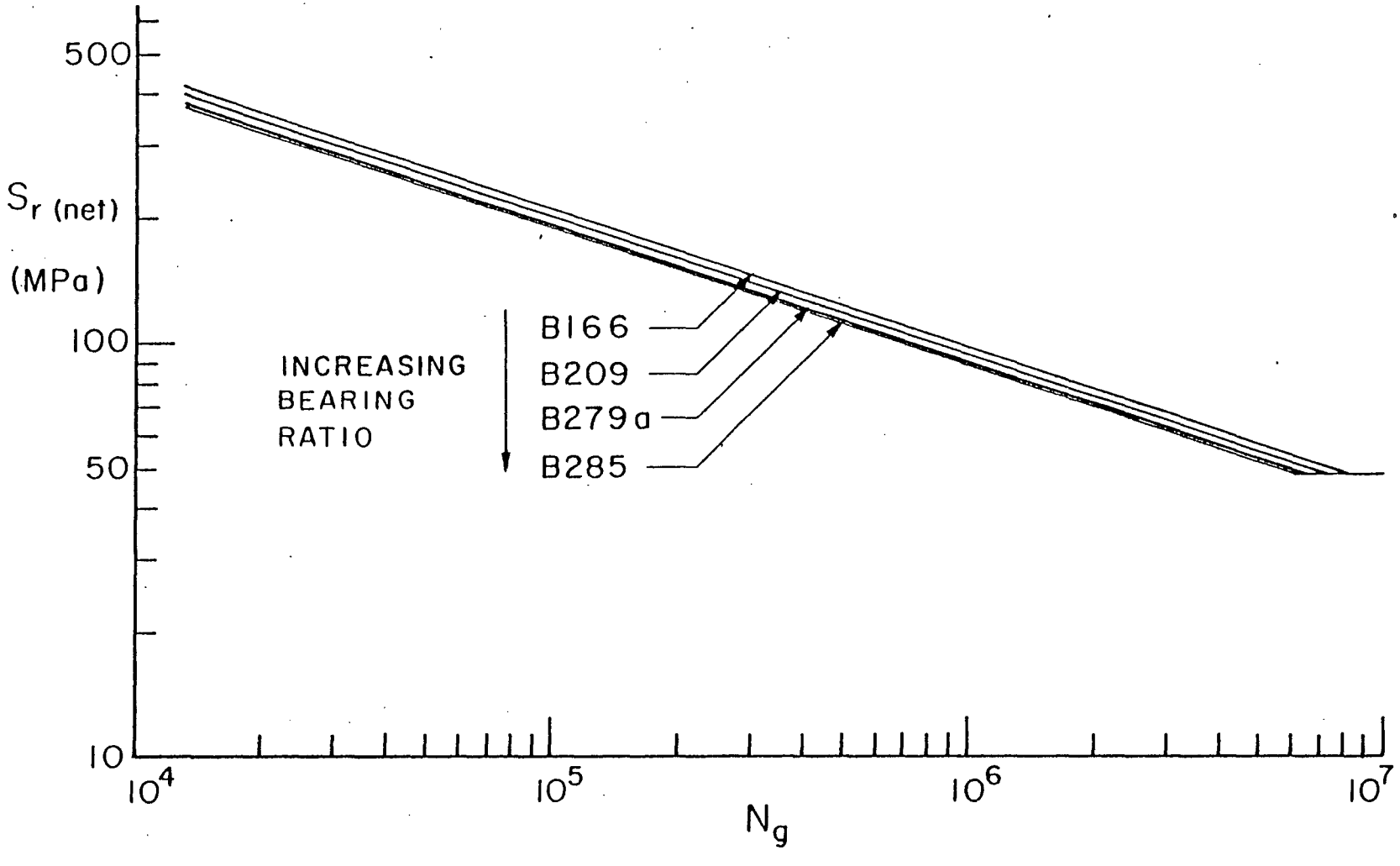

Fig. 5.6 Effects of Bearing Ratio on Fatigue Life of Riveted Truss Joints

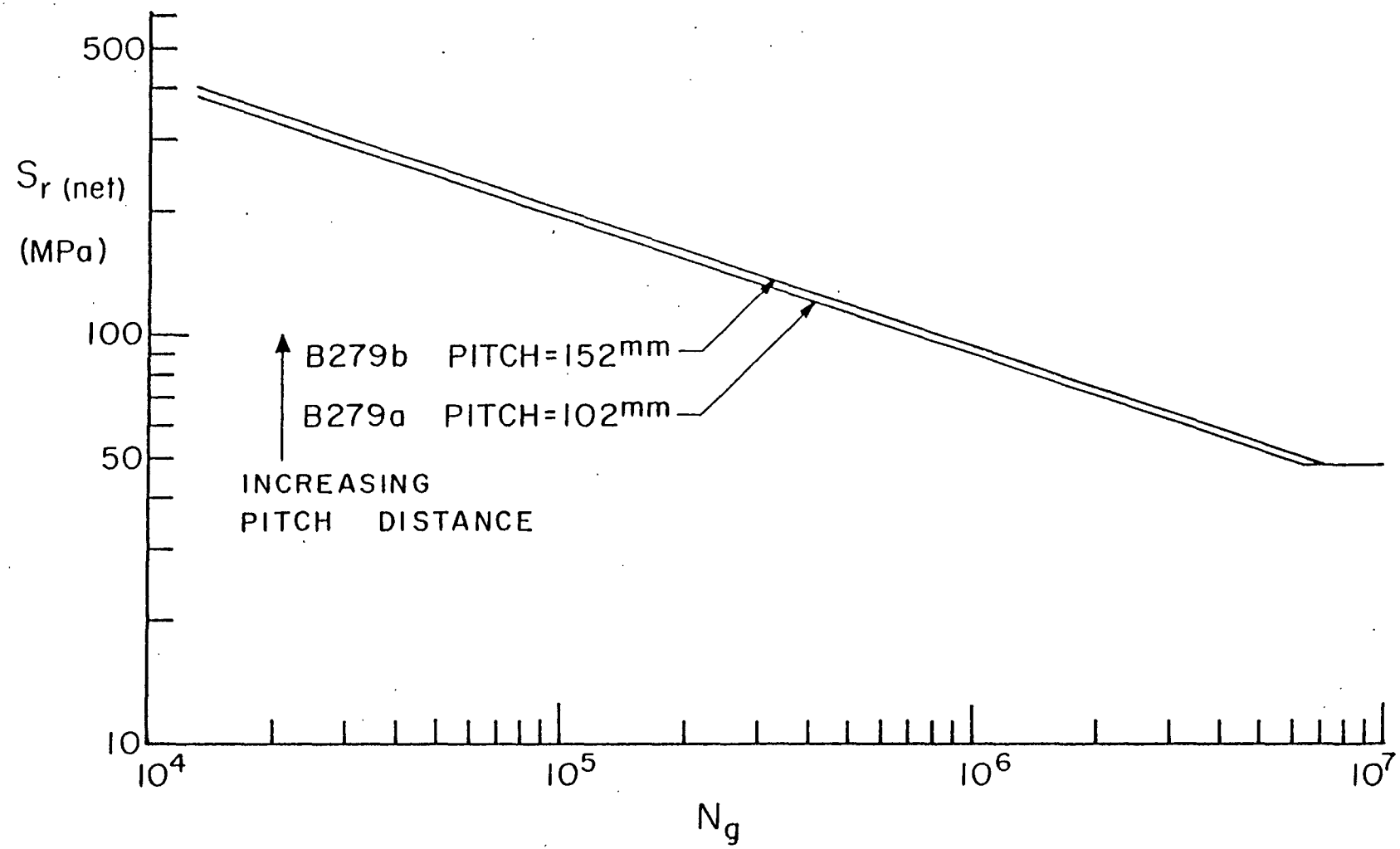

Fig. 5.7 Effects of Pitch Distances on Fatigue Life of Riveted Truss Joints (Gage Distance = 15.24 cm)

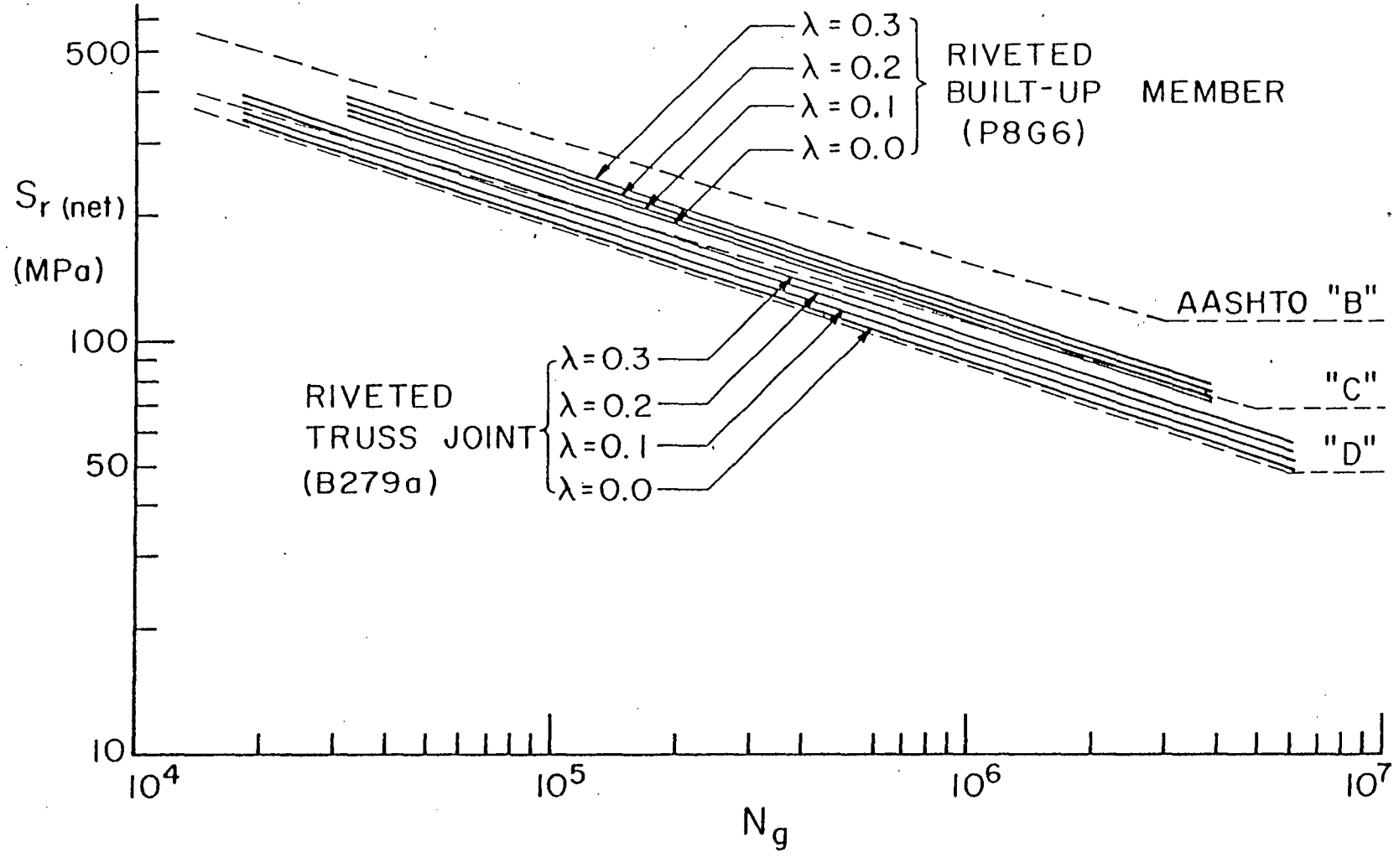

Fig. 5.8 Effects of Bending Moments on Fatigue Life of Riveted Truss Joints

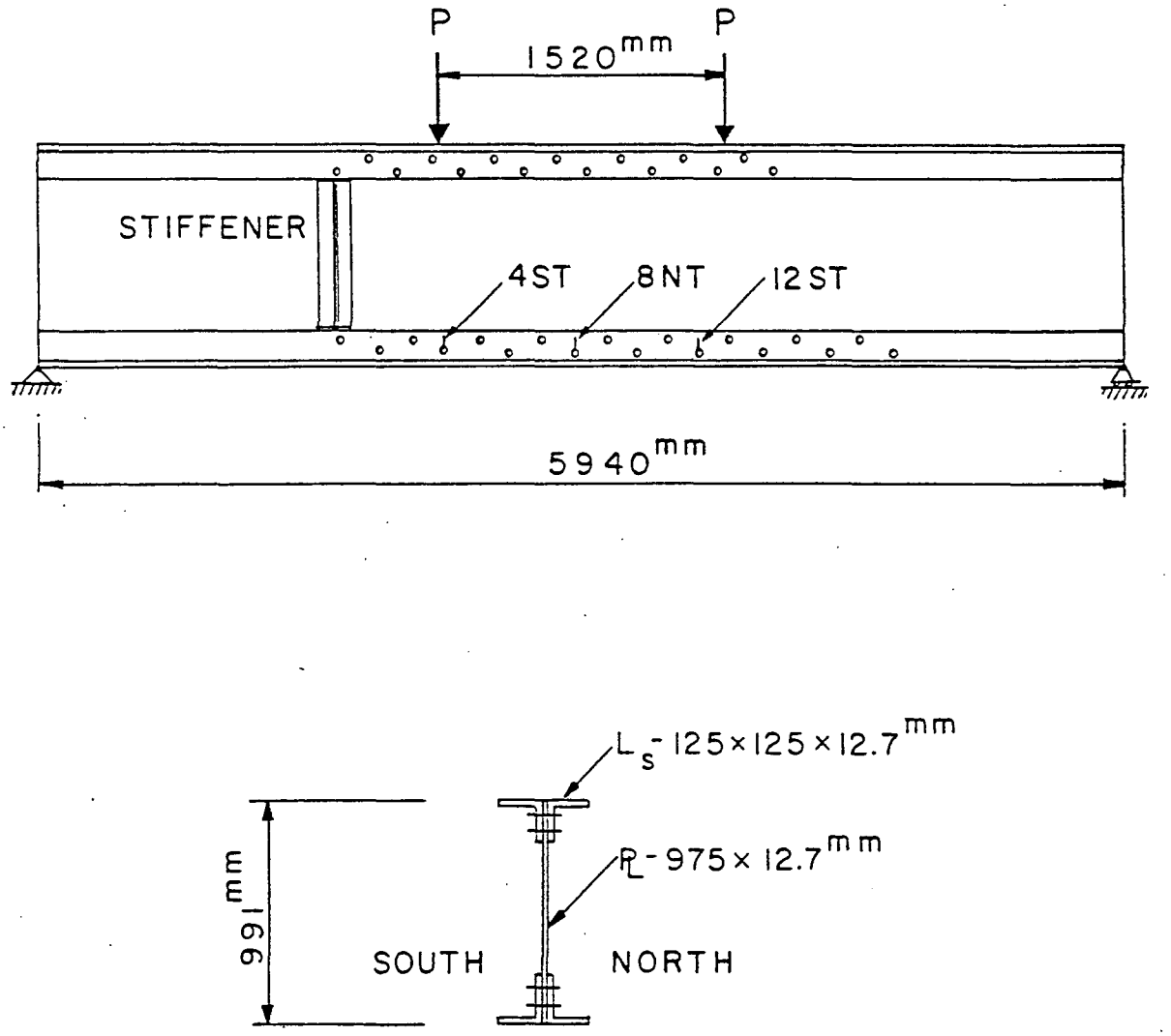

Fig. 5.9 Details and Crack Locations of Riveted Floor Beam in Testing

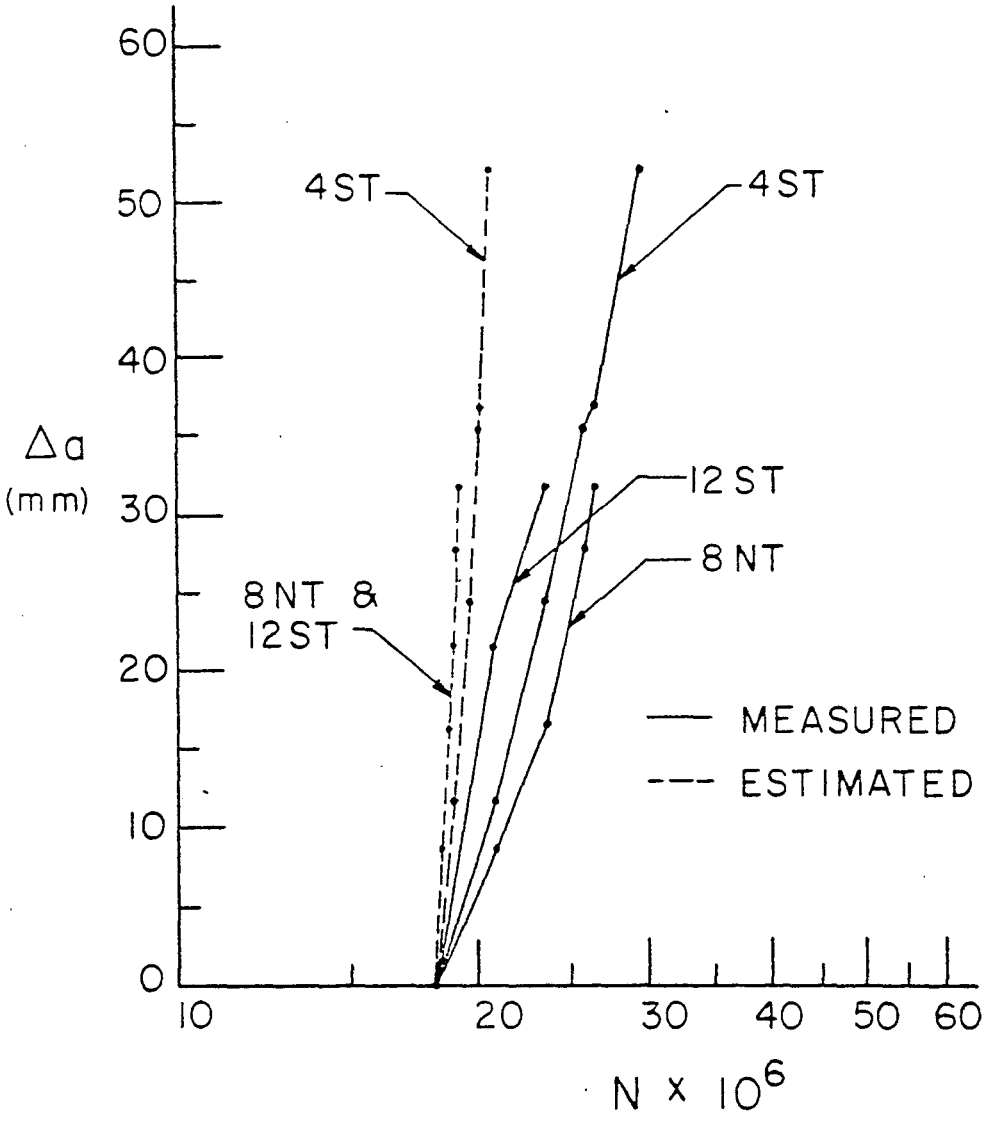

Fig. 5.10 Measured and Estimated Fatigue Crack Propagation in Riveted Floor Beam

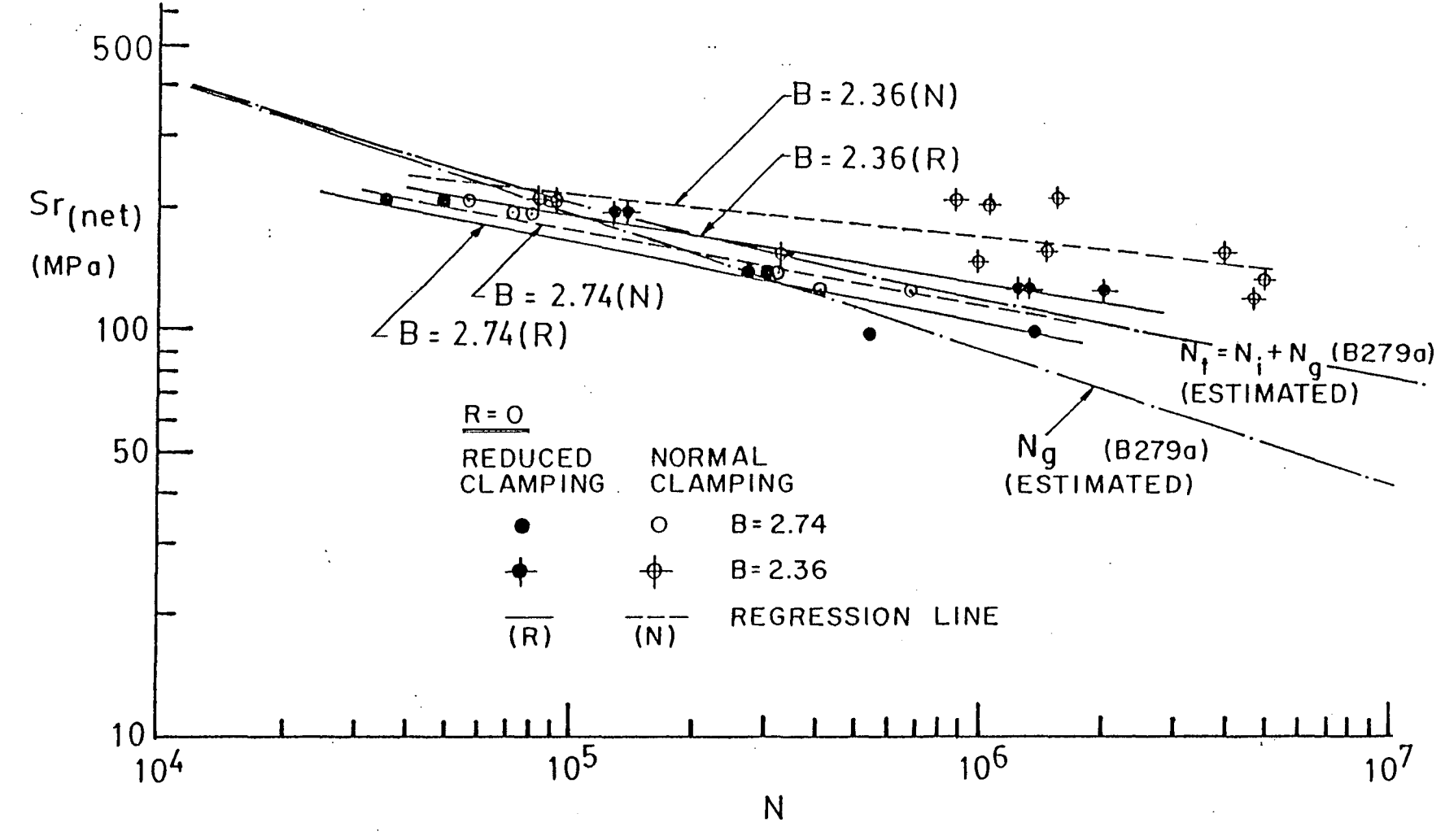

Fig. 5.11 Estimated Fatigue Strength and Test Result of Reference [60] for Bearing Ratio 2.74 and 2.36; R = 0

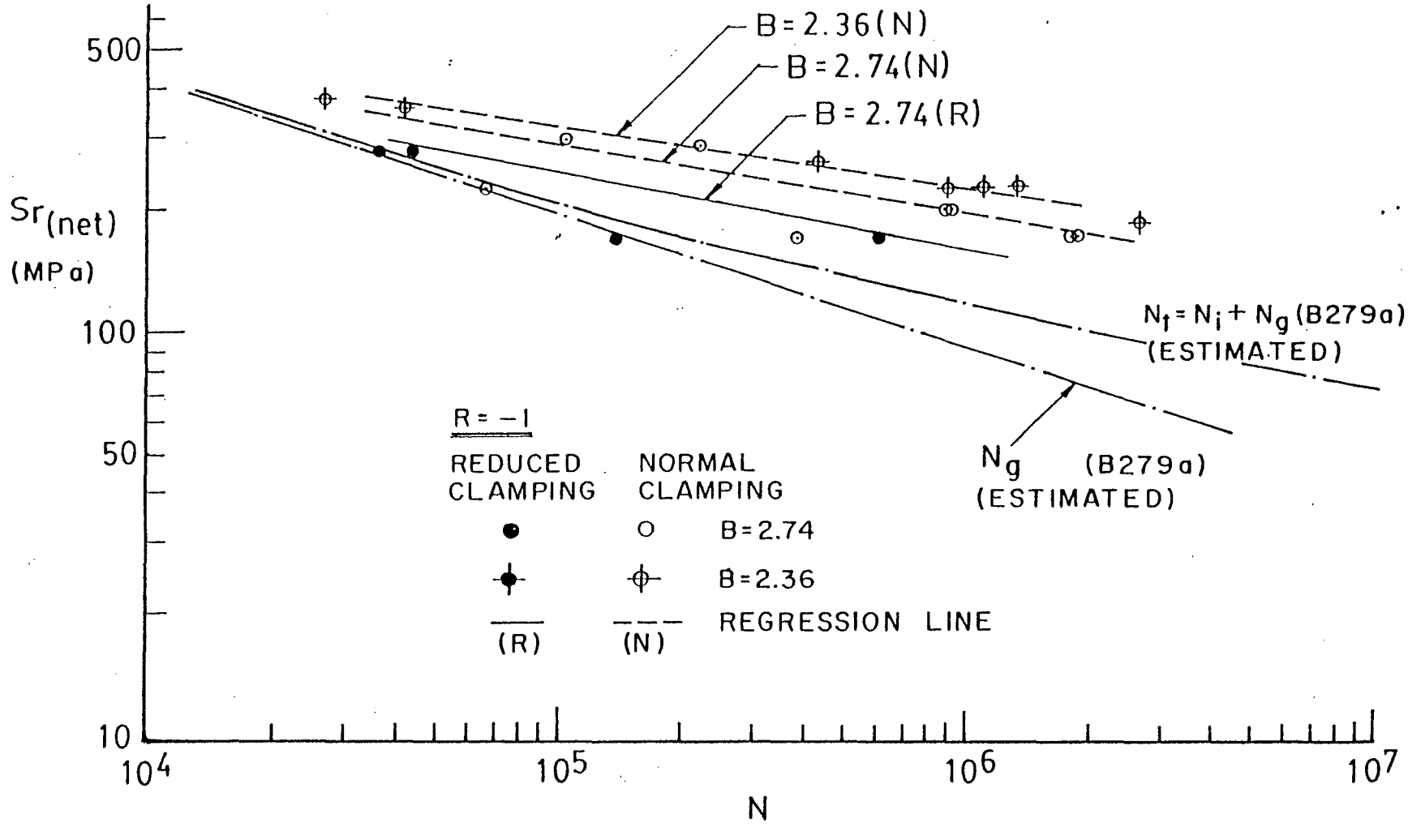

Fig. 5.12 Estimated Fatigue Strength and Test Result of Reference [60] for Bearing Ratio 2.74 and 2.36; R = -1

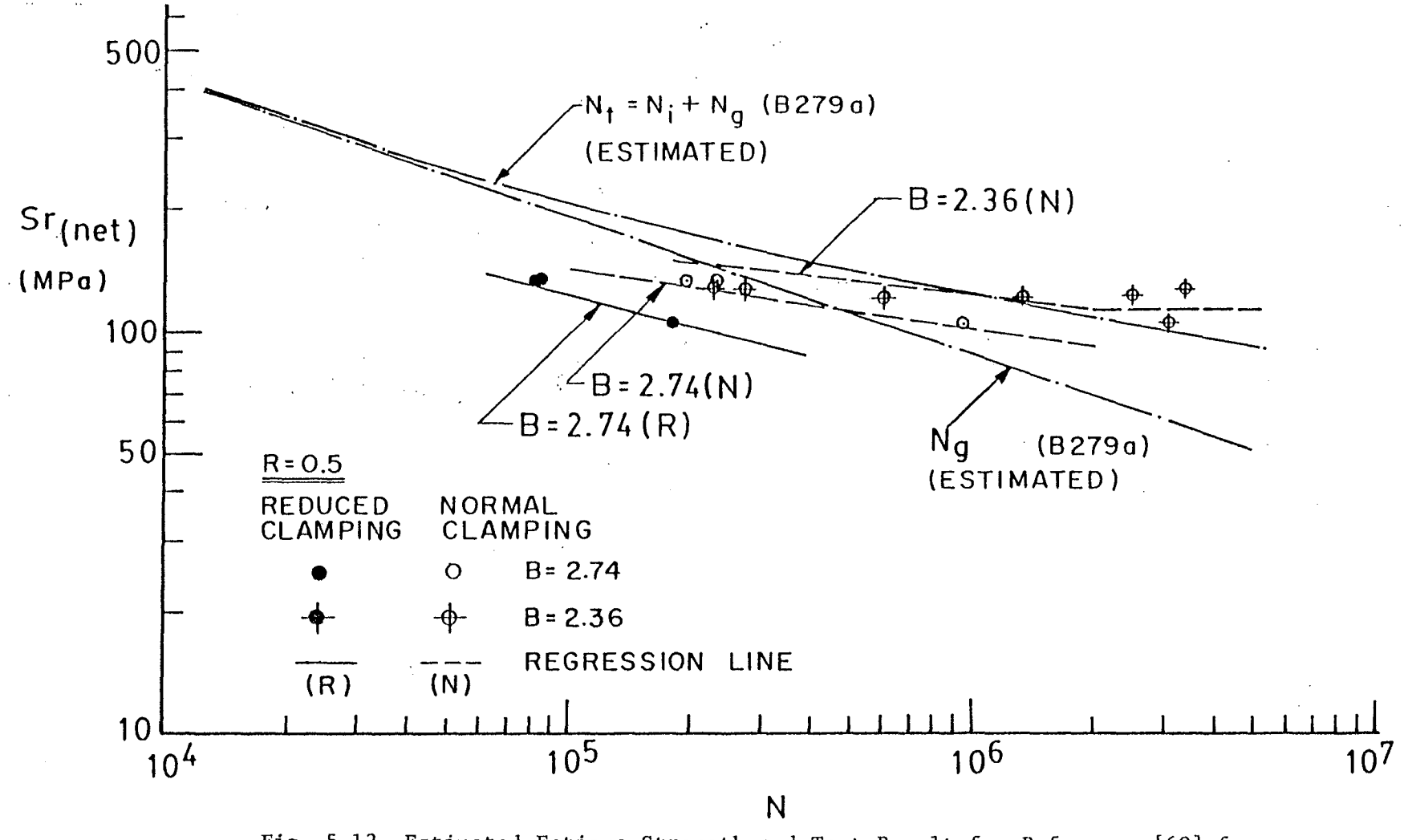

Fig. 5.13 Estimated Fatigue Strength and Test Result for Reference [60] for Bearing Ratio 2.74 and 2.36; R = 1/2

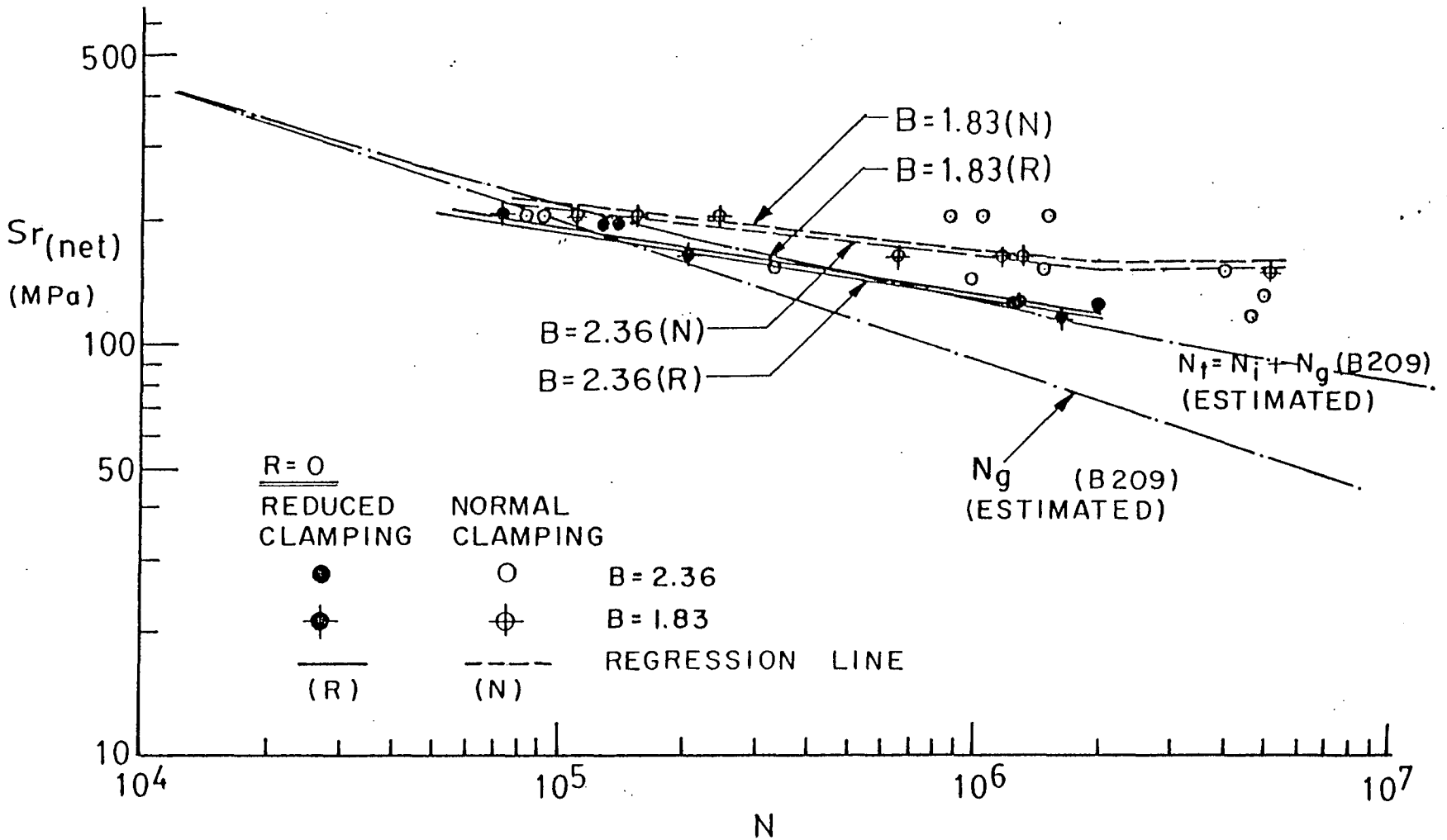

Fig. 5.14 Estimated Fatigue Strength and Test Result of Reference [60] for Bearing Ratio 2.36 and 1.83; R = 0

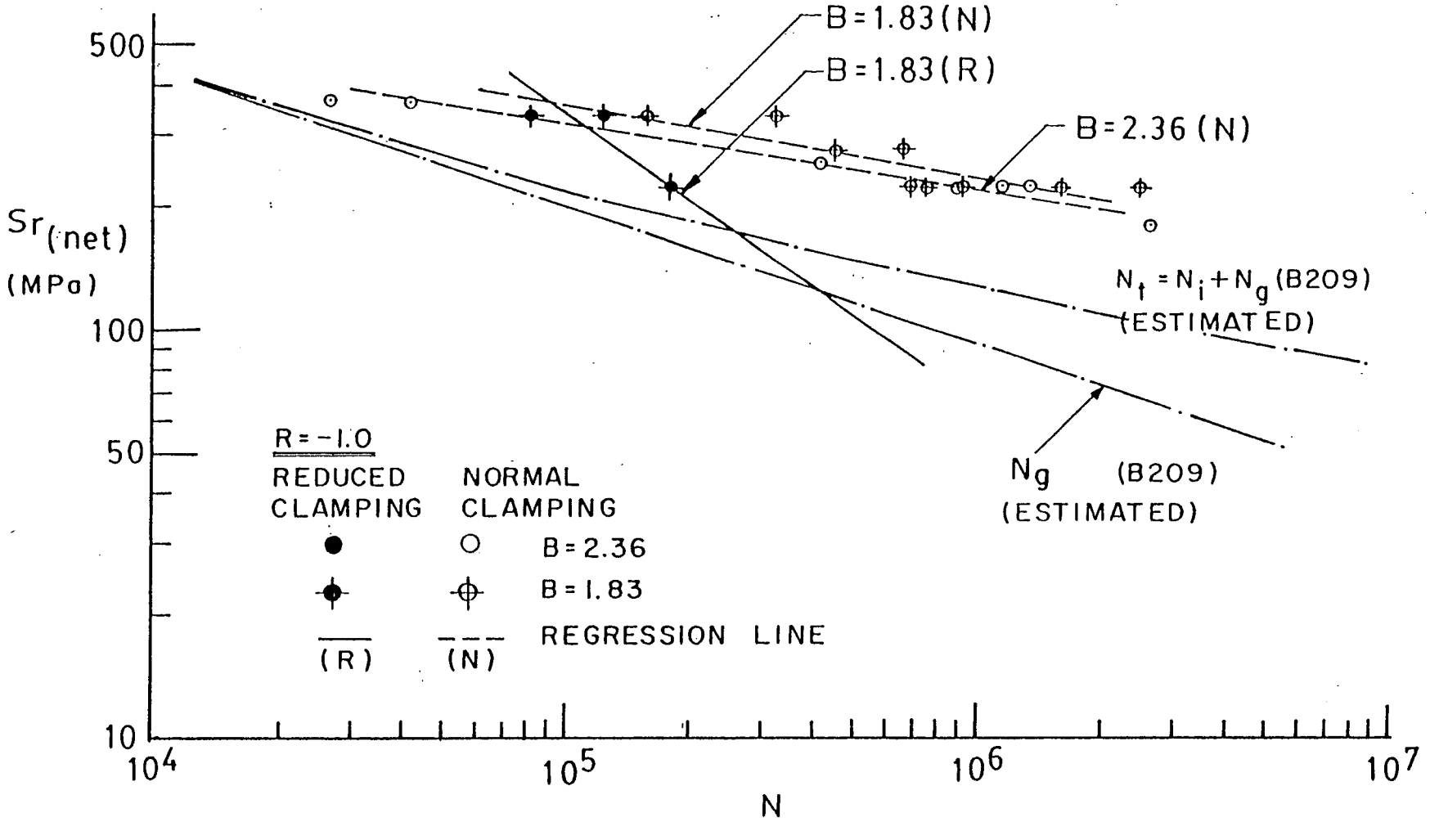

Fig. 5.15 Estimated Fatigue Strength and Test Result of Reference [60] for Bearing Ratio 2.36 and 1.83; R = - 1

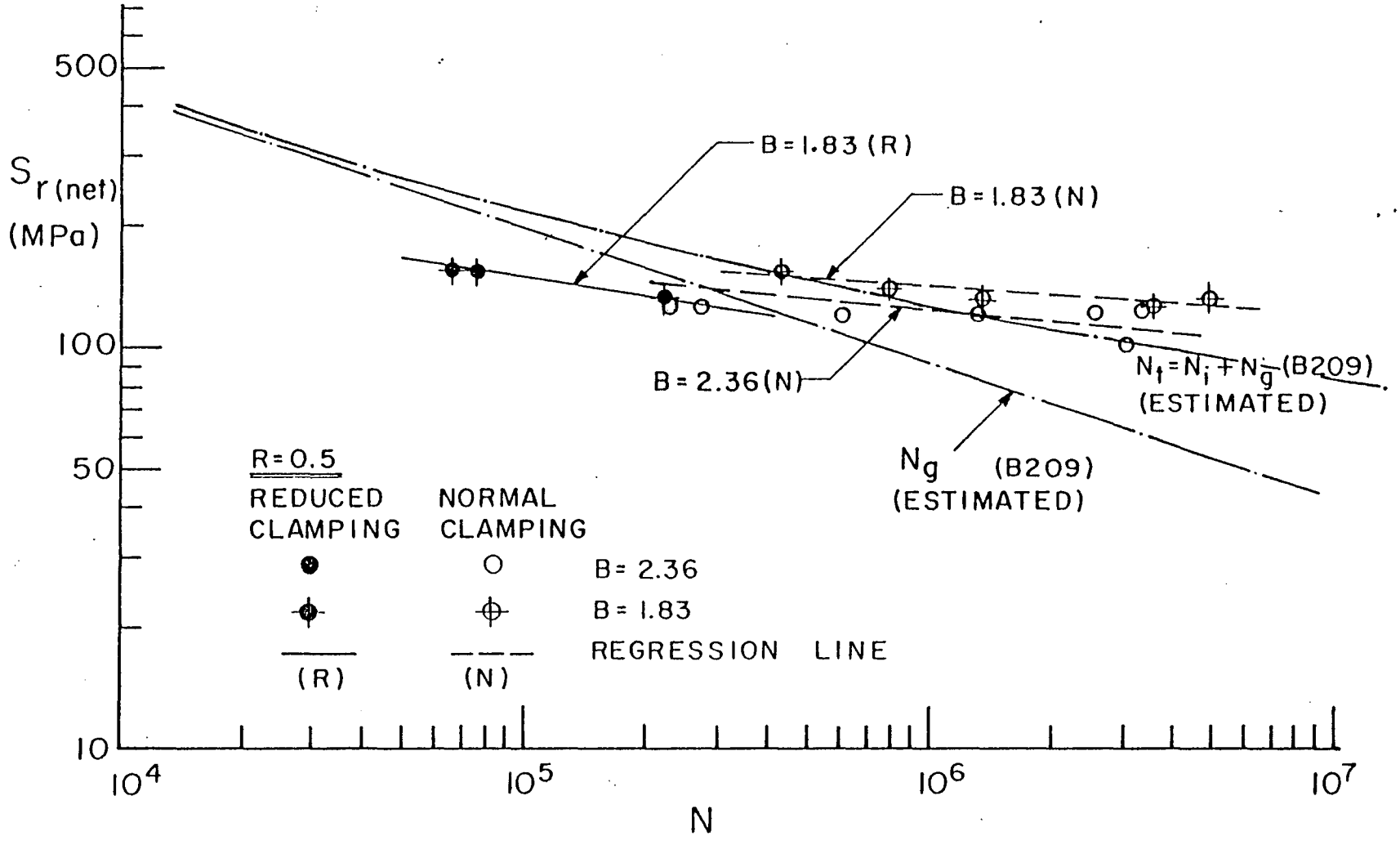

Fig. 5.16 Estimated Fatigue Strength and Test Result of Reference [60] for Bearing Ratio 2.36 and 1.83; R = 1/2

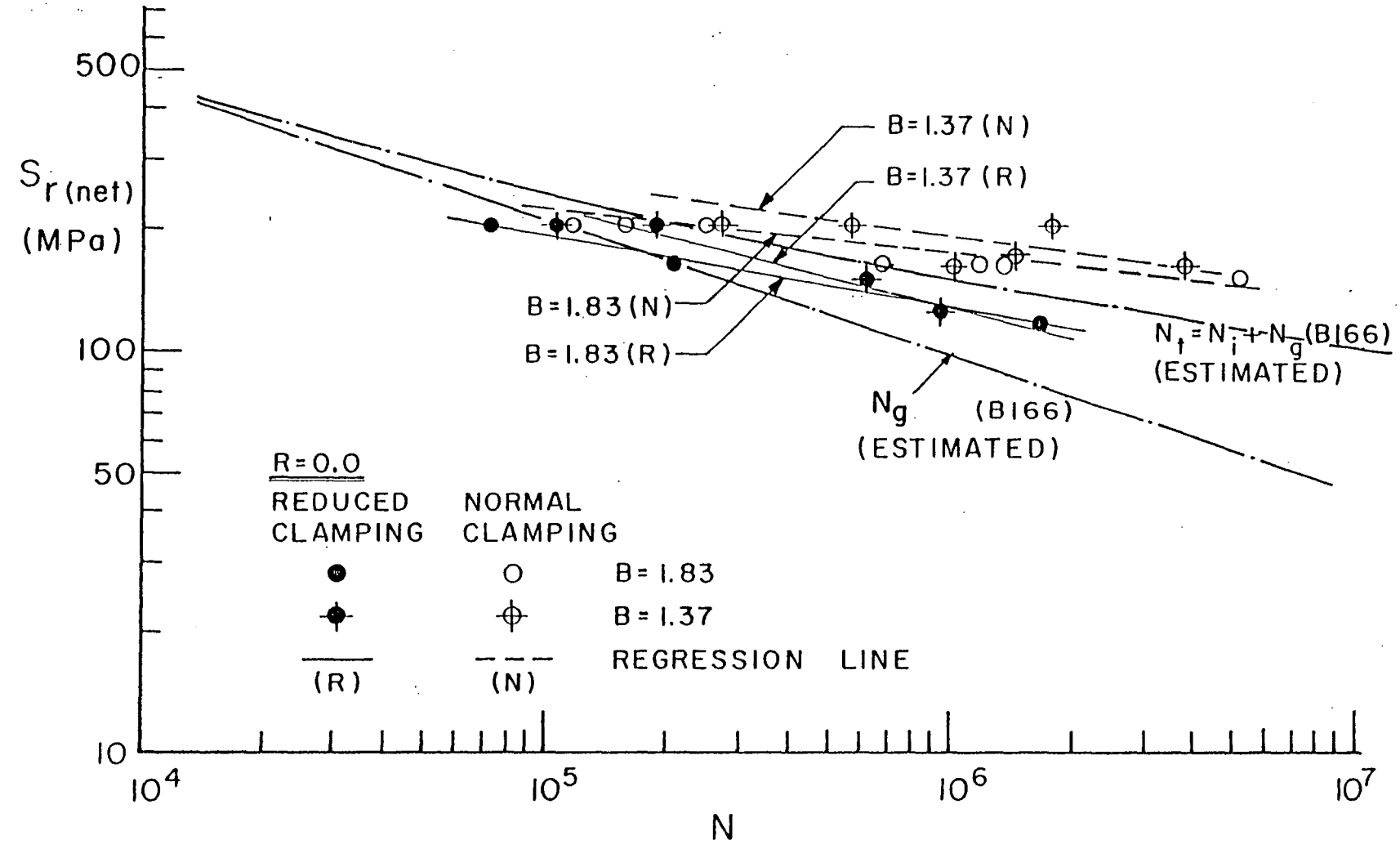

Fig. 5.17 Estimated Fatigue Strength and Test Result of Reference [60] for Bearing Ratio; 1.83 and 1.37; R = 0

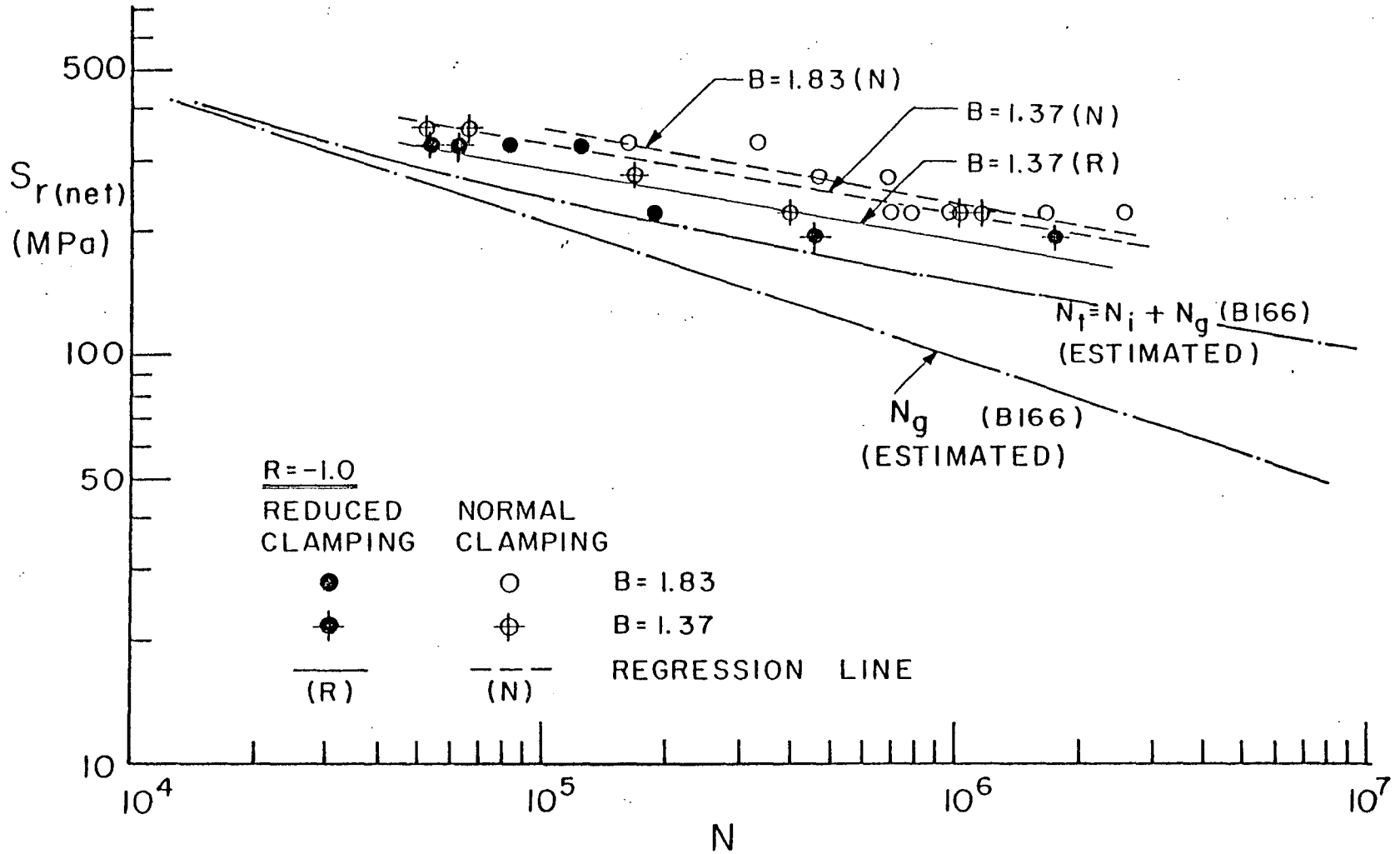

Fig. 5.18 Estimated Fatigue Strength and Test Result of Reference [60] for Bearing Ratio 1.83 and 1.37; R = - 1

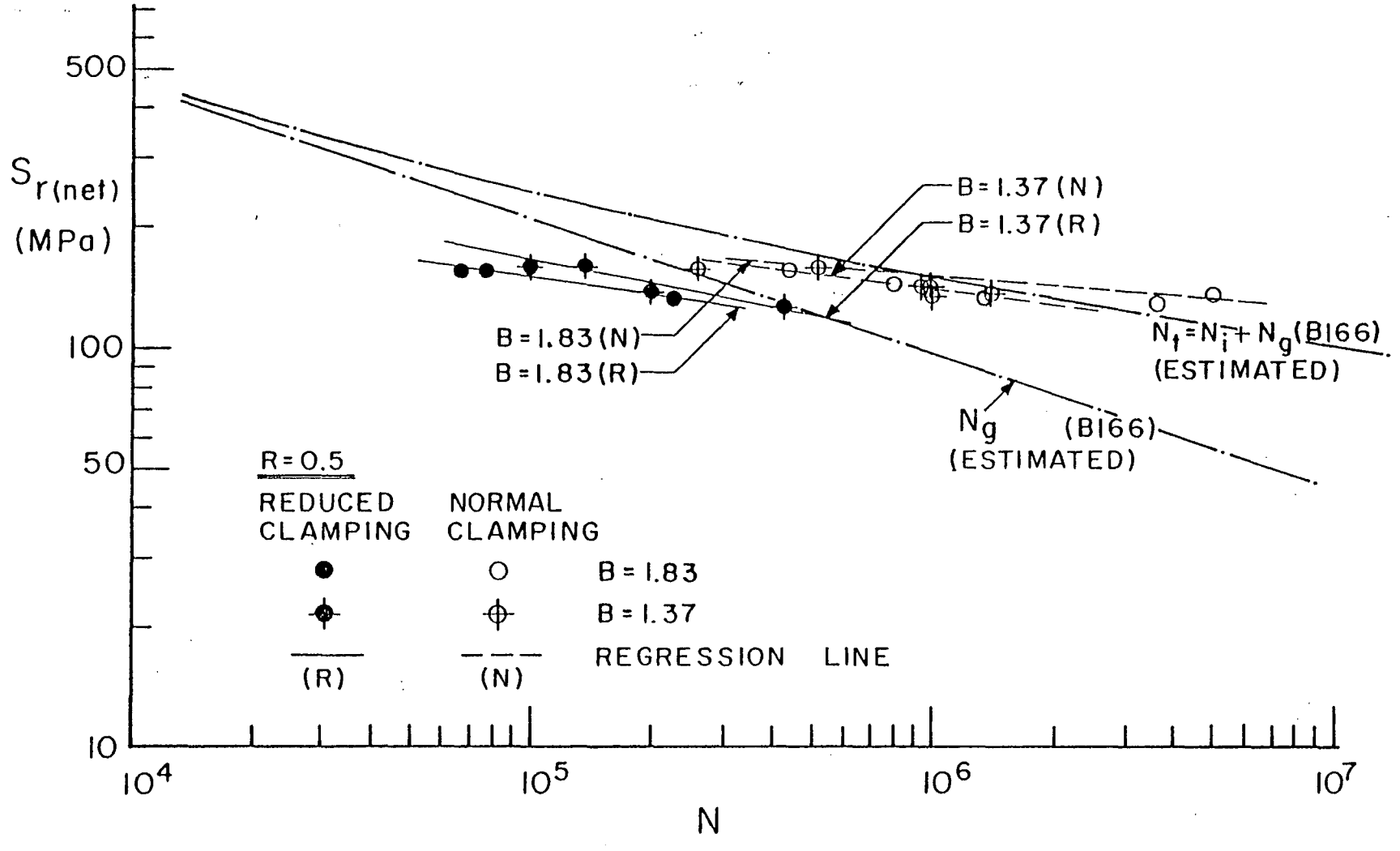

Fig. 5.19 Estimated Fatigue Strength and Test Result of Reference [60] for Bearing Ratio 1.83 and 1.37; R = 1/2

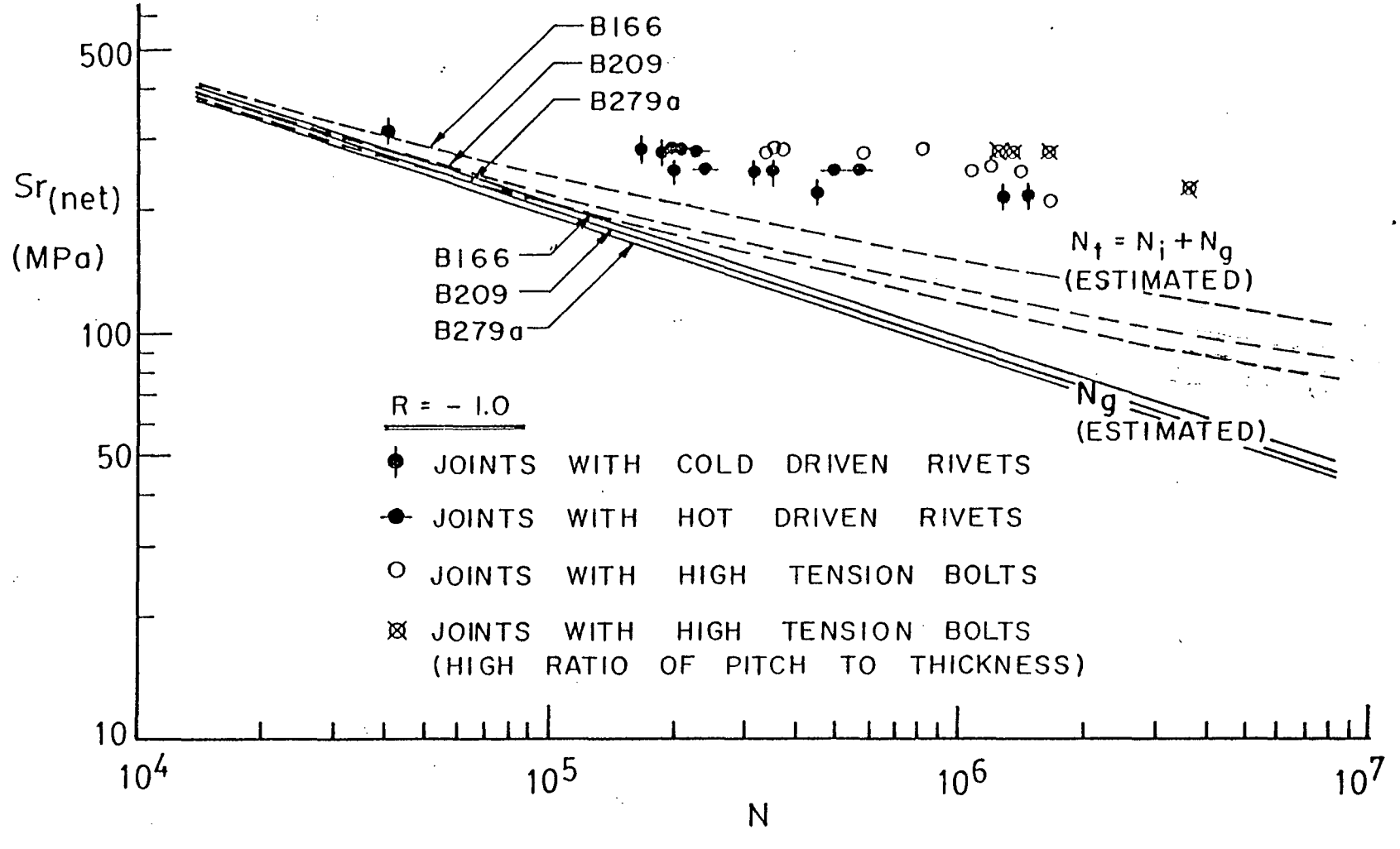

Fig. 5.20 Estimated Fatigue Strength and Test Result of Reference [48] for Riveted and Bolted Joints

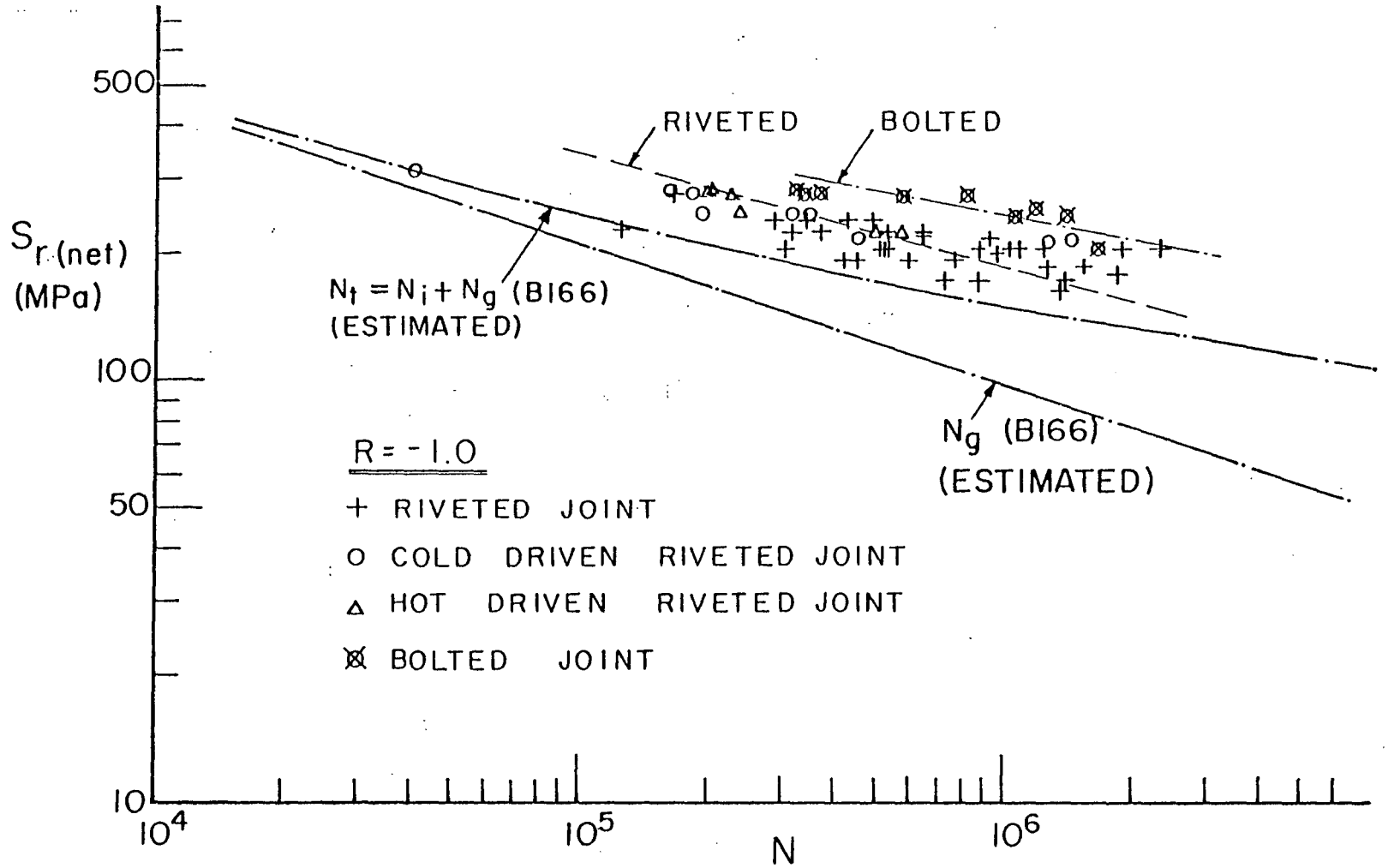

Fig. 5.21 Estimated Fatigue Strength and Test Result of Reference [78]

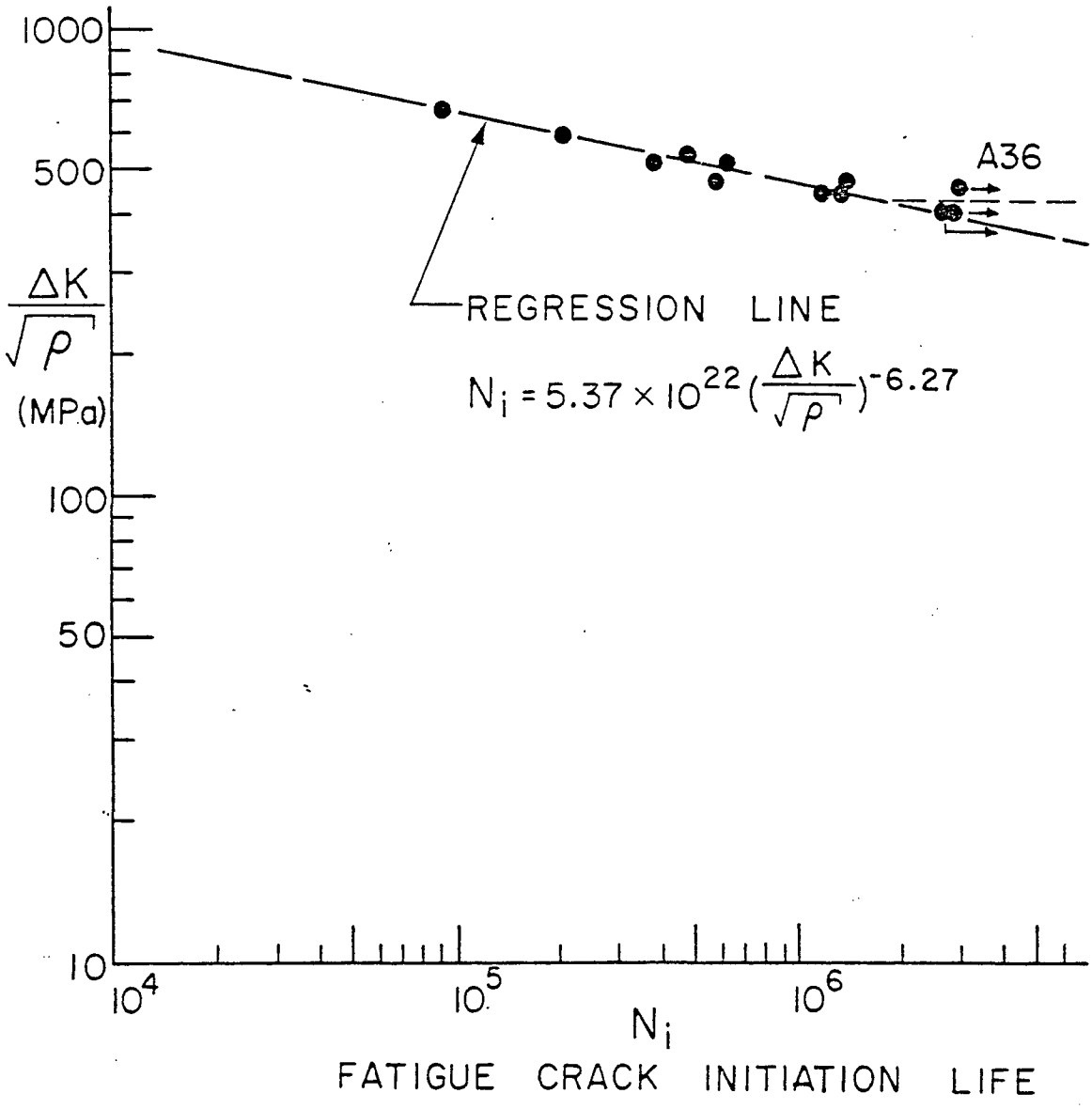

Fig. 5.22 Fatigue Crack Initiation Behavior of A36 Steel [63]

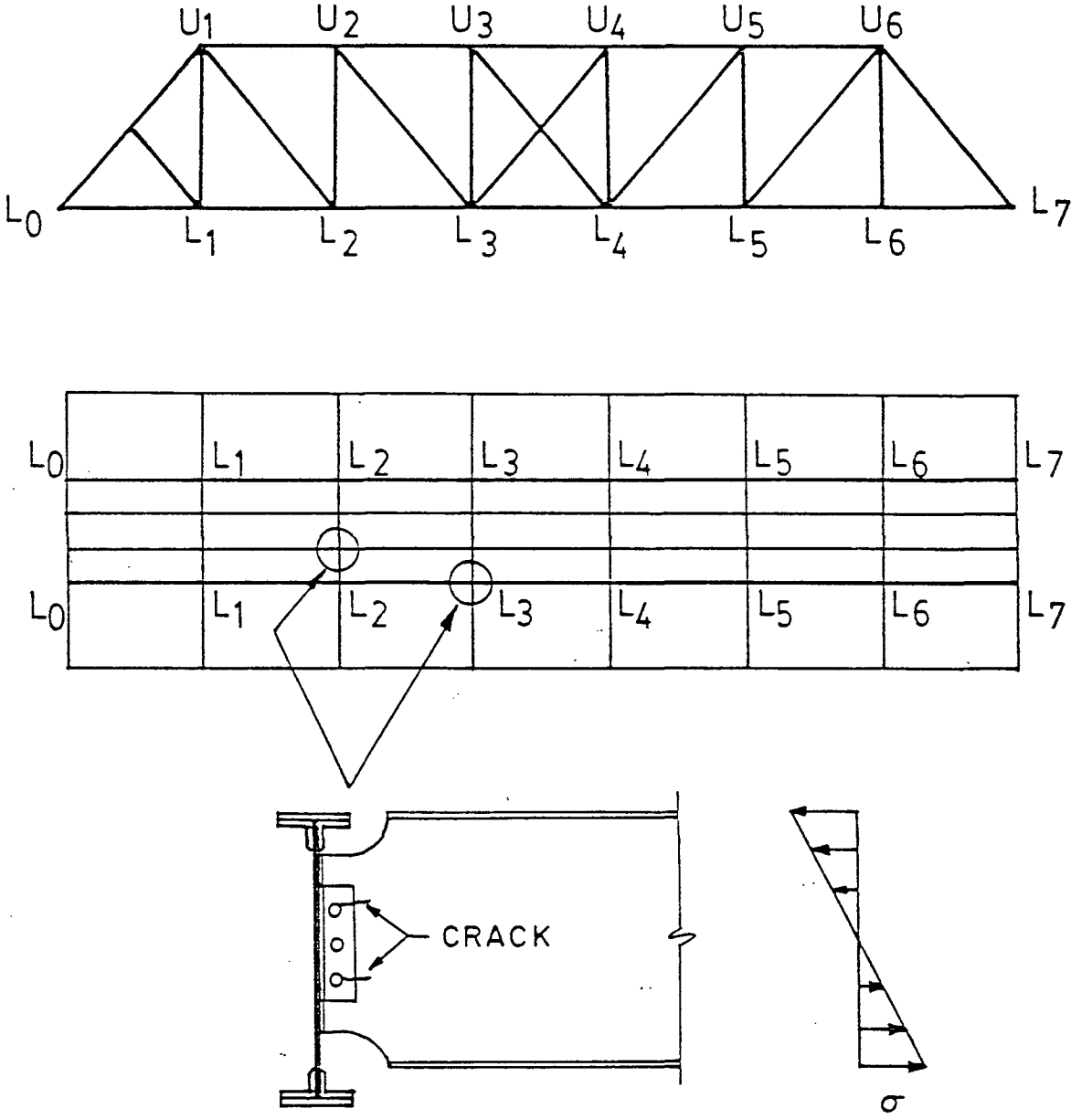

Fig. 5.23 Cracks in Coped Section of Floor System

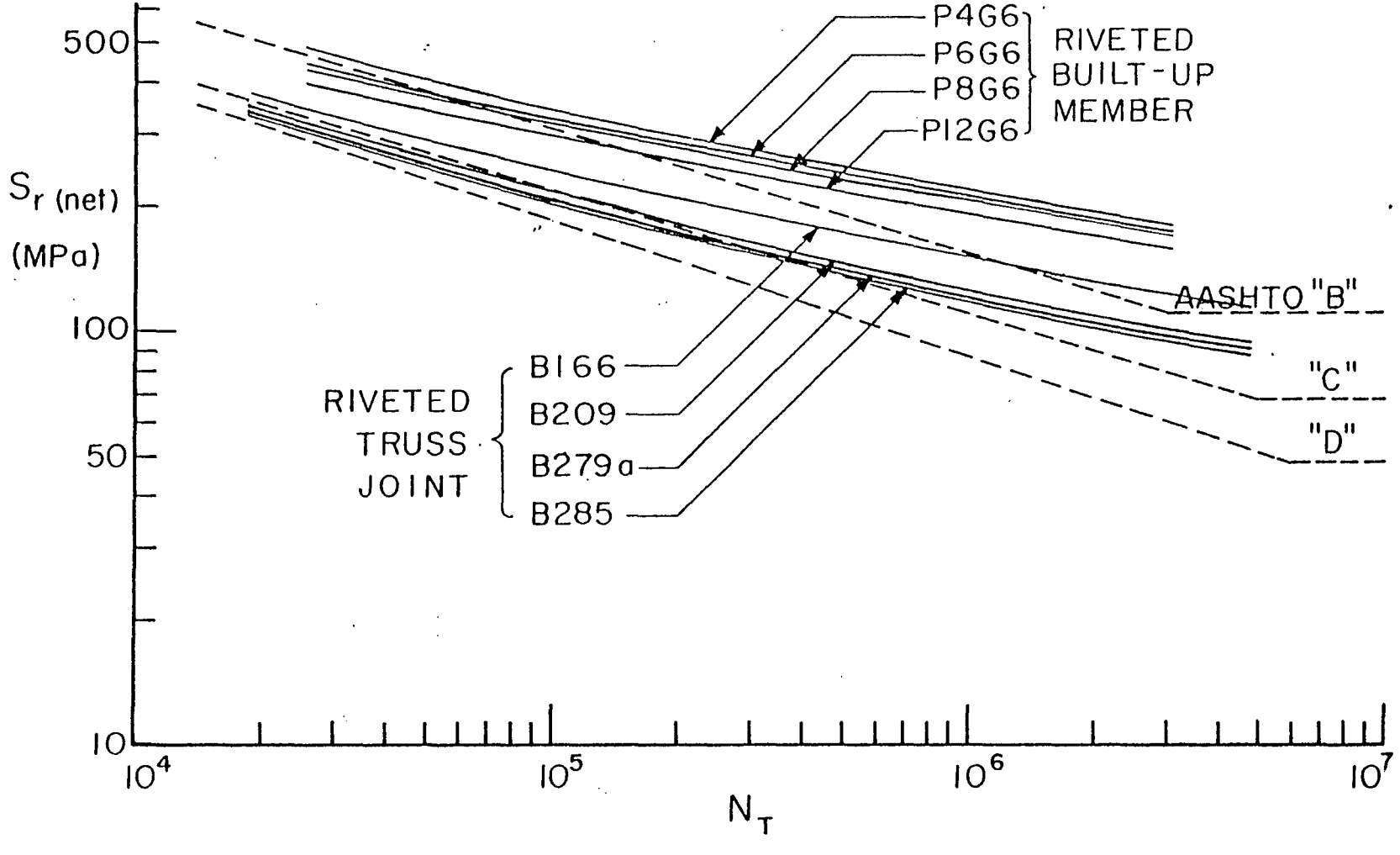

Fig. 5.24 $S_{r\ (net)}$ - N_T Curves of Present Study and AASHTO Fatigue Category B, C and D

R E F E R E N C E S

[1] American Association of State Highway Officials.
Standard Specification for Highway Bridges
11 th edition, American Association of State Highway Officials, Washington, D. C., 1981.

[2] American Railway Engineering Association.
Manual for Railway Engineering
American Railway Enginnering Association, Chicago, Illinois, 1979.

[3] AREA Committee on Iron and Steel Structures.
Stress Distribution in Bridge Frames-Floorbeam Hangers.
In Proceedings, pages 470-503. American Raiload Engineering Association, 1950.
Vol 51.

[4] Association of American Railroads.
Field Investigation of Two Truss Spans on the Southern Pacific Company.
Report ER-82, AAR Research Center, May, 1968.
Chicago.

[5] Baron, F. and Larson E. W., Jr.
The Effect of Grip upon Fatigue Strength of Riveted and Bolted Joints.
Second Progress Report Project 5, Northwestern University, 1951.

[6] Baron, F., Larson, E. W. and Kenworthy, K. J.
The Effect of Certain Rivet Patterns on the Fatigue and Static Strength of Joints.
Bulletin , Northwestern University, Evanston, Illinois, February, 1955.

[7] Barsoum, R. S.
On The Use of Isoparametric Finite Elements in Linear Fracture Mechanics.
International Journal for Numerical Methods in Engineering Vol. 10:pp. 25-37, 1976.

[8] Barsoum, R. S.
Triangular Quarter-Point Elements as Elastic and Perfectly-Plastic Crack Tip Elements.
International Journal for Numerical Methods in Engineering Vol. 11:pp. 85-88, 1977.

[9] Bathe, K.J., Wilson, E. L. and Peterson, F. E.
SAPIV, A Structural Analysis Program for Static and Dynamic Responce of Linear Systems.
Report EERC 73-11, Earthquake Engineering Research Center, June, 1973.

[10] Batho, C.
The Partition of Load in Riveted Joints.
Journal of The Franklin Institute Vol. 182:pp. 553, 1916.

[11] Benzley, S. E.
Representation of Singularities with Isoparametric Finite Elements.
International Journal for Numerical Methods in Engineering Vol. 8:pp. 537-545, 1974.

[12] Benzley, S. E. and Beisinger, A. E.
CHILES-a Finite Element Computer Program that Calculates the Intensities of Linear Elastic Singularities.
Technical Report SLA-73-0894, Sandia Laboratories, 1973.

[13] Bleich, F.
Theorie und Berechnung der Eisernen Brucher.
Julius Springer, Berlin, 1921.

[14] Burk, J. D. and Lawrence, F. V., Jr.
Influence of Bending Stresses on Fatigue Crack Propagation Life in Butt Joint Welds.
Welding Journal Vol. 56:pp. 43s, 1977.

[15] Byskov, E.
The Calculation of Stress Intensity Factors Using The Finite Element Method with Cracked Elements.
International Journal of Fracture Mechanics Vol. 6(No. 2):pp. 159-167, June, 1970.

[16] Carter, J. W., Lenzen, K. H. and Wyly, L. T.
Fatigue in Riveted and Bolted Single-lap Joints.
Transactions of The American Society of Civil Engineers Vol. 120, 1955.

[17] Chan, S. K., Tuba, I. S. and Wilson, W. K.
On the Finite Element Method in Linear Fracture Mechanics.
Engineering Fracture Mechanics Vol. 2:pp. 1-17, 1970.

[18] Chesson, E., Jr. and Munse, W. H.
Riveted and Bolted Joints : Truss-Type Tensile Connection.
Journal of the Structural Division, ASCE Vol. 89(ST1, Part1):pp. 67-106 , February, 1963.

[19] O'Connor, Colin.
Design of Bridge Superstructures.
John Wiley & Sons Inc., New York, 1971.

[20] Davis, C. S.
Computer Analysis of the Stresses in a Plate.
Master Thesis, University of Washington, Seattle, Washington, 1967.

[21] De Luca, A.
Estimated Fatigue Damage in a Railway Truss Bridge ; An Analytical and Experimental Evaluation.
Master Thesis, Lehigh University, Bethlehem, Pennsylvania, October, 1981.

[22] Fairburn, W.
Experimental Inquiry into the Strength of Wrought Iron Plates and Their Riveted Joints as Applied to Shipbuilding and Vessels Exposed to Severe Strains.
Philosophical Trans. Vol. 140, Royal Society, London, 1850.

[23] Fisher, J. W.
The Analysis of Bolted Plate Splices.
PhD thesis, Lehigh University, Bethlehem, Pennsylvania, 1964.

[24] Fisher, J. W. and Daniels, J. H.
An Investigation of the Estimated Fatigue in Members of the 380 Ft. Main Span, Fraser River Bridge.
In Proceedings, Bulletin 658, Vol.77. American Raiload Engineering Association, June-July, 1976.

[25] Fisher, J. W. and Rumpf, J. L.
Analysis of Bolted Butt Joints.
Journal of the Structural Division, ASCE Vol. 91(No. ST5):pp. 181-203, 1965.

[26] Fisher, J. W. and Struik, J. H. A.
Guide to Design Criteria for Bolted and Riveted Joints.
John Wiley & Sons Inc., New York, 1974.

[27] Fisher, J. W., Albrecht, P. A., Yen, B. T., Klingerman, D. J., and McNamee, B. M.
Fatigue Strength of Steel Beams with Welded Stiffeners and Attachments.
NCHRP Report 147, Transportation Research Board, 1974.

[28] Fisher, J. W. and Beedle, L. S.
Bibliography on Bolted and Riveted Joints
The American Society of Civil Engineers, Task Committee on Structural Connections, New York, N. Y., 1967.

[29] Francis, A. J.
The Behavior of Aluminium Alloy Riveted Joints.
Research Report No. 15, The Aluminium Development Association, London, England, 1953.

[30] Frank, K. H.
Fatigue Strength of Fillet Welded Connections.
PhD thesis, Lehigh University, Bethlehem, Pennsylvania, October, 1971.

[31] Gallagher, R. H.
Survey and Evaluation of the Finite Element Method in Linear Fracture Mechanics Analysis.
Paper L6/9, Conference on Structural Mechanics in Reactor Technology, September, Berlin, 1971.

[32] Graf, O.
Dauerversuche mit Nietverbindungen.
Technical Report, Deutscher Stahlbau-Verbund, 1935.

[33] Hansen, N. G.
Fatigue tests of Joints of High-Strength Steel.
Transactions of The American Society of Civil Engineers Vol. 126, Part 2:pp. 750-763, 1961.

[34] Hardin, B. O.
Experimental Investigation of the Primary Stress Distribution in the Gusset plates of a Double-Plane Pratt Truss Joint with Chord Splice at the Joint.
Bulletin No. 49, University of Kentucky, Engineering Experiment Station, Lexington, Kentucky, September, 1958.

[35] Heins, C. P. and Firmage, D. A.
Design of Modern Steel Highway Bridges.
John Wiley & Sons Inc., New York , 1979.

[36] Hellen, T. K. and Blackburn, W. S.
The Calculation of Stress Intensity Factors in Two and Three Dimensions Using Finite Elements.
In Rybicki, E. F. and Benzley, S. E. (editor), Computational Fracture Mechanics, pages 103-120. ASME, 1975.
Presented at the 2nd National Congress on Pressure Vessels and Piping.

[37] Henshell, R. D. and Shaw, K. G.
Crack Tip Elements Are Unnecessary.
International Journal for Numerical Methods in Engineering Vol. 9:pp. 495-507, 1975.

[38] Hertzberg, R. W.
Deformation and Fracture Mechanics of Engineering Materials.
John Wiley & Sons, New York, N. Y., 1976.

[39] Hibbitt, H. D.
Some Properties of Singular Isoparametric Elements.
International Journal for Numerical Methods in Engineering Vol. 11:pp. 180-184, 1977.
Short Communications.

[40] Hinton, E. and Owen, D. R. J.
Computational Mathematics and Applications: Finite Element Programming.
Academic Press, London, England, 1977.

[41] Hirt, M. A. and Fisher, J. W.
Fatigue Crack Growth in Welded Beams.
Engineering Fracture Mechanics Vol. 5:pp. 415-429, 1973.

[42] Hrennikoff, A.
The Work of Rivets in Riveted Joints.
Transactions, ASCE Vol. 99:pp. 437-489, 1939.

[43] Irons, B. M.
A Technique for Degenerating Brick-Type Isoparametric Elements Using Hierarchial Mid-side Nodes.
International Journal for Numerical Methods in Engineering Vol. 8:Short Communication, pp.203-209, 1974.

[44] Irvan, W. G., Jr.
Experimental Study of Primary Stresses in Gusset Plates of a Double Plane Pratt Truss.
Bulletin No. 46, University of Kentucky, Engineering Experiment Station, Lexington, Kentucky, December, 1957.

[45] De Jonge, A. E. R.
Riveted Joints ; A Critical Review of the Literature Covering Their Development.
ASME, New York , 1945.

[46] Kloppel, K.
Gemeinschaftsversuche zur Bestimmung der Schwellzug-Festigkeit Voller.
Der Stahlbau Gelochter und Genieteter Stabe(St.37 und St. 52), 1936.

[47] Kommers J. B.
An Investigation of the Fatigue of Metals.
Bulletin No.136, University of Illinois, Engineering Experiment Station, May, 1923.

[48] Lenzen, K. H.
The Effect of Various Fasteners on the Fatigue Strength of a Structural Joint.
Bulletin 481, Vol. 51, AREA, June-July, 1949.

[49] Lobbet, J. W. and Robb, E. A.
Thermo-mechanical Analysis of Structural Joint Study.
WADD-TR61-151.
1962.

[50] van Maarschalkerwaart, H. M. C. M.
Fatigue Behavior of Riveted Joints.
Technical Report, Netherlands Railways, Utrecht, April, 1981.

[51] Marcotte, D. J.
Estimated Fatigue Damage of The Blue Nile Bridge in Khartoum, Sudan.
Master Thesis, Lehigh University, Bethlehem, Pennsylvania, November, 1981.

[52] Moore, H. F.
An Investigation of the Fatigue of Metals.
Bulletin No.124, University of Illinois, Engineering Experiment Station, October, 1921.

[53] Munse, W. H.
Research on Bolted Connections.
Transactions of The American Society of Civil Engineers Vol. 121:pp. 1255-1266, 1956.

[54] Munse, W. H. and Chesson, E., Jr.
Riveted and Bolted Joints : Net Section Design.
Journal of the Structural Division, ASCE Vol. 89(ST1, Part1), February, 1963.

[55] Munse, W. H., Wright, D. T. and Newmark, N. M.
Laboratory Tests of Bolted Joints.
Transactions of The American Society of Civil Engineers Vol. 120:pp. 1299-1321, 1955.

[56] Newton, R. E.
Degeneration of Brick-Type Isoparametric Elements.
International Journal for Numerical Methods in Engineering Vol. 7:Short Communication, pp.579-581, 1973.

[57] Paris, P. C.
The Fracture Mechanics Approach to Fatigue.
In Fatigue-An Interdisciplinary Approach, pages pp. 107. Syracuse University Press, New York, N. Y., 1964.
10th Sagamore Conference.

[58] Paris, P. C. and Erdogan, F.
A Critical Analysis of Crack Propagation Laws.
Journal of Basic Engineering Series D(Transaction of ASME 85(4)):pp.528, December, 1963.

[59] Paris, P. C. and Sih, G. C.
Stress Analysis of Cracks.
In Special Technical Publication 381, pages . Amarican Society for Testing and Materials, 1964.

[60] Parola, J. F., Chesson, E. Jr. and Munse, W. H.
Effect of Bearing Pressure on Fatigue Strength of Riveted Connections.
Bulletin 481, Vol. 63 No. 27, Engr. Exp. Station, University of Illinois, 1965.

[61] Reemsnyder, Harold S.
Fatigue of Riveted and Bolted Joints ; A Literature Survey.
Homer Research Laboratories, Bethlehem, PA., 1968.

[62] Rice, J. R. and Tracey, D. M.
Numerical and Computer Methods in Structural Mechanics: Computational Fracture Mechanics.
Academic Press, New York, pp. 585-623, 1973.

[63] Rolfe, S. T. and Barsom, J. M.
Fracture and Fatigue Control in Structures.
Prentice-Hall, Inc., Englewood Cliffs, New Jersey, 1977, .

[64] Rumpf, J. L.
The Ultimate Strength of Bolted Connections.
PhD thesis, Lehigh University, Bethlehem, Pennsylvania, 1960.

[65] Shih, C. F.,de Lorenzi, H. G. and German, M. D.
Crack Extension Modeling with Singular Quadratic Isoparametric Elements.
International Journal of Fracture Mechanics Vol. 12:pp. 647-651, 1976.

[66] Struik, John H. A.
Application of Finite Element Analysis to Non-Linear Plane Stress Problems.
PhD thesis, Lehigh University, Bethlehem, Pennsylvania, 1972.

[67] Sweeney, R. A. P. and Elkholy, I. A. S.
Estimated Fatigue Damage of the Assiniboine River Bridge in Nattress, Manitoba, Canada.
report, Canadian National Railways, Montreal, Quebec, Canada, August, 1980.

[68] Tada, H., Paris, P. C. and Irwin, G. R.
The Stress Analysis of Cracks Handbook
Del Research Corporation, Hellertown, Pa., 1973.

[69] Tate, M. B. and Resenfeld, S. J.
Preliminary investigation of the Loads Carried by Individual Bolts in Bolted Joints.
Tech. Memo. No. 1051, NACA, Washington, D. C., 1946.

[70] Taylor D. W. and Gifford, L. N. Jr.
APES-Second Generation Two-dimensional Fracture Mechanics and Stress Analysis by Finite Elements.
Report 4799, Structures Department, Research and Development Report, December, 1975.

[71] Tong, P., Pian, T. H. H. and Lasry, S. J.
A Hybrid-Element Approach to Crack Problems in Plane Elasticity.
International Journal for Numerical Methods in Engineering Vol. 7:pp. 297-308, 1973.

[72] Vasarhelyi, D. D.
Test of Gusset Plate Models.
Journal of the Structural Division, ASCE Vol. 97(No. ST2), February, 1971.

[73] Vogt, F.
Load Distribution in Bolted or Riveted Structural Joints in Light-Alloy Structures.
Tech. Memo. No. 1135, NACA, Washington, D. C., 1947.

[74] Ward, B. A.
An Analytical Study of a Truss Bridge ; Modeling Techniques and Stress Redistribution.
Master Thesis, Lehigh University, Bethlehem, Pennsylvania, October, 1982.

[75] Whitmore, R. E.
Experimental Investigation of Stresses in Gusset Plates.
Bulletin No. 16, University of Tennessee, Engineering Experiment Station, May, 1952.

[76] Wilson, E. L., Bathe, K. J. and Doherty, W. P.
Direct Solution of Large Systems of Linear Equations.
In Computers & Structures, pages 363-372. Pergamon Press, England, Vol. 4, 1974.

[77] Wilson, J. S. and Haigh B. P.
The Influence of Rivet Holes on the Strength and Endurance of Steel Structure.
British Association Meeting at Hull secton G-Trans, September, 1922.

[78] Wilson, W. M. and Thomas, F. P.
Fatigue Tests of Riveted Joints.
Bulletin No. 302 Vol. 63, No. 79, University of Illinois, Engineering Experiment Station, May, 1938.

[79] Wyly, L. T., Scott, M. B., McCammon, L. B. and Lindner, C. W.
A Study of Behavior of Floorbeam Hangers.
Bulletin 482, American Raiload Engineering Association, October, 1949.

[80] Yen, B. T., Seong, C. K. and Daniels, J. H.
Fatigue Resistance of Frankford Elevated Line Viaduct.
Report No. 451.1, Fritz Engineering Laboratory, Lehigh University, Bethlehem, Pennsylvania, June, 1980.

[81] Yen, S. W. and Smillie, D. G.
Computer analysis of Fastener Load Distribution In a Multi-Row Joint.
In Computers & Structures, pages 1293-1320. Pergamon Press, England, Vol. 3, 1973.

[82] Zettlemoyer, N.
Stress Concentration and Fatigue of Welded Details.
PhD thesis, Lehigh University, Bethlehem, Pennsylvania, October, 1976.

[83] Zienkiewicz, O. C.
The Finite Element Method.
3rd Edition, McGraw-Hill, London, England, 1977, .

APPENDIX I

ISOPARAMETRIC FINITE ELEMENT FORMULATION

I.1 Isoparametric Finite Element [83]

The displacement field in an element of general shape is given by,

$$\begin{aligned} u &= \Sigma\, N_i\ (\xi,\ \eta,\ \zeta)\ u_i \\ v &= \Sigma\, N_i\ (\xi,\ \eta,\ \zeta)\ v_i \\ w &= \Sigma\, N_i\ (\xi,\ \eta,\ \zeta)\ w_i \end{aligned} \qquad \text{(I.1)}$$

in which N_i is a shape function in the curvilinear coordinates ξ, η and ζ, and i is the node number as shown in Fig.3-4.

The coodinates x, y and z inside the element domain can be described in a similar manner by

$$\begin{aligned} x &= \Sigma\, M_i\ (\xi,\ \eta,\ \zeta)\ x_i \\ y &= \Sigma\, M_i\ (\xi,\ \eta,\ \zeta)\ y_i \\ z &= \Sigma\, M_i\ (\xi,\ \eta,\ \zeta)\ z_i \end{aligned} \qquad \text{(I.2)}$$

where M_i is a function to define the element geometry in the curvilinear coordinates ξ, η and ζ.

For a particular case, when the shape functions defining the displacement fields (N_i) and those defining

the geometry (M_i) are the same, then the element is termed isoparametric [83].

For the quadratic (8 node) plane two-dimensional element in Fig.3-4, the general equation of the shape function for corner nodes where $\xi_i=\eta_i=\pm 1.0$ is,

$$N_i = \frac{1}{4}(1+\xi\xi_i)(1+\eta\eta_i)(\xi\xi_i+\eta\eta_i-1)$$

for mid-side nodes with $\xi_i=0$, $\eta_i=\pm 1.0$,

$$N_i = \frac{1}{2}(1-\xi^2)(1+\eta\eta_i) \qquad (I.3)$$

and for mid-side nodes with $\eta_i=0$, $\xi_i=\pm 1.0$,

$$N_i = \frac{1}{2}(1+\xi\xi_i)(1-\eta^2)$$

Isoparametric finite element representation is most efficient for modelling a body with curved boundaries. The equation of the form,

$$\begin{Bmatrix} x \\ y \\ z \end{Bmatrix} = [\,N\,] \begin{Bmatrix} x_i \\ y_i \\ z_i \end{Bmatrix} \qquad (I.4)$$

can be considered a transformation between cartesian coordinates and curvilinear coordinates if [N] is a matrix of shape functions of order higher than the first order. Eq.(I.4) represents the mapping of a straight-sided element in local coordinates into a

curve-sided element in the global cartesian coordinate system. This approach permits the modelling of complex geometrical shapes with fewer elements than when elements with straight sides only are used. The important limitation on the isoparametric finite element is that the transformation must be unique such that one-to-one correspondence between points in the two coordinate systems exists. In other words, the mapping must not cause such distortions that element may fold back upon itself.

I.2 Element Stiffness Matrix for the Isoparametric Element [40]

The element stiffness matrix [K] for a two-dimensional isoparametric element is formulated by the following procedure.

The equations relating strains and displacements are,

$$\varepsilon = \begin{Bmatrix} \varepsilon_x \\ \varepsilon_y \\ \varepsilon_{xy} \end{Bmatrix} = [B] \begin{Bmatrix} u_i \\ v_i \end{Bmatrix} \tag{I.5}$$

where,

$$[B] = \begin{bmatrix} \frac{\partial N_i}{\partial x} & 0 \\ 0 & \frac{\partial N_i}{\partial y} \\ \frac{\partial N_i}{\partial y} & \frac{\partial N_i}{\partial x} \end{bmatrix}$$

The expression of [B] matrix can not be performed directly since N_i's are functions of ξ and η.

By chain rule of differentiation,

$$\begin{Bmatrix} \frac{\partial N_i}{\partial \xi} \\ \\ \frac{\partial N_i}{\partial \eta} \end{Bmatrix} = \begin{bmatrix} \frac{\partial x}{\partial \xi} & \frac{\partial y}{\partial \xi} \\ \\ \frac{\partial x}{\partial \eta} & \frac{\partial y}{\partial \eta} \end{bmatrix} \begin{Bmatrix} \frac{\partial N_i}{\partial x} \\ \\ \frac{\partial N_i}{\partial y} \end{Bmatrix} = [J] \begin{Bmatrix} \frac{\partial N_i}{\partial x} \\ \\ \frac{\partial N_i}{\partial y} \end{Bmatrix} \tag{I.6}$$

where [J] is defined as a Jacobian matrix evaluated from Eq.(I.2) and Eq.(I.3) for each element and is given by,

$$[J] = \begin{Bmatrix} \frac{\partial N_1}{\partial \xi}, & \frac{\partial N_2}{\partial \xi}, & - & - & , & \frac{\partial N_n}{\partial \xi} \\ \\ \frac{\partial N_1}{\partial \eta}, & \frac{\partial N_2}{\partial \eta}, & - & - & , & \frac{\partial N_n}{\partial \eta} \end{Bmatrix} \begin{Bmatrix} x_1 & y_1 \\ x_2 & y_2 \\ & \\ & \\ x_n & y_n \end{Bmatrix} \tag{I.7}$$

Therefore, the desired derivatives are

$$\begin{Bmatrix} \frac{\partial N_i}{\partial x} \\ \\ \frac{\partial N_i}{\partial y} \end{Bmatrix} = [J]^{-1} \begin{Bmatrix} \frac{\partial N_i}{\partial \xi} \\ \\ \frac{\partial N_i}{\partial \eta} \end{Bmatrix} \tag{I.8}$$

Similarly,

$$dxdy = |J| \, d\xi d\eta \tag{I.9}$$

where $|J|$ is the determinant of [J].

The stress and strain are related by

$$\{\sigma\} = [D]\ \{\epsilon\} \tag{I.10}$$

where [D] is the stress-strain matrix. Therefore, the element stiffness matrix [K] is,

$$[K] = \int_{-1}^{1}\int_{-1}^{1} [B]^T[D][B]\ |J|\ d\xi d\eta * h \tag{I.11}$$

where h is the thickness of the plate.

I.3 Consistent Nodal Forces and Pressure Loading Applied to Element Edges [40]

For concentrated loads, the known force components can be simply assigned to a node at the point of load application. However, a distributed traction acting on an element boundary is not simple to deal with when quadratic or higher order isoparametric elements are used. As an example, the allocation of uniformly distributed traction force on a rectangular element edge is shown in Fig. I-1.

For the arbitrarily distributed traction force, the proper allocation of traction can be achieved by virtual work consideration.

Manual calculation of consistent load vector which

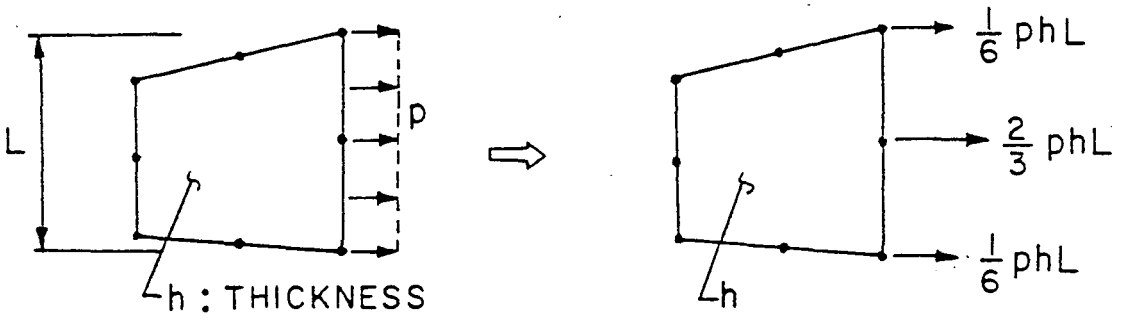

Figure I-1: Consistent Nodal Force Vector For Uniformly Distributed Traction Force

is staticaly equivalent to the distributed traction has the following procedure.

For quadratic isoparametric element, an arbitrarily distributed traction force on an element edge can be assumed as of parabolic distribution without much discrepancy if the element size is small. This parabolic distribution of traction force can be written in terms of p_1, p_2 and p_3, as shown in Fig.I-2.

$$P = 2(p_1-2p_2+p_3)y^2/L^2 + (p_3-p_1)y/L + p_2$$

or,

$$a = 2(p_1-2p_2+p_3)/L^2$$

$$b = (p_3-p_1)/L$$

$$c = p_2$$

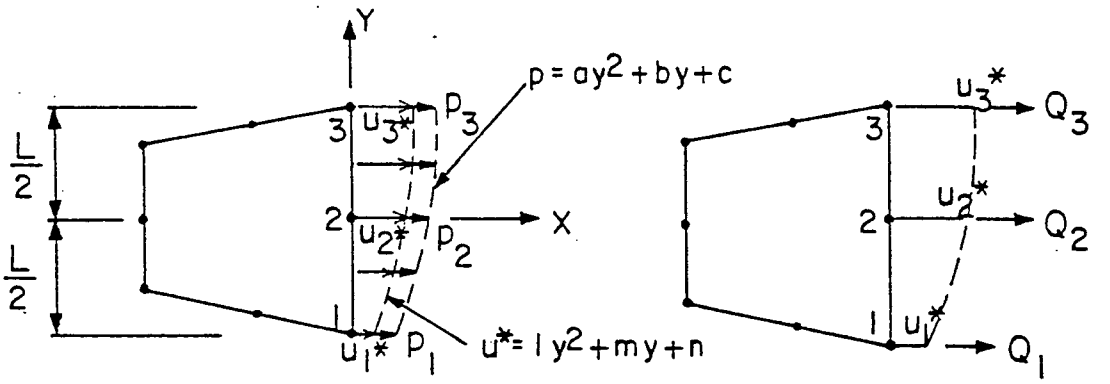

Figure I-2: Consistent Nodal Force Vector for Arbitrarily Distributed Traction Force

The virtual edge displacement u^* also can be assumed parabolic,

$$u^*=[y^2, \quad y, \quad 1] \begin{Bmatrix} l \\ m \\ n \end{Bmatrix}$$

When this virtual displacement take place, the edge load, P, does virtual work . Over an incremental length dy of edge, the work done is,

$$dW_p=(P)(u^*)(h)dy=(ay^2+by+c)[y^2, \quad y, \quad 1] \begin{Bmatrix} l \\ m \\ n \end{Bmatrix} hdy$$

The virtual work done on the entire edge is,

$$W_p{}^*=\int_{-L/2}^{L/2} dW_p=h[\frac{3aL^5+20cL^3}{240}, \quad \frac{bL^3}{12} , \quad \frac{aL^3+12cL}{12}] \begin{Bmatrix} l \\ m \\ n \end{Bmatrix}$$

When a concentrated load system Q_1, Q_2, and Q_3 move through virtual displacements u_1^*, u_2^* and u_3^* as shown in Fig.I-2, the virtual work done by the load system is,

$$W_p=[Q_1,\ Q_2,\ Q_3]\begin{Bmatrix} u_1^* \\ u_2^* \\ u_3^* \end{Bmatrix}$$

where,

$$\begin{Bmatrix} u_1^* \\ u_2^* \\ u_3^* \end{Bmatrix}=\begin{Bmatrix} u^*_{y=-L/2} \\ u^*_{y=0} \\ u^*_{y=L/2} \end{Bmatrix}=\begin{bmatrix} (-L/2)^2 & -L/2 & 1 \\ 0 & 0 & 1 \\ (L/2)^2 & L/2 & 1 \end{bmatrix}\begin{Bmatrix} l \\ m \\ n \end{Bmatrix}$$

By equating the virtual work done by the edge load P to that by the concentrated loading system, it is obtained,

$$[Q_1,Q_2,Q_3]\begin{bmatrix} \frac{L^2}{4} & -\frac{L}{2} & 1 \\ 0 & 0 & 1 \\ \frac{L^2}{4} & \frac{L}{2} & 1 \end{bmatrix}\begin{Bmatrix} \ell \\ m \\ n \end{Bmatrix} = h\left[\frac{3aL^5+20cL^3}{240},\ \frac{bL^3}{12},\ \frac{aL^3+12cL}{12}\right]\begin{Bmatrix} \ell \\ m \\ n \end{Bmatrix} \qquad (I.12)$$

and Q_1, Q_2 and Q_3 become,

$$Q_1 = hL\ (4p_1+2p_2-p_3)/30$$

$$Q_2 = hL\ (p_1+8p_2+p_3)/15$$

$$Q_3 = hL\ (-P_1+2p_2+4p_3)/30$$

when $p_1=p_2=p_3=p$, then,

$$Q_1 = p\ hL/6$$

$$Q_2 = 2p\ hL/3$$

$$Q_3 = p\ hL/6$$

which give the same results as shown in Fig.I-1 for uniformly distributed edge traction.

The above calculations are involved when the element edges are not straight. The best way of computation in this situation is to employ a computer to calculate the consistent nodal vectors for specified pressure value input of edge traction force at each nodal points of the element edge.

Let the shape function defining a parabolic variation along the element edge be N_1, N_2 and N_3 which are identical to the three shape functions N_1^*, N_5^* and N_2^* of Eq.(3.7) respectively.

Then the distributed traction intensity at any point along the loaded edge is given by,

$$\begin{Bmatrix} p_n \\ p_t \end{Bmatrix} = \sum_{i=1}^{3} N_i \begin{Bmatrix} (p_n)_i \\ (p_t)_i \end{Bmatrix} \qquad (I.13)$$

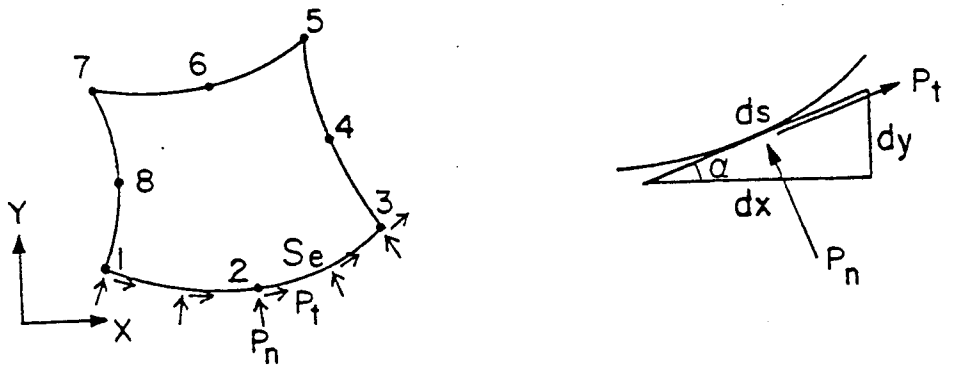

Figure I-3: Consistent Nodal Force Vector for Traction force on Curved Edge

The components of force acting in the x and y directions on an incremental length dS of the loaded edge are, respectively,

$$dP_x=(p_t dS \cos\alpha - p_n dS \sin\alpha)=(p_t dx - p_n dy)$$

$$dP_y=(p_n dS \cos\alpha + p_t dS \sin\alpha)=(p_n dx + p_t dy)$$

Since

$$dx = \frac{\partial x}{\partial \xi} d\xi \ , \quad dy = \frac{\partial y}{\partial \xi} d\xi$$

then,

$$dP_x = (p_t \frac{\partial x}{\partial \xi} - p_n \frac{\partial y}{\partial \xi}) d\xi$$

$$dP_y = (p_n \frac{\partial x}{\partial \xi} + p_t \frac{\partial y}{\partial \xi}) d\xi$$

By applying the principle of virtual work, the equivalent consistent nodal forces are,

$$P_{xi} = \int_{Se} N_i \left(p_t \frac{\partial x}{\partial \xi} - p_n \frac{\partial y}{\partial \xi} \right) d\xi$$

$$P_{yi} = \int_{Se} N_i \left(p_n \frac{\partial x}{\partial \xi} + p_t \frac{\partial y}{\partial \xi} \right) d\xi$$

where integration is taken along the loaded element edge, Se. For the integration, Gaussian Quadrature numerical technique is employed.

V I T A

The author was born in Seoul, Korea on June 6, 1947, the first child of Mr. Nak Yong Seong and Mrs. Sang Yul Nam, Seong. He received his primary education at DonAm Elementary School, KyungGi Junior and Senior High School, in Seoul, Korea.

He received his Bachelor of Science Degree in Feb. 1970 and Master of Science Degree in Feb. 1975 in Architectural Engineering from the Seoul National University, Korea. From Sept. 1970 to Jun. 1973, he was drafted to fulfill his military service.

After graduation, he worked as a design engineer for the HyunDai Construction Company for one and half year. From Sept. 1976 until July 1979, he was an Assistant Professor in the Department of Architectural Engineering at Ulsan Institute of Technology, Ulsan, Korea. He took a leave of absence from this position in Aug. 1979 to enter the Graduate School at Lehigh University. He has been a Research Assistant in Fritz Engineering Laboratory and exposed to the study on the fatigue and fracture problems in bridges.

He was married to former Sung Hee Choi in March, 1976 and has a daughter, Ki Won and a son, Ki Suk.